NATIONAL COOPERATIVE HIGHWAY RESEARCH PROGRAM REPORT **163**

DESIGN OF BENT CAPS FOR CONCRETE BOX-GIRDER BRIDGES

TRANSPORTATION RESEARCH BOARD
NATIONAL RESEARCH COUNCIL

NATIONAL COOPERATIVE HIGHWAY RESEARCH PROGRAM
REPORT 163

DESIGN OF BENT CAPS FOR CONCRETE BOX-GIRDER BRIDGES

J. E. CARPENTER, J. M. HANSON A. E. FIORATO,
H. E. RUSSELL, D. F. MEINHEIT, I. ROSENTHAL,
W. G. CORLEY, AND E. HOGNESTAD
PORTLAND CEMENT ASSOCIATION
SKOKIE, ILLINOIS

RESEARCH SPONSORED BY THE AMERICAN ASSOCIATION OF STATE HIGHWAY AND TRANSPORTATION OFFICIALS IN COOPERATION WITH THE FEDERAL HIGHWAY ADMINISTRATION

AREAS OF INTEREST:
BRIDGE DESIGN
CONSTRUCTION

TRANSPORTATION RESEARCH BOARD
NATIONAL RESEARCH COUNCIL
WASHINGTON, D.C. 1976

NATIONAL COOPERATIVE HIGHWAY RESEARCH PROGRAM

Systematic, well-designed research provides the most effective approach to the solution of many problems facing highway administrators and engineers. Often, highway problems are of local interest and can best be studied by highway departments individually or in cooperation with their state universities and others. However, the accelerating growth of highway transportation develops increasingly complex problems of wide interest to highway authorities. These problems are best studied through a coordinated program of cooperative research.

In recognition of these needs, the highway administrators of the American Association of State Highway and Transportation Officials initiated in 1962 an objective national highway research program employing modern scientific techniques. This program is supported on a continuing basis by funds from participating member states of the Association and it receives the full cooperation and support of the Federal Highway Administration, United States Department of Transportation.

The Transportation Research Board of the National Research Council was requested by the Association to administer the research program because of the Board's recognized objectivity and understanding of modern research practices. The Board is uniquely suited for this purpose as: it maintains an extensive committee structure from which authorities on any highway transportation subject may be drawn; it possesses avenues of communications and cooperation with federal, state, and local governmental agencies, universities, and industry; its relationship to its parent organization, the National Academy of Sciences, a private, nonprofit institution, is an insurance of objectivity; it maintains a full-time research correlation staff of specialists in highway transportation matters to bring the findings of research directly to those who are in a position to use them.

The program is developed on the basis of research needs identified by chief administrators of the highway and transportation departments and by committees of AASHTO. Each year, specific areas of research needs to be included in the program are proposed to the Academy and the Board by the American Association of State Highway and Transportation Officials. Research projects to fulfill these needs are defined by the Board, and qualified research agencies are selected from those that have submitted proposals. Administration and surveillance of research contracts are responsibilities of the Academy and its Transportation Research Board.

The needs for highway research are many, and the National Cooperative Highway Research Program can make significant contributions to the solution of highway transportation problems of mutual concern to many responsible groups. The program, however, is intended to complement rather than to substitute for or duplicate other highway research programs.

NCHRP Report 163

Project 12-10 FY '70
ISBN 0-309-02428-5
L. C. Catalog Card No. 76-1352

Price: $6.80

Notice

The project that is the subject of this report was a part of the National Cooperative Highway Research Program conducted by the Transportation Research Board with the approval of the Governing Board of the National Research Council, acting in behalf of the National Academy of Sciences. Such approval reflects the Governing Board's judgment that the program concerned is of national importance and appropriate with respect to both the purposes and resources of the National Research Council.

The members of the advisory committee selected to monitor this project and to review this report were chosen for recognized scholarly competence and with due consideration for the balance of disciplines appropriate to the project. The opinions and conclusions expressed or implied are those of the research agency that performed the research, and, while they have been accepted as appropriate by the advisory committee, they are not necessarily those of the Transportation Research Board, the National Research Council, the National Academy of Sciences, or the program sponsors.

Each report is reviewed and processed according to procedures established and monitored by the Report Review Committee of the National Academy of Sciences. Distribution of the report is approved by the President of the Academy upon satisfactory completion of the review process.

The National Research Council is the principal operating agency of the National Academy of Sciences and the National Academy of Engineering, serving government and other organizations. The Transportation Research Board evolved from the 54-year-old Highway Research Board. The TRB incorporates all former HRB activities but also performs additional functions under a broader scope involving all modes of transportation and the interactions of transportation with society.

Published reports of the

NATIONAL COOPERATIVE HIGHWAY RESEARCH PROGRAM

are available from:

Transportation Research Board
National Academy of Sciences
2101 Constitution Avenue, N.W.
Washington, D.C. 20418

(See last pages for list of published titles and prices)

Printed in the United States of America.

FOREWORD

By Staff

Transportation Research Board

This report contains the findings from research related to the design of bent caps for reinforced concrete box-girder bridges. The study was primarily experimental in nature but also included a significant analytical phase. The findings should be of interest to structural engineers involved in the design and construction of concrete bridges.

Recent emphasis on safe and aesthetic design of reinforced concrete highway bridges has resulted in substructure configurations that depart from the traditional footing-column-cap frame design. Aesthetic considerations often dictate the concealment of massive concrete caps and reduction of the number of vertical columns. Current design procedures are not necessarily applicable to these new configurations. At the time this research was initiated there existed a general belief that current procedures resulted in overdesigned structures containing much more reinforcing steel than was necessary.

The Portland Cement Association carried out NCHRP Project 12-10 with the objective of developing more appropriate design procedures. Although the ultimate need is to establish valid procedures applicable to many configurations of bridge bent caps, this project was limited to investigation of integral bent caps concealed in straight, continuous, reinforced concrete box-girder bridges. Because many similar bridges are being built, even a small reduction in the amount of reinforcing steel used in each bridge might result in substantial total savings. This project showed that reductions are possible.

The research comprised both analytical and experimental phases, with emphasis on the latter. Analytical studies of load distribution throughout the structures and stress distribution in bent caps were conducted on two prototype bridges. The experimental phase included construction of seven scale models. Two of the models, built to one-fifth scale of the prototype bridges, were representative of popular reinforced concrete box girder designs. Testing of these models provided information on the distribution of loads in the vicinity of integral bent caps. The other five models represented transverse strips of bridge superstructures parallel to, and including, the bent caps and columns. Column flare and the amount and distribution of bent cap reinforcement varied in these models. These tests also provided information about critical sections and the effective width of bent caps.

The research findings relate primarily to design assumptions rather than provisions of the specifications, and none of the recommendations is in conflict with current practice. As a result, implementation should be relatively easy. No changes are recommended in the method of distributing loads to the bent cap. With respect to the spreading of reinforcement and the effective flange width, the specifications have no explicit provisions for bent caps; however, the recommendations herein are slightly more conservative than what might be inferred. The findings with respect to support effectiveness and the location of the critical design section simply clarify the specifications.

Because the findings result from a carefully designed and executed experimental program as well as from consideration of the results of a sophisticated analytical study, it is believed that they are highly reliable and can be used immediately for improved design methods.

CONTENTS

ACKNOWLEDGMENTS

The research reported herein was directed from and the experimental portion was carried out in the Structural Development Section of the Portland Cement Association. Principal Investigator for the project was James E. Carpenter, Principal Structural Engineer, SDS, PCA (now Manager, Structural Research and Development, Concrete Technology Corporation, Tacoma, Wash.)

The other authors include: John M. Hanson, Assistant Manager, SDS, PCA (now Director of Structural Research, Wiss, Janney, Elstner and Associates, Northbrook, Ill.); Anthony E. Fiorato, Structural Engineer, SDS, PCA; Henry G. Russell, Senior Structural Engineer, SDS, PCA; Donald F. Meinheit, Associate Structural Engineer, SDS, PCA (now Assistant Professor, University of Notre Dame, South Bend, Ind.); Israel Rosenthal, Visiting Engineer, SDS, PCA (now Senior Research Fellow, Building Research Station, Technion, Israel Institute of Technology, Haifa, Israel); W. Gene Corley, Manager, SDS, PCA (now Director, Engineering Development Department, PCA); and Eivind Hognestad, Director, Engineering Development Department, PCA (now Director, Technical and Scientific Development, PCA).

Other members of the PCA professional staff who participated in the project include: H. T. Capell, M. Fintel, P. G. Griffin, T. Helgason, C. L. Freyermuth, V. Cervenka, and M. Haddadin. Members of the technician and clerical staff who worked on various phases of the project include: B. W. Fullhart, R. K. Richter, A. G. Aabey, D. C. Bell, B. J. Doepp, W. H. Graves, W. Hummerich, Jr., R. McCarley, Jr., C. C. Tenant, O. A. Kurvits, B. G. Firstenberger, Jr., J. S. Zintel, A. M. Parisi, R. Kohn, and A. A. Nelson.

DESIGN OF BENT CAPS FOR CONCRETE BOX-GIRDER BRIDGES

SUMMARY

Design recommendations for integral bent caps in straight, continuous, reinforced concrete box-girder bridges were developed from the results of a combined experimental and analytical investigation.

The results of the investigation indicate that reductions in the amount of flexural reinforcement in the bent cap of up to 40 percent can be made without reducing safety and while maintaining adequate serviceability. Even greater reductions in the amount of reinforcement can be made for bent caps with flared columns. Most of this improved economy results from a change from the working stress method of design to the load factor method of design.

Test variables included the distribution of loads on the bent cap, the effect of flaring the column in the plane of the bent, the effective flange width of the bent cap in tension and in compression, the effect of spreading the main tensile reinforcement into the adjacent superstructure, and the location of the critical design sections.

The experimental program included tests on two one-fifth scale models of complete box-girder bridges, four two-fifths scale models of single-column bent cap portions of the bridges, and one one-fifth scale model of a double-column bent cap portion of a bridge. The analytical studies included (1) development of a computer program using the elastic folded-plate method to predict the load-carrying mechanism of the complete bridges and (2) development of a finite element model simulating in detail the behavior of the bent cap through cracking of the concrete and yielding of the reinforcement.

Results from tests of the two complete model bridges indicated that at loads approaching ultimate there was little lateral transfer of load from girder to girder. The analytical results, based on elastic material properties, predicted somewhat greater lateral distribution of load. With or without this distribution, moments in the bent cap were found to be essentially the same. Since the assumption of no distribution gave a slightly higher moment, it was more conservative. On the basis of these results, it is recommended that the current design assumption of no lateral distribution of load be used.

The extreme column flare tested in the program had a support surface that formed an angle of 45 degrees with the vertical. This flare, and one that was similar but less extreme, were found to be fully effective as supports. Stress induced in the concrete of the flare itself was not excessive. Similarly, reinforcement strains in the bent cap were comparable to those at corresponding locations over the cylindrical column. On the basis of these results, it is recommended that all flares up to 45 degrees be considered effective supports. Similar provisions already exist in building codes.

Existing provisions for compressive flange widths in box girders, restated in terms of overhanging flanges, were found to be applicable to bent caps. For tension

flanges, recommendations of effective widths similar to those for compression flanges are made with the additional restriction that the effective overhanging flange width be limited to one-fourth of the box web spacing. This width ensures that reinforcement is not over-stressed by secondary effects.

The effectiveness of flexural reinforcement was found to diminish rapidly with increasing distance from the bent cap web. However, the recommendation is made that reinforcement spread to the limits of the effective flange width in tension be considered completely effective.

The critical design section for negative moment in the bent cap was found to be at the face of the support. This section is defined as the intersection of the extremity of the effective support with the bottom of the bent cap. The critical design section for positive moment was found to be at midspan of the tested double-column bent.

CHAPTER ONE

INTRODUCTION AND RESEARCH APPROACH

PROJECT STATEMENT

The project statement furnished by NCHRP Project 12-10 noted that bridge superstructures usually consist of main load-carrying members that span between abutments and piers. In traditional designs, support at piers is provided by a footing-column-cap frame similar to that shown in Figure 1. However, recent emphasis on safe and aesthetically pleasing designs has resulted in the development of highly efficient reinforced concrete box-girder bridges. This type of structure makes desirable the concealment of the cap in the box-girder superstructure as shown in Figure 2.

Currently, bent caps concealed within and thereby integrated into the bridge superstructure are being proportioned by the same procedures used in the design of traditional caps. A general belief exists, however, that bent caps contain considerably more reinforcing steel than is necessary and that development of improved design procedures is urgent.

Although the ultimate need is to establish valid design procedures applicable to many configurations of bridge bents, this project was limited to investigation of bent caps concealed in straight, continuous, reinforced concrete box-girder bridges.

Within the general scope of the investigation, the project statement as amended restricted the investigation to the following items:

1. A review of the relevant technical literature.
2. Investigation of bent caps with the following configurations:
   a. Single column with:
      (1) Constant circular cross section.
      (2) Flare in the plane of the bent to twice the column diameter.
      (3) Flare in the plane of the bent to three times the column diameter.
   b. Single column with constant circular cross section, but with the bent cap reinforcement spread out into the adjacent roadway slab thickened for the purpose.
   c. Two columns of the same constant circular cross section.
3. Determination of a design procedure, using the results of items 1 and 2, for single- and multiple-column bents.
4. Specifying those changes required in the AASHTO specifications to permit the use of the new design procedures.

The project statement as amended also specified that the bridges studied should have girder spans of approximately 80 ft and depth-to-span ratios of 0.055. Columns were either round or square with a lateral dimension of 5 ft and an 18-ft minimum length. Multiple columns were to be spaced at about 40-ft centers in the bent. Grade 60 reinforcing steel was specified.

The investigation was conducted by a combination of analytical studies and tests on adequately scaled, reinforced concrete models.

Models were to be designed and loaded in accordance with AASHTO specifications (*1*) for bridge design.

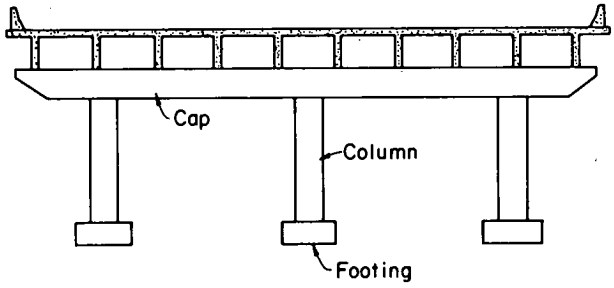

Figure 1. Footing-column-cap frame.

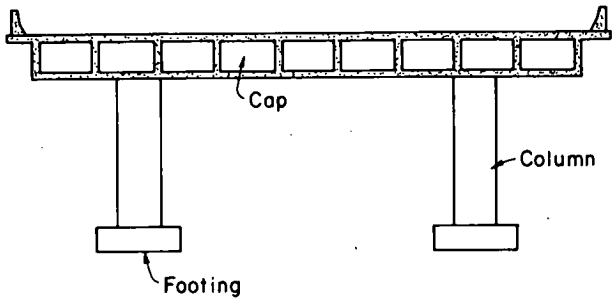

Figure 2. Cap concealed in box-girder bridge.

SPECIFIC OBJECTIVES

The over-all goal of the project was to develop a design procedure for bent caps. The design procedure was to cover the following specific items:

1. Location and distribution of the critical AASHTO loading for the bent cap.
2. Effect of flaring the column.
3. Effective width of the bent cap.
4. Effect of spreading the bent cap reinforcement into the adjacent box-girder slab.
5. Location of the critical cross sections for design of the bent cap.

RESEARCH PLAN

For planning purposes, the over-all project was divided into six phases, which are given in Table 1. Several phases were further subdivided as indicated. The scope of each phase is described.

1. *Literature review.* A literature review was carried out to bring the investigators up to date on the latest information in order to avoid duplication of work.

2. *Analytical studies.* The load distribution portion of the analytical studies was the analytical equivalent of the model bridge tests. The aim was to develop by elastic analysis a method of predicting the loads transmitted to the bent cap by the box-girder superstructure. The bent cap would then be designed to carry those loads.

The bent analysis portion of the analytical studies was the analytical equivalent of the model bent tests. Its purpose was to develop by the finite element method a mathematical model of the bent cap portion of the bridge so that all details of behavior, including stresses in the concrete and reinforcement, could be predicted.

3. *Model bridge tests.* In the first part of the testing program, two complete bridge models were built to one-fifth scale. The first bridge contained a single-column bent and the second, a wider bridge, contained a double-column bent. Both structures were designed by the working stress method, and had dimensions satisfying the requirements of the project statement.

The main purpose of the bridge tests was to determine experimentally the location and distribution of the critical AASHTO loading for the bent cap. The bent cap portions of the model bridges were also instrumented to obtain information on behavior.

4. *Model bent tests.* The experimental investigation of variables No. 2 through No. 5 listed under "Specific Objectives" was carried out by means of testing the five bent cap models, which are given in Table 1. Data from all five models were used in the study of effective width of the bent cap and the location of the critical design section. The effect of flaring the column was evaluated by comparing the results of tests on models SC-3, SF-4, and SF-5, the latter two of which had flared columns. The effect of spreading the bent cap reinforcement was studied by comparing the results of the tests on models SC-3 and ST-6.

Each bent cap model, including the bent cap and column, represented the central portion of a bridge between the lines of inflection in either span. The single-column models were constructed at two-fifths scale and the double-column model at one-fifth scale. The load factor method was used to design the models to resist a single pattern of loads representing increments of dead load plus a uniformly distributed live load.

5. *Design procedure.* Recommendations for changes to the AASHTO specifications are discussed in the latter part of Chapter Three. These recommendations are based on analysis of data developed in this investigation.

6. *Modification to the plan.* A number of NCHRP-approved changes were made in the project working plan after the investigation had begun. As a result, the working plan described herein was the one followed.

TABLE 1

PROJECT PLAN

PHASE	PART
Literature review	
Analytical studies	Load distribution
	Bent analysis
Model bridge tests	Single-column bridge
	Double-column bridge
Model bent tests	Single-column bent SC-3
	Single-column bent SF-4, flared column
	Single-column bent SF-5, flared column
	Single-column bent ST-6, spread reinforcement
	Double-column bent DC-9
Design procedure	
Final report	

IMPLEMENTATION OF THE RESEARCH PLAN

Analytical Studies—Load Distribution

The part of the project dealing with analytical studies of load distribution was carried out by Professor Alex C. Scordelis, of the University of California at Berkeley. A specially developed computer program called MUPDI-3 was used. The program treats the box-girder superstructure as an elastic folded-plate system that is simply supported on the ends and carried at the center by a flexible bent of zero dimension spanwise of the bridge. Stiffnesses of the elastic bent are selected to approximate those of the bridge. The Goldberg-Leve (*2*) solution is used for analysis of the folded plates.

Output of the program can be in terms of shears, moments, and axial forces in the bent cap and girders. Other items of information can also be obtained. Thus, within the limits of the elastic analysis, the program gives the distribution of loads among the various girders.

The program was used to analyze the two prototype bridges. Distributions for dead load and for all live-load patterns were obtained. The effect of adding integral continuous parapets was also determined.

An elevation of the bridges analyzed is shown in Figure 3. The cross section of the single-column bridge is shown in Figure 4; that of the double-column bridge is shown in Figure 5.

Additional introductory material concerning the analytical approach to the problem is contained in Appendix A. A comprehensive report describing this part of the project is included as Appendix B.

Analytical Studies—Bent Analysis

Analytical studies of the bent were carried out by Professor Paul P. Lynn of the University of Colorado. A finite element program was used to analyze the single-column bent cap specimen and its loading. The finite element used has provisions for nonlinear combined action of the reinforcement and concrete, including the effects of cracking and of slip between the reinforcement and concrete. Output includes steel stresses.

Additional introductory material describing the method is contained in Appendix A. A comprehensive report describing this part of the project is included as Appendix C.

Model Bridge Tests

The two prototype designs developed for the model bridge test phase had basic geometry and loading specified by the problem statement. Within the geometric limitations, dimensions were chosen so that, when the structure was scaled down to model size, it would fit the constraints of the laboratory test floor.

The prototype bridges were designed by working stress methods. The design was based on concrete with a compressive strength of 3,500 psi and reinforcement meeting the requirements of ASTM A615, Grade 60. Thus, allowable stresses were 1,400 psi for the concrete and 24,000 psi for the reinforcement.

Dimensions of the prototype bridges are shown in Figures 3 through 5. An elevation is shown in Figure 3. Depth of the prototype box-girder superstructure was 5 ft. The width of the bent cap for the single-column bridge was 6 ft 6 in. However, this width was reduced to 5 ft 6 in. for the double-column bridge. Each bridge was supported by 5-ft-diameter columns having a height of 18 ft.

The single-column prototype shown in Figure 4 has a roadway width of 40 ft plus an overhang of 2 ft on each side for a parapet. Center-to-center spacing of the webs was 7 ft 6 in.; the web thickness was 8 in. in the main part of the span. Each web was thickened to 12 in. near the bent cap. The thicknesses of the top and bottom slabs were 7 in. and 5½ in., respectively.

Figure 5 shows a section through the double-column prototype. This bridge had a roadway width of 70 ft. Dimensions of all other elements in the double-column bridge were similar to those in the single-column bridge.

In the prototype design, the following criteria were used:

1. The location and distribution of the critical AASHTO loading for the bent cap was based on current AASHTO methods.
2. The effective width of the bent cap was based on current AASHTO specifications for box girders. The same re-

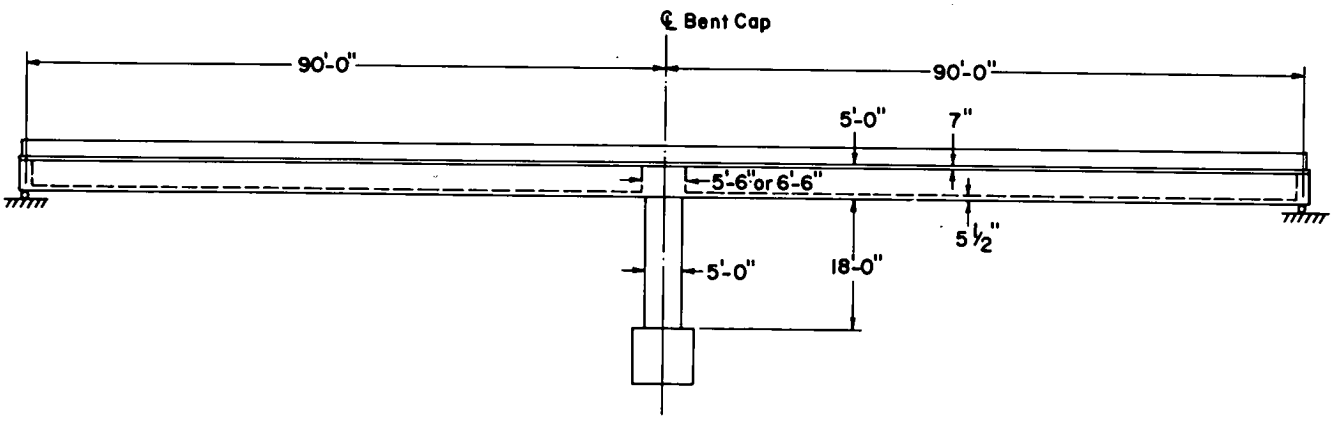

Figure 3. Elevation of prototype bridge.

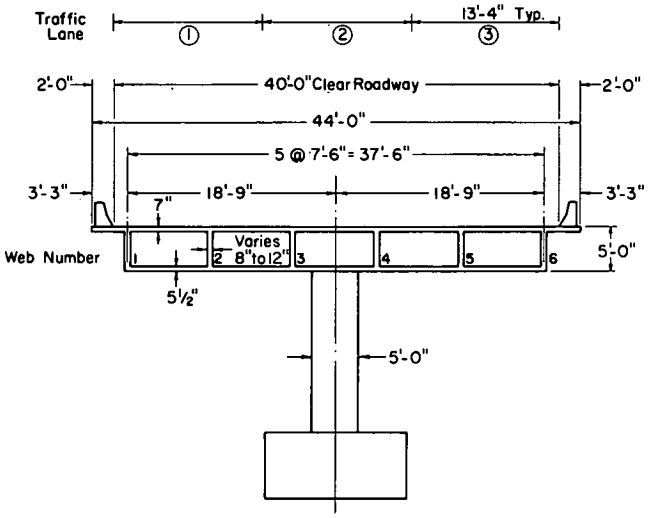

Figure 4. Prototype bridge section showing single-column bent cap.

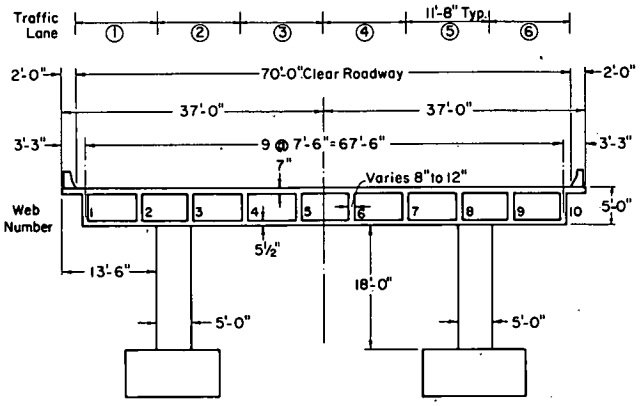

Figure 5. Prototype bridge section showing double-column bent cap.

quirements were used to determine the compression flange width for both the girders and the bent cap. No determination had to be made for effective width of the bent cap in tension because all necessary reinforcement was contained within the width of the bent cap web.

3. The critical design section for bent cap negative moment was taken at one-sixth the column diameter from the column centerline, as suggested in the California *Manual of Bridge Design Practice* (*3*).

4. The effect of column flare did not apply to these bridges.

5. The effect of spreading bent cap reinforcement did not apply to these bridges.

6. The critical design section for negative moment in the girders was taken at one-half the column diameter from the bent cap centerline.

Criteria adopted for the design of the model bridges were that the stress and strain scales should both be unity in order that the stresses and strains for a particular properly scaled load pattern on the model would be the same as for an identical load pattern on the prototype bridge. As a result, the models were geometrically similar to the prototype. Similarly, the design material properties were the same as those for the full-sized structure. This is an example of the "direct" method of structural modeling as described in detail elsewhere (*4*).

A scale factor of one-fifth was chosen so that the model could be accommodated in the laboratory. The elevation of the model bridges is shown in Figure 6. Figure 7 shows a cross section of the single-column bridge; Figure 8 shows a cross section of the double-column bridge. The models were similar to the prototype designs except for the addition of column-base blocks to enable reactions to be measured.

Reinforcement could not be scaled down bar by bar. Instead, the steel areas were scaled and then the model reinforcement selected with consideration for available sizes. Reinforcement sizes ranged from No. 4 bars to annealed deformed wire of 0.01-sq. in. cross-sectional area. The concrete mix was designed with a nominal maximum aggregate size of ⅜ in.

Reduced-scale structures made of the same materials as the prototype are deficient in dead-load stresses, as discussed by Mattock (*4*). The deficiency in dead-load stresses

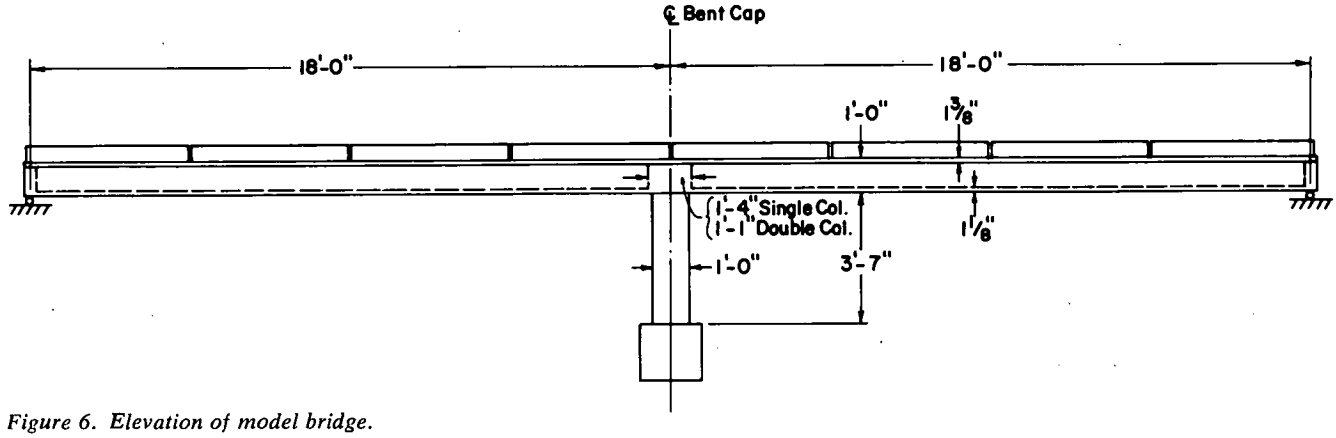

Figure 6. Elevation of model bridge.

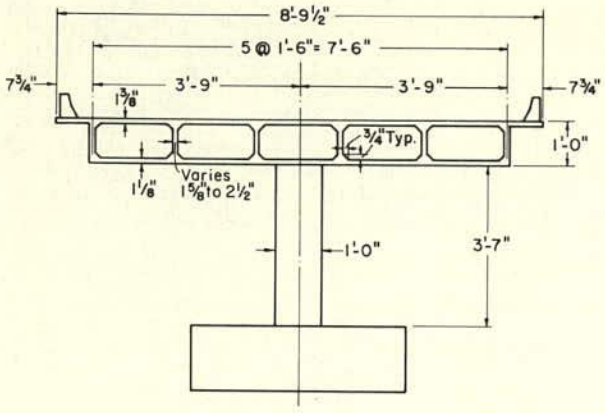

Figure 7. Cross section of single-column model bridge.

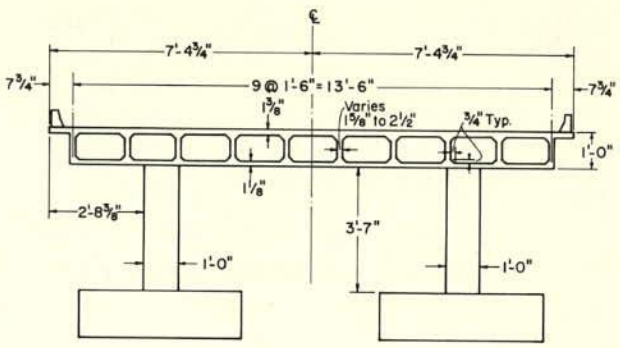

Figure 8. Cross section of double-column model bridge.

was made up by application of load through the same hydraulic system that supplied increments of dead load. This "dead-load makeup" was removed only for the purpose of obtaining new "zero" readings on the instrumentation, a process required only a few times during each test.

The loading apparatus was arranged so that uniform loads were simulated by point loads spaced at 3-ft intervals along the webs. Lane loads were applied at the proper lateral position. Concentrated load portions of the AASHTO live loads were also applied through a hydraulically actuated system. In addition to the hydraulically applied loads, the effect of applying a single point load was measured by placing a weight successively at several points on the bridge deck.

Loads were measured by observation of the pressure in the hydraulic loading system, by signals from load cells installed in the loading system, and by signals from load cells measuring the abutment and column reactions. Strains were measured by electrical resistance strain gages, mounted either on the reinforcement or on the concrete surface, and by a Whittemore mechanical strain gage. Deflections were measured both by means of linear potentiometers and by observation of targets through a surveyor's level (*5, 6*). Crack widths were measured by a hand microscope containing graduations to 0.001 in.

Signals from the electrical sensors were measured by a scanning digital voltmeter and were recorded on both punched and printed paper tapes. The punched tape was fed into a computer that reduced the data. The printed tape was available for inspection during the test and as a cross check for errors in the punched paper tape. A total of 344 channels of data were recorded during the single-column bridge test and 555 during the double-column bridge test.

Casting of the single-column model bridge proceeded in four steps. First, the column base was cast. This was followed by casting of the column. Next, the soffit, webs, and bent cap up to the bottom of the deck were cast in a single lift. Finally, the deck concrete was placed.

After the concrete had cured, the model bridge was lifted from the casting platform and placed in the test location. End diaphragms were then added, reactions adjusted, loading apparatus installed, and the instrumentation completed and calibrated. The model ready for testing is shown in Figure 9.

The test program commenced with the application of the continuously maintained force to make up the deficiency in dead load. A series of loadings, given in Table 2, was then applied to the model.

Capacity of the model was reached in Phase 6 at 2.3 times the design ultimate load of $[1.5D + 2.5\ (L + I)]$, where D equals dead load and $(L + I)$ equals live load plus impact. The observed cause of distress was slipping of a splice in the positive moment girder reinforcement near the end of the span. Following the initial test to destruction, the superstructure was repaired and additional tests, Phases 1 and 8, were performed.

Casting and preparation for test of the double-column model followed the same procedures used for the single-column bridge. The significant difference between the two models was that the restraint conditions of the bases of the columns of the double-column bridge could potentially influence the test results. Consequently, provision was made for introducing column base rotations as one of the tests to be performed. Figure 10 shows the model ready for test.

As with the single-column bridge, the testing started with application of a continuously applied force to make up the

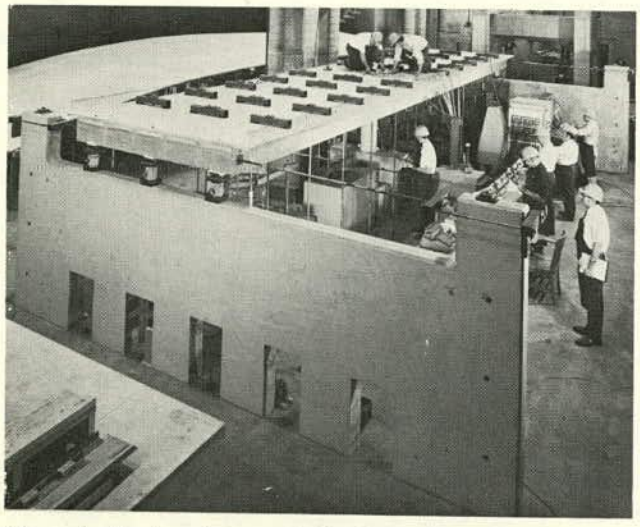

Figure 9. Single-column model bridge ready for test.

TABLE 2

TEST PROGRAM FOR SINGLE-COLUMN MODEL BRIDGE

PHASE	LOADING
1	A 2-kip concentrated load applied successively at points 3 ft apart on each web Equivalent AASHTO service loadings 1.0 $[D+(L+I)]$
2	Reapplication of AASHTO service loadings after adding parapet
3	Overload $1.75D+2.0\ (L+I)$
4	A 4-kip concentrated load applied successively at points 3 ft apart on each web
5	Equivalent AASHTO design ultimate loadings $1.5D+2.5\ (L+I)$
6	Test to destruction
7	Test to destruction of repaired complete model
8	Test to destruction of bent cap portion of model

dead load deficiency. Testing continued with the application of loadings, which are given in Table 3. Capacity was reached at a load of 2.2 times the design ultimate condition of $[1.5D + 2.5\ (L + I)]$. The test was ended when distress occurred in a box girder near the bent cap.

Details of the model bridge test program are described in Appendix D.

Model Bent Tests

The model bent specimens were designed using criteria different from those used for the model bridges. Rather than being designed to simulate a structure subjected to a variety of load patterns and hence "overdesigned" at most sections for a particular load pattern, the bent cap models were designed throughout to resist a single critical load pattern. Furthermore, the load factor method was used in design so that the capacity of the structure was at the same time better defined and at a lower total than for the bridges. The design was purposely biased to favor flexural yielding of the bent cap for first distress.

The following design assumptions were used:

1. For location and distribution of the critical AASHTO loading for the bent cap, all lanes were assumed loaded. Furthermore, all girders were assumed to be equally loaded, in accord with results from the model bridge tests.
2. The effective width of the bent cap compression flange was based on extant AASHTO specifications for box girders. Similar criteria were used for determining the compression flange width for the girders.
3. The critical design section for bent cap negative moment was taken as one-fourth the superstructure depth outside the face of the support. This assumption was based on preliminary analysis of results from the tests on the model bridges.
4. Flared columns were considered to be as effective as cylindrical columns having a cross section the same as that at the top of the flare.
5. Spread reinforcement was considered to be fully effective.

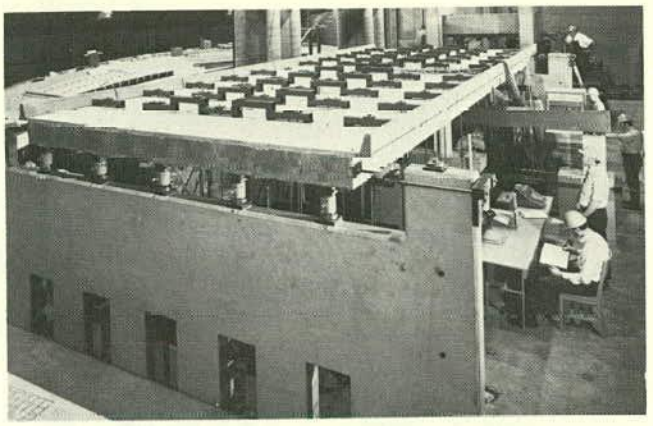

Figure 10. Double-column model bridge ready for test.

TABLE 3

TEST PROGRAM FOR DOUBLE-COLUMN MODEL BRIDGE

PHASE	LOADING
1	Equivalent AASHTO service loadings 1.0 $[D+(L+I)]$
2	Reapplication of AASHTO service loadings after adding parapet
3	Equivalent AASHTO design ultimate loadings $1.5\ D+2.5\ (L+I)$
4	Special tests, including application of concentrated loads, and settlement and rotation of columns
5	Test to destruction

6. The critical design section for negative moment in the girder was taken at the face of the bent cap.

The bent cap models represented the central portion of the bridge, including the bent cap and column, located between lines of inflection a distance $l/4$ either side of the bent cap centerline, where l is the span of the bridge. Location of the line of inflection, taken to be the same as for a uniformly loaded continuous beam, was essentially that indicated by the analytical studies and by the results of the tests on the model bridges. Cutting the structure along the line of inflection enabled the influence of the missing portions to be represented by concentrated shear loads applied at the cut ends. The dimension of the specimen, in the direction of the bridge span, was great enough to include the entire effective width of the bent cap.

Test methods for the bent cap tests closely paralleled those for the bridges. However, the loading apparatus was less complex due to the equal distribution of live loads, and the loading program was shorter.

The loading program was carried out in two phases. The first phase involved application of service load $[1.0D + 1.0\ (L + I)]$; the second was the test to destruction.

Instrumentation was similar to that installed on the model bridges, except that reactions were not measured. Data acquisition and reduction were handled in the same manner as for the model bridges.

The four single-column bent specimens were two-fifths scale. This larger size provided some advantages in construction without any serious disadvantages due to increased loading requirements or absolute size.

The elevation of the first three single-column bent specimens is shown in Figure 11. That of the fourth specimen is shown in Figure 12. Cross sections of the specimens are shown in Figures 13 and 14. Dimensions shown are geometrically in proportion to those of the corresponding prototype bridge except that the girder webs are not flared. Elimination of the web flares resulted from change to the load factor method of design. The column height was 5 ft rather than the scale 7 ft 2⅜ in.; no column-base blocks were used. The column height, which had no effect on the test, was reduced for ease of construction. Figure 15 shows a specimen ready for test.

The single-column model bents were constructed with the same concrete mix used for the model bridges. The construction sequence was also similar.

Main negative-moment reinforcement for specimens SC-3, SF-4, and SF-5 consisted of 12 bars extending the full length of the bent cap. Sizes used were Nos. 7, 6, and 5, respectively. Specimen ST-6, with the full-length bent cap reinforcement spread, contained 36 No. 4 bars. These gave the same total area of reinforcement as specimen SC-3.

Each test was conducted within a period of two days. The dead-load makeup was not applied separately but was included as part of the total load. On the first day, service load was applied in increments of 0.25 D to 1.0 D followed by increments of [0.25 $(L + I)$] to a total of [1.0 D + 1.0 $(L + I)$]. On the second day, the specimen was loaded to ultimate in increments of 0.05 K, where $K = 1.0$ is equal to [1.8 D + 3.0 $(L + I)$], the design ultimate load. Strengths and observed causes of distress for each of the four specimens are given in Table 4.

The double-column bent specimen was designed at one-fifth scale, the maximum that could be accommodated in the laboratory. The elevation and cross section are shown in Figures 16 and 17. Girder design was geometrically similar to that for the single-column bents. Bent cap flexural reinforcement, both positive and negative, was provided by 16 6-mm deformed bars. This reinforcement would be the equivalent of 14 No. 4 bars in the two-fifths scale, single-column specimens.

Materials, construction techniques, instrumentation, and data acquisition and reduction were the same as for the single-column bents except that no Whittemore mechanical strain gages were used. The loading program was also

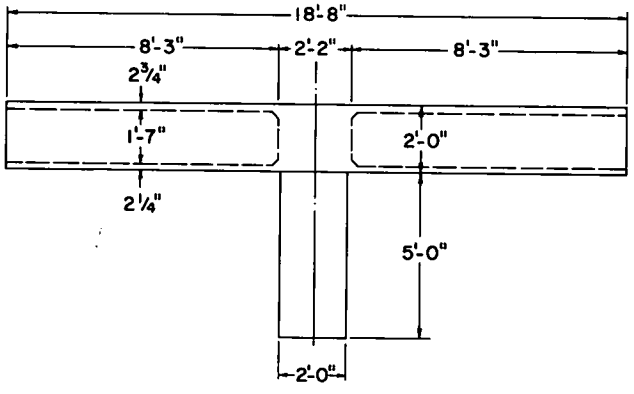

Figure 11. Elevation of single column bents SC-3, SF-4, and SF-5.

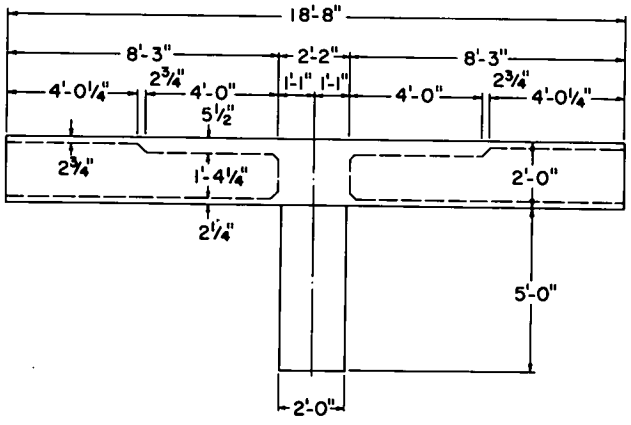

Figure 12. Elevation of single-column bent ST-6.

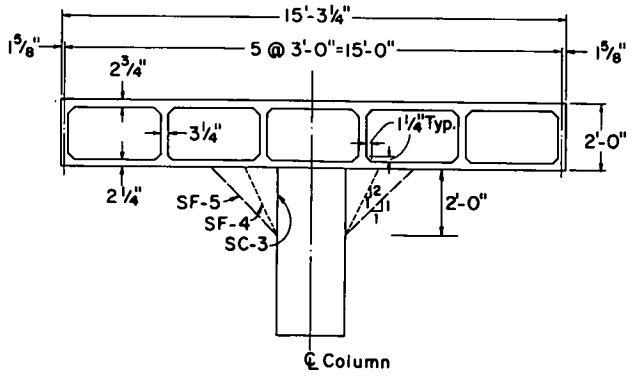

Figure 13. Cross sections of single-column bents SC-3, SF-4, and SF-5.

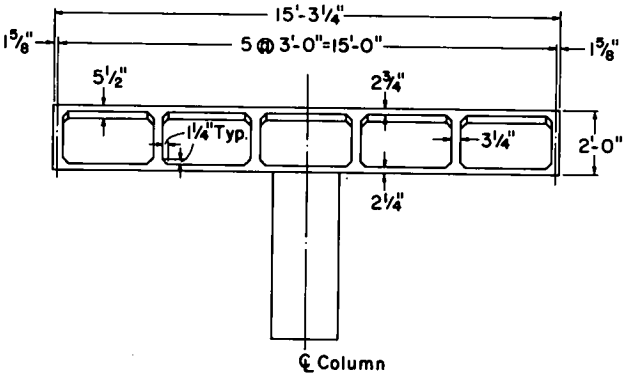

Figure 14. Cross section of single column bent ST-6.

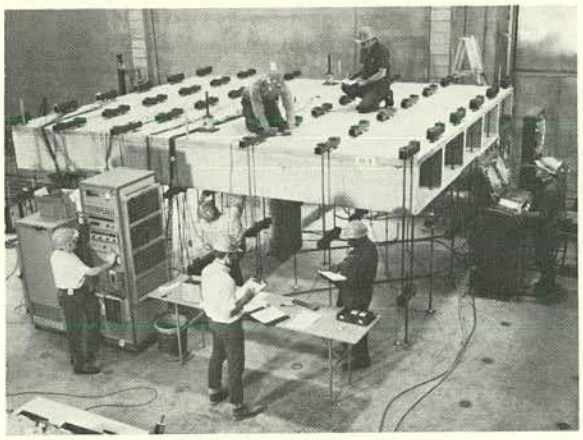

Figure 15. Single-column bent ready for test.

similar to that for the single-column bents. Figure 18 shows this model ready for test.

The ultimate load was reached at $K = 1.15$ with a local failure at a construction joint. Upon retesting the undamaged portion of the bent, a load of $K = 1.40$ was sustained prior to crushing of the lower flange of an exterior girder. This was the same type of distress noted in two of the single-column bents.

Details of the model bent test program are described in Appendix E.

TABLE 4

TEST RESULTS FOR SINGLE-COLUMN BENTS

BENT	ULTIMATE LOAD, K [a]	CAUSE OF DISTRESS
SC-3	1.25	Horizontal shear in girder web
SF-4	1.25+	Crushing in lower flange of exterior girder
SF-5	1.30	Crushing in lower flange of girders
ST-6	1.20	Crushing in lower flange of exterior girder

[a] $K = \dfrac{\text{Observed ultimate load}}{1.8\,D + 3.0\,(L+I)}$

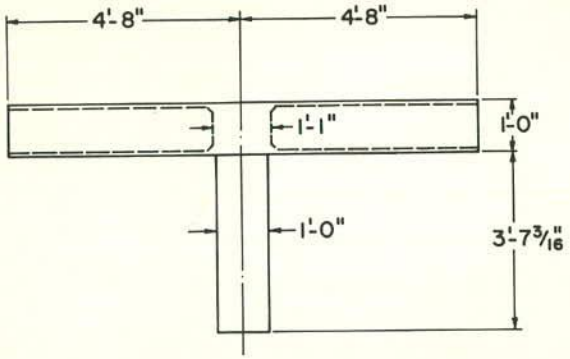

Figure 16. Elevation of double-column bent DC-9.

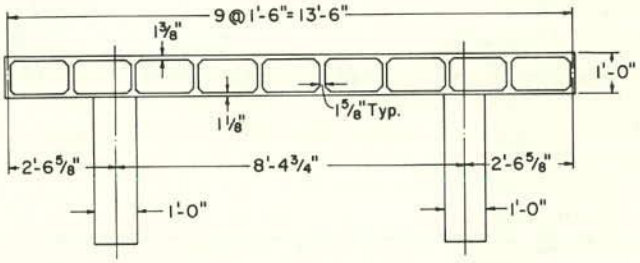

Figure 17. Cross section of double-column bent DC-9.

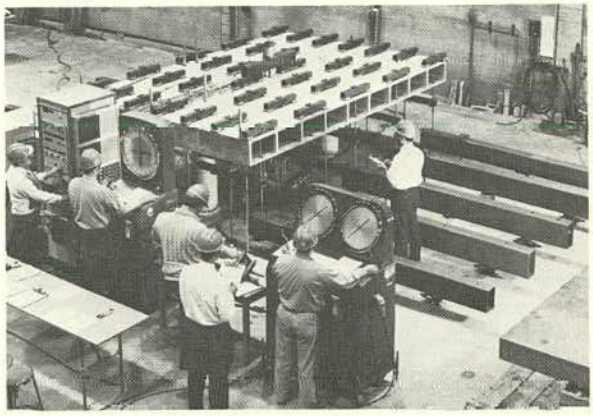

Figure 18. Double-column bent ready for test.

CHAPTER TWO

FINDINGS

LOAD DISTRIBUTION IN BRIDGES

Controlling Loading Distribution

The live loading found to control the bent cap design was always some combination of the AASHTO lane loadings, rather than the truck loadings. Controlling distributions for design of the bent caps in both bridges are given in Table 5. Lane designations are shown in Figures 4 and 5 for the single-column and double-column bridges, respectively.

In Table 5, and in the discussion that follows, "current design method" refers to the AASHTO Specifications (*1*). The folded-plate analysis of this project as described in Appendix B is referred to as "the analysis" and the experimental results from both model bridge and model bent tests are referred to as "the experimental results."

For the design of the bent cap of the single-column bridge, the current design method indicated that the controlling load distribution is with lanes 1 and 2 loaded. However, both the analysis and the experimental results indicated that the controlling load distribution was with all three lanes loaded.

For the design of the bent cap of the double-column bridge for exterior negative moment, the current design method predicts that the maximum moment at the design section is produced by loading the adjacent exterior lane. According to the assumptions, loading the opposite exterior lane has no effect on the moment being considered. Thus, defining as the controlling loading case either one or both exterior lanes loaded gives the same maximum moment. For ease in comparison with the symmetrical loading cases considered in the analytical program and in the experimental program, the controlling case for the current design method was taken as the two exterior lanes, lanes 1 and 6, loaded.

Four symmetrical loading cases were considered for the double-column bridge in both the analytical and experimental programs. These were all six lanes loaded, the two exterior lanes loaded, the two center lanes loaded, and the four interior lanes loaded. It would have been impractical to study unsymmetrical cases because it would have been necessary to consider the entire cross section of the bridge. To do so would have overtaxed the capacity of both the computer program for analysis and the data acquisition system for the test. With symmetrical loadings, it was necessary to consider only one-half the bridge cross section.

For exterior negative moment, both the analysis and the experimental results indicated that the controlling condition was with all six lanes loaded.

For interior negative moment, the current design procedure indicates that the unsymmetrical condition with the five nearest lanes loaded results in a larger moment than the symmetrical case of all six lanes loaded. The difference is 16 percent for live-load moment and 4 percent for total moment. Six lanes loaded, the controlling symmetrical

TABLE 5

CONTROLLING DISTRIBUTION OF LIVE LOADS BY LANE FOR BENT CAP DESIGN

BRIDGE TYPE	LOCATION	METHOD	INDICATED CRITICAL LIVE-LOAD DISTRIBUTION (AASHTO LANE LOADINGS)	
			NO. OF LANES LOADED	LANE NO.
Single-column	−M	Current design	Two exterior lanes	1 2
		Analysis	All three lanes	1 2 3
		Experimental	All three lanes	1 2 3
Double-column [a]	−M exterior	Current design	Two outside lanes	1 6
		Analysis	All six lanes	1 2 3 4 5 6
		Experimental	All six lanes	1 2 3 4 5 6
	−M interior	Current design	All six lanes	1 2 3 4 5 6
		Analysis	All six lanes	1 2 3 4 5 6
		Experimental	All six lanes	1 2 3 4 5 6
	+M	Current design	Two center lanes	3 4
		Analysis	Two center lanes	3 4
		Experimental	Two center lanes	3 4

[a] Symmetrical loadings only considered. Current design indicates five lanes loaded critical for −M interior.

case, was used for comparison with the analysis and with the experimental results.

Both the analysis and the experimental results indicated that, of those considered, the controlling condition was with all six lanes loaded.

For positive moment at midspan of the bent cap, all three methods indicated that the controlling condition was with the two center lanes loaded.

Load Distribution Characteristics of Bridges

To give a qualitative picture of the lateral load distribution characteristics of the bridges as predicted by different methods of analysis and design, Tables 6 and 7 were prepared for the single-column and double-column bridges, respectively. In these tables, the input per girder was defined as the load applied to that girder over a particular length. The output was defined as the resulting shear at the end of that length of girder closest to the bent cap. The ratio of output to input was then a measure of what portion of its applied load a particular girder was carrying.

For the current design method, no lateral distribution of load is assumed. Consequently, the ratio of output to input is always unity.

Output shears for the analysis were taken at the points of inflection of the girders. Inputs for each girder were based on the length between the abutment and the point of inflection. The output shears and the location of the point of inflection are displayed graphically, in Appendix B, for each loading case as Part 11 of a set.

In Tables 6 and 7, the absolute values of shear are given. It should be noted that for the single-column bridge, the sums of input and output need not be the same, since transverse distribution of load across the bridge centerline can occur.

In addition to the loading cases for dead load and for live load in all lanes, a loading case for equal line loads on all webs of the single-column bridge was included. The plot for this case, equivalent to the plots for the other load cases given in Appendix B, is shown in Figure 19.

As can be seen by comparing the input loads with those of the other analytical loading cases in Table 6, the input loads for this case are more uniform than either of the

TABLE 6

DISTRIBUTION PROPERTIES OF SINGLE-COLUMN BRIDGE

METHOD AND LOADING CASE	INPUT OR OUTPUT	FORCE ON WEB (KIPS)			OUTPUT/INPUT RATIO ON WEB		
		1	2	3	1	3	3
Current design method	—	—	—	—	1.00	1.00	1.00
Analytical distribution:	I	13.81	13.37	13.33			
Equal loads	O	8.00	13.74	17.74	0.58	1.03	1.33
Case 1, all lanes,	I	12.67	15.81	17.08			
live load	O	7.61	14.59	18.40	0.60	0.92	1.08
Case 4, dead load	I	45.26	54.40	54.00			
	O	33.30	53.70	65.91	0.74	0.99	1.22
Experimental distribution	I	32[a]	32[a]	36[a]			
	O	30[a]	35[a]	35[a]	0.94	1.09	0.97

[a] In percent.

TABLE 7

DISTRIBUTION PROPERTIES OF DOUBLE-COLUMN BRIDGE

METHOD AND LOADING CASE	INPUT OR OUTPUT	WEB					OUTPUT/INPUT RATIO ON WEB				
		1	2	3	4	5	1	2	3	4	5
Current design method		—	—	—	—	—	1.00	1.00	1.00	1.00	1.00
Analytical distribution:											
Case 6, all lanes,	I	12.31	16.03	15.54	17.04	20.01					
live load	O	13.01	17.60	19.62	15.72	13.79	1.06	1.10	1.26	0.92	0.69
Case 10, dead load	I	44.87	54.40	54.40	54.64	55.20					
	O	44.6	58.7	63.2	51.5	45.2	0.99	1.08	1.16	0.94	0.82
Experimental distribution	I	19[a]	19[a]	21[a]	18[a]	23[a]					
	O	20[a]	20[a]	21[a]	18[a]	21[a]	1.05	1.05	1.00	1.00	0.91

[a] In percent.

other loading cases. However, the output/input ratios show more range than in any other analytical loading case. The analysis predicts that uniform loading will be nonuniformly distributed.

For the experimental results, inputs and outputs were calculated at the face of the bent cap. Due to the necessity for making adjustments in absolute values, only distributions of loads are given. The distributions are taken from Table D-11 of Appendix D in which details of the computations are found.

Throughout both Tables 6 and 7 it can be seen that the range of output/input ratios is greater for the analytical cases than for the experimental distribution.

Loadings on the Bent Cap

Due to different assumptions and different distributions of applied load, the design loadings on the bent cap appear to vary considerably. Figures 20 and 21 show the design loadings for the indicated critical distributions of lane loadings needed to produce maximum negative moment in the single-column and double-column bridges, respectively. For multiple lanes loaded, the appropriate reduction factors are applied.

Bent cap loads for the current design method are easily obtained. Girder dead loads are concentrated at the web centerlines, and the effects of the lane loadings are concentrated at the lane centerlines.

For the bent cap loading from the analysis, the respective shears from Part 11 of the relevant loading cases were combined. These shears, taken from figures equivalent to Figure 19, include the forces on the free body of the central portion of the bridge out to the line of inflection.

The girder shears to be applied to the bent cap using the experimental results were obtained by applying the experimentally determined distributions to the calculated sum of the reactions. Details are described in Appendix D.

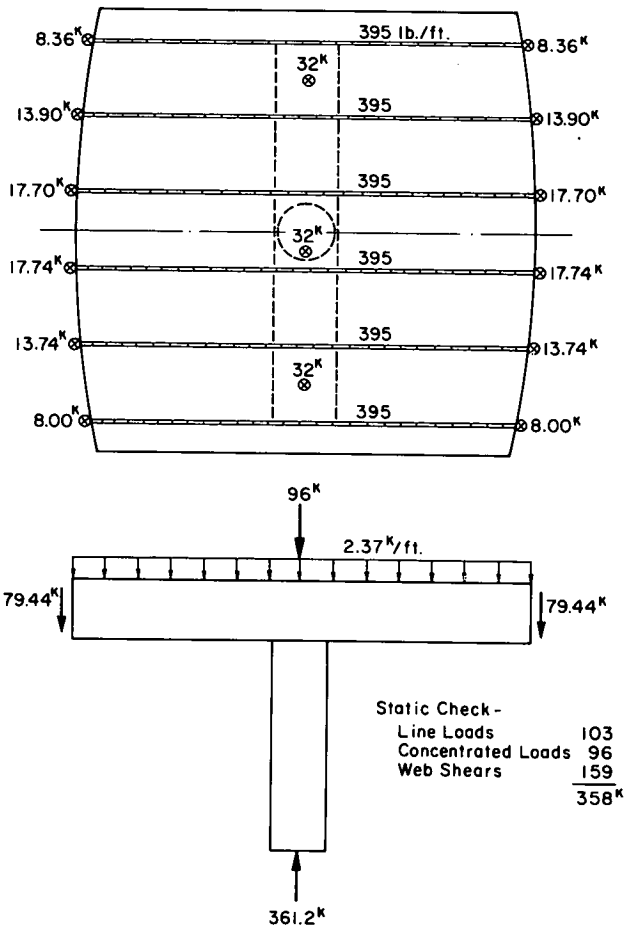

Figure 19. Analytical results for equal line loads on webs of single-column bridge, Part 11.

Bending Moments in the Bent Cap

Equivalency, or lack thereof, between the various loadings for the bent caps shown in Figures 20 and 21 is not obvious from study of the loads themselves because forces of different magnitudes are applied at different points. However, bending moments should be similar if the various methods are valid. The bending moments resulting from the various loadings are plotted for the single-column and double-column bridges in Figures 22 and 23, respectively.

In the double-column bridge, the interior span moments for the present design method and for the experimental distribution were based on a two-dimensional-frame analysis using centerline dimensions and no flanges on the bent cap. Analytical moments were obtained directly from the free bodies.

In both bridges, the bent cap moments predicted by the different methods are in good agreement. A more detailed discussion is contained in Chapter Three.

Experimental distributions are not available for the loading of the two center lanes in the double-column bridge, which is the condition calculated to create maximum positive moment in the bent cap. Moments predicted by the analysis and by the current design method are shown in Figure 24.

EFFECT OF COLUMN FLARE

Model bents with columns flared in the plane of the bent were tested to determine whether the flared column would act as effectively as a cylindrical column having the same noncircular cross section as the top of the flare.

Specimens SF-4 and SF-5 had single columns with two-to-one and one-to-one flares, respectively, as shown in Figure 13. The test results for these two specimens were compared with the results for SC-3, a model with a circular cylindrical column. Except for the flare detail, all three specimens had the same nominal dimensions. The main flexural reinforcement consisted of 12 No. 7 bars for SC-3, 12 No. 6 bars for SF-4, and 12 No. 5 bars for SF-5.

The effectiveness of the flares was evaluated by comparing the longitudinal tensile and compressive stresses in the bent caps with those in the concrete of the flare for specimens SF-4 and SF-5.

The distributions of stresses in the main flexural reinforcement and in the concrete at the bottom of the bent cap for SC-3, SF-4, and SF-5 are shown in Figure 25. To facilitate comparisons, the distance between the face of the

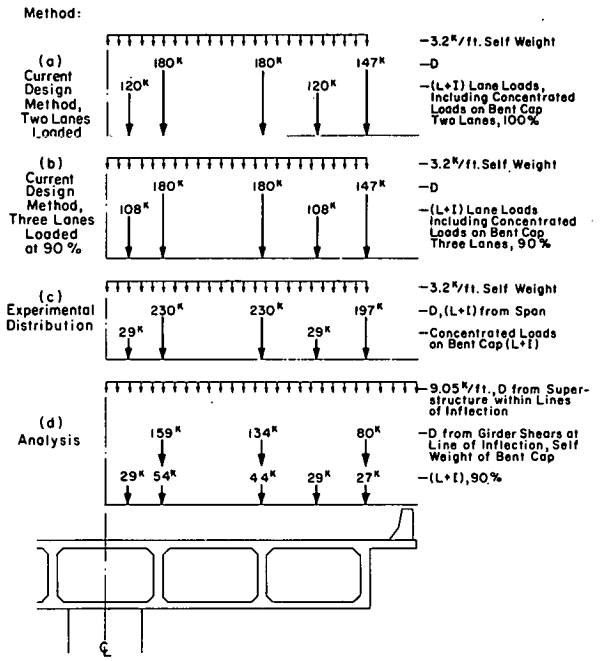

Figure 20. Service loadings on bent cap of single-column bridge.

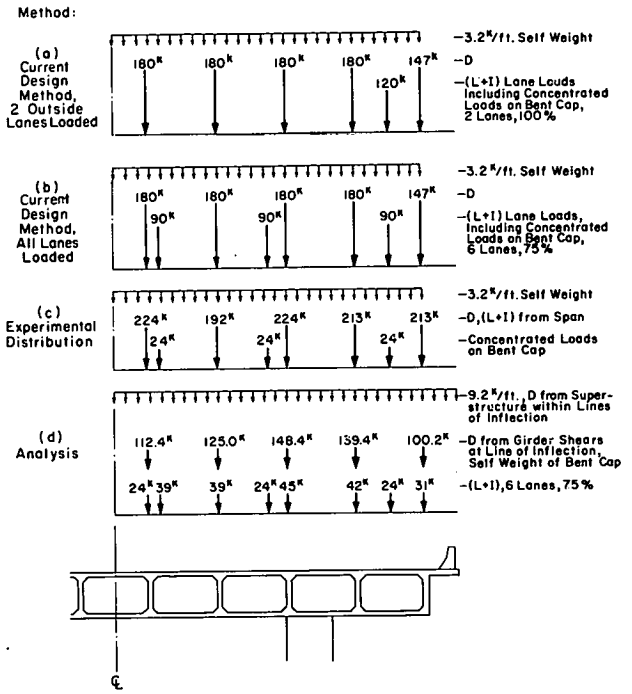

Figure 21. Service loadings on bent cap of double-column bridge.

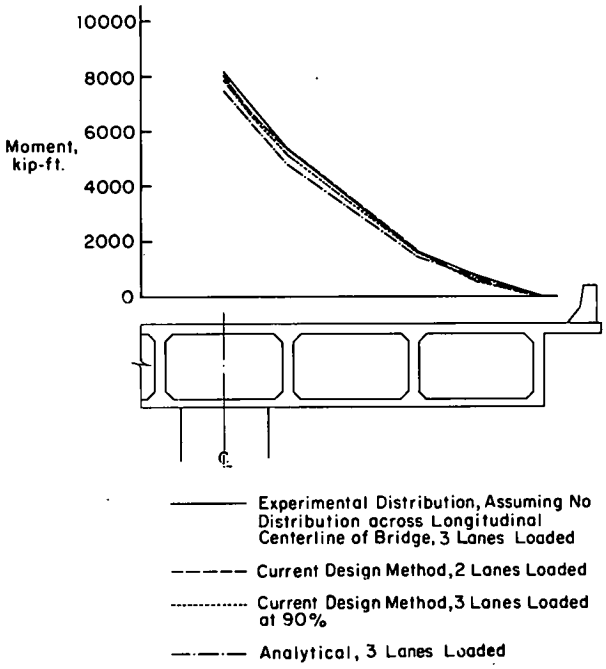

Figure 22. Bent cap moments for single-column bridge.

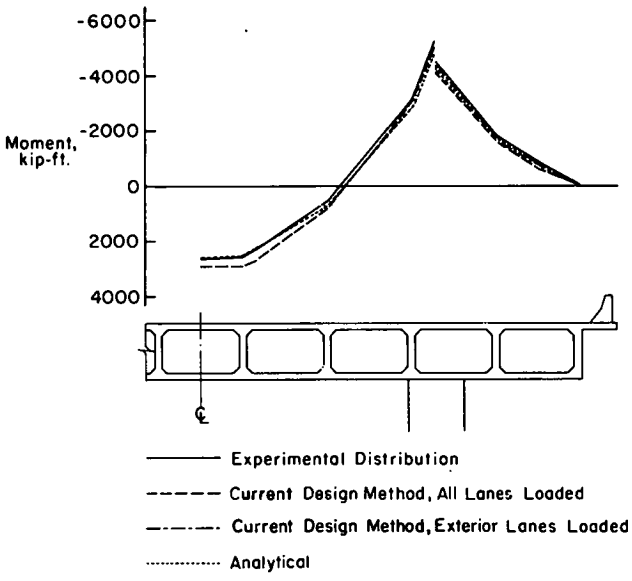

Figure 23. Bent cap negative moments for double-column bridge.

support and the center of the exterior web has been drawn as though constant for the three specimens. The face of support is the intersection of the surface of the straight or flared column with the bottom surface of the bent cap at the longitudinal centerline of the bent cap. The stresses, plotted at the design ultimate load, were determined from the measured strains using stress-strain relationships obtained from control tests.

In Figure 25 and subsequent figures, the load is given as the ratio, K, of the total applied load to the design ultimate load. Thus, $K = 1.0$ represents the load corresponding to $1.8\,D + 3.0\,(L + I)$.

Figure 25 shows that the distributions of reinforcement

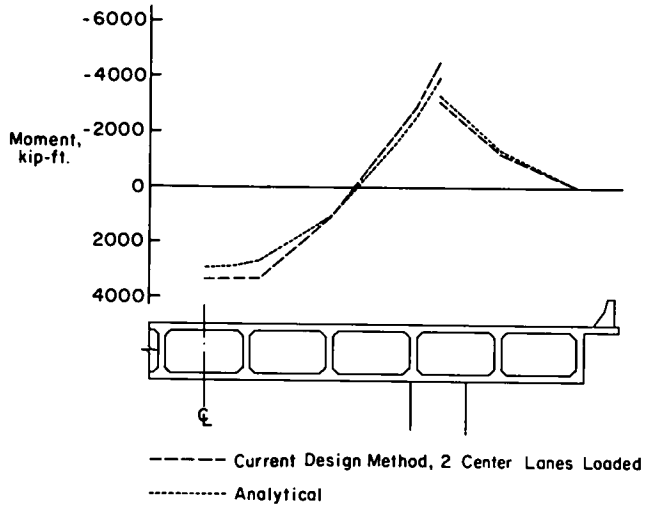

Figure 24. Bent cap positive moments for double-column bridge.

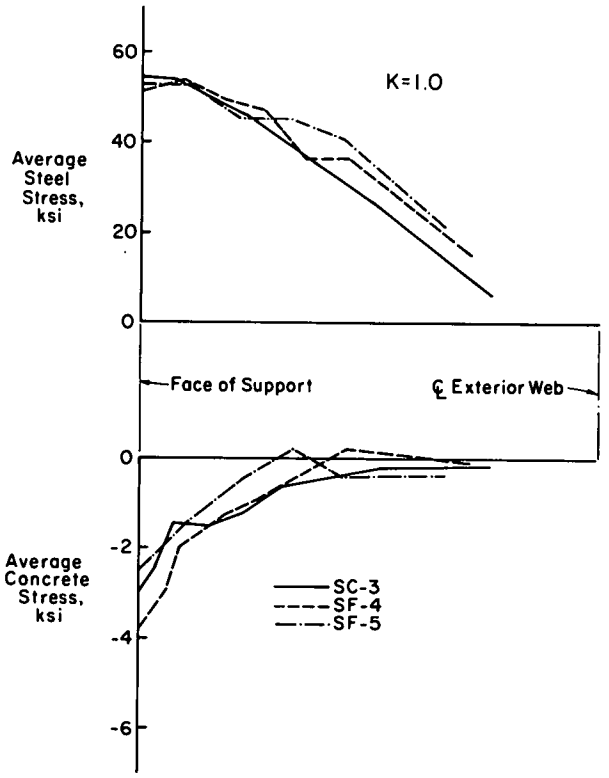

Figure 25. Distribution of stresses in bent cap of specimens SC-3, SF-4, and SF-5.

stresses are similar for the three specimens, particularly in the vicinity of the face of the support. Compressive stresses in the concrete also match well for the straight and flared column models.

To determine whether the concrete in the most highly stressed region of the flare showed any signs of distress, strains were measured for SF-4 and SF-5 on the face of the flared column 3 in. below the bottom of the bent cap. The concrete strain in SF-5, which had the widest flare, was slightly greater than the corresponding strain in SF-4 at all load levels. In neither specimen, however, did the strain at the design ultimate load indicate that the concrete in the flare was overstressed. At the design ultimate load, the maximum measured strain in the concrete of the flare was 1420 millionths for SF-4 and 1550 millionths for SF-5. At service load, the maximum strains were 390 millionths for SF-4 and 460 millionths for SF-5.

For both the straight and flared column specimens, strains measured in the bent cap stirrups located above the column were insignificant, even at higher load levels.

The presence of the column flare did affect bent cap deflections. As would be expected, flaring the column decreased the deflection of the bent cap.

Based on measured strains in the bent cap and on the face of the flared column, it can be concluded that a flared column was as efficient a support for the bent cap as would be an equivalent cylindrical column.

EFFECTIVE SLAB WIDTH

In addition to the effect of the column flare, the model bent specimens were used to determine the extent of participation of the soffit and deck slabs in resisting the bending moment applied to the bent cap.

The effectiveness of the tension flange as well as the compression flange was investigated. In single-column bents, and in the negative-moment regions of double-column bents, the deck and soffit slabs serve as the tension and the compression flanges, respectively. In the positive moment region of double-column bents, the roles of the deck and soffit slabs are reversed.

Transverse distributions of strains parallel to the longitudinal centerline of the bent cap were used to obtain a measure of the participation of the deck and soffit slabs. Based on measured strains in the main tensile reinforcement for the bent cap and the top reinforcement in the deck slab, and in the concrete on the bottom surface on the soffit slab, the representative distributions shown in Figure 26 were constructed for the single-column bent cap models. Results similar to those shown in Figure 26 were obtained in the negative-moment regions of the double-column bent cap.

In Figure 26, the strains are plotted as a percentage of the strain at the bent cap centerline. Strains decrease in magnitude with increasing distance from the bent cap. This decrease is indicative of shear lag in the slabs. As can be seen, effectiveness of the slab portions farther away from the bent cap is reduced.

Negative Moment Compression Flange

The negative-moment compressive strains, shown in Figure 26, indicate the participation of the soffit slab. Because of high strain concentrations at the intersection of the bent cap with the support, the drop-off in the cencrete compressive strain distribution is accentuated at the section along the support face. Therefore, a representative distribution along a section which is 6 in. outside the face of support is also plotted in Figure 26.

The strain distributions indicate that the soffit slab acted

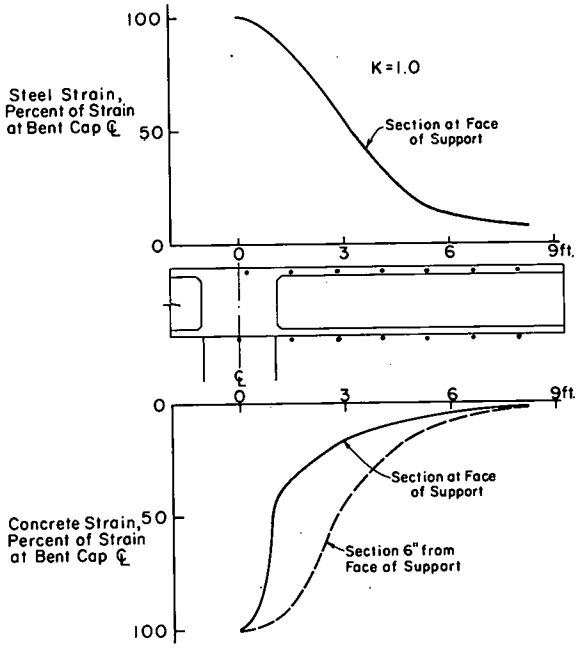

Figure 26. Representative transverse distributions of strains parallel to longitudinal centerline of bent cap.

as a compression flange in resisting the applied bent cap moment. The effectiveness of the soffit slabs decreased in portions of the slab farther from the bent cap in a manner similar to that observed by Jackson and Lord (*7*) in T-beam flanges.

Negative Moment Tension Flange

The deck slab reinforcement did contribute to the moment resistance of the bent cap, but the effectiveness of this reinforcement decreased as its distance from the bent cap increased.

Figure 27 provides a more specific illustration of the contribution of the deck reinforcement. This figure shows the force distribution in the bent cap and deck reinforcement along a section transverse to the bent cap at the face of support. The forces were calculated based on the measured strains in SF-5 at the design ultimate load and the measured moduli of elasticity for the bent cap and deck reinforcement. The distribution of strains was assumed to be linear between gage locations, and the reinforcement was considered to be uniformly distributed along a continuous strip. Specimen SF-5 was chosen for this calculation because the section at the face of the flared column falls at the centerline of a box section. Along this section, secondary bending in the slabs due to shear distortion of the boxes is not expected to significantly influence the measured reinforcement strains.

From the tensile force distribution in Figure 27, it was found that the deck reinforcement contributed approximately 40 percent to the total tensile force developed. Similar calculations at the service load level showed that the deck reinforcement contributed approximately 35 percent to the total tensile force developed.

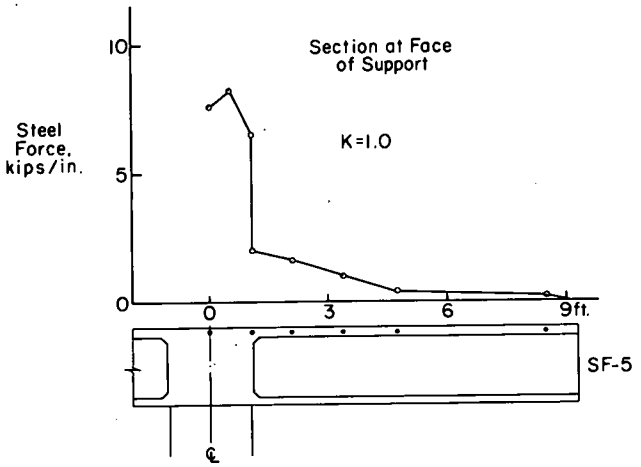

Figure 27. Distribution of force in bent cap and deck slab reinforcement for specimen SF-5.

Positive Moment Tension and Compression Flanges

At loads below the design ultimate load, $K = 1.0$, the strains measured at the section of maximum positive moment in double-column bent specimen DC-9 followed patterns similar to those obtained in the negative moment regions. As expected, the soffit slab was in tension and the deck slab was in compression. Strains decreased with increasing distance from the bent cap. At loads above $K = 1.0$, the measured strains indicated a redistribution of internal forces.

EFFECT OF SPREADING BENT CAP TENSILE REINFORCEMENT

Specimen ST-6 had a thickened deck, as shown in Figure 12, to accommodate a portion of the bent cap tensile reinforcement. Spread bent cap reinforcement might be used when the width of the bent cap is not large enough to accommodate the required flexural reinforcement.

Figure 28 shows the effect on steel stresses within the bent cap when the tensile reinforcement is spread. To construct the figure, the strains measured on the longitudinal reinforcement within the bent cap were averaged and converted to stresses using stress-strain relationships determined by test. The two specimens compared, SC-3 and ST-6, had the same total amount of reinforcement. Specimen SC-3, with no spread reinforcement, contained 12 No. 7 bars within the bent cap. Specimen ST-6, with spread reinforcement, contained 36 No. 4 bars. However, only eight of these bars were placed within the width of the bent cap.

As indicated in Figure 28, the maximum stresses were higher in specimen ST-6 than in specimen SC-3. In addition to higher bent cap reinforcement stresses, specimen ST-6 had greater bent cap deflections than specimen SC-3. For example, at the service load level, the deflection measured at the end of the bent cap in ST-6 was 7 percent greater than that in SC-3. At the design ultimate load the deflection of ST-6 was 45 percent greater than that of SC-3.

Since the model with the spread reinforcement had higher

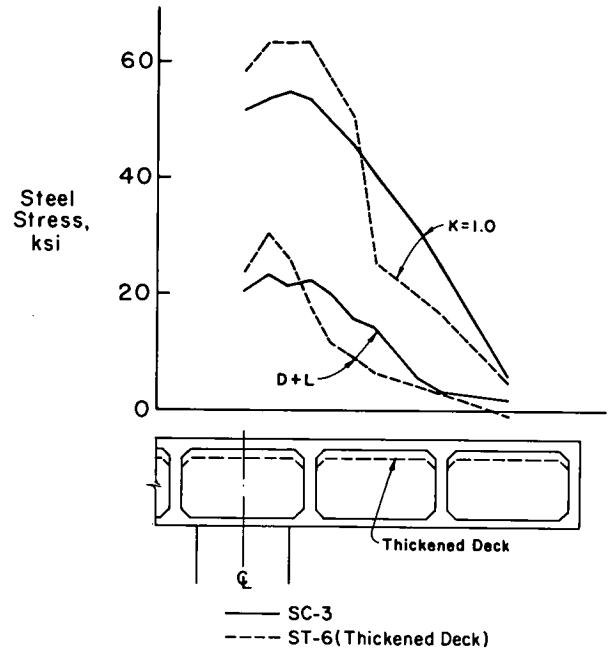

Figure 28. Effect of spreading bent cap tensile reinforcement on steel stresses within the bent cap.

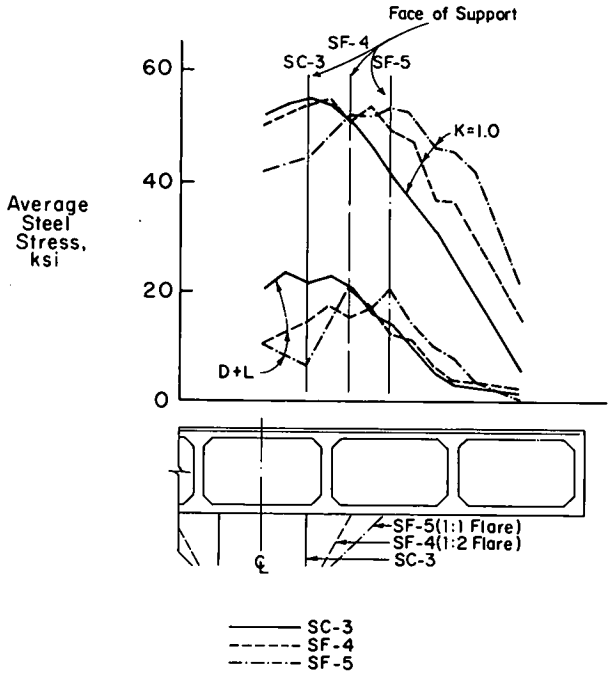

Figure 29. Stresses in bent cap reinforcement of single-column bents.

maximum stresses and greater deflections, it would appear that wide spreading of the main bent cap reinforcement is not a desirable design practice.

LOCATION OF CRITICAL SECTION FOR BENT CAP DESIGN

The most significant requirement for determining a critical design section was that it be located where the maximum stresses occur. Distributions of the average longitudinal tensile stresses in the single-column bent caps are shown in Figure 29. These curves show that the stresses are maximum at or near the face of support. For any particular curve, the stress gradient tends to be relatively flat in the vicinity of the face of the support. At the center of the support, the reinforcement stresses tend to be smaller than at the face of support. This is presumably because the support serves to increase the effective depth of the bent cap.

The data shown in Figure 29 support the selection of the critical design section at or near the face of the column.

Figure 30 shows the observed variations in average longitudinal tensile and compressive stresses in the double-column bent cap. These results indicate that the maximum negative tensile stresses occur in the vicinity of the face of the column, as was the case for the single-column specimens. The maximum positive moment tensile stresses occur at midspan of the bent cap as expected.

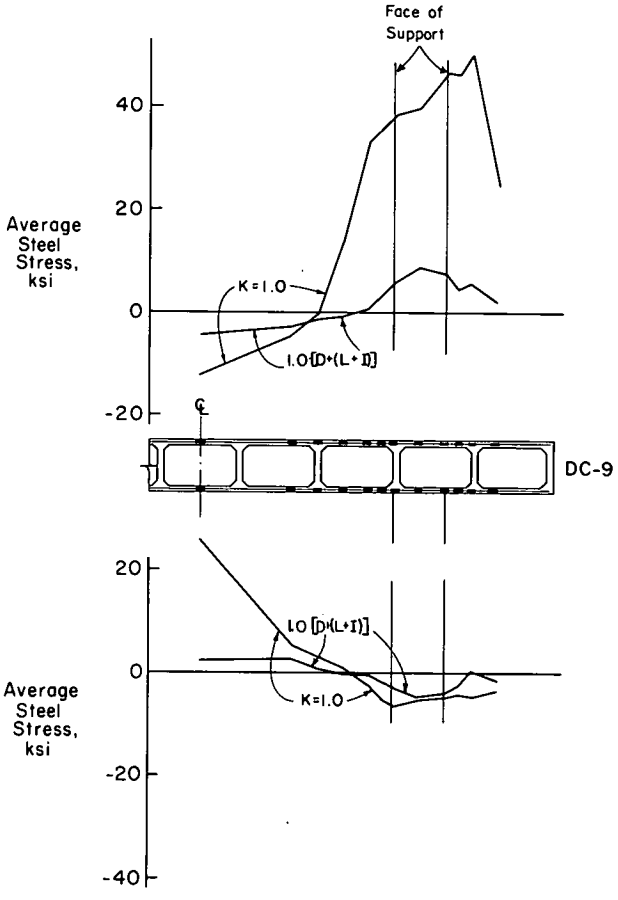

Figure 30. Stresses in bent cap reinforcement of double-column bent.

CHAPTER THREE

INTERPRETATION AND APPLICATION

LOAD DISTRIBUTION IN BRIDGES

Governing Specifications

Both the load factor method and the working stress method use the same AASHTO loading provisions (*1*). Thus, the process for the determination of the controlling load pattern is the same for either method.

Controlling Load Pattern

For live load plus impact in any given lane, the distributed lane loading clearly predominated over the truck loading for design of the bent cap. Consequently, the truck loading was not considered either in the analytical studies or in the experimental program. However, according to information previously given in Table 5, the controlling pattern of lane loads was not the same for all methods.

For negative-moment design of the single-column bent, the controlling loading pattern for the current design method is for two lanes loaded. However, both the analysis and the experimental results indicate that the largest moment is created with all three lanes loaded. The lateral distribution characteristics implicit in each method as well as the intensity reductions specified by AASHTO when more than two lanes are loaded contribute to disagreements in the controlling loading pattern.

In the current design method, no lateral distribution of loads is assumed. On the bent cap, two lanes lie on one side of the column centerline and the third lane lies on the other side. With two lanes loaded on one side of the bent cap, certain moments are produced. The only effect on that side of the bent cap of adding the third lane is to reduce by 10 percent the intensity of the lane loadings already in place. When this is done, moments are also reduced by 10 percent. Keeping in mind that dead-load effects are about four times live-load effects, it should be noted that a reduction of 10 percent in live load results in a reduction of only 2 or 3 percent in total moments.

The analysis predicts some lateral distribution of load. When the same two lanes are loaded as before, the analytical method predicts moments in the bent cap on both sides of the column. Similarly, applying load to the third lane adds moments in the bent cap on both sides of the column. On the side of the column first loaded, the additional moments from loading the third lane overcome the decrease in moments from the first two lanes due to the reduction in lane load intensity. The net result is a slight increase in total moments.

The bent cap moments measured experimentally also show values slightly larger for three lanes loaded to 90-percent intensity than for two lanes loaded to 100 percent.

In the analysis, the service load moment for three lanes loaded at 90-percent intensity is 2 percent higher than for two lanes loaded to 100 percent. The experimentally measured values, as determined from reinforcement strains at design ultimate load, are too close to the same value at the two loadings to assign a percentage difference. Thus, within a single method, the choice of the controlling loading for the bent cap as lanes 1 and 2 loaded, or lanes 1, 2, and 3 loaded, makes little difference in the calculated moment.

For the exterior negative moment of the double-column bent cap, the current design method indicates that the maximum moments occur with the two exterior lanes loaded. Both the analysis and the experimental results indicate that the maximum moments occur with all lanes loaded.

For the current design method, live-load moments are reduced 25 percent from the controlling case by use of the multiple-lane provisions after loading the four interior lanes. At service load, the over-all moment is reduced about 5 percent.

For the analysis, the increase in exterior moment due to loading the interior lanes again overcomes the decrease due to the multiple-lane reduction factor. However, the difference in the totals is less than 1 percent. At design ultimate, the experimentally determined strains under the two load patterns were indistinguishable when multiple-lane reduction factors were taken into account. Thus, within a particular method, the choice of exterior lanes 1 and 6 loaded, or all six lanes loaded, makes very little difference in the calculated value of the exterior negative moment.

When symmetry is maintained, the controlling loadings predicted by all three methods are the same for the interior negative moment and the positive moment in the double-column bent cap.

The bent cap moments calculated by the various methods are affected not only by the choice of the loading pattern, but also by the assumed or measured load distribution characteristics of the bridges. As can be seen from the output-input ratios given in Tables 6 and 7, the experimental results show considerably less lateral distribution of load than predicted by the analysis.

The reasons why the experimental results show less than the analytically predicted amount of lateral distribution of load is not immediately apparent. In two tests of models of reinforced concrete box-girder bridges carried out at the University of California at Berkeley, good correspondence was reported between measured and predicted distributions. In one of these models, a simple span bridge (*8, 9*), results also were reported to correlate well with those obtained by loading the prototype structure.

The second model test at the University of California was on a 1/2.82-scale model of a two-span continuous bridge with a single-column bent. This model was similar in proportions to the single-column model of the present project. Test results, for loadings in the span, were reported (*10, 11, 12*) to agree well with those predicted by

another version of the same MUPDI computer program used in the present project.

Uniformly distributed dead load and relatively uniformly distributed lane loads are considered in the preceding discussion. It might be argued that if the correspondence between analysis and experimental results is not complete for these loadings, it is possible that even less correspondence might exist for point loads. However, other investigators have shown that the effect of point loads on bridges in service is not particularly significant. As pointed out in University of California reports (*10, 11, 12*) and by others (*13*), applied live loads on real bridges reasonably approximate distributed loads. This is due to the fact that multiple wheels some distance apart are always involved. Thus, it is sufficient to discuss the effect of distributed loads.

For prediction of the distributed loads carried by each girder to the bent cap, the discrepancy between the test results and the analysis is of theoretical significance. It is also of some importance as far as the design of the girders is concerned. However, the observed difference has little effect on the design moments for the bent cap, as can be seen in Figures 22 and 23.

The largest ratio between maximum experimental and analytical moments is 1.09, occurring at the centerline of the column of the single-column bent. The equivalent ratios of the double-column bent for the interior and exterior sides of the column centerline, respectively, are 1.06 and 1.07. As already noted, the experimental moments were increased somewhat by the small overload applied to the exterior girders as a result of the application of equal dead-load makeup to all girders. If the smaller dead load of the exterior girders had been taken into account, it would be expected that the experimentally determined bent cap moments would have been slightly decreased. The correspondence between analysis and test results would then have been even closer.

For both the single-column bridge and the double-column bridge as respectively shown in Figures 22 and 23, the moments obtained by the current design method lie between those derived from both the analytical and the test results. Because the percentage differences lie within the range calculated above and because the experimental values are slightly increased by the loading technique, it is believed that the current design method gives a sufficiently accurate evaluation of bent cap moments.

Because of the loading sequence, no test results are available for the comparison for maximum positive moments in the double-column bent cap. However, the trend of moments obtained by the current design method and predicted by the analysis are similar, as shown in Figure 24. The current design method gives a moment 16 percent greater than that predicted by analysis. Consequently, the use of the current design method is conservative for this case.

The tendency in all cases for the moments obtained by the current design method to lie close to both test results and analytically predicted values leads to the conclusion that the current design method for distributing loads gives satisfactory results.

Only the distribution of loads to the bent cap is considered here. Scordelis et al. (*11, 14*) have pointed out that present methods of choosing the design loads may be unconservative. Discussion of this point is beyond the scope of this report.

In the interest of brevity, bent cap shears have not been discussed. As in the case with moments, no significant differences exist regardless of the method of calculation.

For design, it is recommended that all loads in the span first be locally distributed to the girders. The girders are then assumed to carry the loads to the bent cap. This procedure provides a better indication of shears and moments than assuming that live loads are applied on the bent cap at the lane centerline. The latter assumption is particularly unrealistic when the lane centerline is at or near the center of a cell. In this case it is obvious that the lane loads cannot be carried to the bent cap through the roadway slab. The proposed change might result in a minor change in stirrup arrangement for the bent cap.

DEVELOPMENT OF BENT CAP DESIGN PROCEDURE

As outlined in the project statement, the primary objective of this investigation was to establish a valid design procedure for single- and multiple-column bridge bents for straight, continuous, reinforced concrete box girder bridges. The following discussion concerns findings from the model bent tests, presented in Chapter Two, and their significance in bent cap design.

Column Flares

The tests on model bent caps with straight and flared columns showed that a flared column performed as effectively as a column having a cross section the same as that at the top of the flare. The longitudinal strains measured in the bent cap gave no indication that the flared column provided support different in any way from that of a column with an equivalent constant noncircular cross section. Strains measured in the bent cap stirrups over both the straight and flared columns were insignificant. This indicates that the flared columns provided completely effective support from the standpoint of shear as well as flexure. In addition, the column flares showed no signs of being overstressed.

The surface of the widest flare tested had a maximum angle of 45 degrees with the vertical along the longitudinal centerline of the bent cap, as can be seen in Figure 13. Since no information was obtained for surfaces with larger angles, this angle is recommended as a limit for the design of column flares. The 45-degree limit is consistent with that specified in the ACI Building Code (*15*) and the British Code of Practice (*16*) for flat slab supports.

The cross section at the top of the flared columns tested had parallel sides and elliptical ends. Results are not considered applicable for sections of less compact shape.

Effective Flange Width in Compression

The test results showed that the box-girder soffit slab acted as a compression flange in resisting bent cap negative moments. The effectiveness of the soffit slab decreased in portions of the slab farther from the bent cap. This behavior

is attributed to the well-known phenomenon of shear lag.

Strain distributions observed in the flanges of the bent cap specimens are shown idealized in Figure 26. The distributions observed are similar to those found in the flanges of T-beams, reported by Jackson and Lord (*7*).

In the design of T-beams, it is common to approximate the actual compressive stress distribution by a uniform stress distributed over a predetermined effective width of the flange. Using the effective width concept, T-beams can be desiged by elementary beam theory. The effective flange width is determined such that the maximum bending stress calculated using elementary beam theory corresponds to correct maximum stress in the flanged section (*7, 17*). Although the effective flange width is determined by elastic analysis, Brendel (*18*) has indicated that flange participation increases with increasing loads. Thus, the effective width based on elastic theory is considered reasonable for use in calculating moment capacity of the section.

The effective width of the compression flange depends upon several variables. These have been discussed by Brendel (*18*). Included are type of load on the beam (distributed or concentrated), relative thickness of the flange with respect to the depth of the beam, width of the web, spacing of the beams, and span length.

In the interest of simplicity, most building codes prescribe a limiting value for the effective flange width rather than attempting to account for all the variables mentioned previously. For example, AASHTO (*1*) limits the effective flange width of T-beams and box girders to the smallest of the following:

1. One-fourth of the span length of the girder.
2. The distance center to center of the girders.
3. Twelve times the least thickness of the slab plus the width of the girder stem.

These requirements are the same as those specified for T-beams in the ACI Building Code (*15*), except that it places a limit of 16 times, rather than 12, the slab thickness. Although the Code criteria represent a simplification of the actual behavior of flanged sections, they have proven to be adequate for design.

For design of bent caps, the existing AASHTO provisions provide an acceptable concept. Because the strength of the bent cap is relatively insensitive to the width of the chosen compression flange, there is no need for more complicated provisions. However, the provision limiting the over-all flange width to one-fourth the span length should be restated because it was developed for beams with narrow webs. When applied to bent caps with relatively wide webs, this provision could often result in small or even negative flange overhangs.

In terms of overhang, the flange width is currently one-eighth the span minus one-half the stem or web width. For bent cap design, an overhang of one-tenth the span is recommended as a conservative restatement of the existing provisions.

An indication of the insensitivity of the bent cap strength to the width of compression flange is given in Figure 31. Curves in this figure represent the calculated strength of the two sections shown as a function of compression flange

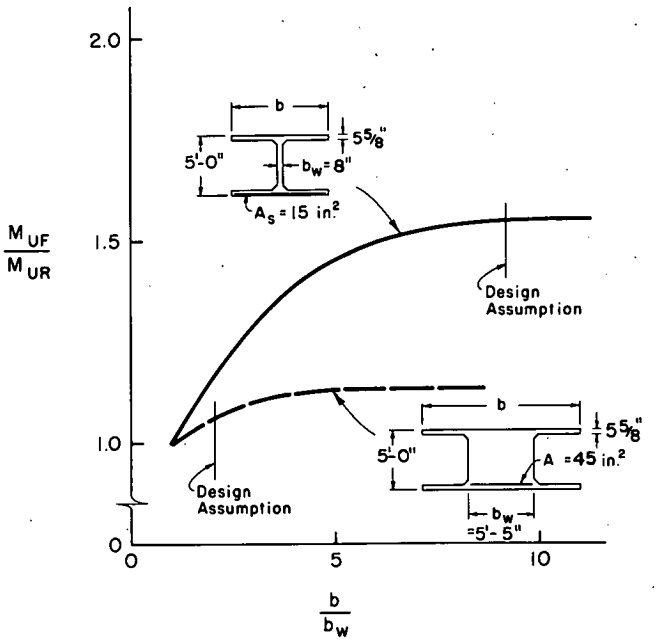

Figure 31. Effect of compression flanges on capacity of bent cap and box-girder sections.

width. The strengths are plotted as the ratio of the moment capacity of the flange section, M_{UF}, to that of a rectangular section with a width equal to that of the web, M_{UR}. Moment capacities were calculated using common design expressions given in Reference 19. Material properties were the same as those used for design of the model bent caps. The cross section with the thin web was overreinforced as a rectangular section. In this case, the expression developed by Kriz and Lee (*20*) was used to calculate moment capacity.

It is evident from Figure 31 that the section with the wide web, the bent cap section, is less sensitive to increases in the compression flange width. The cross section with the thin web represents an interior girder of the box section. The flange widths assumed in the design of the models according to AASHTO (*1*) are also indicated on the figure.

In practice, most bent cap sections have proportions similar to the one tested.

Effective Flange Width in Tension

Measurement of strains on the tensile reinforcement in the bent cap and box-girder slabs showed that the slab reinforcement did contribute to the moment resistance of the bent cap. However, the effectiveness of this reinforcement decreased as its distance from the bent cap increased. This observation has been made by other investigators.

On the basis of the observed distribution of steel strains, Kaar (*21*) reached similar conclusions about the effectiveness of reinforcement in isolated T-beams. Mattock and Kaar (*13*) found that the longitudinal tensile strains in the I-beams of continuous bridges peaked over the webs. As in the case of the compression flange, this behavior is attributed to shear lag. As reported in Appendix E, the shear

lag phenomenon was also evident in the box girders of the model bent tests.

The reduced effectiveness of flexural reinforcement placed away from the bent cap was particularly evident in the model bent cap with spread reinforcement. For a given load, this specimen exhibited larger deflections and greater crack widths than the corresponding straight-column model that had all flexural reinforcement within the bent cap. Thus, in terms of serviceability, the specimen with spread reinforcement was less satisfactory.

Based on the test results, a limitation on the width of the tension flange that can be considered effective is necessary. For design, the current AASHTO provisions for effective flange width, listed previously, are recommended as limits on the tension flange width. However, the overhanging width for tension flanges is further restricted to one-fourth the box-girder web spacing. This is intended to ensure that effects of concentrated loads and box distortion do not reduce the capacity of the reinforcement in the flanges.

The somewhat arbitrary choice of one-fourth the web spacing was based on the premise that concentrated loads placed within these limits would be transmitted directly to the nearby bent cap rather than to the more remote girder webs. Also, in this region, the flange is forced to follow the deflection curve of the bent cap thus minimizing the secondary stresses resulting from shear distortion of the box sections.

Over-all effectiveness of the bent cap tensile reinforcement can be evaluated from the test results. Measurements indicate that, at loads below those causing yield of the flexural reinforcement, bars at the specified extremities of the tension flanges will be stressed about 75 percent as much as the bars over the bent cap web. If the reinforcement is distributed uniformly across the tension flange of a bent cap of usual proportions, about 60 percent of the reinforcement will be located above the web. Assuming linear variation of effectiveness of the reinforcement in the flanges, the over-all effectiveness becomes 95 percent, a figure higher than the equivalent effectiveness for box girders tested. Post-yield rotation of the section, plus participation of the portion of the superstructure outside the assumed flange, provides the required strength of the bent cap.

It would be expected that in a bridge of the usual proportions reinforcement originally designed as deck flexural reinforcement would be found within the defined limits of the tension flange of the bent cap. Following the reasoning that led to the proposed specification, these bars can also be considered as part of the bent cap reinforcement.

Effect of Spreading Bent Cap Tensile Reinforcement

The model bent cap with spread reinforcement had higher maximum stresses and greater deflections than the equivalent model whose reinforcement was all within the stem width of the bent cap. In bridge designs, all required tension reinforcement should be placed within the stem width whenever possible. However, placing bent cap flexural reinforcement within the bounds defined by the effective tension flange will minimize the detrimental effects of spread reinforcement on serviceability.

It is expected that the reduced amount of reinforcement required by the load factor method of design will help to alleviate the need for widely spread reinforcement.

Location of Critical Section for Bent Cap Design

The choice of location of the critical design section was based on measured strains in the bent cap flexural reinforcement. These strains indicated that maximum stresses occurred at or near the face of support, defined as the intersection of the surface of the straight or flared column with the bottom surface of the bent cap at the longitudinal centerline of the bent cap. It is recommended that the critical section for design be taken at the face of support.

Considerations that led to determining the critical design section at the face of support are shown in Figures 32 through 35. These figures show the experimental and calculated stresses in the longitudinal flexural reinforcement of the single-column and double-column model bent caps. Results are given for service load 1.0 $[D + (L + I)]$ and the design ultimate load $(K = 1.0)$.

Reinforcement stresses were determined from the measured strains and experimentally determined stress-strain relationships. The strains used were the average across the width of the bent cap.

Calculated stresses were determined from the applied moment diagram for the bent caps. Reinforcement stresses corresponding to the applied moment were determined for the cross section in question by satisfying the applicable conditions of equilibrium and compatibility of strains. The basic procedure has been outlined by Pfrang, Siess, and Sozen (*22*).

In the figures, the calculated curves are designated "with" or "without" the tension flange. Calculations designated with tension flange include the slab reinforcement falling within the effective flange width defined previously. As would be expected, lower steel stresses are obtained when the slab reinforcement is included in the calculations.

Comparisons of the experimental and calculated stresses for the single-column models are shown in Figures 32 through 34. For all three specimens, the experimental stress is lower than that calculated at the face of support. The same result is obtained even when the tension flange slab reinforcement is considered.

Several factors contribute to the difference in stresses. More deck slab reinforcement may contribute to the moment resistance of the bent cap than is permitted by the effective flange width limits. If additional slab reinforcement does participate, the stresses in the bent cap reinforcement would be lower than calculated using the effective width concept.

Another feature evident in the curves shown in Figures 32 through 34 is that the experimental stresses toward the end of the bent cap are higher than those calculated. The difference is most apparent for the wide flared supports. This difference in stresses is attributed to the formation of inclined cracks in the bent cap. Similar behavior was observed by dePaiva and Siess (*23*) in tests of deep beams. Once the inclined cracks form, "tied-arch action" results in higher steel stresses toward the end of the bent cap.

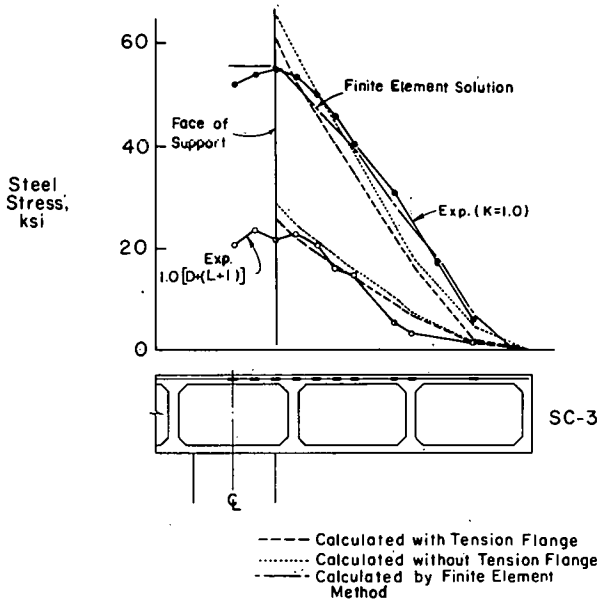

Figure 32. Experimental and calculated stresses in bent cap of specimen SC-3.

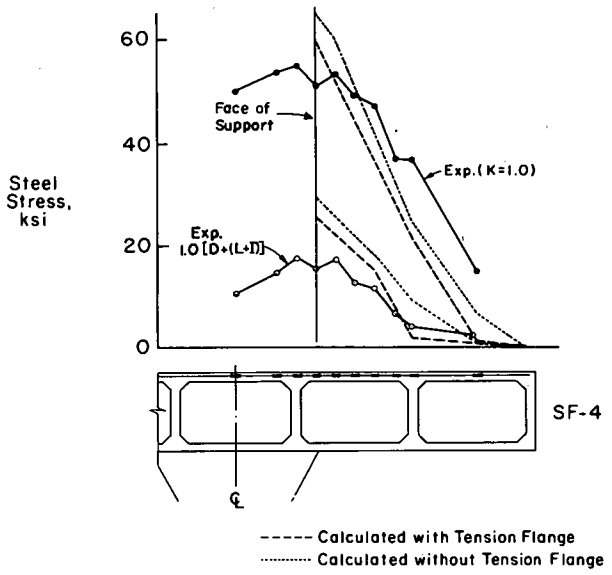

Figure 33. Experimental and calculated stresses in bent cap of specimen SF-4.

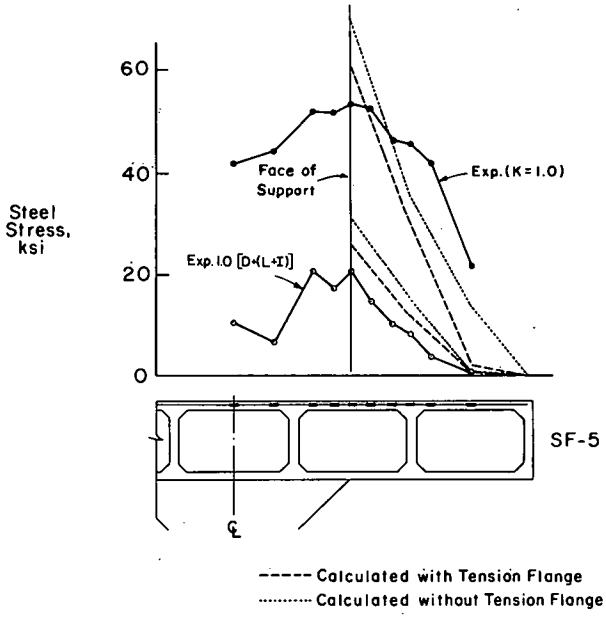

Figure 34. Experimental and calculated stresses in bent cap of specimen SF-5.

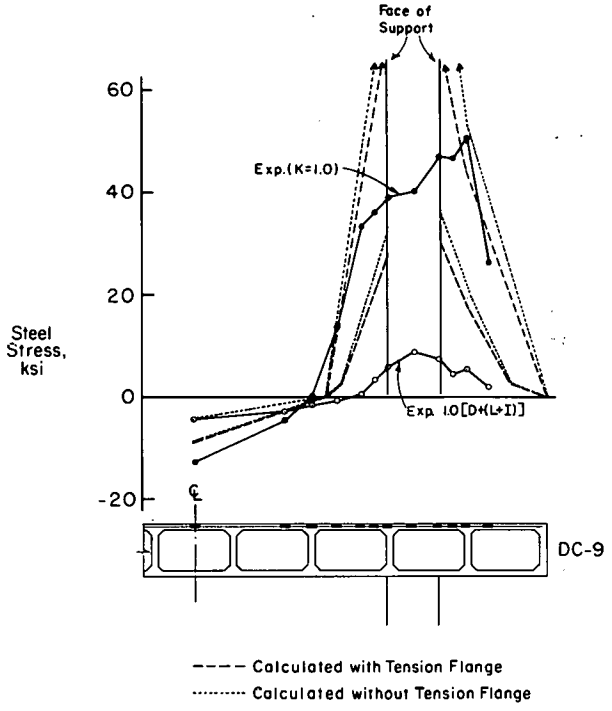

Figure 35. Experimental and calculated stresses in bent cap of specimen DC-9.

Further evidence of this behavior is apparent from a comparison of the experimental stress distributions at service load 1.0 $[D + (L + I)]$ and at the design ultimate load $(K = 1.0)$. At service load the distributions outside the support are concave upward with a shape similar to the applied-moment diagram. At the design ultimate load, when inclined cracks were well formed, the distributions are concave downward, indicating an increase in stresses away from the support.

The finite element analysis, described in Appendix C, was also used to predict longitudinal stresses in the bent cap. The results are shown in Figure 32 for SC-3, the specimen with the straight column. The finite element solution does yield a good prediction of the stresses and apparently accounts quite well for the stress distribution in the vicinity of the support.

Figure 35, showing the bent cap stresses in the double-column model, is based on a moment diagram calculated using centerline dimensions. The stresses calculated at the

interior and exterior column faces are considerably higher than the corresponding experimental stresses in the vicinity of the column.

The moment diagram for the double-column model was also calculated considering finite member widths rather than centerline dimensions. When this was done, moment at the interior column face was increased about 15 percent, with a corresponding reduction in the midspan positive moment.

For the geometric proportions and loads of the double-column bent cap tested, the calculated moments based on either method would result in approximately the same design. It is not possible to predict, based on this test, which method would be preferable for other multiple-column bents.

Based on the results discussed above, the choice of the critical design section at the face of support appears reasonable.

Conditions at the face of support are uniformly conservative in that predicted stresses are higher than those measured. Toward the points of zero moment, the calculations tend to underestimate stresses, but this may occur in any beam where diagonal cracking develops. Traditionally, the provisions for extension of reinforcement have been used to compensate for this underestimation of stresses.

Over-all, correspondence between calculated and measured stresses appears to be the best that can be obtained without the introduction of complex design expressions.

REDUCTION IN THE AMOUNT OF REINFORCEMENT

One of the primary aims of the project was to determine whether current design methods resulted in more reinforcement than needed in the bent cap. Because of the wide variety of proportions possible within the specified geometry, no exact reductions can be calculated but a range of values can be determined.

Flexural Reinforcement

The major factor determining the amount of flexural reinforcement is the design method used. For box-girder bridges of the proportions specified, the change from working stress to load factor design results in a reduction of roughly 30 to 35 percent in bent cap flexural reinforcement. This reduction is evidence that an indirect effect of the current specifications is to require that a bridge designed by the working stress method have more load-carrying capacity than one designed by the load factor method.

The amount of column flare can have a substantial effect on the amount of flexural reinforcement required. In the series tested, the bent cap having the column with the widest flare would require about 30 percent less reinforcement than the similar bent cap having a nonflared column.

Choice of critical design section can also influence the amount of flexural reinforcement required, particularly for wide column flares or for regions of steep moment gradients such as encountered in the negative-moment regions of multiple-column bents. Reinforcement savings can amount to 10 to 20 percent when the design section is moved from one-sixth the support diameter from the column centerline to the face of support.

The effective flange width chosen has little effect on the amount of flexural reinforcement required.

Shear Reinforcement

The amount of shear reinforcement required is not significantly different whether a given bent cap is designed by working stress or load factor methods. The only variables that have an effect on shear reinforcement requirements are the column flare and critical design section location. In the recommendations of this report, these two variables combine to widen the support and, thus, increase the length of bent cap calculated to have zero shear and minimum shear reinforcement.

RECOMMENDED DESIGN PROCEDURE

On the basis of this investigation, the following provisions are recommended for the design of bent caps. Where appropriate, suggested wording for incorporation in the AASHTO Specifications is given.

Determination of Design Loading on Bent Cap

Use present AASHTO design methods.

Effect of Column Flare

For an integral support to be considered effective, the angle of greatest slope of the surface of the support shall not exceed 45 degrees from the vertical.

Effective Flange Width in Compression

The effective width of an overhanging compression flange on either side of the web of an integral bent cap shall not exceed the following:

1. One-tenth the span length of the bent cap. For cantilevers, the span used shall be twice the length of overhang.
2. One-half the clear distance to the next bent cap.
3. Six times the least thickness of the slab.

Effective Flange Width in Tension

The effective width of an overhanging tension flange on either side of the web of an integral bent cap shall not exceed the following:

1. The effective width defined for compression.
2. One-fourth the average spacing of the intersecting box-girder webs.

All longitudinal reinforcement located within the specified flange widths may be considered fully effective.

Design Section for Negative Moment

Moments at the face of support may be used for design of the bent cap. The face of support is defined as the limit of the effective support along the centerline of the bent cap.

Effect of Spreading Reinforcement

Use the provisions specified previously for "Effective Flange Width in Tension."

COMMENTS

Design Loading

Analysis of the experimental results obtained from this project indicates that the lateral distribution of load in box-girder superstructures in these bridges was not large. Consequently, the present design methods that assume no lateral distribution of loads can be used.

It is believed that application of the recommended design methods, in conjunction with the load factor method, will yield structures more closely exhibiting the intended behavior than any previous method. However, this report deals only with the strength, serviceability, and load distribution characteristics of box-girders bridges. Determination of whether or not the magnitude of the design loadings is representative of actual loadings on the bridges was beyond the scope of this program. As pointed out in Chapter Four, more refined design methods increase the importance that design loadings correspond to actual loadings.

No evidence was gathered in this project on the local distribution to the adjacent girder webs of live loads applied to the deck. Present design methods commonly place the entire lane load reaction directly on the bent cap at the lane centerline. If the lane centerline happens to be at or near a box centerline, it is physically impossible for the lane load to be applied to the bent cap at that point. A more logical approach would be to consider some distribution of the live loads to the girders, which would then be assumed to carry the loads to the bent cap.

Assuming the live load applied through the girder webs would result in minor local changes in the moment diagram, there would also be changes in the location and magnitude of the steps in the shear diagram for the bent cap.

Since the present specifications are silent on this point, no formal changes are proposed.

Column Flare

The proposed provisions were developed from tests on flared columns, in which the shape of the support at the bottom of the bent cap had parallel sides and rounded (elliptical) ends. The provisions should not be applied to supports of less compact cross section than those tested. For example, they should not be applied to a section with pointed ends.

These provisions follow the intent of long-standing specifications for supports in flat slabs in the ACI Building Code (*15*), and the British Code of Practice (*16*).

Flange Widths

Compression flange width provisions are a restatement in terms of overhanging flanges of current provisions. Test results and calculations both indicate that strength of the bent cap is very insensitive to the choice of the compression flange width. Consequently, the present provisions are satisfactory.

Overhanging widths for tension flanges are further restricted to one-fourth the average box-girder web spacing to ensure that effects of concentrated loads and box distortion do not reduce the capacity of the reinforcement in the flanges.

Design Section for Negative Moment

The experimental results indicated that, for design, the best choice of location for the maximum moments and reinforcement stresses was at the face of support.

Spreading Reinforcement

The reduced amount of reinforcement that meets the requirements of the load factor method of design will probably eliminate the need for spreading reinforcement outside the limits of the bent cap web width. However, if spreading is required, the test results indicate that reinforcement placed anywhere within the specified tension flange may be considered effective.

CHAPTER FOUR

CONCLUSIONS AND SUGGESTED RESEARCH

CONCLUSIONS REGARDING ANALYSIS AND DESIGN

Load Distribution

Experimental results in this project indicated only a small amount of lateral distribution of loads when applied loadings approached the capacity of the bridge. On the other hand, the elastic analysis predicted a considerable amount of lateral distribution.

For the design of the bent cap, the smaller the amount of lateral distribution assumed, the more conservative the design. Consequently, no changes were recommended in the current design method, since it assumes no lateral distribution of loads within the structure.

Effect of Column Flare

All flared columns tested in this project were found to be fully effective as supports. The flares were as effective as straight columns having a noncircular cross section the same as at the top of the flare at its intersection with the bent cap. The surfaces of the flares made angles of up to 45 degrees with the vertical.

Effectiveness of the flares as supports for the bent was judged by determining whether or not reinforcement and concrete stresses in the bent at the face of the flares exhibited the same behavior as at the face of the circular cylindrical column. Behavior was found to be indistinguishable. Consequently, all the flares tested were judged to be completely effective. No overstress was found within the flares themselves.

Effective Flange Width in Tension and Compression

The effectiveness of reinforcement was found to decrease rapidly with distance from the bent cap web. The effect was assumed to be primarily due to shear lag. In a prototype bridge subjected to traffic, bars outside the bent cap web would also be stressed by concentrated loads on the deck. To take into account the reduced effectiveness and the stresses due to loadings not included in this test program, restrictions were placed on the assumed flange width for tension.

All properly oriented reinforcement within the specified flange width can be considered effective. The proximity to the bent cap web minimizes secondary stresses due to concentrated loads and to shear distortion of the box girder cells.

The effective flange width of the bent cap in compression was found to be adequately defined by existing specifications (*1*) for the width of compression flanges in box girders and T-beams.

Effect of Spreading Bent Cap Reinforcement

The effect of spreading bent cap reinforcement is closely related to the problem of effective flange width. Consequently, conclusions for that problem apply.

Critical Design Section

The critical design section for moment was found to be at the face of support. This is defined as the extreme point of the column or flare at its intersection with the bent cap.

CONCLUSIONS REGARDING EXPERIMENTAL TECHNIQUES

To properly evaluate stresses for any particular loading, it was found necessary to take into account residual stresses introduced during the test program. In the tests of the model bridges, residual stresses in the reinforcement under dead load near the end of the program were substantially higher, in the range of 10 ksi, than the stresses under the same load at the beginning of the test. Details are discussed in Appendix A.

In the determination of internal moments from experimentally measured strains, it was found that the calculated tensile and compressive resultants were not equal. Possible reasons for the apparent departure from the statically required equality, and the method used to obtain usable results, are discussed in Chapter Three and Appendix D.

SUGGESTED RESEARCH

Proof Test

The original project statement indicated that a proof test of a complete model bridge, designed according to the recommendations of this report, should be included. This proof test would provide direct physical evidence of the soundness of the design recommendations. The load factor method would be used so that the performance of a complete box-girder bridge built according to this design concept could also be evaluated.

It is strongly recommended that this test be performed to satisfy the original project statement.

Loadings

The lane loads that govern the design of the bridges discussed in this report are significantly lighter than a lane of "AASHTO" trucks. Such a lane would have a loading approaching 2.0 kips per foot, assuming the standard 72-kip truck-trailer combination with axles 17 ft apart, and some interval between vehicles. This contrasts with the 0.64-kip-per-foot lane load plus a concentrated load or

loads assumed in design. Taking into account the concentrated load, the effect of the line of trucks might be two to three times that assumed in the design.

The current load factors (*24*) require a capacity of 1.3 $[D + 5/3(L + I)]$, or $1.30D + 2.17\ (L + I)$. The reserve capacity of $1.17\ (L + I)$ appears to be rather small considering the possibility of the occurrence of live loads larger than the lane loadings used for design. It is recommended that the latest studies on the frequency and magnitude of applied loads be compared with the reduced capacities resulting from the suggested refinements in design before revised specifications are adopted.

REFERENCES

1. American Association of State Highway Officials, *Standard Specifications for Highway Bridges,* Tenth Edn., Washington, D.C. (1969) 384 pp.
2. Goldberg, J. E., and Leve, H. L., "Theory of Prismatic Folded Plate Structures." *International Assoc. Bridge and Structural Eng.,* Vol. 17 (1957) pp. 59-86.
3. *Manual of Bridge Design Practice,* Second Edn., State of California, Highway Transportation Agency, Dept. of Public Works, Div. of Highways, Bridge Dept. (1963).
4. Mattock, A. H., "Structural Model Testing—Theory and Application." *J. PCA Research and Development Lab.,* Vol. 4, No. 3 (Sept. 1962) pp. 12-23. Reprinted as *Development Dept. Bull. D56,* Portland Cement Assoc., Skokie, Ill.
5. Hognestad, E., Hanson, N. W., Kriz, L. B., and Kurvits, O. A., "Facilities and Test Methods of PCA Structural Laboratory." *J. PCA Research and Development Lab.,* Vol. 1, No. 1 (Jan. 1959); pp. 12-20, 40-45; Vol. 1, No. 2 (May 1959); pp. 30-37; Vol. 1, No. 3 (Sept. 1959); pp. 35-41. Reprinted as *Development Dept. Bull. D33,* Portland Cement Assoc., Skokie, Ill.
6. Hanson, N. W., Hsu, T. T. C., Kurvits, O. A., and Mattock, A. H., "Facilities and Test Methods of PCA Structural Laboratory—Improvements 1960-65." *J. PCA Research and Development Lab.,* Vol. 3, No. 2 (May 1961) pp. 27-31; Vol. 7, No. 1 (Jan. 1965) pp. 2-9; Vol. 7, No. 2 (May 1965) pp. 24-38. Reprinted as *Development Dept. Bull. D91,* Portland Cement Assoc., Skokie, Ill.
7. Jackson, N., and Lord, W. D., "Stresses in Wide-Flanged T-Beams." *Concrete Constructional Eng.,* Vol. 60, No. 6 (June 1965) pp. 205-212.
8. Davis, R. E., Kozak, J. J, and Scheffey, C. F., "Structural Behavior of a Concrete Box Girder Bridge." *Hwy. Res. Rec. No. 76* (1965) pp. 32-82.
9. Davis, R. E., Scheffey, C. F., Castleton, G. A., and Evans, E. E., "Model and Prototype Studies of Box Girder Bridge." *Proc. Am. Soc. Civil Engrs.,* Vol. 98, No. ST1 (Jan. 1972) pp. 165-183.
10. Bouwkamp, J. G., Scordelis, A. C., and Wasti, S. T., "Structural Behavior of a Two Span Reinforced Concrete Box Girder Bridge Model, Vol. I." *Structures and Materials Res. Rept. No. SESM 71-5,* Dept. Civil Eng., Univ. of California (Berkeley) (Oct. 1971).
11. Scordelis, A. C., Bouwkamp, J. G., and Wasti, S. T., "Structural Behavior of a Two Span Reinforced Concrete Box Girder Bridge Model, Vol. II." *Structures and Materials Res. Rept. No. SESM 71-16,* Dept. Civil Eng., Univ. of California (Berkeley) (Oct. 1971).
12. Scordelis, A. C., Bouwkamp, J. G., and Wasti, S. T., "Structural Behavior of a Two Span Reinforced Concrete Box Girder Bridge Model, Vol. III." *Structures and Materials Res. Rept. No. SESM 71-17,* Dept. Civil Eng., Univ. of California (Berkeley) (Oct. 1971).
13. Mattock, A. H., and Kaar, P. H., "Precast-Prestressed Concrete Bridges. 6. Test of Half-Scale Highway Bridge Continuous Over Two Spans." *J. PCA Research and Development Lab.,* Vol. 3, No. 3 (Sept. 1961) pp. 30-70. Reprinted as *Development Dept. Bull. D51,* Portland Cement Assoc., Skokie, Ill.
14. Scordelis, A. C., Davis, R. E., and Lo, K. S., "Load Distribution in Concrete Box-Girder Bridges." First International Symposium on Concrete Bridge Design, *Publ. SP-23,* American Concrete Inst., Detroit (1969) pp. 117-136.
15. *Building Code Requirements for Reinforced Concrete (ACI 318-71),* American Concrete Inst., Detroit (1971).
16. *Code of Practice for the Structural Use of Concrete, Part 1. Design, Materials and Workmanship,* CP110, British Standards Inst., London (Nov. 1972).
17. Timoshenko, S., and Goodier, J. N., *Theory of Elasticity.* Second Ed., McGraw-Hill, New York (1951) 506 pp.
18. Brendel, G., "Strength of the Compression Slab of T-Beams Subject to Simple Bending." *J. American Concrete Inst.,* Vol. 61, No. 1 (Jan. 1964) pp. 57-76.
19. "Proposal for Load Factor Design of Reinforced Concrete Highway Bridges." Prepared by Portland Cement Assoc. for the AASHO Bridge Comm., Subcomm. on Reinforced Concrete (March 1971).
20 Kriz, L. B., and Lee, S. L., "Ultimate Strength of Over-Reinforced Beams." *Proc. Am. Soc. Civil Engrs.,* Vol. 86, No. EM3 (June 1960) pp. 95-105. Reprinted

as *Development Dept. Bull. D36,* Portland Cement Assoc., Skokie, Ill.

21. KAAR, P. H., "High Strength Bars as Concrete Reinforcement, Part 8. Similitude in Flexural Cracking of T-Beam Flanges." *J. PCA Research and Development Lab.,* Vol. 8, No. 2 (May 1966) pp. 2-12. Reprinted as *Development Dept. Bull. D106,* Portland Cement Assoc., Skokie, Ill.
22. PFRANG, E. O., SIESS, C. P., and SOZEN, M. A., "Load-Moment-Curvature Characteristics of Reinforced Concrete Cross Sections." *J. American Concrete Inst.,* Vol. 61, No. 7 (July 1964) pp. 763-778.
23. DE PAIVA, H. A. R., and SIESS, C. P., "Strength and Behavior of Deep Beams in Shear." *Proc. Am. Soc. Civil Eng,* Vol. 91, No. ST5 (Oct. 1965) pp. 19-41.
24. AMERICAN ASSOCIATION OF STATE HIGHWAY OFFICIALS, "Interim Specifications, 1972—Interim No. 2 Load Factor Design." Comm. on Bridges and Structures, Washington, D.C.
25. SCORDELIS, A. C., "Analysis of Simply Supported Box Girder Bridges." *Structures and Materials Res. Rept. No. SESM 66-17,* Dept. of Civil Eng., Univ. of California (Berkeley) (Oct. 1966).
26. SCORDELIS, A. C., "Analysis of Continuous Box Girder Bridges." *Structures and Materials Res. Rept. No. SESM* 67-25, Dept. of Civil Eng., Univ. of California (Berkeley) (Nov. 1967).
27. LIN, C. S., and SCORDELIS, A. C., "Computer Program for Bridges on Flexible Bents." *Structures and Materials Res. Rept. No. SESM 71-24,* Dept. of Civil Eng., Univ. of California (Berkeley) (Dec. 1971).
28. SCORDELIS, A. C., and DAVIS, R. E., "Stresses in Continuous Concrete Box Girder Bridges." Second International Symposium on Concrete Bridge Design, *Publ. SP-26,* American Concrete Inst., Detroit (1971) pp. 284-318.
29. HOLAND, I., and BELL, K., Ed., *Finite Element Methods in Stress Analysis.* Tapir Forlag, Trondheim, Norway (1970) 500 pp.
30. CLOUGH, R. W., "The Finite Element Method in Structural Mechanics." *Stress Analysis,* Ed. by O. C. Zienkiewicz and G. S. Holister, Wiley, New York (1965) pp. 85-119.
31. ZIENKIEWICZ, O. C., *The Finite Element Method in Structural and Continuum Mechanics.* McGraw Hill, New York (1967) 272 pp.
32. PRZEMIENIECKI, J. S., *Theory of Matrix Structural Analysis.* McGraw Hill, New York (1968) 468 pp.
33. NGO, D., and SCORDELIS, A. C., "Finite Element Analysis of Reinforced Concrete Beams." *J. American Concrete Inst.,* Vol. 64, No. 3 (March 1967) pp. 152-163.
34. NILSON, A. H., "Nonlinear Analysis of Reinforced Concrete by the Finite Element Method." *J. American Concrete Inst.,* Vol. 65, No. 9 (Sept. 1968) pp. 757-766.
35. FRANKLIN, H. A., "Nonlinear Analysis of Reinforced Concrete Frames and Panels." *Structures and Materials Res. Rept. No. SESM 70-5,* Dept. of Civil Eng., Univ. of California (Berkeley) (March 1970).
36. NGO, D., FRANKLIN, H. A., and SCORDELIS, A. C., "Finite Element Study of Reinforced Concrete Beams With Diagonal Tension Cracks." *Structures and Materials Res. Rept. No. SESM 70-19,* Dept. Civil Eng., Univ. of California (Berkeley) (Dec. 1970).
37. ISENBERG, J., and ADHAM, S., "Analysis of Orthotropic Reinforced Concrete Structures." *Proc. Am. Soc. Civil Engrs.,* Vol. 96, No. ST12 (Dec. 1970) pp. 2607-2624.
38. CERVENKA, V., and GERSTLE, K. H., "Inelastic Analysis of Reinforced Concrete Panels: Theory." *International Assoc. Bridge and Structural Eng.,* Vol. 31, No. II, pp. 31-45 (1971).
39. ROLL, FREDERIC, "Materials for Structural Models." *Proc. Am. Soc. Civil Engrs.,* Vol. 94, No. ST6 (June 1968) pp. 1353-1382.
40. BREEN, JOHN E., "Fabrication and Tests of Structural Models." *Proc. Am. Soc. Civil Engrs.,* Vol. 94, No. ST6 (June 1968) pp. 1339-1352.
41. AMERICAN CONCRETE INSTITUTE, "Models for Concrete Structures." *Spec. Publ. SP-24,* Detroit (1968).
42. ZIA, PAUL, WHITE, RICHARD N., and VAN HORN, DAVID A., "Principles of Model Analysis." *Models of Concrete Structures, Publ. SP-24,* American Concrete Inst., Detroit (1971) pp. 19-41.
43. CERVENKA, VLADIMIR, "Inelastic Finite Element Analysis of Reinforced Concrete Panels Under In-Plane Loads." Ph.D. Thesis, Univ. of Colorado (1970).
44. CERVENKA, VLADIMIR, "Finite Element Analysis of the Single-Column Model Bridge Bent." Internal Rept., Portland Cement Assoc.
45. PETER, J., "Zur Bewehrung von Scheiben und Schalen für Hauptspannungen schiefwiklig zur Bewehrungrichtung." Dr. Ing. Dissertation, T. H. Stuttgart (1964).
46. WATSTEIN, D., and MATHEY, R. G., "Strains in Beams Having Diagonal Cracks." *J. American Concrete Inst.,* Vol. 55, No. 6 (Dec. 1958) pp. 717-728.

APPENDIX A

BACKGROUND AND REVIEW OF LITERATURE

Introduction

This appendix serves two purposes. First, it presents some background material for Appendixes B and C, and second, it provides information on experimental methods common to both Appendixes D and E.

Appendixes B and C are, respectively, the reports on the Load Distribution part of the Analytical Studies, done by A. C. Scordelis, and the Bent Analysis part of the Analytical Studies, done by P. P. Lynn and S. Arya. Except for some condensation in the Load Distribution report, the two reports are presented as received. Due to the informal nature of the reports and the fact that they were done concurrently with the experimental program, some added explanation is needed to show how the reports fit into the project. To maintain the reports as separate entities, this added material was placed in Appendix A.

Scaling considerations, construction techniques, loading apparatus, instrumentation and data reduction techniques common to both the Model Bridge Tests described in Appendix D and the Model Bent Tests described in Appendix E are discussed in Appendix A.

Also contained in Appendix A are comments on data analysis, "new maximum" loadings and design methods.

Folded Plate Method of Analysis for Box Girder Bridges

A detailed description of the folded plate method has been reported by Scordelis in his study of simply supported box girder bridges.[25] This method was extended to include the analysis of continuous bridges with simple supports at the extreme ends.[26] Lin and Scordelis[27] have developed a

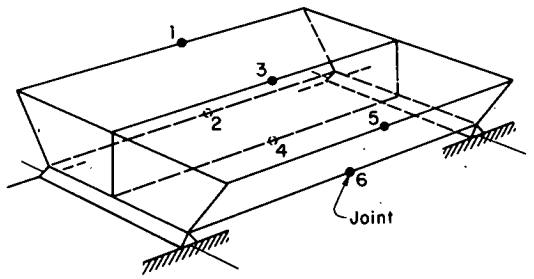

Fig. A-1 Simply Supported Cellular Folded Plate as Described in Ref. 25

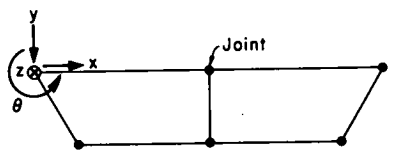

Fig. A-2 Degrees of Freedom at Each Joint

computer program, based on the folded plate method of Goldberg and Leve[2], to analyze prismatic structures with flexible interior diaphragms or supports. The summary that follows is derived from these three references. For simplicity, the method of handling interior rigid or flexible diaphragms will not be discussed.

The initial report by Scordelis[25] contains a review of analytical models used to represent simply supported box girder bridges; also included is a selected bibliography. More recent references are given by Lin and Scordelis.[27]

Assumptions. In the development of the folded plate solution, it is assumed that the box girder structure is made up of uniformly thick rectangular plates that are elastic and homogeneous. Superposition is considered valid. Because a harmonic analysis is used, the structure must be simply supported at its extreme ends.

Analysis of a Simply Supported Box Girder Bridge by the Folded Plate Method. The box girder bridge is considered as a system of interconnected rectangular plates as shown in Fig. A-1. The structure may be analyzed for applied loads of arbitrary longitudinal distribution using a harmonic analysis representing the loads by a Fourier series. The harmonic analysis makes it possible to treat an entire longitudinal joint as a single nodal point. Each joint or nodal point has four degrees of freedom as shown in Fig. A-2.

The forces and displacements in each plate caused by loads normal to the plane are calculated by the classical bending theory for thin plates. Forces and displacements caused by loads in the plane of the plate are calculated by the plane stress theory of elasticity.

A direct stiffness method of analysis is used to solve for the internal forces and displacements in each plate. Using classical plate theory and plane stress theory, expressions are derived for the plate edge forces caused by the surface loads for the case of the longitudinal edges fixed against displacement. These four forces at each edge are then related to the corresponding edge displacements to yield an element stiffness matrix. The element stiffnesses are assembled to form the structure stiffness matrix, K, which relates the applied loads, F, to the unknown joint displacements, u. After the equilibrium equations, $F = Ku$, are solved for u, the plate element internal forces and displacements can be calculated.

Analysis of a Box Girder Bridge Supported by a Planar Frame Bent. The folded plate solution outlined above has been extended by Lin and Scordelis[27] to permit analysis of bridges supported by flexible planar frame bents. Interior support bents are assumed to be incapable of carrying loads normal to their own plane. The solution combines the stiffness and flexibility methods.

The interior support bent is accounted for by using a flexibility (force) method of analysis in which the interaction forces between the folded plates and the supporting frame bents are taken as redundants as illustrated in Fig. A-3. The analysis consists of the following steps:

1. Redundants are set equal to zero and the folded plate structure is analyzed for the given loads as described in the previous section. From this analysis the displacements, $\{\Delta_0\}$, are defined at the points where the redundants act.
2. The folded plate structure is analyzed to determine unit values of each redundant force and the corresponding flexibility matrix

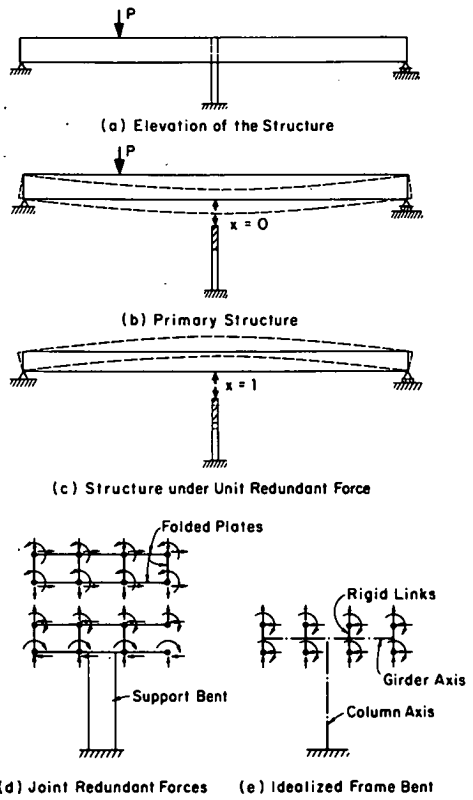

Fig. A-3 Analysis of a Folded Plate Structure on a Flexible Bent as Described in Ref. 27

Davis, et. al. have found that the folded plate method correlated well with model and prototype tests in the determination of the distribution of box girder resisting moments.(9)

Application of the Folded Plate Method of Analysis. Since the structures of this project are prismatic, except for the minor flaring of the box girder webs, the folded plate method of analysis appears applicable. However, in the vicinity of the bent cap, the correspondence is less exact since the analysis assumes a cap of zero width in the direction of the span of the bridge. Since accurate prediction of stresses in the bent cap was a primary objective of the project, the folded plate method is deficient in this respect. However, this deficiency should not affect the accuracy of predictions of quantitities such as load distribution among the girders, a quantity related to the overall characteristics of the structure.

Both concentrated and distributed loads can be accurately represented in the folded plate method. Consequently, all loadings used in this project are adequately represented by the analysis.

As a method based on assumed linear elastic behavior, the folded plate analysis will satisfactorily simulate the behavior of a reinforced concrete structure only in the range of loadings in which the structure exhibits no marked changes in behavior due to cracking or nonlinear material properties.

Adaptation of Scordelis' Report for Appendix B. Scordelis' report on the Load Distribution part of the Analytical Studies was condensed for publication as Appendix B. The condensation consisted of the elimination of many figures, the renumbering of those remaining, and slight modifications of the text to make it compatible with the new agreement.

is formed. This matrix relates the displacements at the points where the redundants act, $\{\Delta_1\}$, to the unit forces.

3. The planar bent frame is analyzed by the direct stiffness method and the frame stiffness matrix is condensed to eliminate the degrees of freedom that do not correspond to the redundant forces. The stiffness matrix is then inverted to obtain the flexibility matrix. This matrix relates the frame displacements at the points where the redundant forces act, $\{\Delta_2\}$, to the unit redundant forces.
4. Unknown redundant forces are determined by satisfying geometric compatibility which requires that $\{\Delta_0\} + \{\Delta_1\} + \{\Delta_2\} = 0$.
5. The folded plate structure and the planar frame bent are then analyzed for the known loads and the known redundant forces to determine the stresses and displacements in the actual structure.

A typical support beam consisting of a transverse girder and a column may be idealized as a planar frame with fictitious vertical rigid links connecting the girder axis to the joints of the folded plate system as shown in Fig. A-3.

Advantages and Disadvantages of the Folded Plate Method. Scordelis(26,28) has compared the folded plate method to other elastic analyses such as the finite segment and finite element methods. This comparison indicated that the folded plate method is the most accurate. This method yields a complete solution in a reasonable amount of computer time. However, it is restricted to analysis of continuous, homogeneous, prismatic structures with simple supports at the extreme ends.

As originally submitted, the report contained a complete set of figures for each of 11 loading cases, five for the single-column bridge and six for the double-column bridge. For each case 15 figures and two tables were shown. Each loading case concerned with the double-column bridge included two additional figures and an additional table. Besides these items, four figures and two tables of a general nature were included in the text. Thus, the complete report contained 181 figures and 30 tables. It was felt that the inclusion of all this material relating to only one phase of the project would make the final report unnecessarily long.

To form Appendix B, the text and the four figures and two tables of a general nature were retained. The figures appear as Figs. B-1 through B-4, respectively.

The subdivisions of the various loading cases, originally named "figures" were renamed "parts". Figures illustrating the results of all the parts for loading cases 1 and 6, live loading of all lanes in the single-column and double-column bridges, respectively, were retained. Figures illustrating the results of parts 11 and 12, related to loadings calculated for the bent caps, were retained for all loading cases. Some additional figures were also retained. The figures were renumbered by loading case and part. The condensation contains 60 figures and two tables.

Finite Element Analysis of Reinforced Concrete Structures

This section presents a brief description of the finite element method and its application to reinforced concrete structures. It is intended for this material to serve as a background for the presentation in Appendix C of Lynn and Arya's results on the finite element analysis of the bent cap specimen.

Detailed descriptions of the finite element method are presented elsewhere.[29,30,31,32]

Finite Element Concept. The finite element method is a technique for approximating solutions to stress analysis problems of continuum mechanics by replacing the actual continuous structure with a system of discrete elements having known physical properties. The method allows complex two-and three-dimensional structures to be analyzed by the same basic matrix displacement or force techniques used for frame structures. With the finite element method, the effects of anistropy, nonlinear response, temperature, and time-dependent phenomena can be incorporated.

The first step in the finite element analysis is idealization of the continuous structure as an assemblage of discrete elements. To illustrate this procedure, Fig. A-4 shows a beam divided into a system of triangular elements interconnected at nodal points. The displacements of the nodal points are the basic unknowns of the problem, just as in the matrix displacement analysis of a frame. Thus, the beam continuum is reduced to a structural system having a finite number of degrees of freedom.

The discrete elements that replace the continuous system are not merely pieces of the original structure connected at the points. Such a system would be much more flexible than the original structure because continuity would only be satisfied at the joints. Rather, the elements are developed to represent, as closely as possible, the displacement pattern of the original structure.

The second and most critical step in the analysis is the determination of the stiffness characteristics of the individual elements. To accomplish this, it is necessary to develop the element stiffness matrix that relates the nodal point displacements to the nodal point forces.

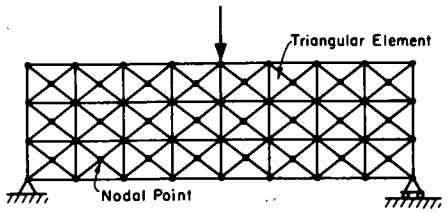

Fig. A-4 Finite Element Idealization of Beam

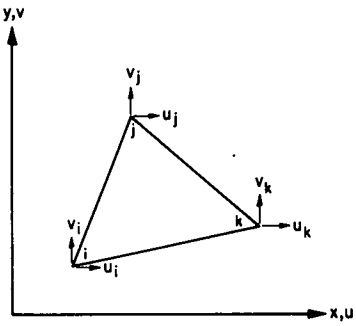

Fig. A-5 Triangular Element

A representative triangular element, with two degrees of freedom at each node, is shown in Fig. A-5. In deriving the element stiffness matrix, displacement functions are selected to define the state of deformation within each element in terms of the nodal point displacements of the element.

Once the displacement functions are chosen, the strains within the element can be defined in terms of the nodal point displacements. Then, through a stress-strain relationship, the stresses within the element are also related to the nodal point displacements. Finally, the principle of virtual work is applied to obtain the element stiffness matrix by imposing arbitrary virtual nodal point displacements on the element and then equating the external work to the internal work.

After the continuous structure has been idealized and the element stiffness matrix has been derived, the next step in the analysis is to assemble the structure stiffness matrix by systematic addition of the individual element stiffnesses. The structure stiffness matrix, K, relates the unknown nodal point displacements, u, to the external nodal point loads, F. Using matrix notation, the equilibrium equations may be expressed as follows:

$$\{F\} = [K]\{u\} \qquad \text{(A-1)}$$

Once the stiffness matrix is assembled, Eq. A-1 can be solved to obtain the unknown nodal point displacements. Subsequently, the element stresses and strains can be computed. For nonlinear problems, incremental or iterative procedures are used to account for changes in the structure stiffness with increasing load.

Through the use of matrix algebra, the finite element technique is readily adapted to programming for the digital computer.

Application to Reinforced Concrete Structures. Application of the finite element method to reinforced concrete beams was described by Ngo and Scordelis.[33] Figure A-6 shows their finite element idealization of a reinforced concrete beam. Triangular elements were used to represent both the steel and the concrete, and a special linkage element was used to represent the bond between the concrete and steel. A linear relationship between the bond slip and bond stress was assumed. Cracking was incorporated into the model by separating the concrete elements on either side of a crack.

Nilson[34] has extended Ngo and Scordelis' work to include nonlinear material properties, progressive cracking, and a more complex bond slip to bond stress relationship.

Franklin[35] has also used the finite element method for the nonlinear analysis of reinforced concrete structures, including open and infilled frames.

Reinforced concrete beams with diagonal tension cracks have been modeled by Ngo, Franklin, and Scordelis.[36] They simulated the progression of diagonal cracking and determined the stress state at various stages of cracking. Beams with and without web reinforcement were analyzed. Their work includes a study of the effects of aggregate interlock, dowel forces, and horizontal splitting.

Isenberg and Adham[37] have presented an approach to the finite element analysis of reinforced concrete structures that differs from the process described by Ngo and Scordelis. Rather than idealizing the structure as a system of concrete elements, steel elements, and bond links, Isenberg and Adham derived stress-strain relationships for a composite reinforced concrete element as shown in Fig. A-7. The composite model is developed

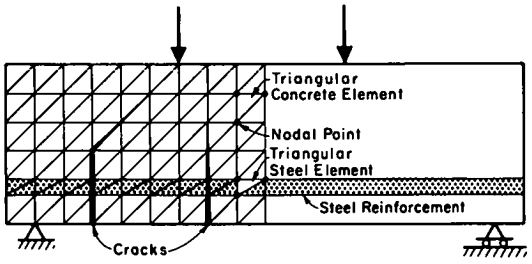

Fig. A-6 Finite Element Idealization of Reinforced Concrete Beam as Described in Ref. 33

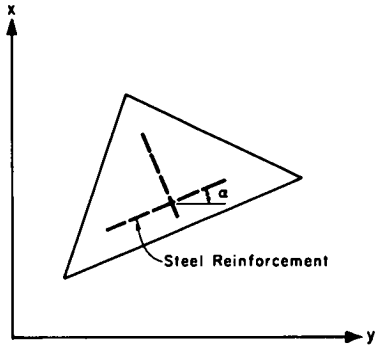

Fig. A-7 Reinforced Concrete Element

a concrete mix with reduced maximum aggregate size, these structures were, in almost every detail, reduced size structures geometrically similar to the prototype.

The capabilities and limitations of reduced scale models are discussed in several recent publications, including those by Roll[39], Breen[40] and the American Concrete Institute Symposium Volume SP-24.[41] The latter publication, concerned with all phases of modeling of concrete structures, contains 18 papers. Some of these are referred to elsewhere in this report.

Capabilities. To assess how well the model bridges in this study model the behavior of the prototype, it is necessary to evaluate the relative importance of various types of behavior. It is assumed that properties of the reinforcement, with the possible exception of bond, are modeled very well. Similarly, structural properties of concrete are modeled well except for some small, easily measured increases in tensile strength.

By nature of the design, the predominant action is flexural. The flexural action of primary interest is in the post cracking range. For the small reinforcement percentages used on the test specimens, flexural behavior is almost completely a function of reinforcement properties. Consequently, behavior of the prototype is well modeled.

Shear behavior is another consideration in the performance of the models. That portion of shear behavior attributable to the concrete may be slightly influenced by the higher tensile strength of the model concrete. In these structures, however, the major portion of the shear resistance is provided by the reinforcement. Again, since the reinforcement properties are well modeled, shear behavior should be well represented.

to account for (1) the combined properties of the concrete and steel, (2) the change in principal directions of stresses and the orientation of cracks, (3) progressive bond failure between concrete and steel, (4) orthotropy due to different moduli in different directions under multiaxial compression and (5) orthotropy due to cracking. With the composite element, cracking is accounted for by changes in the stiffness of the composite element, not by disconnecting the elements at their common nodes.

Cervenka and Gerstle[38] have also used the composite element approach to evaluate the nonlinear effects of cracking and plasticity in the analysis of reinforced concrete panels under in-plane forces. Lynn and Arya's analysis of the bent cap presented in Appendix C is based on the composite element model approach.

Limitations of the Method. The accuracy of results obtained from the analysis is dependent on the ability of the mathematical model to represent the actual structure geometry, material properties and loading conditions. As more refined experimental data becomes available concerning the multiaxial stress-strain relationships for concrete, the bond slip between concrete and reinforcement, and the effective shear modulus of reinforced concrete planar elements, mathematical models will be improved. In addition, more work is necessary to determine the effects of dowel action, aggregate interlock, creep, and shrinkage. Until better information concerning these items is available, finite element analysis of reinforced concrete structures must still be considered to be in the development stage.

Model Testing - Reduced Scale

To simulate the behavior of the prototype at all loads through ultimate, models were constructed at reduced scale. Using steel reinforcement and

Bond, though not particularly well modeled, should not be a factor entering into the behavior of either prototype or model, since designs are proportioned to avoid bond problems.

Cracks may be expected to form at relatively wider spacings in the model, as pointed out by Kaar[21] and others. Consequently, individual cracks will tend to be relatively wider in the model than in the prototype. In addition, the onset of cracking may be slightly retarded by higher tensile strength in the model concrete.

Deflections are affected by the proportions of cracked to uncracked sections in a structure. Consequently, higher tensile strengths in the model concrete somewhat reduce the relative deflections.

Scaling Considerations. The laws of similitude define an infinite variety of material properties that will satisfy the requirements of modeling. However, as pointed out by Zia, White and VanHorn[42] and Roll[39], as well as others, from a practical standpoint it is convenient for strength models to use materials having in all details the same properties as those in the full scale structure. When this is done, the stress scales and strain scales are unity for the model, i.e., throughout the model the stresses and strains are the same as those in the prototype for the equivalent loading. Therefore, effort was made to duplicate the assumed properties of the prototype materials in the model.

With the stress scale and strain scale set at unity, the scaling of loads and forces becomes very straightforward. If the scale factor λ is defined as

$$\lambda = \frac{\ell_m}{\ell_p} \qquad \text{(A-2)}$$

where ℓ is a characteristic length dimension and the subscripts m and p

refer to model and prototype respectively, then

$$P_m = \lambda^2 P_p \tag{A-3}$$

$$\left[P/\ell\right]_m = \lambda \left[P/\ell\right]_p \tag{A-4}$$

$$w_m = w_p \tag{A-5}$$

where P is a concentrated load (force), P/ℓ is a load per unit length (for example, pounds per foot) and w is load (force) per unit area (for example, psi stress, psf load).

The choice of the unity strain scale means that all quantitites containing a dimension factor obey Eq. (A-2). Of greatest interest is the fact that deflections are in proportion to the scale factor, assuming that modeling of behavior is accurate.

The fact that strains are equal in model and prototype is an aid in interpretation of test data. Care must be taken, of course, to see that strains are measured over an appropriately short gage length in the model to avoid invalid averaging of values in regions of steep strain gradients.

The use of concrete in the model having material properties similar to those of the prototype concrete insures that the effects of creep and shrinkage will be present in the model in the same general manner as in the prototype.

As discussed above, the fundamental characteristics of the reduced scale strength models assure adequate modeling of behavior for all of the needed and well-defined properties. In addition, the use of concrete and reinforcement in the model similar to those in the prototype helps assure that less well-defined characteristics, such as failure criteria for the concrete, will also be modeled correctly.

One complication of the use of concrete and steel in the models is that, with the densities of prototype and model materials the same, then

$$\sigma_{D_m} = \lambda \sigma_{D_p} \tag{A-6}$$

where σ_D are stresses due to dead load. To make up the deficiency in dead load stresses in order to satisfy Eq. (A-5), additional dead load must be applied.

Model Tests

Scale. The choice of scale for the specimens was intended to provide a balance between favorable and unfavorable factors. Construction costs decrease along with model size until difficulties related to the need for greater precision begin to elevate costs. Reduced load requirements make smaller models attractive. On the other hand, installation of strain gages on the smaller models is more difficult. According to Breen[40], for a somewhat similar bridge system the optimum scale is in the range $\lambda = 1/4$ to $\lambda = 1/16$. For the two model bridges a factor within this range, $\lambda = 1/5$, was chosen. The choice was primarily governed by the capacity of the laboratory equipment and by size and weight of the finished models.

A scale factor of $\lambda = 2/5$ was chosen for the single-column bent cap models. However, at this scale the weight of the double-column bent cap model, DC-9, became greater than the capacity of the laboratory crane. Consequently, this model was constructed at $\lambda = 1/5$ to reduce weight and allow the model to be lifted from the casting platform.

Concrete Mix Design. A mixture using a maximum aggregate size of about 5/16 in. was adopted for the box girder and bent cap portions of all specimens. Type I cement, sand and pea gravel were combined in the ratios

of about 1.0:3.7:4.4. In addition, an agent was added to produce about 6 percent entrained air.

Mixtures of similar proportions were designed to meet specific strength requirements for columns, column bases, and parapets.

The physical properties of the various mixes as obtained from tests on standard 6-in. by 12-in. cylinders are tabulated in the sections describing the individual tests. A representative stress versus strain relationship for the concrete is shown in Fig. A-8.

Reinforcement. Required reinforcement percentages for the model bridge were obtained from the prototype designs. Specific reinforcement sizes were then chosen by consideration of the scaled prototype bar sizes and the actual bar and wire sizes available. The model bents were designed directly.

In the models, ASTM Designation: A-615 Grade 60 sizes No. 7, No. 6, No. 5, No. 4, and No. 3 were used to represent large bars. Deformed 6mm hot rolled bars (A = 0.044 sq. in., d_{nom} = 0.236 in.) with similar properties were also used. Deformed wire size D-5 (A = 0.05 sq. in.) was used in some specimens. Smaller deformed wires, sizes D-3 (A = 0.03 sq. in.), D-2 (A = 0.02 sq. in.) and D-1 (A = 0.01 sq. in.) were used to represent smaller bar sizes.

The deformed wires as purchased had a rounded stress-strain curve and a tensile strength of about 85 ksi. By heat treating the properties were altered so that a well defined yield stress of about 60 ksi was produced. Consequently, the deformed wires used had stress-strain characteristics similar to those of Grade 60 bars. The heat treating was accomplished

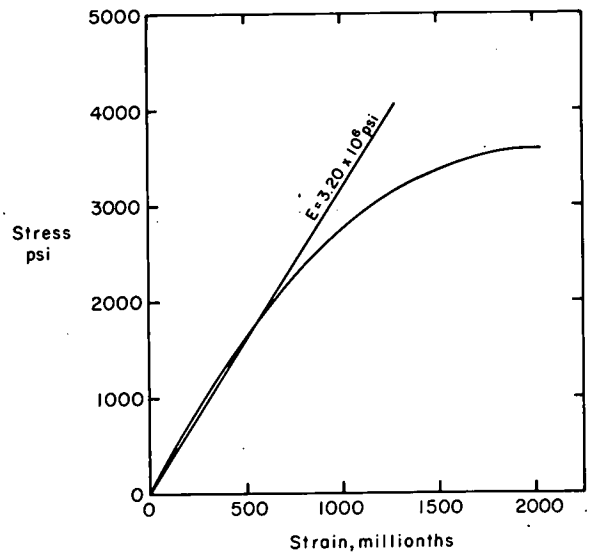

Fig. A-8 Stress versus Strain Relationship for Concrete

by holding a constant temperature for a period of about 6 hours. Temperatures from 975°F to 1050°F were used for different sizes and lots of wire.

Representative stress-strain curves for different sizes of bars and wires are shown in Fig. A-9. Properties of the reinforcement used for specific specimens are listed in the sections describing the tests.

Construction Techniques. All models were cast on a stationary wooden platform leveled to ± 1/16 in. overall. The casting of the superstructure was done in two stages as illustrated in Fig. A-10. In the first casting, the deck was completed. In the bent cap, the construction joint between castings was at about the same elevation as in the girders. Forms for the underside of the deck were removed after the concrete had hardened thereby avoiding any possibility of restraint to the structure from forms left in place. All concrete was compacted using a combination of internal and external vibration.

For the two model bridges and the first bent cap specimen, concrete of the first casting was placed to the tops of the webs in one operation. However, there was some tendency for the fresh concrete to settle away from the horizontal reinforcement in the webs, leaving planes of weakness. This tendency was particularly apparent in the first two-fifth-scale bent cap specimen, where increased web height and clearances tended to aggrevate the problem. In subsequent specimens the concrete of the first casting was carried to just below the lowest horizontal wires, then allowed to take its initial set over a period of a few hours. After that, the rest of the concrete was placed in the webs.

Loading Apparatus. Loads for the models were applied by means of hydraulic equipment described elsewhere.(5) In this system, loading rods

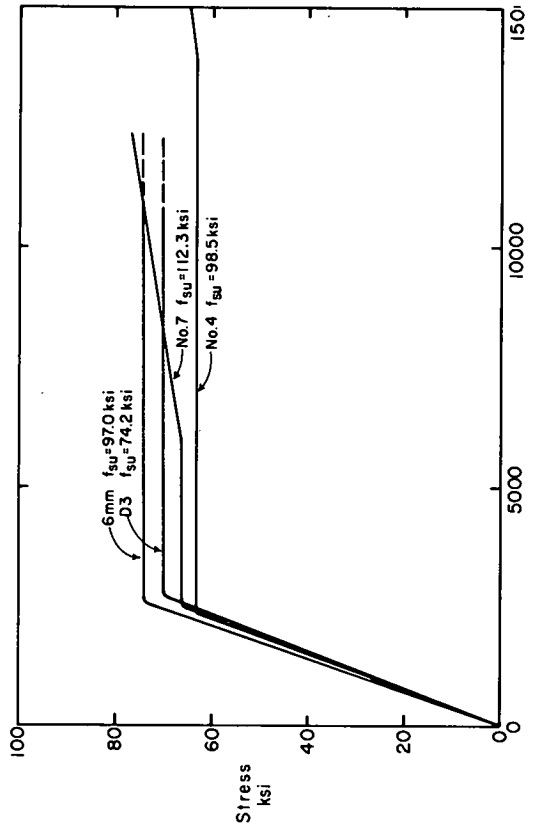

Fig. A-9 Stress versus Strain Relationships for Reinforcement

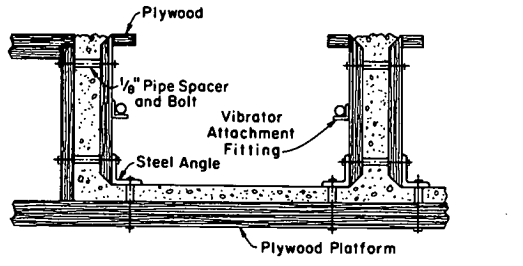

First Casting

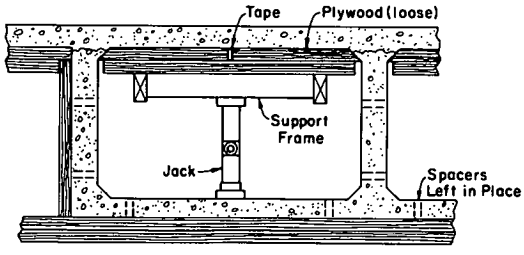

Second Casting

Fig. A-10 Casting Sequence for Model Bridge Superstructure

attached to the test structure extend down through holes in the laboratory floor. The loading rods are connected to hydraulically actuated rams located beneath the test floor. By interchanging components, a variety of loading patterns and forces can be developed. Uniformly distributed loads are approximated by a set of concentrated loads.

To make up the dead load deficiency for correct simulation of dead load stresses in the bridge models, force was maintained throughout the test period. This force was removed only for brief intervals to obtain "zero load" readings from the instrumentation.

In both the single-column and double-column model bridges, the center of application of live load for one or more lanes was offset slightly from the dead load system. Due to this offset, the two loading systems did not have compatible geometry. Consequently, it was necessary to construct reaction frames above the test floor to accommodate the offset. The arrangement for the single-column bridge is shown in Fig. A-11. Similar arrangements were used for the offset lanes in the double-column bridge.

In addition to the hydraulically applied loads, concentrated point loads were applied to the model bridges by placing a concrete block successively in the desired locations. Line loads were applied by piles of bags of cement. Details are described in the sections concerning the particular tests.

For the single-column bent cap specimens, all loads were applied through the hydraulic system. Since the tests were of short duration, it was not necessary to apply the dead load makeup separately. Instead, dead load makeup, dead load increments, and live loads were applied simultaneously through the hydraulic loading system shown in Fig. A-12.

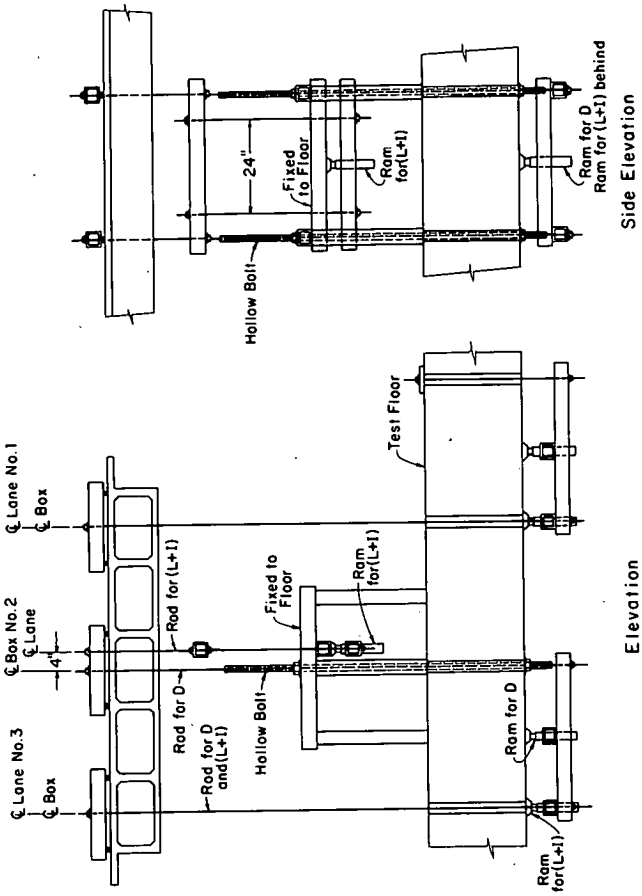

Fig. A-11 Loading Apparatus in Span for Single-Column Model Bridge

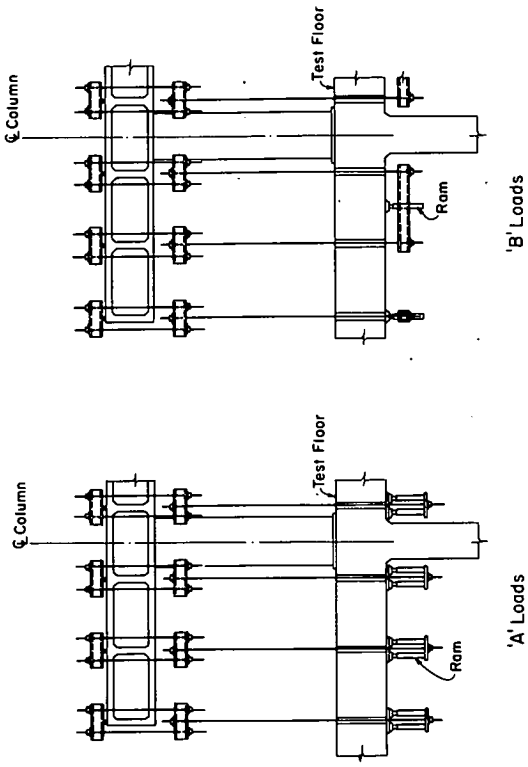

Fig. A-12 Loading System for Single-Column Bents

The same loading criteria were used for the single-column bent cap specimens and the double-column bent cap specimen. Since the single-column specimens were two-fifths scale and the double-column specimen was one-fifth scale, the points of application of load in the latter were at 1.5-ft. centers rather than at 3-ft. centers as used along the girders of the larger model. A lever system, shown in Fig. A-13, was used to adapt the pattern to the floor hole spacing of the laboratory.

Instrumentation. Techniques for instrumentation of structural models are described in detail elsewhere.(5) Some modifications were made in the strain gage installation techniques for the small wires used as reinforcement. Otherwise, the instrumentation was similar in all respects to that used for larger scale specimens.

Strains on reinforcement and on the surface of concrete were measured with electrical resistance strain gages. On both bridge models and on the single-column bent cap specimens, the electrical gages were supplemented with a Whittemore mechanical strain gage system that was used to monitor strains over long periods of time.

Deflections were measured with linear potentiometers. A precision industrial level sighting on targets, was used as an additional check on measured deflections.

Forces were measured with load cells placed at selected locations in the loading apparatus. For the model bridges, reactions at the column bases and at the abutments were also measured.

Crack widths were measured with a hand microscope containing a scale with graduations of 0.001 in.

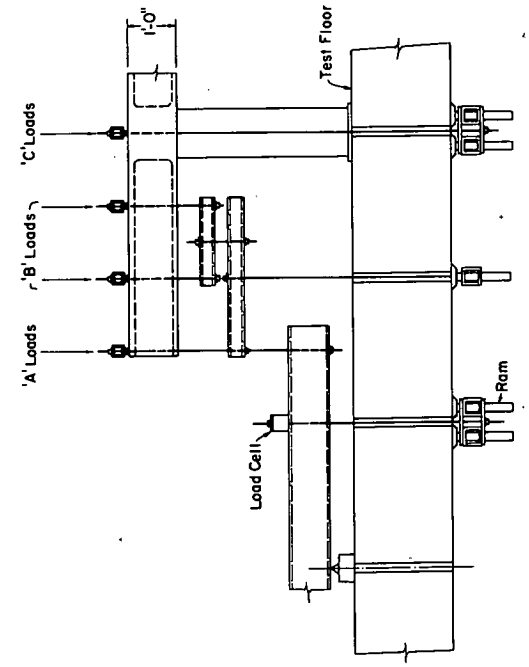

Fig. A-13 Loading System for Double-Column Bent

Details of instrumentation for specific tests are included with the test descriptions.

Analysis of Data

Moments and Shears. The primary objective of the experimental portion of the program was to determine the distribution of internal forces in the test specimens. To do this, stresses were calculated from measured strains, and forces were calculated from the stresses. When appropriate, internal moments were determined from the measured forces. Shears could then be determined from differences in moments.

One of the problems of the experimental analysis was the determination of the absolute value of strain for any particular load. In the analysis of this report, an early load stage was selected for which all strains were taken to be zero, the exact choice being governed by judgment of the creep, shrinkage and dead load stresses present. For the model bridges, the strain increment from the zero load stage to a stage of low load at the beginning of the cycle containing the load of interest was determined by study of both the relevant Whittemore mechanical gage readings and the electrical strain gage readings. Although the mechanical gages have better absolute accuracy, they represent averaging over a relatively long 5-in. gage length. The electrical gages may show drift over a long period of time, but depict strain gradients more accurately due to the shorter gage length.

With the absolute strain at the beginning of the cycle determined, the increment within the cycle to the load of interest was determined using the electrical gage readings.

For the bent cap specimens, the problem of drift of electrical gages over a period of time was not present. Consequently, absolute strains were determined directly from the increment of strains indicated by electrical gages between the chosen zero load stage and the load stage considered.

Stresses corresponding to the measured strains in the reinforcement were obtained by multiplying by the measured value of the modulus of elasticity. To obtain stresses in concrete of the model bridges, time effects due to creep and shrinkage were taken into account as described in more detail in Appendix D.

When moments were determined from forces, tensile and compressive resultants calculated from measured strains were not equal, even in situations where no axial force could be present. The procedures used to adjust for this anomaly are described in the appropriate sections.

Determination of shears from moments, basically a differentation process, magnified experimental errors, reducing the accuracy of the results. However, the end use of the individual girder shears to determine moments in the bent cap, represents an integration process that tends to reduce overall error, if the total shear is statically correct.

Residual Strain. The determination of absolute strains was affected by residual strains that accumulated after any loading. The effect exists for all deformations produced in concrete structures, but is particularly evident in the case of measured reinforcement strains.

A representative load versus strain curve for a strain gage on reinforcement is shown in Fig. A-14. The gage selected was on the bent cap reinforcement of Specimen SC-3. In the figure, it is seen that a certain

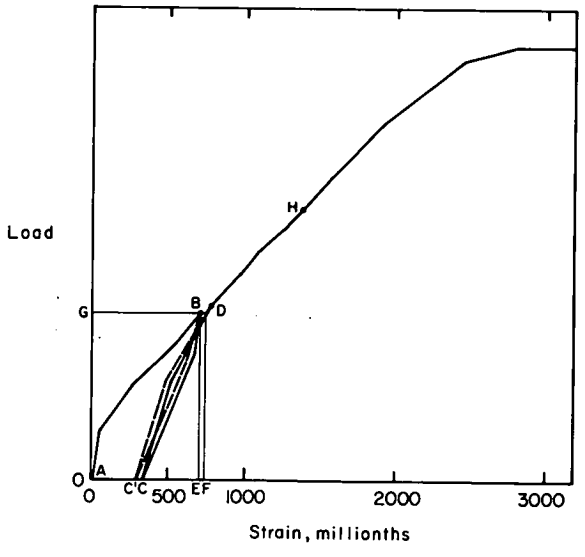

Fig. A-14 Residual Strains

strain increment AE was produced when the load was increased from zero to G. When the load was reduced to zero, the strain did not return to zero, instead, a residual shown as AC remained.

The location of C was not unique. Rather, strains could unload along the dashed curve BC', for a different residual AC'. Experience indicated that further reloadings to level G produced slight shifts of the maximum and minimum strains to the right.

Experience also indicated that reloadings to levels less than G produced loops with minima in the vicinity of C. First loading to a level above G followed along the line DH. This is essentially the same curve that would have been followed if the load had been increased monotonically.

For this investigation it was assumed that only those strains that represented new maxima for the particular location were unique functions of the load. The strain associated with this load can be referred to the original zero, in Fig. A-14, point A.

Any other strain due to a load increment, for example the strain increment CF produced by the same loading that produced the unique strain AE, is called a "response" in this report. The response is a measurable, but non-unique, result of a particular loading. Since a residual strain is present at the beginning of the response, responses are relative rather than absolute.

Load Determination. Loads applied to the test structure by the hydraulic system differ from the nominal calculated on the basis of hydraulic pressure and the ram piston areas. The factors involved, which usually result in a force reduction, are discussed elsewhere [5]. In the tests described in this report, actual force applied might be expected to be 3 or 4

percent less than the nominal force, principally because of friction in the rams.

As mentioned earlier, the values of loads applied at various points were measured by load cells. These measurements are also subject to experimental error.

For consistency, all tests were planned on the assumption that the nominal hydraulically applied loads were correct. The actual loads, as determined by interpretation of the load cell readings, are recorded test by test. Plots are made on the basis of nominal loads unless otherwise indicated.

Bridge Design Methods

The test specimens of this project were designed by two methods. The Working Stress Method was used for the model bridges while the Load Factor Method was used for the bent specimens. Discussion of these two methods is beyond the scope of this report, however, it should be pointed out that the design method and assumptions have an influence on both the absolute strength of the complete structure and on the relative strength of the various parts.

Working Stress Method. The two model bridges were designed as full-scale structures using Working Stress Methods described elsewhere.(1) Geometry and reinforcement were then scaled down for construction of the mold. This design method results in a structure with greater capacity than it would have if designed by the Load Factor Method.

From a testing standpoint, the Working Stress Method has the disadvantage that, since the structure has its components designed one by one to resist the particular loading that causes the maximum stress, the complete

structure is designed for a group of different loadings. However, in the test to destruction, only one load pattern can be applied. Consequently, only those items designed to resist that particular load are being tested. This problem is common to both the Working Stress Method and the Load Factor Method when critical load patterns are used.

Load Factor Method. For the bent cap specimens, the design assumptions of the Load Factor Method were used. However, only the applied load pattern was considered for design. Thus, the relative strengths of the various members were more nearly the same.

APPENDIX B

ANALYSIS OF BOX GIRDER BRIDGE AND BENT SYSTEMS

by

A. C. Scordelis*

Introduction

The objective of this study was to analyze two box girder bridge and bent systems which are presently being studied by the Portland Cement Association (PCA) as part of their research program "Analysis and Design of Bridge Bents." In both cases the bridge is a two span, continuous box girder bridge which is simply supported at the two ends and has a central interior support bent. Each span of the bridge is 90 ft. long. The first bridge system is a five cell bridge with a central interior support bent which consists of a single circular column and a rectangular transverse girder, Fig. B-1a. The second bridge system is a nine cell bridge with a central interior support bent which consists of two circular columns and a rectangular transverse girder, Fig. B-1b.

Each of the two bridge systems were analyzed for a variety of loadings specified by John Hanson of PCA and summarized in Table B-1. These loadings simulated several live load lane and truck loading positions corresponding to lanes as shown in Fig. B-1, and separately one loading case for each bridge system consisted only of dead load. For ease of reference each case has been given a numerical designation from 1 to 11 in Table B-1.

*Professor of Civil Engineering, University of California, Berkeley, California

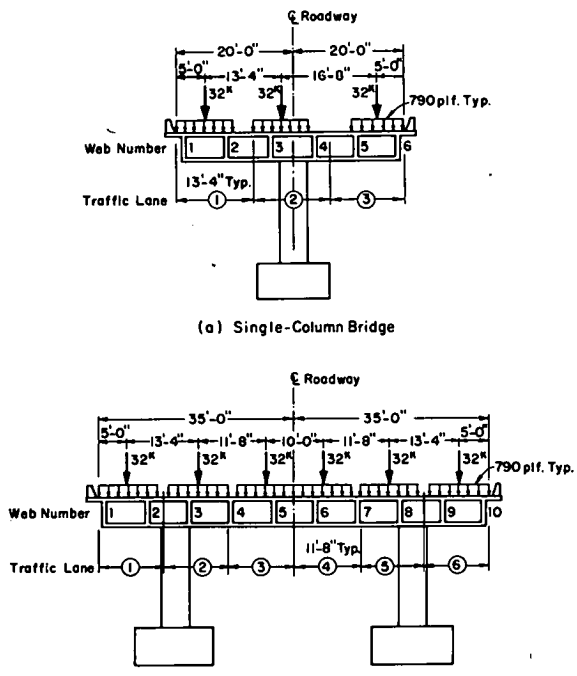

Fig. B-1 Loadings on Prototype Bridges

TABLE B-1 LOADING CASES FOR SINGLE-COLUMN AND DOUBLE-COLUMN BRIDGES

	Case	Live Load* Lane 1	Lane 2	Lane 3	Tributary Loading, Pounds Per Ft. Web 1	2	3	4	5	6	Remarks
Single Column Bridge	1	X	X	X	364.0	463.5	506.2	241.9	424.4	370.0	Slightly modified version of case received with letter dated 2/17/71
	2	X	X	0	363.4	467.0	492.3	294.0	44.1	7.4	
	3	X	0	0	362.6	468.5	-52.1	13.9	-3.5	0.6	Apply dead load of all elements.
	4	0	0	0	0	0	0	0	0	0	
	5	X	X	X	364.0	463.5	506.2	241.9	424.4	370.0	Modify slab overhang to represent parapet
	Case	Lanes 1&6	2&5	3&4	Web 1&10	2&9	3&8	4&7	5&6		
Double Column Bridge	6	X	X	X	362.0	475.4	458.2	493.1	580.9		Received with ltr. dated 4/29/71
	7	0	X	X	-0.6	7.0	510.3	479.4	583.6		
	8	0	0	X	-1.4	8.7	-34.7	201.6	615.6		
	9	X	0	0	362.6	468.4	-52.1	13.7	-2.7		Apply dead load of all elements.
	10	0	0	0	0	0	0	0	0		
	11	X	X	X	362.0	475.4	458.2	493.1	580.9		Modify slab overhang to represent parapet

*"X" indicates HS20-44 live loading multiplied by an impact factor of 23.3 percent.
"0" indicates no live load.

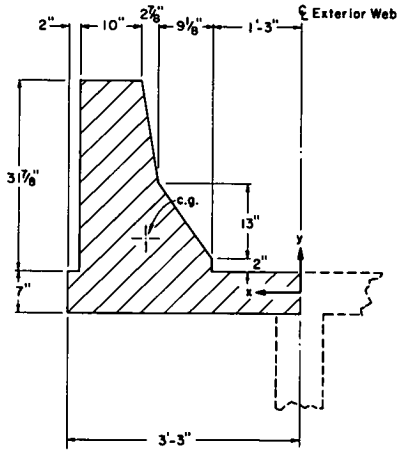

Area = 5.1 ft.^{2} $I_{x_{c.g.}}$ = 3.05 ft.^{4} I_x = 8.34 ft.^{4}
$x_{c.g.}$ = 2.13 ft. $I_{y_{c.g.}}$ = 4.31 ft.^{4} I_y = 26.21 ft.^{4}
$y_{c.g.}$ = 0.89 ft.

Fig. B-2 Parapet Details

Cases 1 to 5 are for the 5 cell single-column bridge, and cases 6 to 11 are for the 9 cell double-column bridge. Cases 4 and 10 are dead load only cases. Cases 1, 2, 3 and cases 6, 7, 8, 9 involve different transverse positions of the live loads only (no dead load is included in these cases). Cases 5 and 11 are identical respectively to cases 1 and 6 with the exception that the parapets at the extreme longitudinal edges of the bridge, which are excluded as part of the structural cross-section in all other cases, are now included. Details of the parapet supplied by PCA are shown in Fig. B-2.

Of particular interest in the analysis were the following items:

1. The transverse distribution and the longitudinal variation of the total moments taken by each girder of the cross-section. A single interior girder was considered to consist of a vertical web and flanges consisting of a half bay width of top and bottom slabs on either side of the web. The exterior top flange of an exterior girder consisted of the cantilever overhang and this girder had no bottom exterior flange. For cases 5 and 11 where the parapets were added they were assumed to be additional girders without flanges. Longitudinal moments for all cases were determined with respect to the same reference horizontal axis, which was taken as the gross section neutral axis of the bridge cross section without parapets.
2. The locations of zero moment (points of inflection) for each girder.
3. The value of the girder vertical shear for each girder at these points of inflection.

4. The interaction forces between the cellular folded plate system and the supporting bent girder in which the girder has a rectangular cross section and the columns have circular cross sections.
5. The axial forces, shear forces and bending moments in the above bent members.
6. The amount of participation of the top and bottom slabs of the cellular system with the rectangular bent girder section in carrying the transverse moments in the bent.

Method of Analysis

In order to obtain the above information an analysis was performed using a computer program entitled MUPDI-3. The program provides a solution for prismatic cellular or open folded plate structures simply supported at the two ends which may have interior flexible diaphragms or supporting frame bents between the two ends.

The computer solution uses a direct stiffness method for the folded plate system. Compatibility at the interior flexible diaphragms or supporting frame bents is accomplished by a force (flexibility) method of analysis. The Goldberg-Leve equations are used to analyze the folded plate system. The flexible supporting frame bents are analyzed as two dimensional planar frames (thus they are assumed to be incapable of carrying loads normal to their own plane). A harmonic analysis with up to 100 non-zero terms of the appropriate Fourier series is used to approximate the loading. In the present examples only 50 non-zero terms were used resulting in a required computer time of about 4 to 6 minutes on the CDC6400 for the complete analysis of each case.

Output from the computer consists basically of the membrane forces, plate bending forces and displacements in the folded plate system and the axial forces, shear forces, bending moments and displacements in the two dimensional planar frame bents.

It should be emphasized that the analysis assumes the structure to be an uncracked homogeneous concrete system.

Description of Results for Each Case

Results for each of the 11 cases studied are presented in this report. For ease of reference, each case is broken down into 15 parts [in the original report figures, plus tables not shown here]. A description of these parts, which present the results of the analyses, is given below. Unless otherwise noted, only those parts dealing with cases 1 and 6 are shown.

Details regarding the physical dimensions are given in Parts 1 and 2 (Figs. B-5 through B-7). The specified loading used is shown in Parts 3 and 4 (Figs. B-9 through B-12).

The joint and element numbering for the folded plate system is shown in Part 5 (Figs. B-13 and B-14). In the program each plate element must be assumed to have constant properties in the longitudinal direction (thickness, modulus of elasticity and Poisson's ratio; E = 492,000 ksf μ = 0.15 were used in all cases).

The joint and element numbering system for the idealized planar frame bent is shown in Part6(Figs B-15 and B-16). For the 5 cell single-column bridge, the entire cross section was used in the analysis since loadings were not symmetrical about the longitudinal centerline. For the 9 cell double-column bridge, because of the symmetry of structure

and loading about the longitudinal centerline of the bridge, only one-half of the structure had to be analyzed. This permitted a large saving in the number of elements used and the computer time required for solution. Section properties consisting of the axial area, shear area and moment of inertia for the girder elastic axis are computed from its rectangular cross section while those for the column elastic axis from its circular cross section. Short vertical ficticious frame elements from the girder elastic axis to the points of assumed connection to the folded plate system are assigned a high value of modulus of elasticity (4.92×10^{11} ksf) to simulate rigid links.

Only selected results are described below although the computer output includes results for all the quantities mentioned in the description of the method of analysis.

The longitudinal variation of the moment M taken by each girder is shown in Part 7 (Figs. B-17 and B-18). A sum of the moments taken by all girders at a section should equal the total statical moment at that section. Each circled point represents information from the computer output. The moment M taken by an individual girder is obtained in the program by a special moment integration routine which sums the contribution of the longitudinal membrane stresses N_x times their lever arm to the cross section neutral axis and the longitudinal slab moments M_x. The contribution of N_x accounts for almost all of the moment M. Location of points of inflection for each girder can easily be found from this figure.

The integration of the longitudinal N_x membrane stresses over the bottom portion, top portion and the total cross section of the girders

is shown in Parts 8, 9 and 10 (Figs. B-19 through B-24). The last value represents the net axial force P in each girder, which is not zero, but if summed for all girders should equal zero.

The values of vertical shear transmitted by each girder at its point of inflection are obtained by integrating numerically the membrane shears N_{xy} in each vertical girder web. The vertical shears associated with slab bending in the top and bottom slabs are neglected as being small. The calculations are not included as part of the program and must be done by hand if desired.

A free body of the portion of the bridge structure between the inflection points on either side of the bridge bent is shown in Part 11. All cases are included, in Figs. B-25 through B-35. A statics check for vertical forces is made by summing the applied downward vertical loads plus the shears from the girders and comparing this sum with the computer output vertical reaction at the bottom of the bridge bent. The check is good in all cases recognizing that the small contribution of the slab shears mentioned in the preceding paragraph are neglected. This Part 11 also gives a visual picture of how the girder shears are distributed across the width of the bridge.

The magnitude and direction of the interaction forces between the folded plate system and the bent, acting on the bent, are shown in Part 12. Again, all cases are included, in Figs. B-36 through B-46. Note that a horizontal, vertical and rotational connection was specified and these are on the rectangular bent girder. Again a statics check was made to verify that the sum of the interaction forces equalled the output reaction at the base of the column bent and good agreement was found.

The values of P, V, M in each girder and column frame element as output by the computer are shown in Part 13 (Figs. B-47 and B-48). Part 14 (Figs. B-49 through B-52) for cases 1, 4, 6 and 10 respectively graphically illustrates that the computer output should be plotted to make a proper estimate of actual bent girder moments which would exist if a continuous interaction were used instead of the discretized system needed in the computer program.

For both the single-and double-column bridge cases 1 to 11, Part 15 (plus Table 2 in the original text), and for the double-column bridge 6 to 11 only, Part 17 (plus Table 3 in the original text), give an indication of how the total maximum transverse moment in the bent is shared by the rectangular bent girder cross section and the top and bottom slabs of the folded plate system. Part 15b and Part 17b show the distribution of the transverse membrane stresses N_y (kips/ft) in the top and bottom slab. Note how they damp out rapidly in most cases by the time they get to a transverse line 22.5 ft. in a longitudinal direction from the bent transverse centerline. The three dimensional free body diagrams shown in Part 15c and Part 17c depict all the internal transverse horizontal forces and moments contributing to the balancing of the external moment produced by the appropriate external forces which can be taken from Part 11. T slab and C slab are obtained by integrating the N_y values in Part 15b and Part 17b. P girder and M girder, acting on the rectangular section are obtained from the frame bent output shown in Part 13. The H forces are obtained by suitably integrating the membrane shears in the top and bottom slabs which are given in the output. Parts 15 and 17 are shown for cases 1, 4, 6 and 10 in Figs B-53 through B-56 and in Figs. B-59 and B-60.

For the two column bridge cases 6 to 11 only, Part 16 illustrates the relative participation of the bent girder, Part 16e, and the horizontal C, T and H forces of the folded plate system, Part 16f, in carrying the total transverse bending moment, Part 16d along the width of the bridge. The values in Part 16d are obtained directly by applying statics to the total forces acting on the free body of Part 11 shown in a transverse elevation view in Part 16a. The values in Part 16e, representing the moment by the bent girder, are taken directly from Part 14. The values in Part 16f, representing the moment taken by the C, T and H forces of the folded plate system, are found simply by subtracting the values in Part 16e from those in Part 16d. Part 16 is shown for cases 6 and 10 in Figs. B-57 and B-58 respectively.

Summary of Results

A summary of certain pertinent results for all cases is given in Table B-2. Col. (1) gives the case number.

Cols. (2) through (10) consider total values for the full bridge width for the single-column bridge cases 1 to 5 and for the half bridge width (because of symmetry about the longitudinal centerline) for the double-column bridge cases 6 to 11.

As shown in Fig. B-3 and in Table B-2, Cols (2), (3), (4) give respectively the concentrated load F (kips) at the central bent, the uniformly distributed bridge load w (kips/ft) and the total load on the bent plus bridge (kips).

Col. (5) gives the total central bent column reaction from Fig. B-3 determined by treating the bridge as a one dimensional frame in the longitudinal direction. Col. (6) gives the output from MUPDI-3 for the

TABLE B-2 SUMMARY OF RESULTS

Case	Conc. Bent Load F (kips)	Distr. Bridge Load w (kips/ft)	Total Load on Bent + Bridge (kips)	Total Bent Column Reaction: Prgm Analysis (kips)	Total Bent Column Reaction: MUPDI-3 (kips)	Applied Load + Shears in Part 11 (kips)	Total Longitudinal Midspan Moments: Prgm Analysis (kip-ft)	Total Longitudinal Midspan Moments: MUPDI-3 From Int. Stresses (kip-ft)	Total Longitudinal Midspan Moments: MUPDI-3 From Ext. Reactions (kip-ft)	Transverse Moments in Bent From MUPDI-3: Int.M^B Girder (kip-ft)	Transverse Moments in Bent From MUPDI-3: Int.M^B Total (kip-ft)	Transverse Moments in Bent From MUPDI-3: Ext.M^B Total (kip-ft)	Transverse Moments in Bent From MUPDI-3: Int.M^B Girder (kip-ft)	Transverse Moments in Bent From MUPDI-3: Int.M^B Total (kip-ft)	Transverse Moments in Bent From MUPDI-3: Ext.M^B Total (kip-ft)
Single Column Bridge															
1	98	2.27	522	365	361.2	358.0	1200	1233	1241	877	1891	1870	508	882	913
2	64	1.58	449	282	280.8	283.0	800	822	827	808	1574	1556	350	1138	1231
3	32	0.79	374	121	120.4	122.4	400	411	418	616	1221	1174	286	948	988
4	135	9.13	1778	1165	1156.0	1145.0	4620	4737	4777	2759	5190	5196	45	315	244
5	98	2.27	522	365	358.9	358.0	1200	1268	1298	885	1964	1943	751	1986	1990
Double Column Bridge															
6	98	2.27	522	365	360.6	358.4	1200	1246	1254	626	1125	1119	309	822	913
7	64	1.58	449	282	279.6	283.9	800	822	824	193	322	296	350	1138	1231
8	32	0.79	374	121	119.5	143.3	400	411	418	96	163	150	286	948	988
9	32	0.79	374	121	121.0	118.0	400	398	400	434	811	804	45	315	244
10	99	7.81	1508	979	970.8	965.0	3960	4076	4145	1715	3109	3073	751	1986	1990
11	98	2.27	522	365	360.1	358.0	1200	1253	1265	648	1220	1214	309	779	797

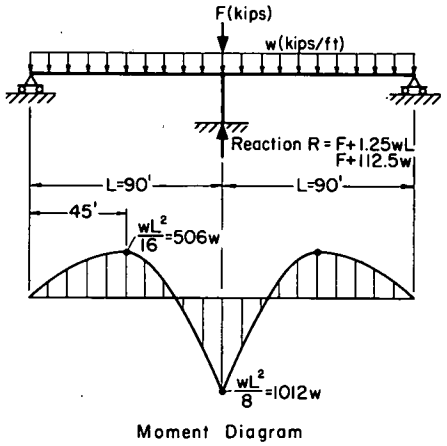

Fig. B-3 One-Dimensional Frame Analysis

central bent column reaction which should equal the value given in Col. (7) which is the total of the applied load plus shears on the free body diagram of Part 11 for each case. It can be seen that the check between Cols. (6) and (7) is quite good in all cases. Comparing the values in Cols. (5) and (6) it can be seen that a one dimensional frame analysis, Col. (5), adequately predicts the column reaction in the three dimensional system analyzed by MUPDI-3, Col. (6). The values in Col. (6) are slightly lower in all cases than those in Col. (5) reflecting the flexibility of the bent which is accounted for in MUPDI-3.

Cols. (8), (9), (10) give respectively the total longitudinal midspan moments (at x = 45 ft.) as obtained from a one dimensional frame analysis, Fig. B-3, as found automatically in MUPDI-3 by integrating the internal longitudinal stresses times their respective lever arms to the gross section neutral axis; and as found from the external reactions from MUPDI-3. For a perfect static check between internal and external moments by MUPDI-3, Cols. (9) and (10) should give identical values. It can be seen that this check is good. By comparing Col. (8) with (9) it can be seen that a one dimensional frame analysis gives a very good approximation of the total moment at a section in the three dimensional system analyzed by MUPDI-3. Of course, unlike MUPDI-3, the one dimensional frame analysis does not give any information on the transverse distribution of the total moment at a section of the bridge.

Cols (11) through (16) give information on the transverse moment in the bent structure at the two important sections indicated in Fig. B-4.

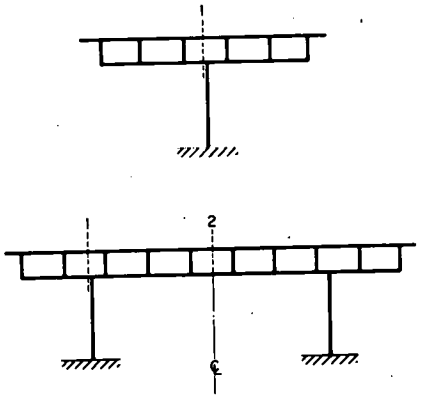

Fig. B-4 Sections for Transverse Moments in Bents

Cols. (11) amd (14) indicate the internal moments taken by the rectangular bent girder alone shown in Parts 15 and 17 for each case. Cols. (12 and (15) give the total internal moment taken by the combined bent girder -folded plate system shown in Parts 15 and 17. Cols. (13) and (16) give the total external moments acting on the same combined system as calculated from the applied loads. The check between total internal and external moments is quite good in almost all cases. Comparing Cols. (11) and (12), it can be seen the girder alone carries roughly only about 50% of the total internal moment at Section 1 for all cases, the balance being carried by the folded plate system. Comparing Cols. (14) and (15), the girder alone carries even a smaller percentage of the total moment at Section 2 and the percentage appears to vary depending on the type and distribution of loading.

B-15

B-16

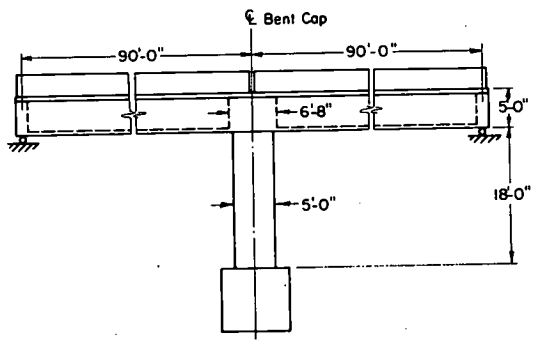

Fig. B-5 Cases 1-5, Part 2, Single-Column Bridge Elevation

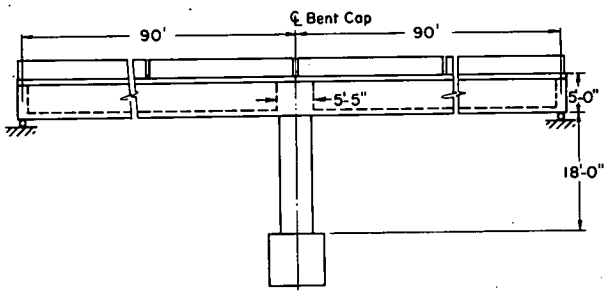

Fig. B-7 Cases 6-11, Part 2, Double-Column Bridge Elevation

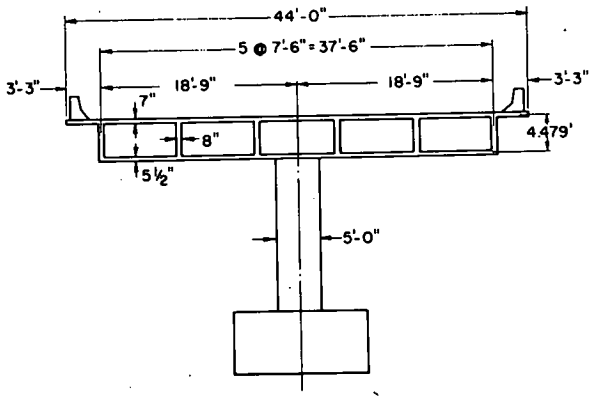

Fig. B-6 Cases 1-5, Part 2, Single-Column Bridge Cross Section

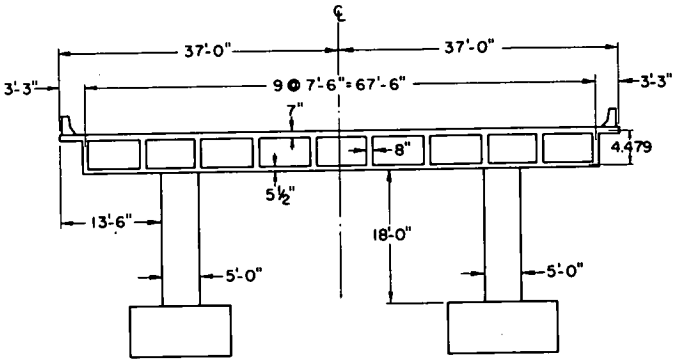

Fig. B-8 Cases 6-11, Part 2, Double-Column Bridge Cross Section

B-17

B-18

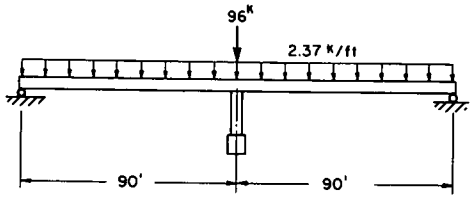

Fig. B-9 Case 1, Part 3, Loading Elevation

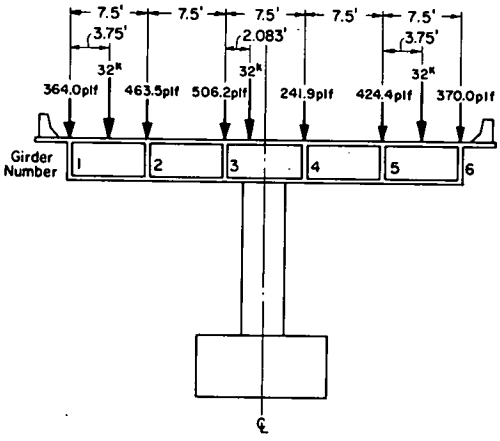

Fig. B-10 Case 1, Part 4, Loading Cross Section

B-20

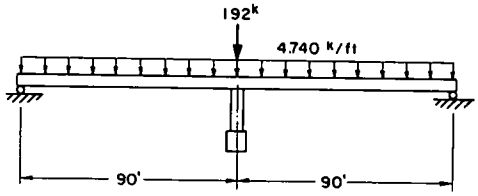

Fig. B-11 Case 6, Part 3, Loading Elevation

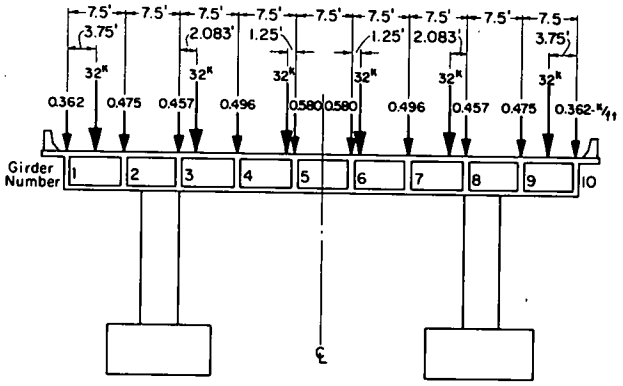

Fig. B-12 Case 6, Part 4, Loading Cross Section

B-21

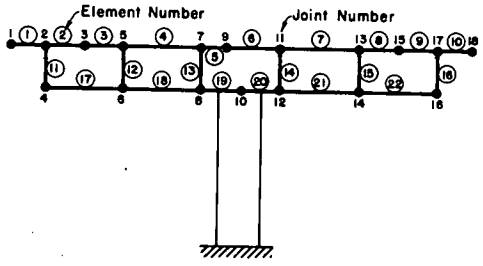

Fig. B-13 Case 1, Part 5, Joint and Element Numbering in the Folded Plate System

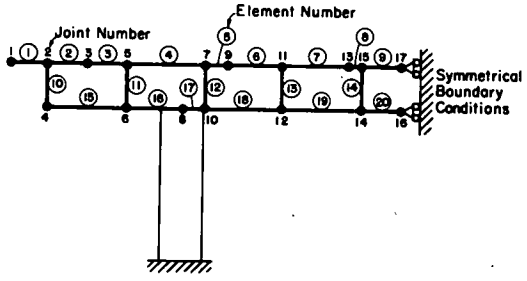

Fig. B-14 Case 6, Part 5, Joint and Element Numbering in the Folded Plate System

B-22

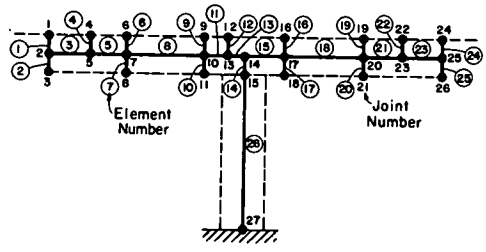

Fig. B-15 Case 1, Part 6, Joint and Element Numbering in the Idealized Frame Bent

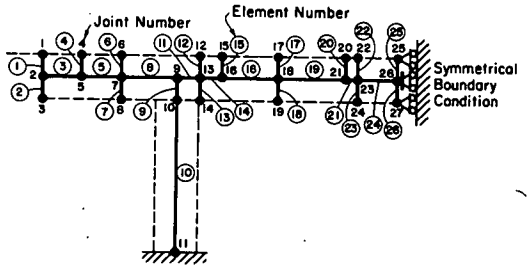

Fig. B-16 Case 6, Part 6, Joint and Element Numbering in the Idealized Frame Bent

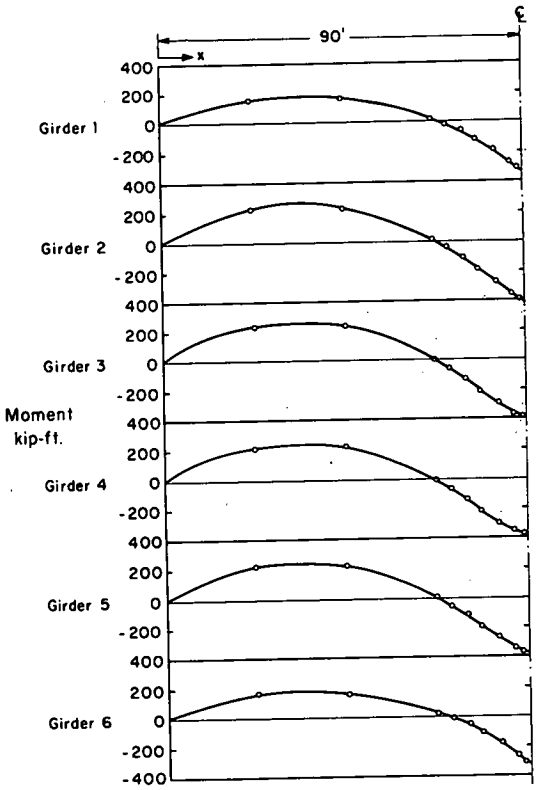

Fig. B-17 Case 1, Part 7, Longitudinal Variation of Moment M Taken by Each Girder

B-23

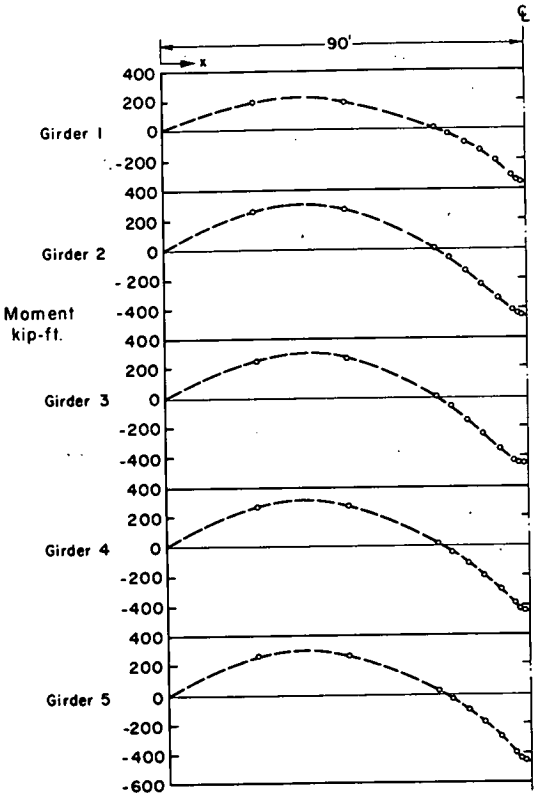

Fig. B-18 Case 6, Part 7, Longitudinal Variation of Moment M Taken by Each Girder

B-24

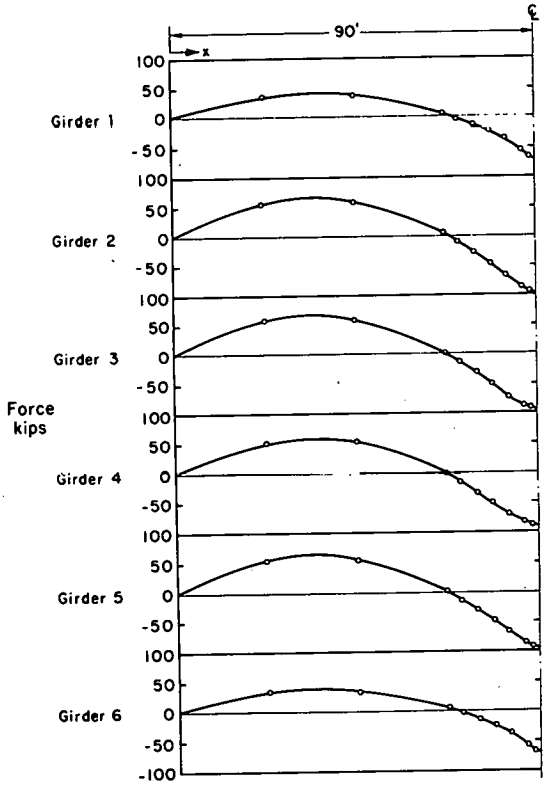

Fig. B-19 Case 1, Part 8, Longitudinal Forces in the Bottom Portions of Girders

B-25

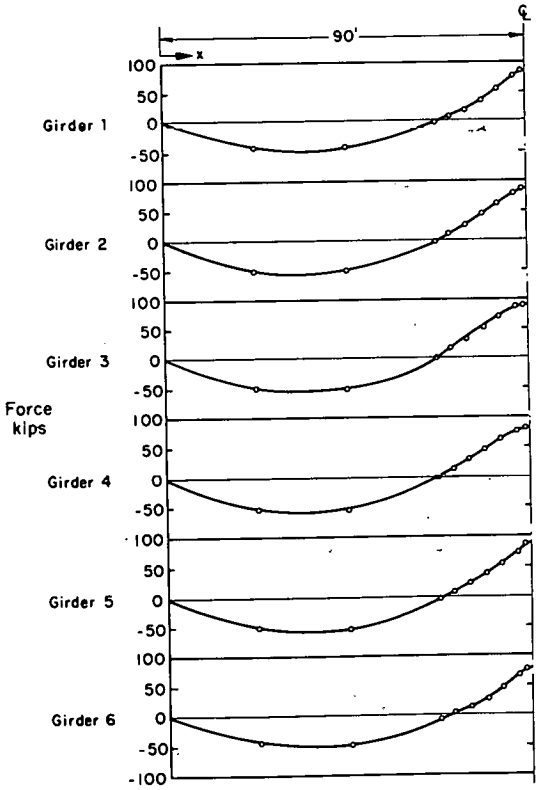

Fig. B-20 Case 1, Part 9, Longitudinal Forces in the Bottom Portions of Girders

B-26

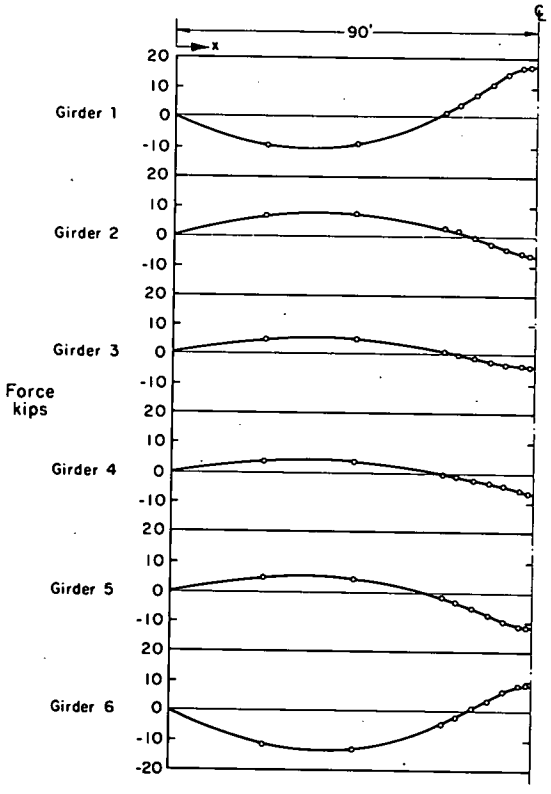

Fig. B-21 Case 1, Part 10, Net Axial Forces P in Each Girder

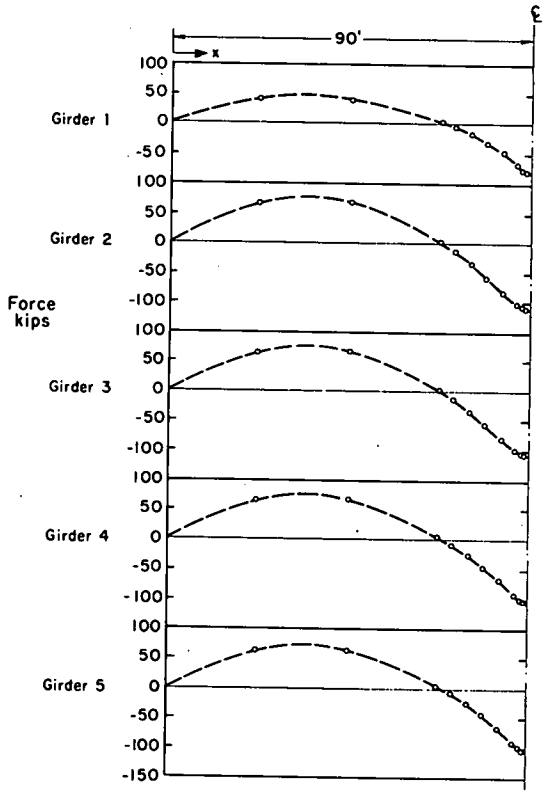

Fig. B-22 Case 6, Part 8, Longitudinal Forces in the Bottom Portions of Girders

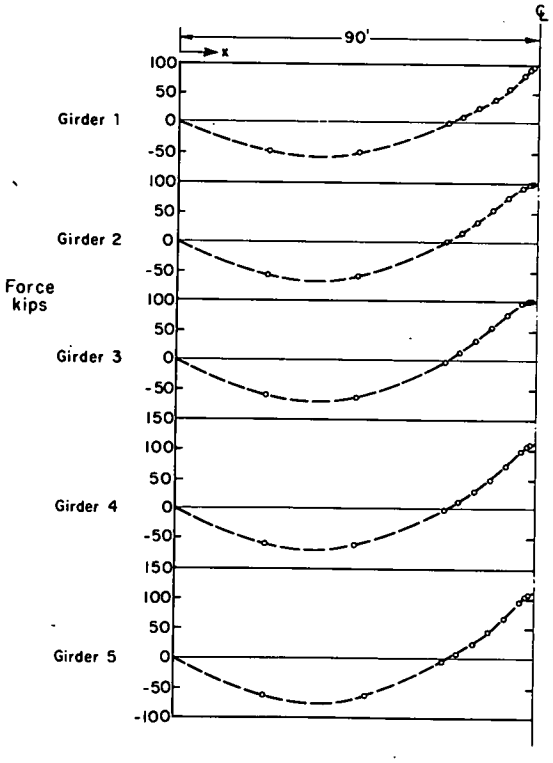

Fig. B-23 Case 6, Part 9, Longitudinal Forces in the Top Portions of Girders

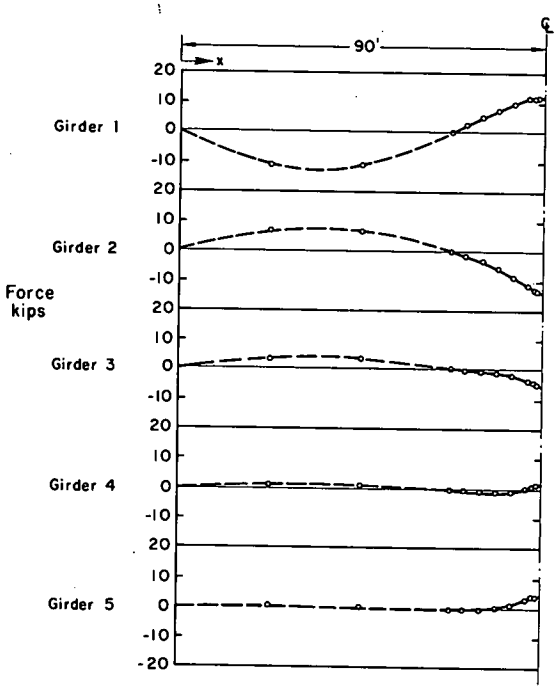

Fig. B-24 Case 6, Part 10, Net Axial Forces P in Each Girder

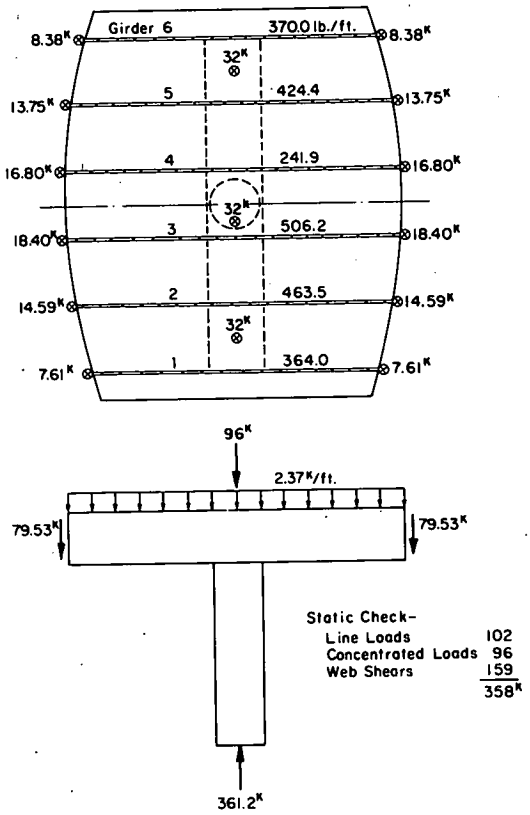

Fig. B-25 Case 1, Part II, Forces Acting on the Bent and the Adjacent Portion of the Bridge

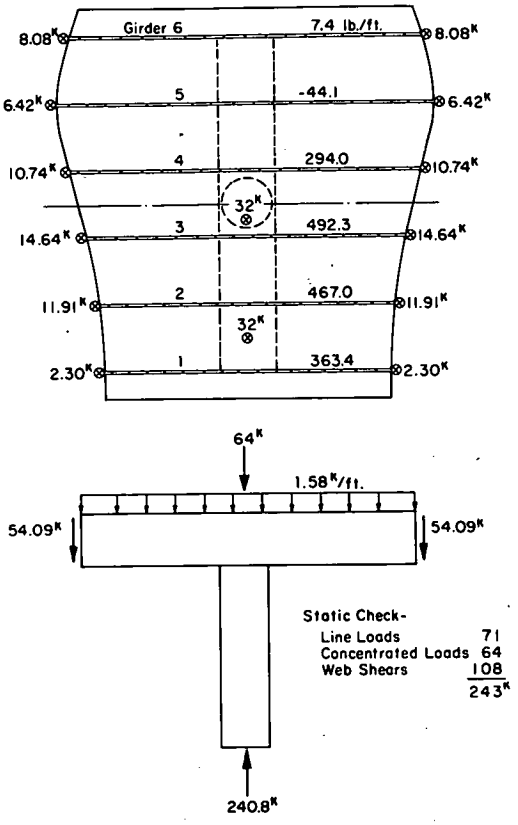

Fig. B-26 Case 2, Part II, Forces Acting on the Bent and the Adjacent Portion of the Bridge

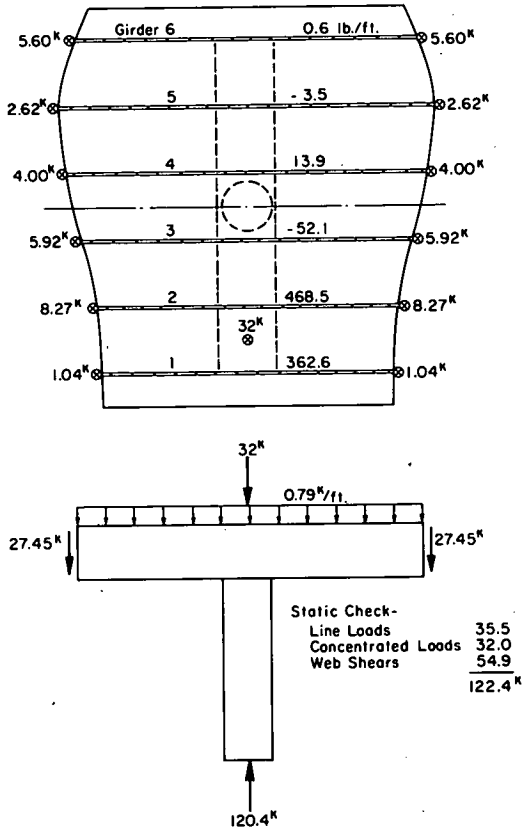

Fig. B-27 Case 3, Part II, Forces Acting on the Bent and the Adjacent Portion of the Bridge

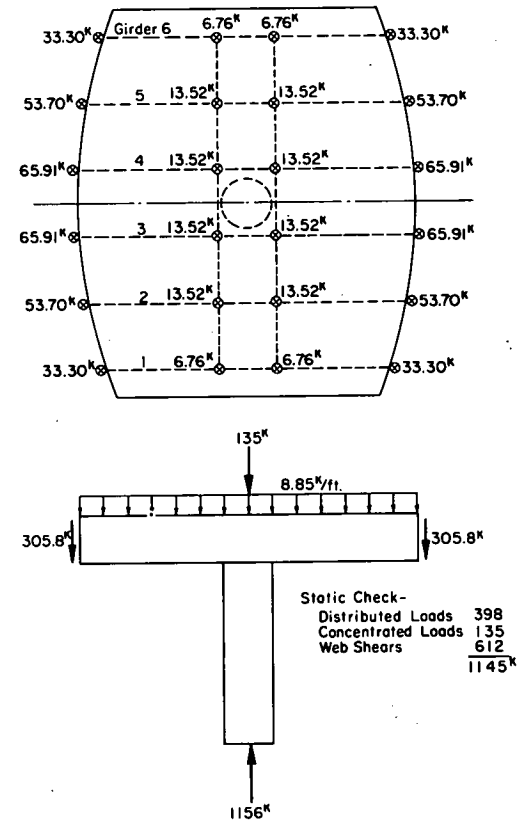

Fig. B-28 Case 4, Part II, Forces Acting on the Bent and the Adjacent Portion of the Bridge

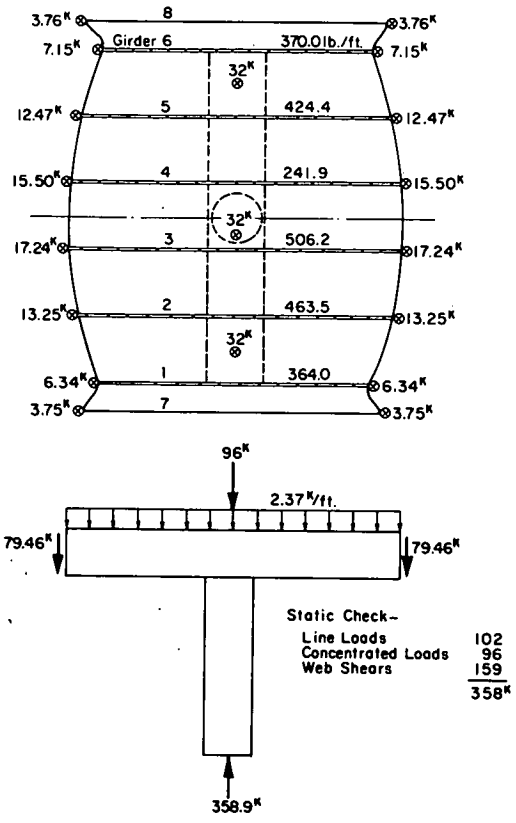

Fig. B-29 Case 5, Part 11, Forces Acting on the Bent and the Adjacent Portion of the Bridge

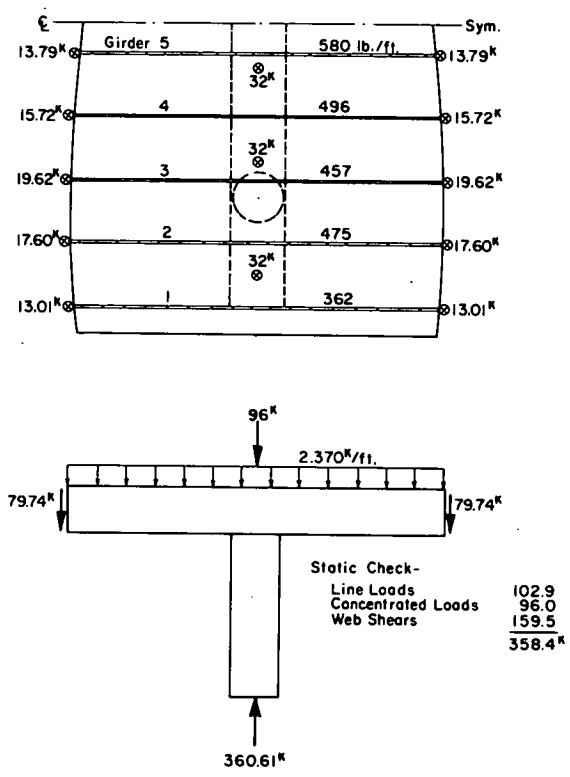

Fig. B-30 Case 6, Part 11, Forces Acting on the Bent and the Adjacent Portion of the Bridge

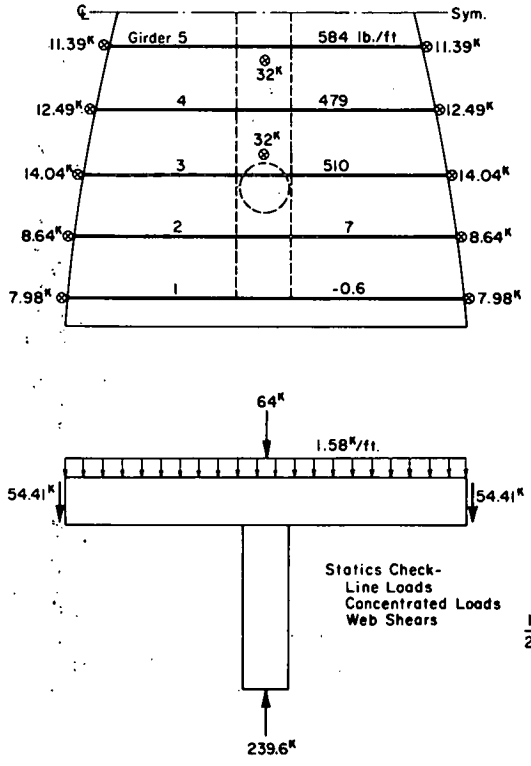

Fig. B-31 Case 7, Part 11, Forces Acting on the Bent and the Adjacent Portion of the Bridge

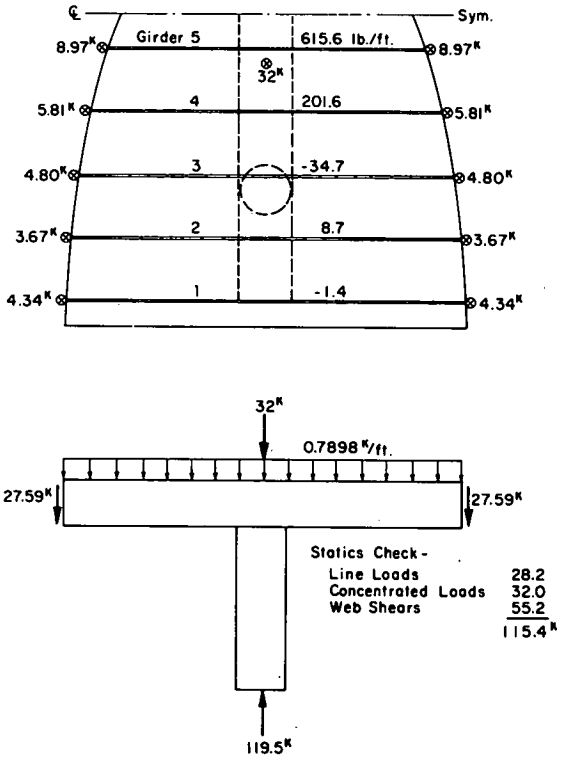

Fig. B-32 Case 8, Part 11, Forces Acting on the Bent and the Adjacent Portion of the Bridge

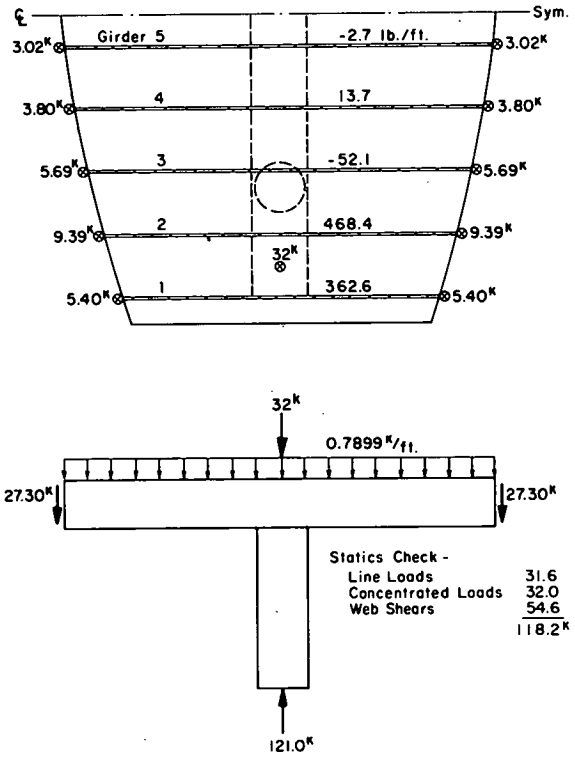

Fig. B-33 Case 9, Part 11, Forces Acting on the Bent and the Adjacent Portion of the Bridge

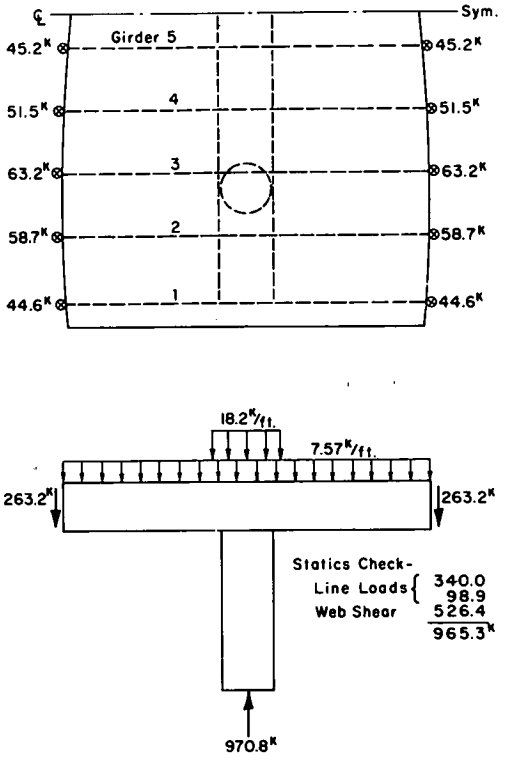

Fig. B-34 Case 10, Part 11, Forces Acting on the Bent and the Adjacent Portion of the Bridge

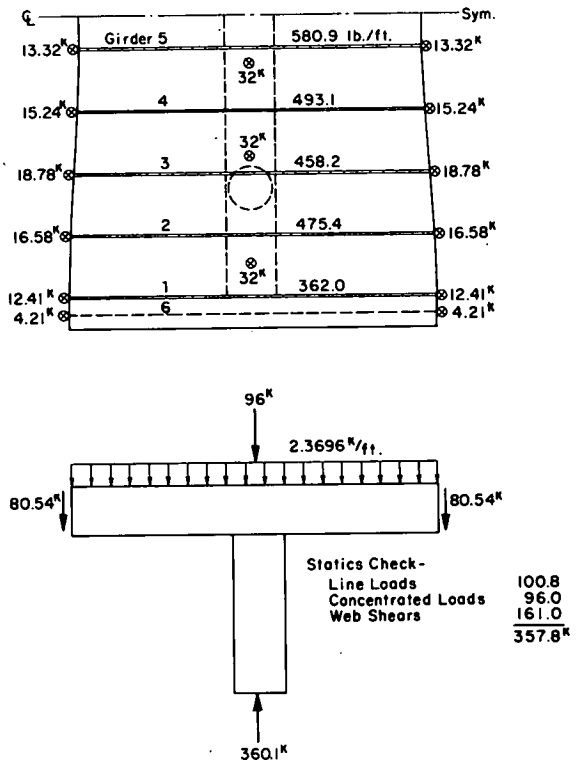

Fig. B-35 Case 11, Part 11, Forces Acting on the Bent and the Adjacent Portion of the Bridge

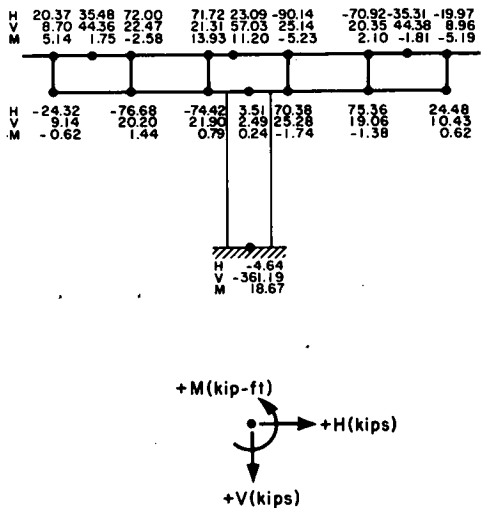

Fig. B-36 Case 1, Part 12, Forces Acting on the Bent

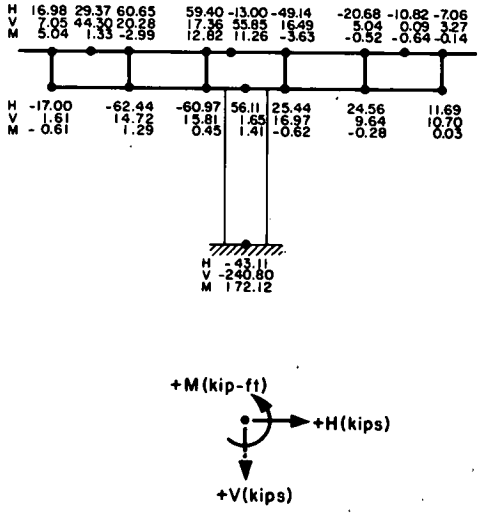

Fig. B-37 Case 2, Part 12, Forces Acting on the Bent

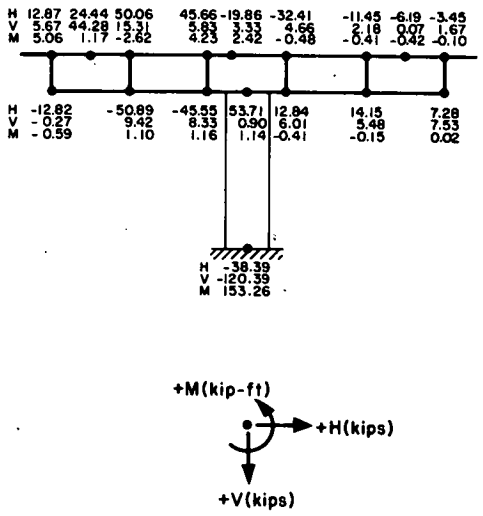

Fig. B-38 Case 3, Part 12, Forces Acting on the Bent

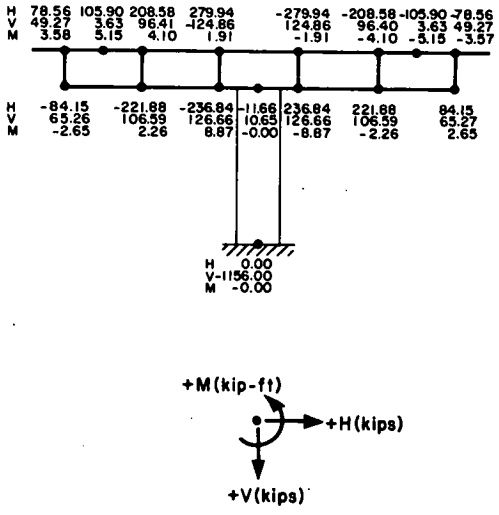

Fig. B-39 Case 4, Part 12, Forces Acting on the Bent

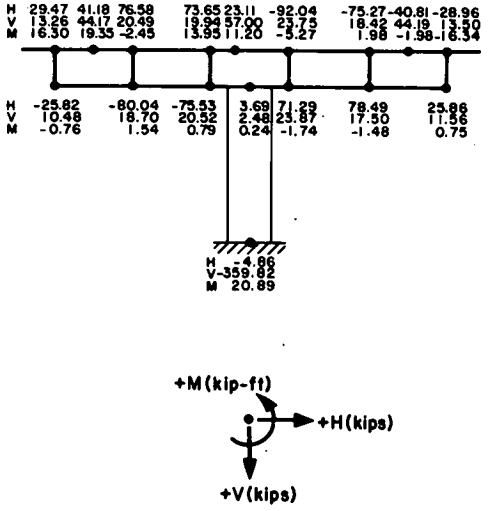

Fig. B-40 Case 5, Part 12, Forces Acting on the Bent

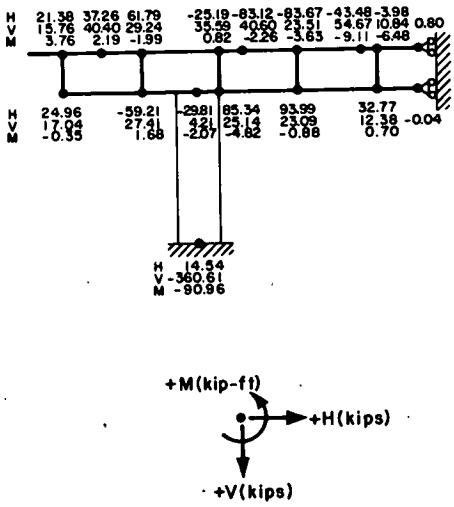

Fig. B-41 Case 6, Part 12, Forces Acting on the Bent

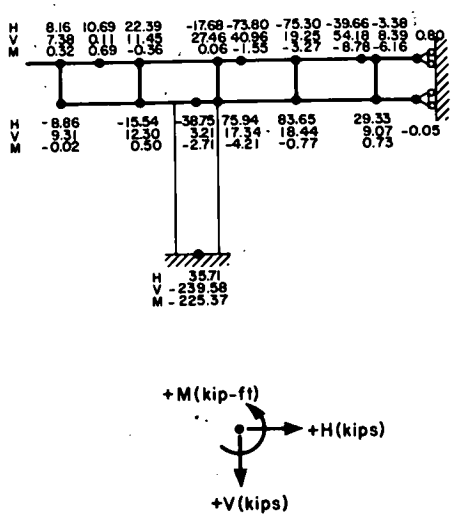

Fig. B-42 Case 7, Part 12, Forces Acting on the Bent

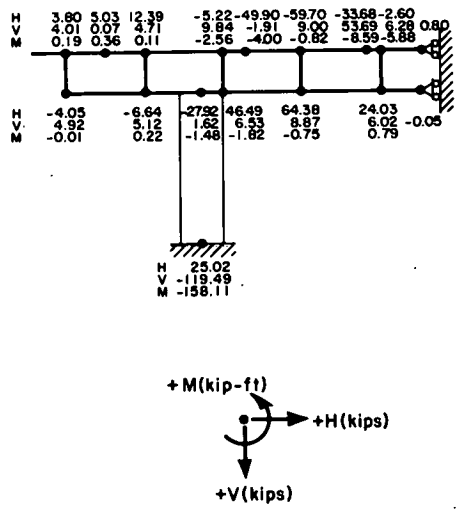

Fig. B-43 Case 8, Part 12, Forces Acting on the Bent

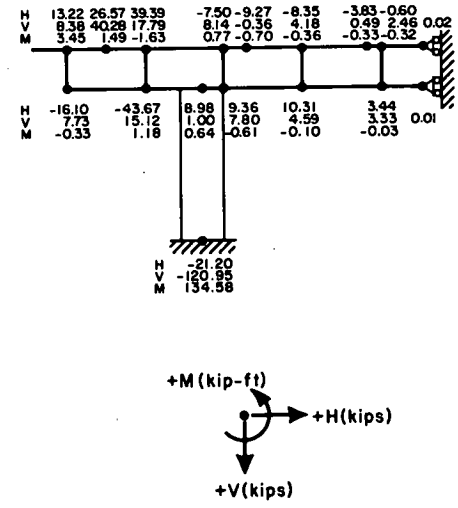

Fig. B-44 Case 9, Part 12, Forces Acting on the Bent

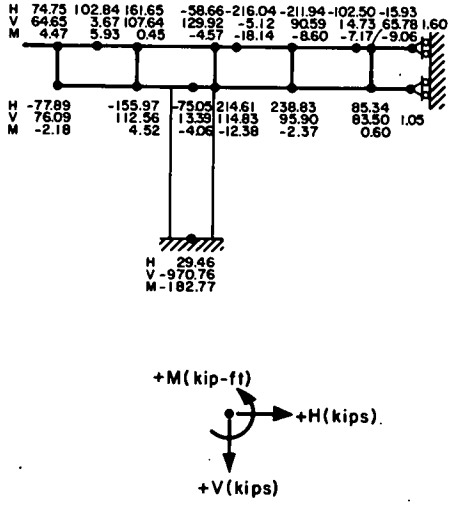

Fig. B-45 Case 10, Part 12, Forces Acting on the Bent

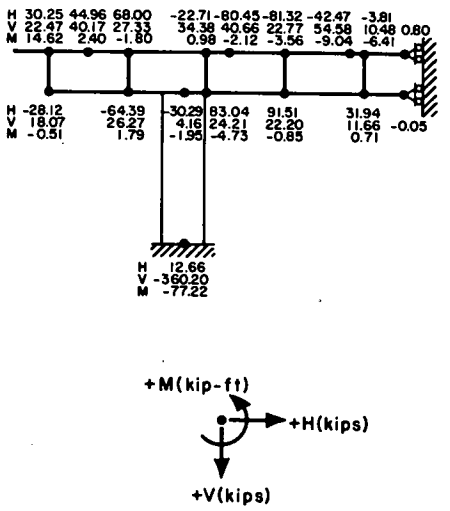

Fig. B-46 Case 11, Part 12, Forces Acting on the Bent

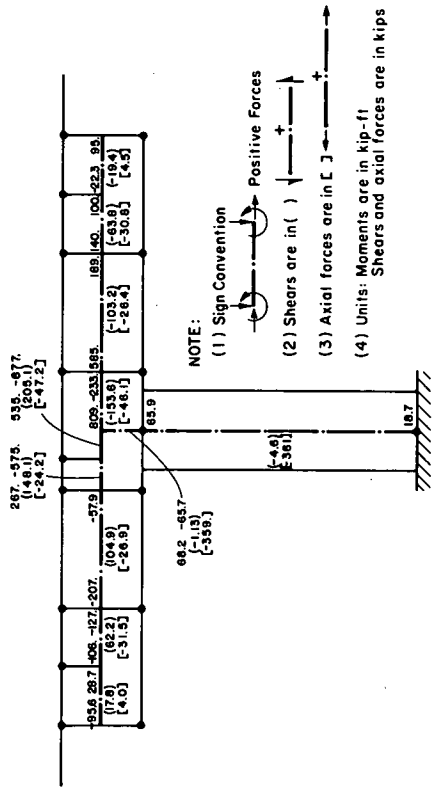

Fig. B-47 Case 1, Part 13, Moments Shears and Axial Forces in the Bent

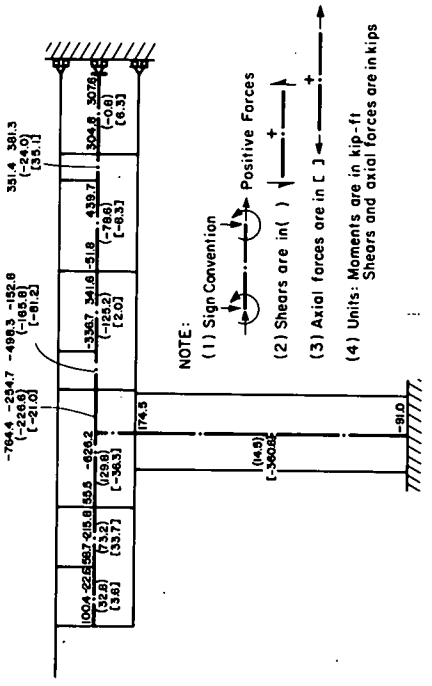

Fig. B-48 Case 6, Part 13, Moments Shears and Axial Forces in the Bent

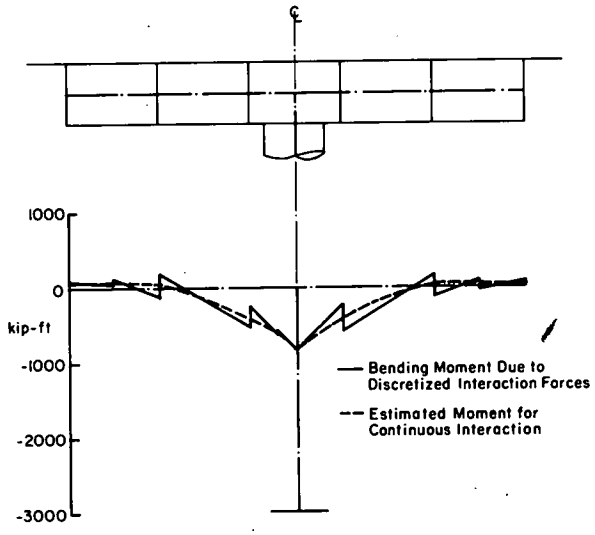

Fig. B-49 Case 1, Part 14, Bending Moments in the Bent Cap

B-55

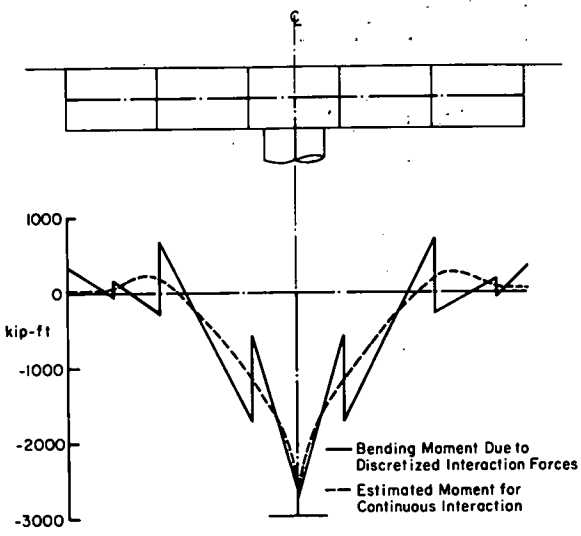

Fig. B-50 Case 4, Part 14, Bending Moments in the Bent Cap

B-56

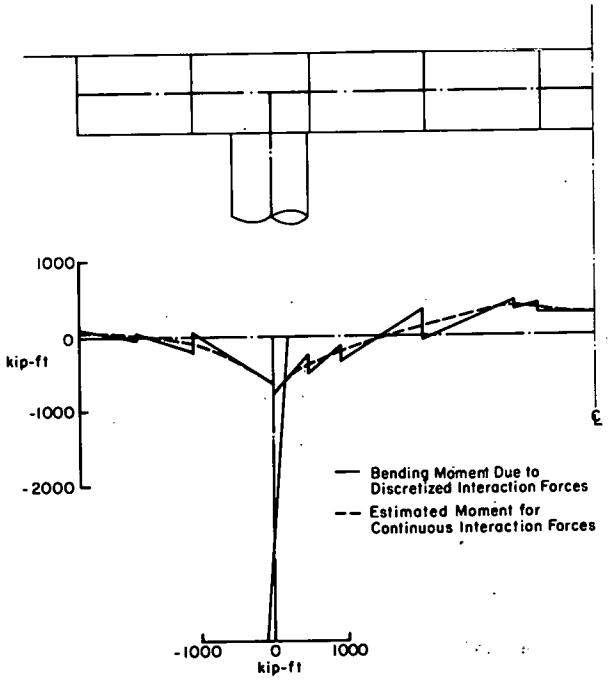

Fig. B-51 Case 6, Part 14, Bending Moments in the Bent Cap

B-57

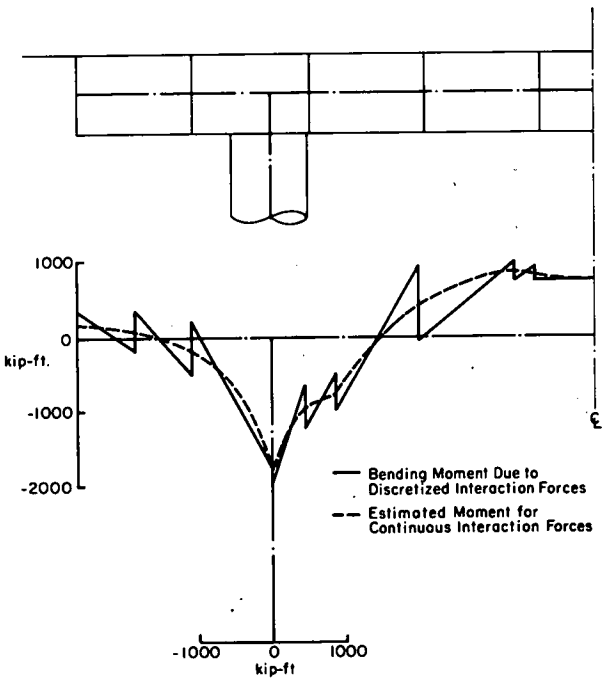

Fig. B-52 Case 10, Part 14, Bending Moments in the Bent Cap

B-58

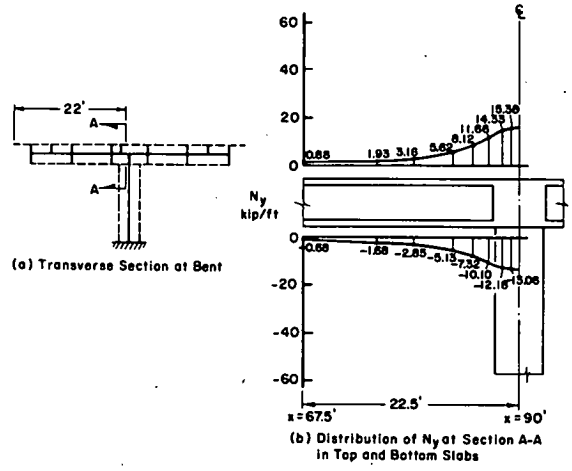

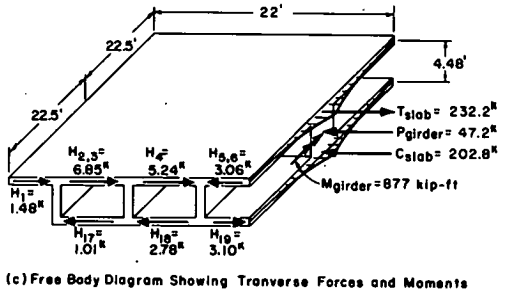

Fig. B-53 Case 1, Part 15, Distribution of Internal Total Transverse Moment in Bent Cap Plus Slabs at Centerline of Column

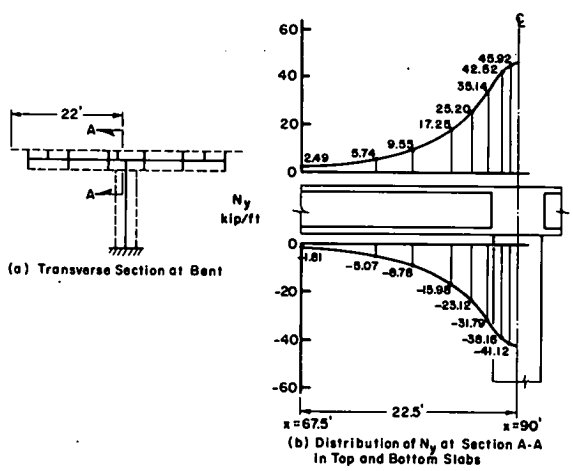

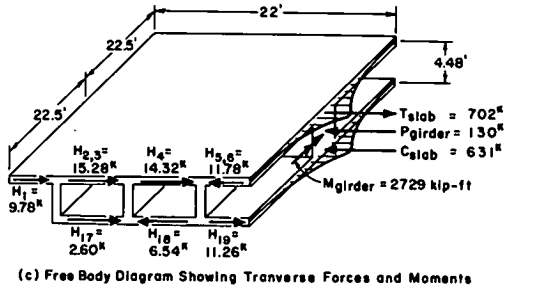

Fig. B-54 Case 4, Part 15, Distribution of Internal Total Transverse Moment in Bent Cap Plus Slabs at Centerline of Column

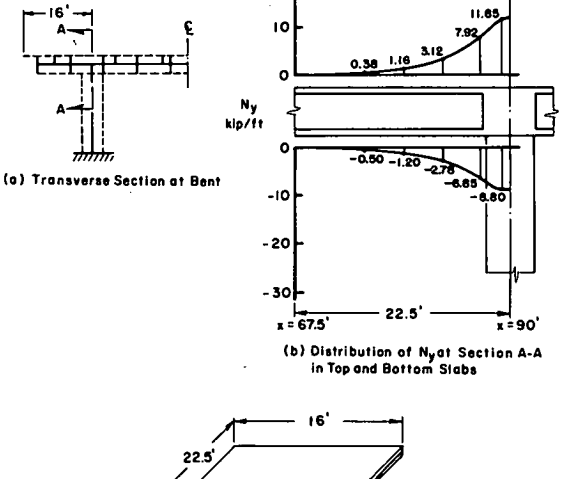

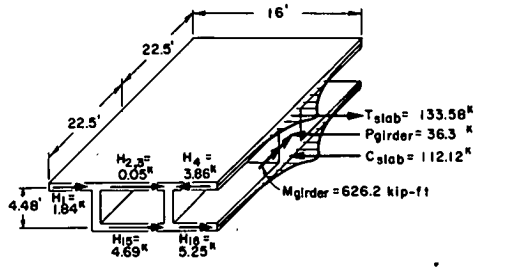

Fig. B-55 Case 6, Part 15, Distribution of Internal Total Transverse Moment in Bent Cap Plus Slabs at Centerline of Column

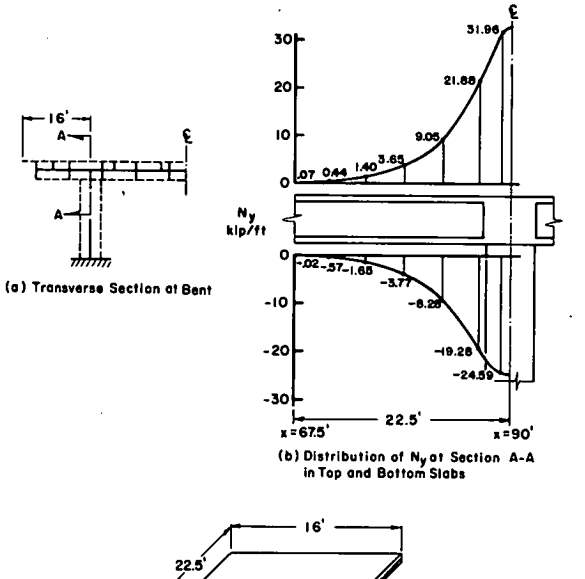

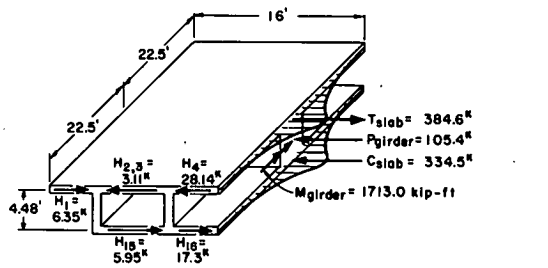

Fig. B-56 Case 10, Part 15, Distribution of Internal Total Transverse Moment in Bent Cap Plus Slabs at Centerline of Column

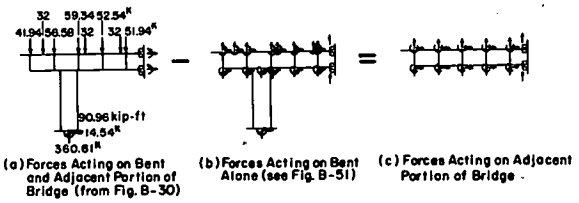

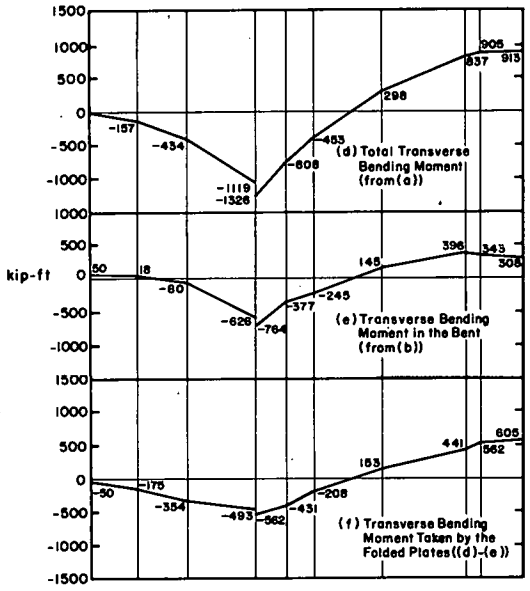

Fig. B-57 Case 6, Part 16, Distribution of Transverse Bending Moment between the Bent and the Folded Plates

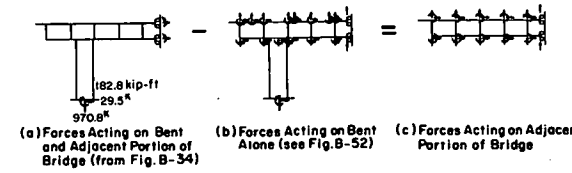

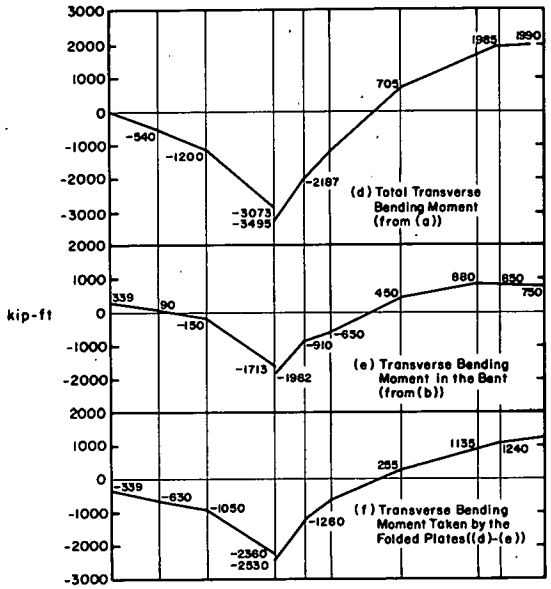

Fig. B-58 Case 10, Part 16, Distribution of Transverse Bending Moment between the Bent and the Folded Plates

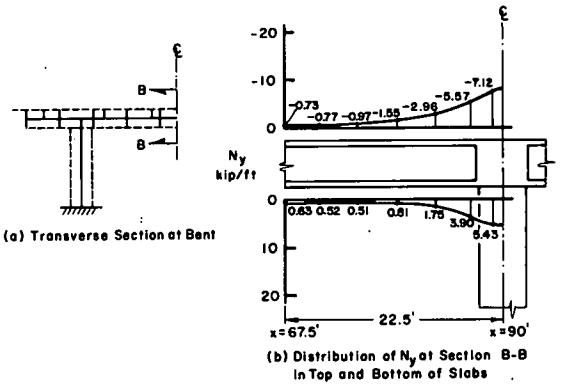

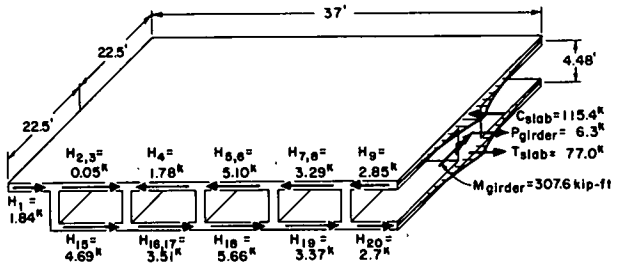

Fig. B-59 Case 6, Part 17, Distribution of Internal Total Transverse Moment in Bent Cap Plus Slabs at Centerline of Bridge

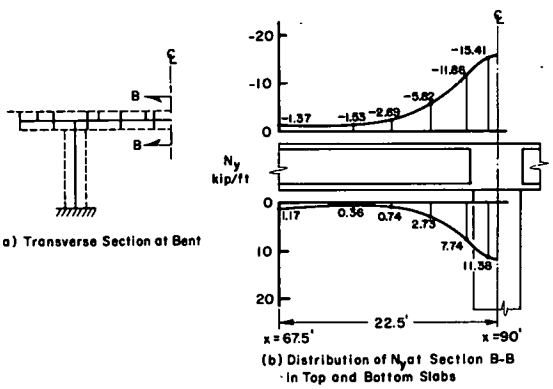

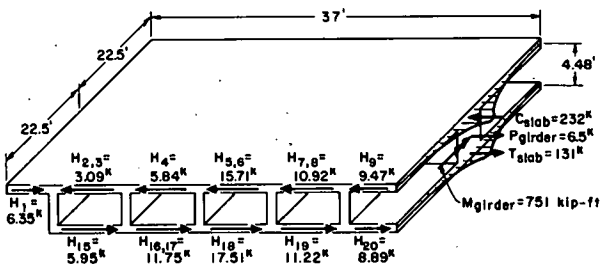

Fig. B-60 Case 10, Part 17, Distribution of Internal Total Transverse Moment in Bent Cap Plus Slabs at Centerline of Bridge

APPENDIX C

FINITE ELEMENT ANALYSIS OF A SINGLE-COLUMN MODEL BRIDGE BENT

by Paul P. Lynn and Santosh Arya*

This report presents the research work sponsored by the Portland Cement Association (PCA) on the finite element non-linear analysis of a single-column model bridge bent described in the working plan of NCHRP Project No. 12-10 (Supplement No. 1).

Introduction

Finite element methods, in a narrow sense, may be considered as modifications of the Rayleigh-Ritz method in the calculus of variations. Ordinarily, the physical body or the reinforced concrete structure is subdivided into an assemblage of a finite number of individual 2 or 3 dimensional elements which are inter-connected at a number of specified nodal points. To each of these elements trial functions for the unknown quantities of interest are defined in a piecewise manner over the assemblage. The constants appearing in the trial functions represent approximate values of the exact solution at the nodes of the elements. The total potential energy of the structure in terms of the element trial functions is then minimized to determine the constants.(31) After replacement of the physical structure by an assemblage of discrete elements, it is necessary to evaluate element stiffness properties. Thus, a successful modelling of the finite element is a vital step in any finite element analysis.

*Associate Professor of Civil Engineering and Graduate Research Assistant, respectively, University of Colorado, Boulder, Colorado

The finite element method has been successfully applied to structures with homogeneous and nonhomogeneous materials. However, in dealing with nonhomogeneous materials, the material properties under the one, two or three-dimensional loadings must be completely known to effect an accurate modelling of the structures. Earlier attempts in the reinforced concrete finite element analysis may be found in Ngo and Scordelis' paper.(33) An application was reported by Cervenka.(43) All these attempts have demonstrated the applicability of the finite element method in the field of reinforced concrete structural analyses. But, due to the lack of accurate reinforced concrete material properties, especially after cracking of concrete, the method is neither accurate nor practical for the practicing structural engineer.

The purpose of the investigation is to obtain a rational reinforced concrete finite element model based on the available properties of reinforcing steel, plain concrete, and slip in the bond between them. In the earlier finite element analysis of the bridge bent by Cervenka(44) the bond stress effect was neglected. Consequently, the steel reinforcement was called on to carry the entire tensile stress right after the onset of concrete cracking. This assumption led to excessively high tensile steel stresses. A careful investigation has revealed that through bond stress between concrete and steel, concrete does carry a considerable amount of tension even after cracking of the concrete. This has been verified experimentally by Peter(45) and Nilson.(34) Isenberg and Adham(37) have taken the bond effect into account in their finite element model with reason-

able success. In the present investigation, a new finite element is formulated which takes into account the cracking of concrete, yielding of steel, and bond slip behavior. A single-column model bridge bent is analyzed and the numerical results are compared with PCA's experimental data.

A Single-Column Model Bridge Bent

The objective of this study is to perform a finite element analysis of a single-column model bridge bent which was experimentally tested by PCA as part of their research program "Analysis and Design of Bridge Bents." The details of the single-column model bridge bent described in the working plan of NCHRP Project No. 12-10 (Supplement No. 1) are shown in Figs. C-1, C-2 and C-3. The main interest of the analysis is to model the bent cap and the column by the finite element method. The finite element idealization of the structure is shown in Fig. C-4 together with the loading considered. As can be seen from Figs. C-3 and C-4, the top and bottom rows of elements in the girder simulate the thicknesses of the top and bottom box girder slabs, respectively. This allows a simple modelling of the physical dimensions of the bent cap by taking the thickness of the elements according to Fig. C-3. The circular column is replaced by a stepped column without altering the steel bars as shown in Fig. C-4. The top and bottom main reinforcement is included in the corresponding elements, the intermediate elements only contain the steel ratios calculated by the actual girder stirrups as provided in Fig. C-2

Finite Element Model of the Reinforced Concrete

In developing the finite element model the uniaxial stress-

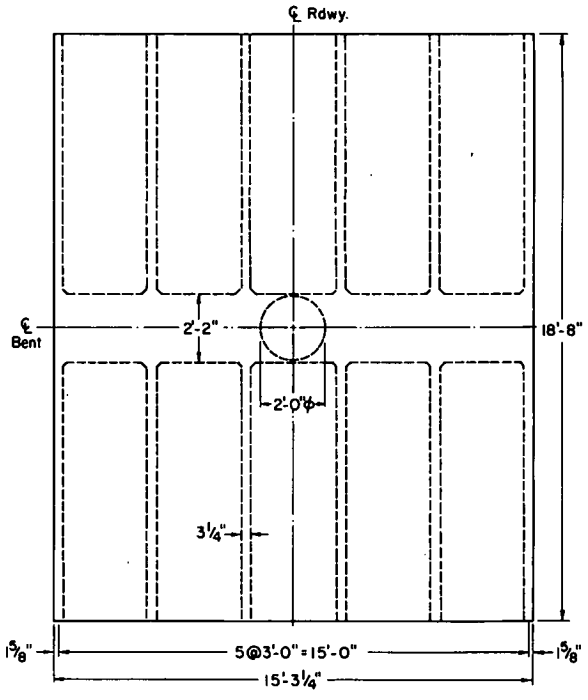

Fig. C-1 Top View of Single-Column Bent Cap

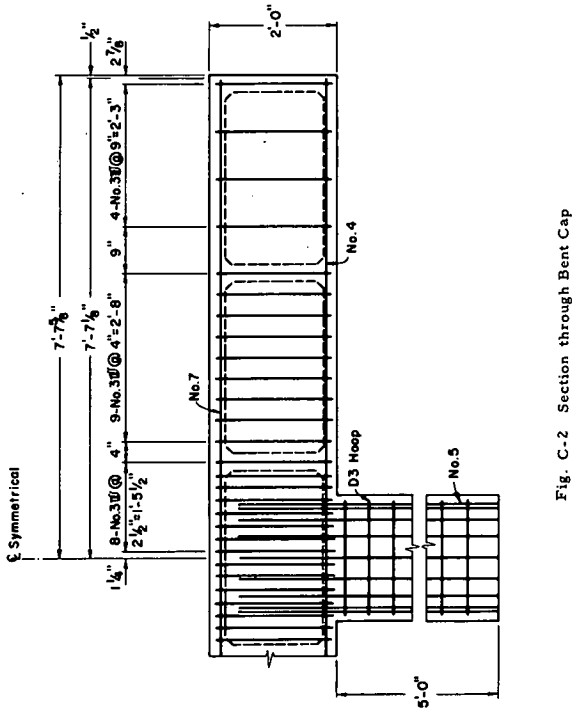

Fig. C-2 Section through Bent Cap

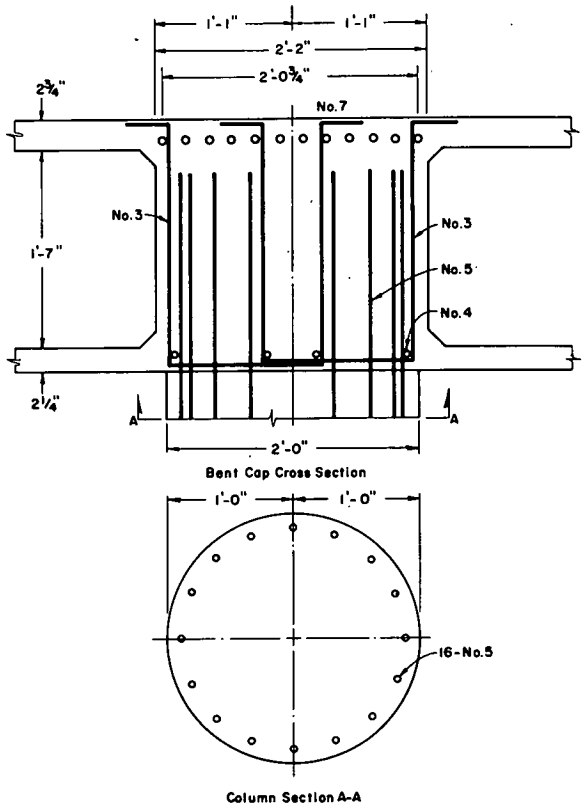

Fig. C-3 Bent Cap Girder and Column Cross Sections

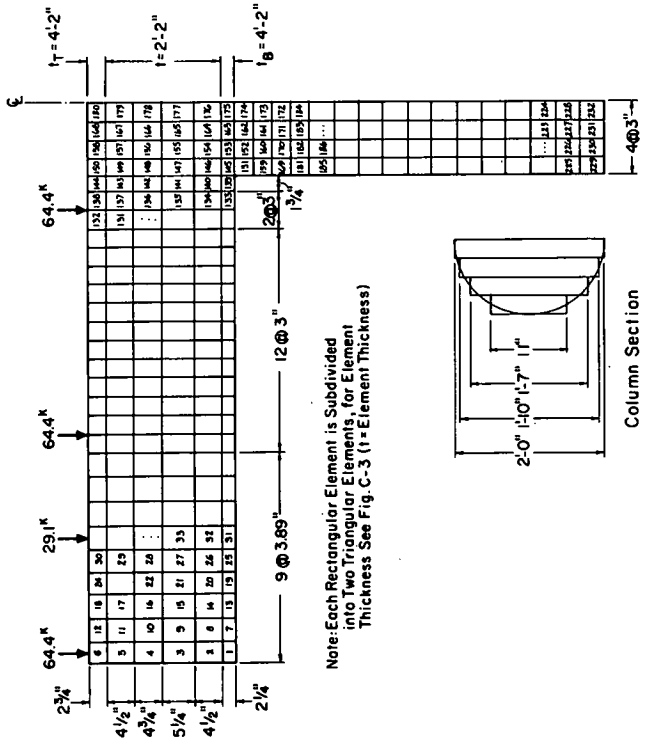

Fig. C-4 Finite Element Idealization of Single-Column Bent

strain relations for concrete and steel are assumed as shown in Fig. C-5. The composite reinforced concrete element is shown in Fig. C-6 together with the idealized composite stress-strain curve which covers three configurations, namely elastic uncracked, elastic cracked, and yielding of steel. This is denoted by the line 0-1-2-3. The other stress-strain curve 0-1-2'-2-3 was employed by Cervenka. In Cervenka's model the onset of concrete cracking is assumed to be the end of concrete tensile load carrying capability. However, it is evident that the uncracked portion of the concrete can still take some tension through the bond effect.

The main difference of the present finite element model and that of Cervenka is the consideration of additional amount of strain energy corresponding to the triangular area 1-2-2' in Fig. C-6. This additional strain energy represents the bond stress effect. Omission of this implies zero bond stress after the cracking of concrete. Under the assumptions described above three stages of reinforced concrete finite elements are formulated as follows:

1) Uncracked Element For the uncracked element with orthogonally placed reinforcing bars, the simple biaxial composite behavior based on the idea of transformed concrete section is used.

2) Cracked Element Without Yielding of Steel The behavior of the finite element in the cracked configuration corresponds to the line segment 1-2 as shown in Fig. C-6. When concrete principal tensile stress exceeds the ultimate concrete tensile stress ($f_t = 0.1\, f'_c$), the cracking of concrete occurs and the tangent modulus of elasticity is

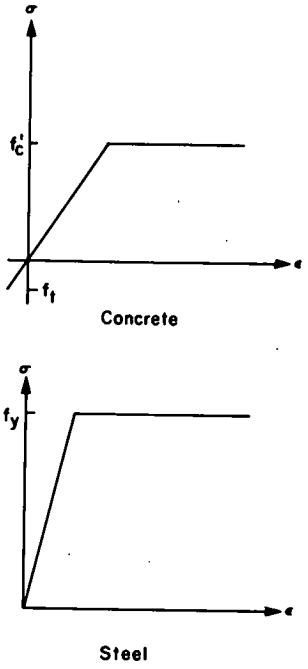

Fig. C-5 Uniaxial Stress-Strain Curves

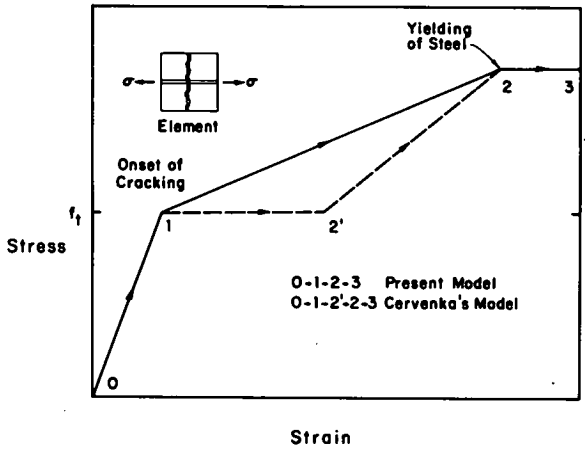

Fig. C-6 Uniaxial Stress-Strain Curve for Reinforced Concrete Cracked Element

modified according to Fig. C-6 (slope of line segment 1-2). This procedure recognizes the existence of the bond effect between concrete and steel. To formulate the composite biaxial stress-strain relations, the modified tangent moduli in x and y directions (E_x and E_y) are first obtained. These can be calculated from the state of stresses at points 1 and 2 (Fig. C-6). E_x and E_y are then substituted into the two-dimensional Hooke's law to yield the stress-strain relations. However, the composite shear modulus creates great difficulties, since its magnitude in the cracked element configuration is dependent on the crack width, aggregate interlock, and steel dowel action. Due to the lack of experimental study in this area, a simple averaging scheme is employed to obtain the composite shear modulus, G_{12}. The method is to average the uniaxial shear modulii in the x and y directions and apply a correction factor α which may be determined experimentally (See Eq. C-1)

$$G_{12} = \frac{1}{\alpha}\left[\frac{E_x}{2(1+\nu)} + \frac{E_y}{2(1+\nu)}\right] \qquad \text{(C-1)}$$

where ν is Poisson's ratio of the concrete.

3) Cracked Element With Yielding of Steel Upon the onset of yielding of the reinforcing steel, zero stiffness is assigned in the direction of the yielding reinforcement.

Based on the above three stages of reinforced concrete models a 6-degree of freedom plane stress triangular element is formulated (Fig. C-7). In the development of this finite element the following material properties, as provided by PCA, are used:

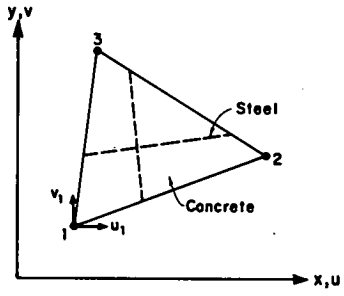

Fig. C-7 6 Degree of Freedom Triangular Element

Concrete

Modulus of elasticity	$E_c = 3.24 \times 10^6$ psi
Poisson's ratio	$\nu = 0.15$
Compressive strength	$f'_c = 3{,}500$ psi

Reinforcement

Modulus of elasticity	$E_s = 29 \times 10^6$ psi
Yield stress	$f_y = 60 \times 10^3$ psi

Finite Element Idealization of the Structure

Figure C-4 shows the finite element subdivision of the single-column model bridge bent. This idealization produces a total of 464 triangular elements with 534 total number of unknown nodal displacements. The ultimate live and dead loads on the bent cap girder caused by reactions of the box girders are idealized and converted to a set of equivalent nodal forces as shown in Fig. C-4.

Numerical Analysis

A computer program for the non-linear load incremental analysis was written for the finite element model described above. A brief flow chart of the program is given in Fig. C-8. Fourteen load increments were used to perform the non-linear analysis which required roughly 45 minutes of CP time on a CDC 6400 computer. The following two numerical analyses were performed:

Case 1. With the composite shear modulus factor $\alpha = 3$, the finite element non-linear analysis was carried out for 14 load increments. A plot of the end deflection of the bent cap versus load factor K is shown in Fig. C-9. The theoretical tensile steel stresses

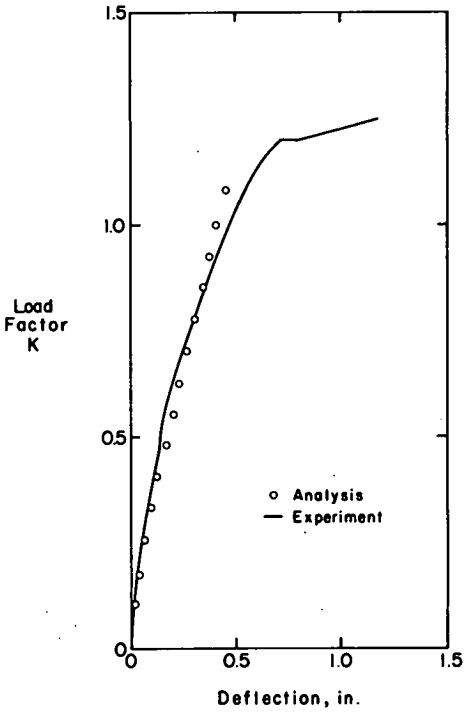

Fig. C-9 Deflection at End of Bent Cap

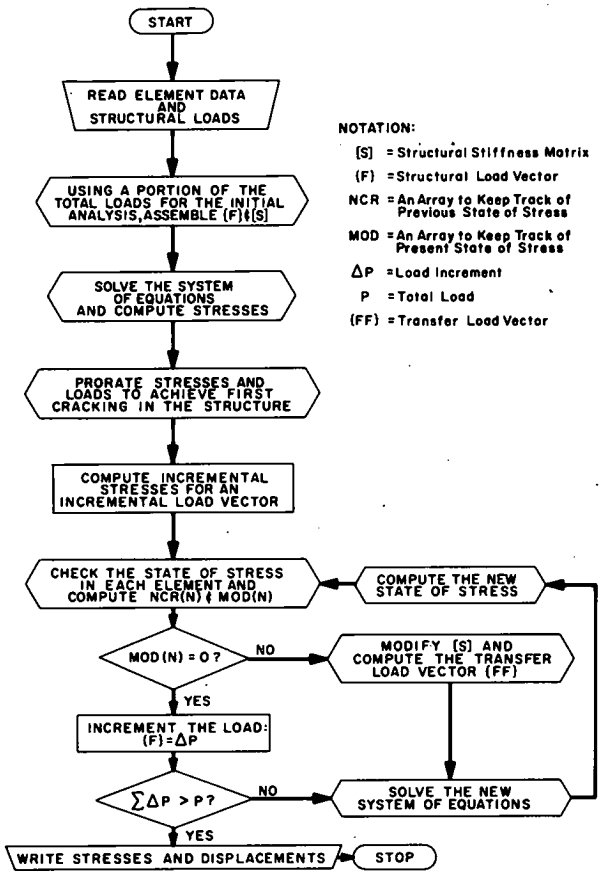

Fig. C-8 Flow Chart for Nonlinear Analysis of Reinforced Concrete Bridge Bents

along the top reinforcement are plotted against PCA's test results in Fig. C-10 for $K = 0.776$ and $K = 1.0$. The theoretical steel stress is defined as the line segment a-b as shown in Fig. C-11 which represents the experimental work carried out by Nilson[34] in the investigation of the bond slip behavior of the reinforced concrete. From Fig. C-10 it can be seen that the theoretical steel stresses agree with the test data reasonably well in the high stress region and disagree with the experimental data in the low stress region. This is due to the disagreement between the theoretical and actual steel stresses as shown in Fig. C-11 by the line segments a-b and a-c, respectively.

Case 2. A careful observation of Fig. C-11 shows that about 1/3 of the concrete stress (line segment b-c) must be transferred to the steel stress in any cracked element. In addition, due to extensive cracking of the bent cap, it was felt that the composite shear modulus correction factor α had to be increased. This increase corresponds to the recognition of progressive spreading and widening of cracks which result in the loss of the shear stiffness and transfer of loads to the steel reinforcement. Accordingly, another analysis was performed with $\alpha = 5$ and the modification of the steel stress mentioned earlier. The improved tensile stresses along the bent cap are plotted in Fig. C-12 for $K = 0.776$, $K = 1.0$, and $K = 1.224$. Dotted lines in Fig. C-12 represent the experimental results. Comparing Figs. C-10 and C-12, it can be observed that considerable improvement has been achieved. Fig. C-12 suggests that the yield stress of steel f_y used in the analysis should be 65 ksi instead of 60 ksi. This discrepancy accounts for somewhat lower steel stress prediction than the experimental result of the load level $K = 1.224$ as shown in Fig. C-12.

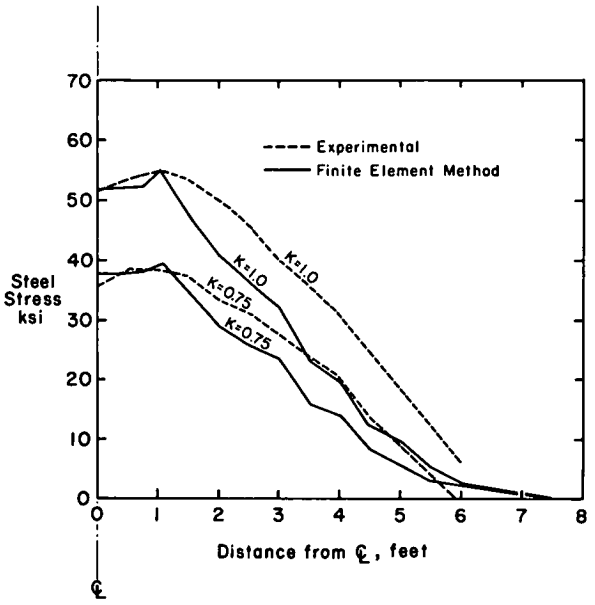

Fig. C-10 Tensile Stress in Top Reinforcement for α = 3

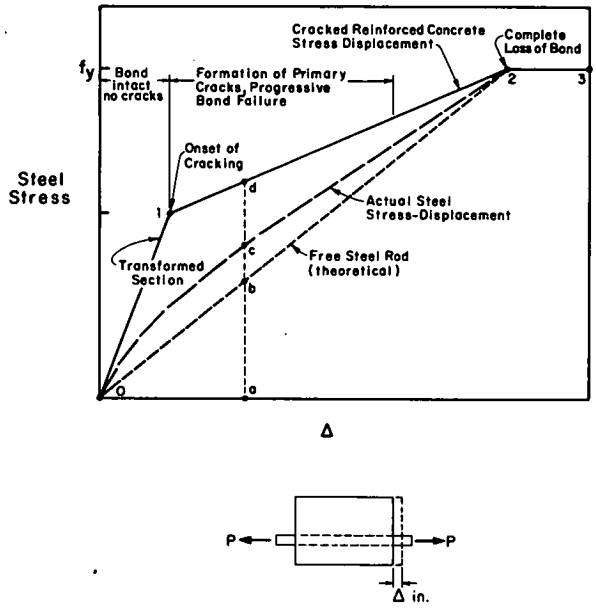

Fig. C-11 Nilson's Test

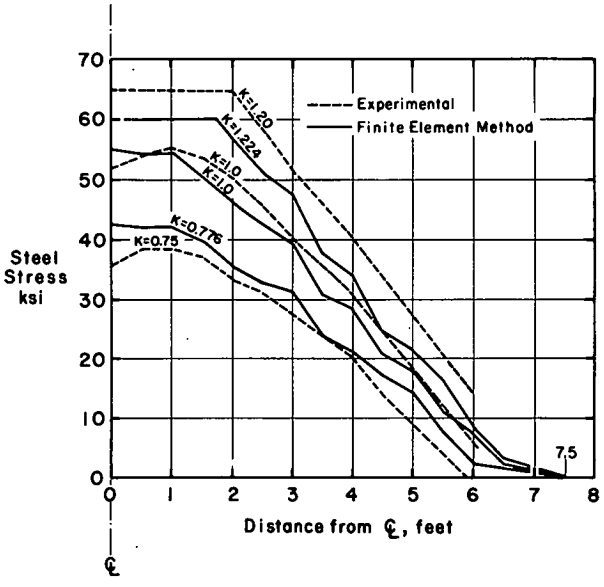

Fig. C-12 Tensile Stress in Top Reinforcement for α = 5

Crack patterns corresponding to the load levels K = 1.0 and K = 0.776 are shown in Fig. C-13.

Conclusion

This finite element analysis of the model bridge bent suggests that extensive basic experimental investigations are needed to formulate an accurate reinforced concrete finite element. The results of this study have demonstrated that the non-linear finite element analysis of reinforced concrete structures is feasible provided sufficient information on the composite action of steel and concrete is known. In the future, more work should be done in the areas of bond slip behavior and shearing rigidity of the cracked reinforced concrete.

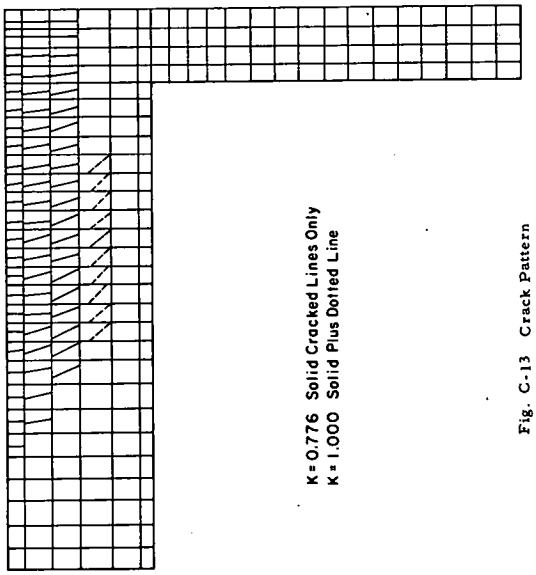

Fig. C-13 Crack Pattern

APPENDIX D

MODEL BRIDGE TESTS

Introduction

The loads carried to the bent cap by the superstructure in two representative box girder bridges designed by current methods were measured in tests of two reduced scale models. One model contained a single-column bent, the other a double-column bent.

Present design methods assume that the critical live load is transmitted directly to the bent cap without lateral distribution. If there is significant lateral distribution of load from more remote girders to those closer to the column, the present assumptions will be unconservative for girders close to the columns and conservative for the bent cap.

In addition to the distribution of load, behavior of the bent caps was also determined. However, more useful information concerning behavior was obtained from the tests on the bent cap models. This was partially due to the fact that the bent cap loading was better defined in the bent cap tests. In addition, bar cutoffs were not at optimum locations for easy interpretation of measurements in the bridge models.

The bridges were designed by Working Stress Methods of the AASHO Specifications[1]. As pointed out elsewhere in this report, the resulting structure has a required total load carrying capacity much greater than that specified by the Load Factor Method. The intrinsic difference in capacity should be kept in mind when making comparisons between results of the model bridge tests, designed by Working Stress Methods, and the model bent tests, designed by the Load Factor Method.

Design of Prototype Bridges

Specifications. The two prototype bridge designs that formed the basis for the bridge test portion of the program were designed in accordance with the Tenth Edition (1969) of the AASHO Standard Specifications for Highway Bridges[1]. The Manual of Bridge Design Practice[3] of the Bridge Department of the California Division of Highways was also used as a reference.

Dimensions, Loading and Materials. Dimensions of the bridges, shown in Figs. 3, 4 and 5, were selected to meet the requirements of the Project Statement. As required by the AASHO Specifications, the 40-ft. roadway of the single-column bridge was divided into three lanes, each 13-ft. 4-in. wide. Within each lane, a ten foot loaded width was placed in the most unfavorable position as shown in Fig. D-1. Following the same rules, the 70-ft. roadway of the double-column bridge was divided into six lanes, each 11-ft. 8-in. wide as shown in Fig. D-2. The required 23.3 percent impact factor is included in the loads shown.

The material properties listed in Table D-1 were used for the design. The allowable stresses, those given in the AASHO Specifications for the assumed materials, are not to be exceeded for the most unfavorable distribution of live loads.

Design. For the deck, 2 in. of cover was provided over the top reinforcement, and 1 in. of cover was provided under the bottom reinforcement.

The bridge was designed to accommodate parapets placed at the sides of the bridge. Each parapet weighed 483 lb. per ft. The controlling deck slab design moment of 5.1 kip-ft. per ft. occurred over the web

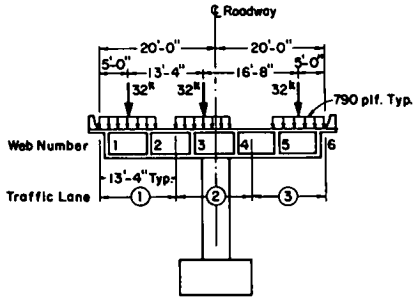

Fig. D-1 Lane Loads on Single-Column Bridge

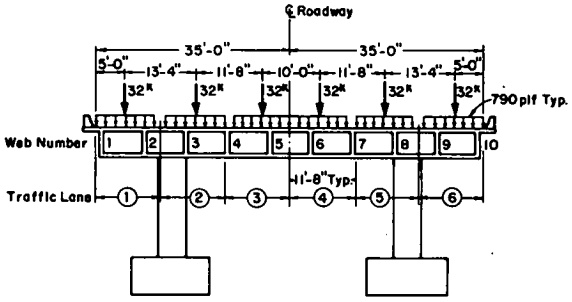

Fig. D-2 Lane Loads on Double-Column Bridge

TABLE D-1 MATERIAL PROPERTIES USED FOR BRIDGE DESIGN

Material	Modulus of Elasticity, E psi	Compressive Strength f'_c at 28 days psi	Yield Strength, f_y psi	Maximum Working Stress psi
Concrete	3,400,000	3500	-	1400
Reinforcement	29,000,000	-	60,000	24,000

of an interior girder. The 7-in. thick slab contained reinforcement amounting to 0.64 sq. in. per ft. of roadway for negative moment, and 0.53 sq. in. per ft. for positive moment. To satisfy the AASHO Specifications, distribution reinforcement of 67 percent of that required for positive moment was placed in the longitudinal direction (parallel to the span of the bridge) in the bottom of the slab. Temperature and shrinkage reinforcement of about 0.125 sq. in. per ft. was provided in the longitudinal direction in the top of the slab.

The thickness of the soffit was determined by the 5 1/2-in. minimum requirement of the AASHO Specifications. Required transverse and longitudinal bottom slab reinforcement was 0.5 percent and 0.4 percent, respectively.

Weight of the parapets was assumed equally distributed among all girders. In addition, 10 percent of the girder weight was added to the dead load for forms and details. As required by the AASHO Specifications, the number of lanes of AASHO live load applied to an interior girder was determined by dividing the girder spacing in feet by 14. This gives 0.535 lanes per girder. For an exterior girder, the fraction of lanes of live load was determined from $W_e/14$, where W_e is the width of an exterior girder. The impact factor was 23.3 percent.

Maximum positive moment of 1786 kip-ft. occured at 0.4 of the distance from the abutment to the central support when an HS 20-44 AASHO truck was on the bridge. Maximum negative moment, considered to be critical at a section one-half the column diameter from the centerline of the bent cap, was 2,400 kip-ft. This moment occurred when the HS 20-44 lane loading was applied. Fourteen and twenty No. 10

bars were selected for the positive and negative moment reinforcement respectively. A cross-section of a typical interior girder at the face of the bent cap is shown in Fig. D-3.

Design moments for the exterior girders were slightly less than those for the interior girders. Twelve and sixteen No. 10 bars were used for positive and negative moment reinforcement, respectively. In the exterior girder, six of the No. 10 bars for positive moment were extended into the bent cap, to function as compressive reinforcement in the region of negative moment. This made it unnecessary to thicken the bottom slab.

For resisting shear, the 8-in. interior girder webs were flared to 12-in. at the bent cap. The exterior girder webs were flared to 10 in. Along each web, No. 5 stirrups were spaced to satisfy the requirements of the AASHO Specifications.

For the design of the single-column bent cap, the dead load reactions of 180 kips and 216 kips from the exterior and interior girders, respectively, were assumed to be concentrated in the girder webs. The AASHO lane loading of 640 lbs. per ft. of load per lane plus a concentrated load of 26,000 lbs. on the bent cap, both multiplied by the impact factor of 23.3 percent, controlled the design of the bent cap. Calculated live load plus impact reaction on the bent cap was 120 kips per lane.

For both moment and shear, the controlling loading condition was with traffic lanes 1 and 2 loaded as shown in Fig. D-1. The critical section for moment in the bent cap was taken at 1/6 of the

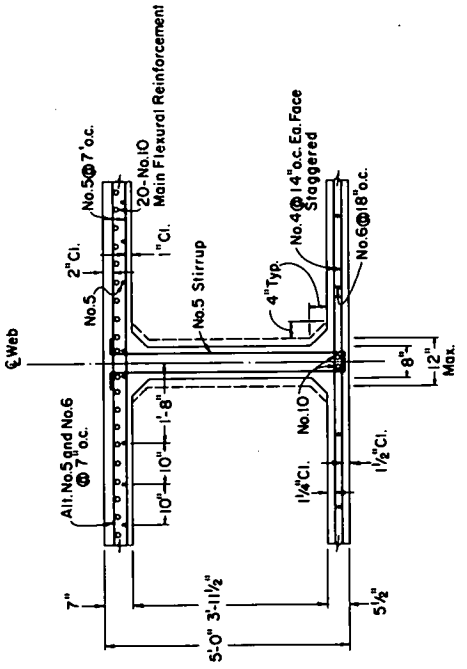

Fig. D-3 Cross Section of Typical Interior Girder of Bridge at Face of Bent Cap

D-7

column diameter from the column centerline. At this location, the calculated design moment was 8,200 kip-ft. A 6-ft. 6-in. wide bent cap reinforced with 20 No. 18 bars in tension and 12 No. 18 bars in compression was used.

The maximum calculated shear stress in the bent cap at the face of the column was 205 psi, somewhat less than the maximum allowable stress of 225 psi permitted by the AASHO Specifications. The shear was resisted by the concrete and by six-legged No. 6 stirrups. A cross section of the bent cap is shown in Fig. D-4.

In the double-column bent, the columns were spaced so that the maximum moment in the bent cap occurred at the inside edge of the columns. However, the difference between the interior and exterior moments was small. The controlling load condition for negative moment was inadvertently taken with traffic lanes 2, 3, 4 and 5 loaded as shown in Fig. D-2. The correct loading condition of all five lanes loaded would have given a somewhat larger negative moment, still at the interior side of the column. For maximum positive moment, the two interior traffic lanes, 3 and 4, were loaded.

The negative and positive bent cap design moments used were 4,500 kip-ft. and 3,800 kip-ft., respectively. These moments were accommodated by a 5-ft. 6-in. wide bent cap containing 12 No. 18 bars as tensile reinforcement and 8 No. 18 bars as compressive reinforcement to resist the negative moment. A total of 10 No. 18 bars as tensile reinforcement and 4 No. 18 bars as compressive reinforcement were used to resist the positive moment.

D-8

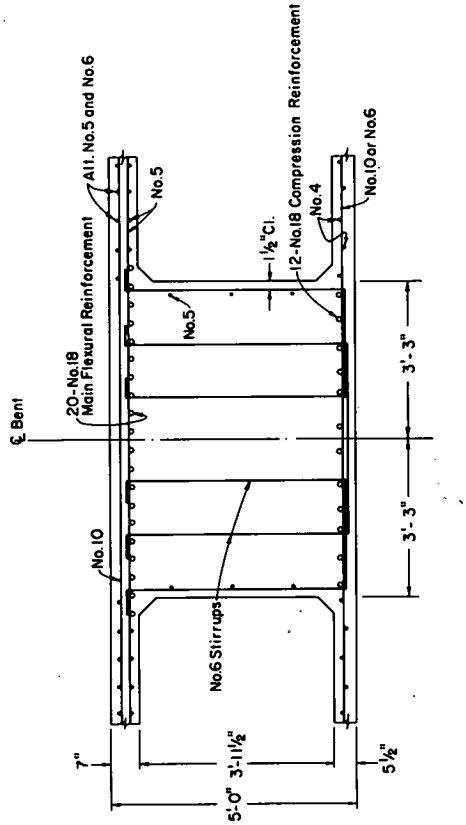

Fig. D-4 Cross Section of Bent Cap of Single-Column Bridge at Region of Maximum Moment

D-9

The maximum calculated shear stress at the interior face of the columns was 227 psi, slightly greater than the allowable stress of 225 psi permitted by the AASHO Specifications. The shear was resisted by the concrete and by six-legged No. 6 stirrups. A cross section for the region of maximum negative moment is shown in Fig. D-5. Details of the cross section for the region of maximum positive moment are shown in Fig. D-6.

The columns were designed using strength design methods. Five-ft. diameter sections were found to be adequate in both the single-column and double-column bridges. Their reinforcement was 23 No. 10 bars and 24 No. 10 bars, respectively, with a No. 5 spiral at 5-in. pitch.

Design of Model Bridges

All external dimensions of the prototype design were scaled by the linear factor 0.2 for the model bridges. The only modification was the addition of the column base blocks through which reactions were measured.

Available sizes of reinforcement for the models were No. 4 and No. 3 Grade 60 deformed bars. In addition, D-5, D-2 and D-1 deformed wire having cross-sectional areas 0.05, 0.02 and 0.01 sq. in., respectively were available. As described in Appendix A, the deformed wire was annealed to have a yield stress of about 60 ksi.

The No. 18 bars comprising the main flexural reinforcement of the prototype bent cap would have been represented at one-fifth scale by bars with a cross-sectional area of 0.16 sq. in., a size between

D-10

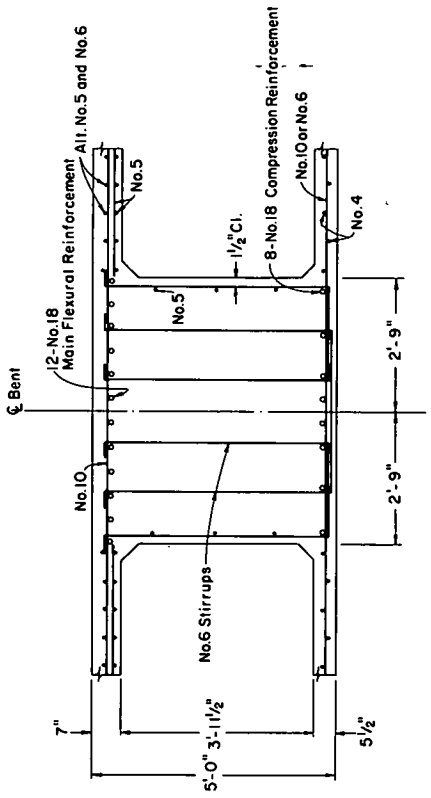

Fig. D-5 Cross Section of Bent Cap of Double-Column Bridge at Region of Maximum Negative Moment

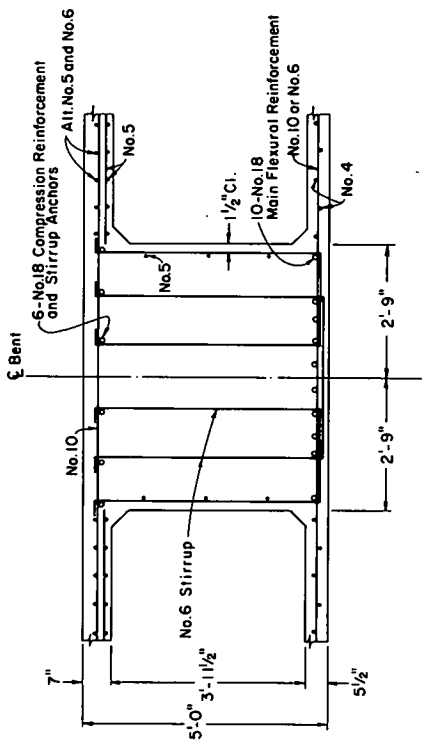

Fig. D-6 Cross Section of Bent Cap of Double-Column Bridge at Region of Maximum Positive Moment

a No. 3 and No. 4 bar. The choice was made to use No. 4 bars, with the number adjusted to give the proper total area of reinforcement. Bar cutoffs were located using the same criteria as the original design. Each bar was extended beyond the point theoretically required by the greater of 15 bar diameters or 1/20 the span. The negative moment bars in the double-column model were inadvertently made about 4 in. shorter than intended.

For the girder flexural reinforcement, the D-5 deformed wires were exact scale representations of the No. 10 bars of the prototype. Therefore, scaling was done bar by bar.

The remainder of the reinforcement for the bridge models was designed by scaling the needed total area from the prototype design, choosing the available reinforcement size closest to the exact scale, then determining the required number and spacing of bars.

Detailed drawings for the model bridges are shown in Figs. D-7 through D-16. The span length of the models was 18 ft. 0 in. with a clear roadway width of 8 ft. 0 in. for the single-column model and 14 ft. 0 in. for the double-column model. The superstructure was 1-ft. 0-in. deep and the width of each box was 1 ft. 6 in.

Test of Bridge Element

Prior to construction and testing of the single-column bridge, a girder element reinforced in a manner similar to the bridge girders was constructed and tested. The girder element represented the negative moment portion of a girder, extending approximately from inflection point to inflection point either side of the bent cap, and including a portion of bent cap. The specimen, shown in Fig. D-17, was 9 ft. 0 in. between supports, 1-ft. 6-in. wide, and 1-ft. 0 in. deep.

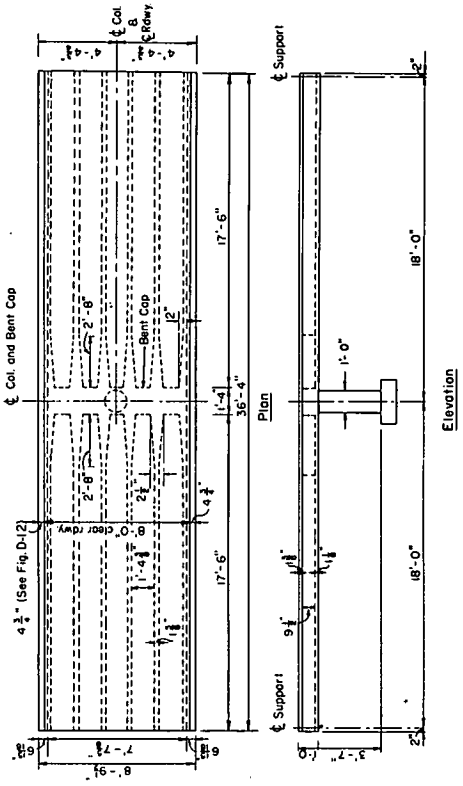

Fig. D-7 Plan and Elevation of Single-Column Model Bridge

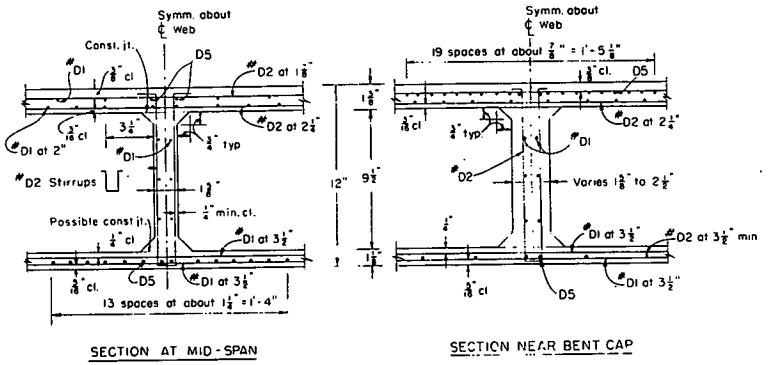

Fig. D-10 Sections of Interior Girder for Model Bridges.

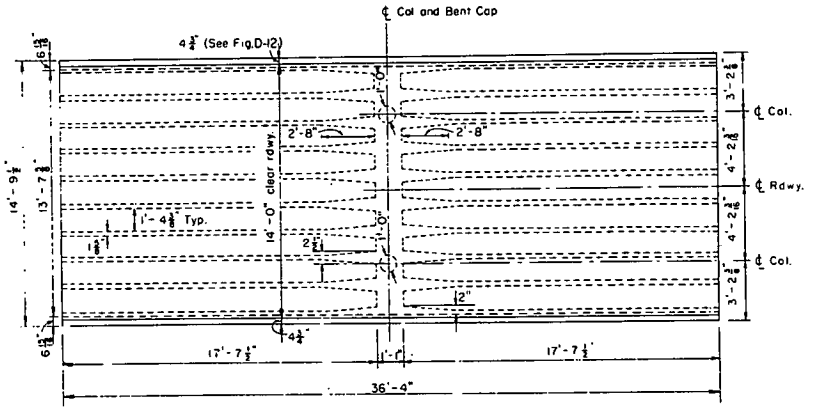

Fig. D-8 Plan of Double-Column Model Bridge

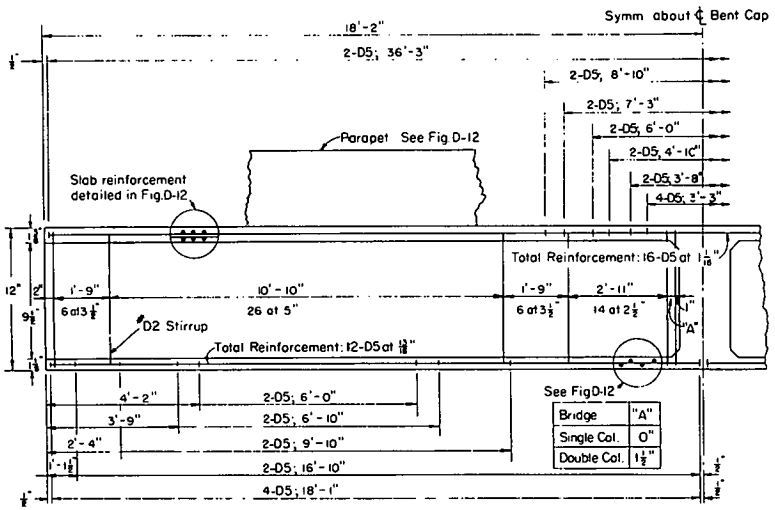

Fig. D-11 Exterior Girder Reinforcement for Model Bridges

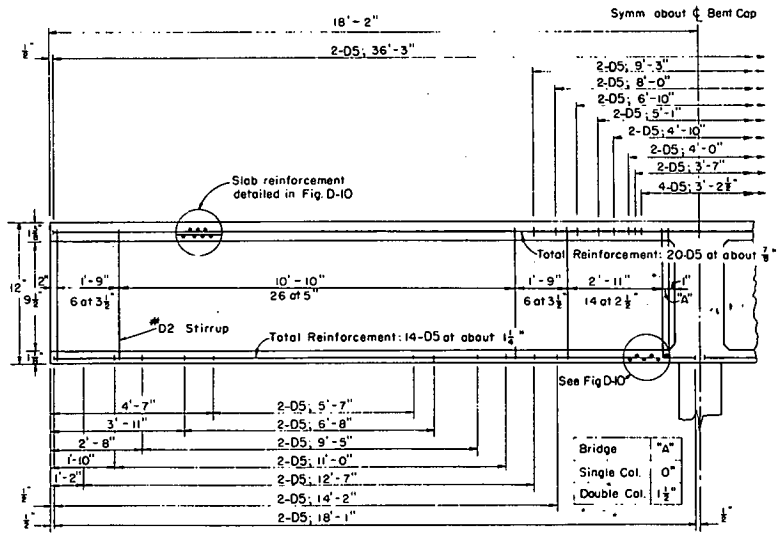

Fig. D-9 Interior Girder Reinforcement for Model Bridges

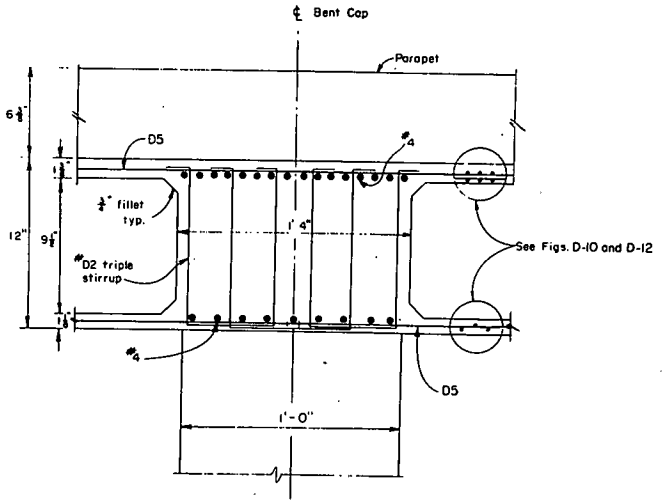

Fig. D-14 Section of Bent Cap in Single-Column Model Bridge

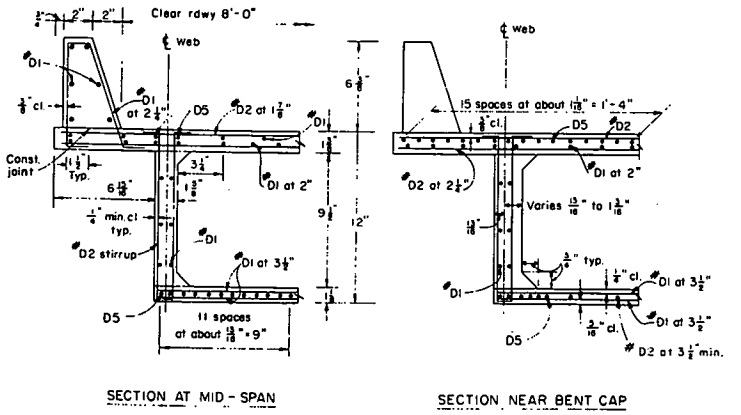

Fig. D-12 Sections of Exterior Girders for Model Bridges

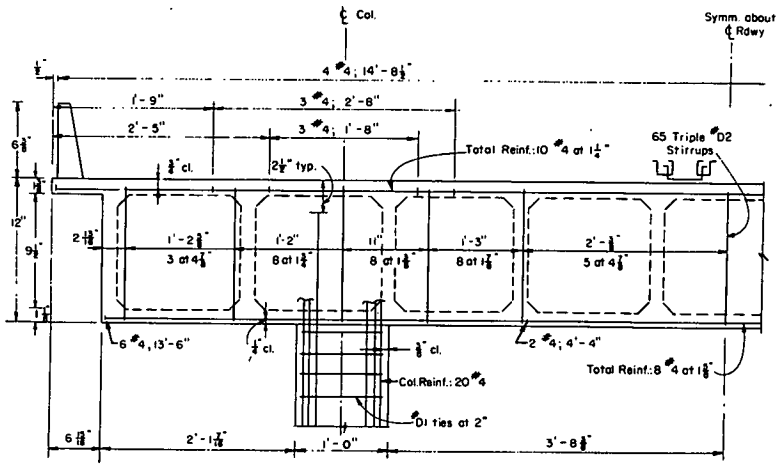

Fig. D-15 Bent Cap Reinforcement in Double-Column Model Bridge

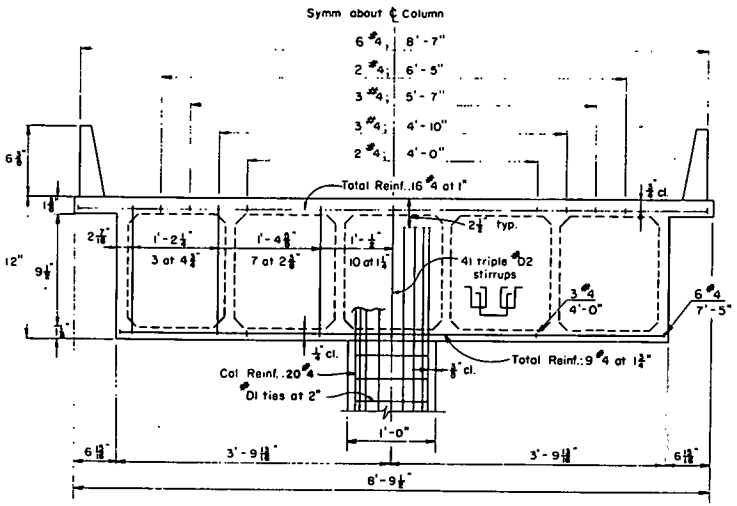

Fig. D-13 Bent Cap Reinforcement in Single-Column Model Bridges

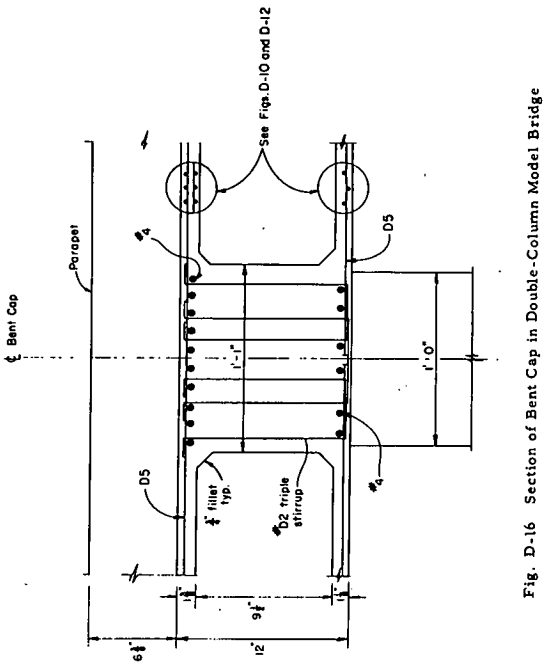

Fig. D-16 Section of Bent Cap in Double-Column Model Bridge

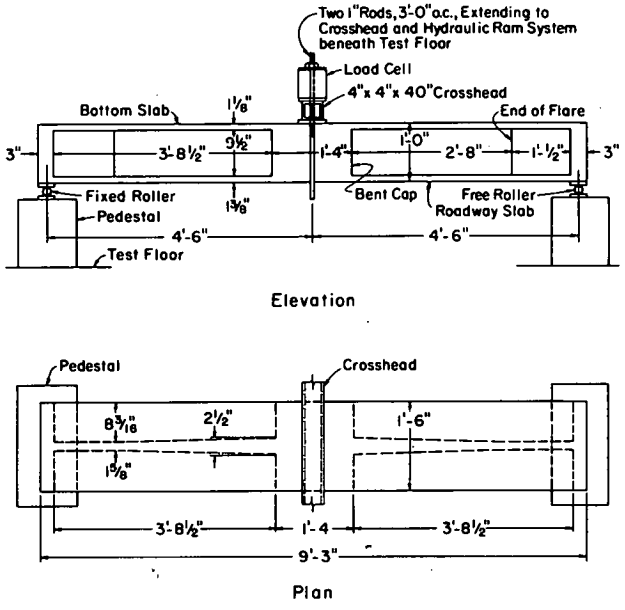

Fig. D-17 Bridge Element Test

The bridge element was tested inverted as a simple beam, supported at the assumed inflection points 1/4 the span or 4 ft. 6 in. either side of the bent cap centerline. It was loaded with a concentrated force applied at the center through the bent cap stub.

The bridge element test had three objectives. First, it tested the planned construction techniques. Second, it was used to determine whether or not the planned instrumentation array would yield the desired information. Finally, by comparison with the known values in this statically determinate test, the results were used to develop means of reducing the experimentally measured strains to moments and shears.

The construction techniques were checked by casting the girder element in a part of the formwork constructed for the double-column bridge. Two complete girder forms were set on the casting platform in the proper position for the future casting. These forms were blocked at the appropriate points in the webs, and temporary bent cap stub forms were added. After the reinforcing cage, manufactured from the same reinforcement used for the model bridges, was set in place, the soffit, webs and a major portion of the bent cap were cast. The web forms were then removed, temporary deck forms were set in place and the remainder of the element was cast.

Instrumentation included strain gages on reinforcement and concrete at various levels on three sections located 1, 7 and 21 in. from the bent cap face along one girder. The strain gage arrangement was the same as that used on each of the instrumented girders of the model bridges. Strain gage locations are shown in Fig. D-18. Applied loads were measured by observing the pressure in the hydraulic loading system,

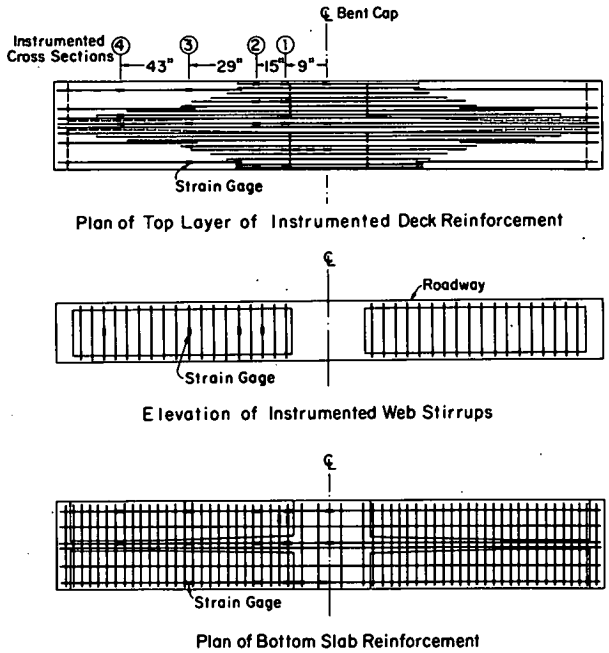

Fig. D-18 Location of Strain Gages in Bridge Element

and by the signals from a load cell. Other instrumentation was also similar to that used for the model bridge tests.

Data were recorded on punched paper tape by means of a VIDAR Digital Data Acquisition System. An IBM 1130 computer was used to process the recorded data. All data processing was done in the same manner as planned for the model bridge tests.

Details of the development of the program for the calculation of moments and shears from observed data are discussed later in this section.

Construction of the girder element proceeded following the same sequence planned for the model bridges. The test was started 31 days after the deck was cast. Material properties at the time of test are shown in Table D-2.

Force was applied in increments of about 2 kips until a load of 9.6 kips, defined as service load, was reached. At this stage, the main girder tensile reinforcement was calculated to be at the working stress of 24 ksi. The 9.6 kip load was removed and reapplied two additional times. After a third unloading, the force was increased in the same 2 kip increments until the strength of the specimen was reached at a load of 27.2 kips. The test was terminated when slip occurred along a horizontal shear plane at midheight of one web.

The load deflection curve recorded during the test is shown in Fig. D-19. The increase in residual deflection due to several applications of service load is seen to be small after the first cycle of loading.

Following the test to destruction, the damaged portion of the bridge element was repaired and strengthened. The ultimate load test was then repeated. Upon reloading, the previously intact half span developed a

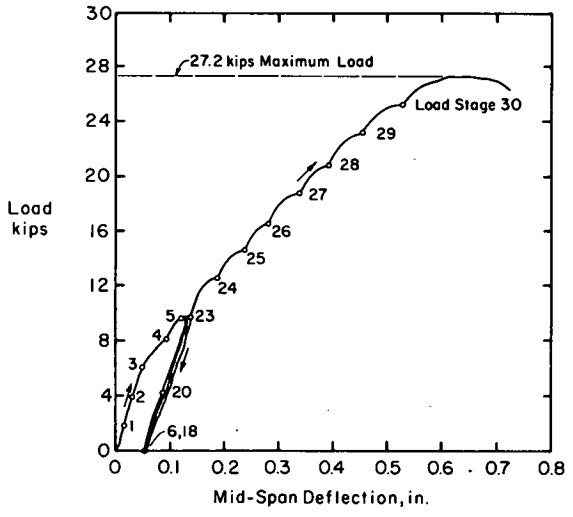

Fig. D-19 Load-Deflection Curve for Bridge Element

TABLE D-2 BRIDGE ELEMENT MATERIAL PROPERTIES AT TIME OF TEST

Material	Size	Location	Compressive Strength psi	Modulus of Elasticity psi	Yield Stress psi
Concrete		Soffit and Webs	4400	3.7×10^6	
		Deck	3450	3.5×10^6	
Reinforcement	D-5				75,500
	D-2				72,300
	D-1				70,700

diagonal tension crack at the same ultimate load as before. This indicated that the horizontal shear distress that occurred in the first test did not reduce the load carrying capacity of the beam.

Data Analysis. The main objective of the data analysis was the development of a suitable method of determining the girder shear force from the measured strains in the tensile and compressive reinforcement. In this statically determinate element the shear was known for each load. Consequently, the accuracy of various methods to convert measured strains to shears could be checked directly.

To convert the measured strains into internal forces, the cross section was divided into five parts as shown in Fig. D-20. Two parts represented the tensile and compressive reinforcement. The other three represented portions of the concrete in compression. It was assumed that the concrete carried no tensile stress. To locate the neutral axis, the vertical strain gradient was assumed to be linear and to be defined by the strains indicated by the gages directly above and below the web. In the transverse direction, a linear distribution of strains was assumed between any two adjacent gages in the flanges.

For each component, the average strain across the depth was determined. The average strains were then converted to stresses using the measured modulus of elasticity. Next, stresses were multiplied by the appropriate area to give the total internal force in each component. The total compressive and tensile forces were obtained by summing the forces in the individual components. The lever arm between the two forces was also calculated.

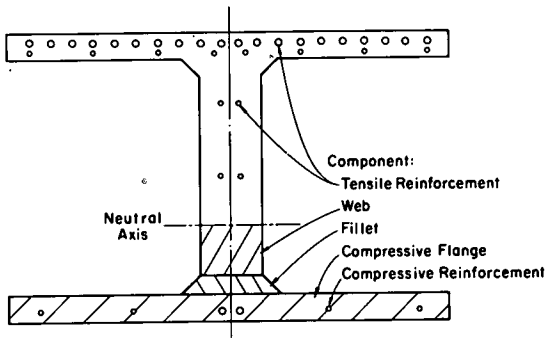

Note: Section is shown in orientation existing in model bridges. Girder element was tested inverted.

Fig. D-20 Division of Girder Cross Section for Determination of Internal Forces

TABLE D-3 INTERNAL FORCES AND LEVER ARMS IN BRIDGE ELEMENT

Load Stage	Section	Internal Force		Lever Arm		
		Compressive kips	Tensile kips	Test in.	Computed in.	Test / Computed
24	1	31.43	25.50	10.57	10.60	1.00
	2	24.27	26.60	10.68	10.65	1.00
	3	11.80	18.66	10.72	10.55	1.02
27	1	47.60	39.11	10.59	10.60	1.00
	2	33.04	39.78	10.69	10.65	1.00
	3	15.49	29.92	10.72	10.55	1.02
30	1	60.27	53.78	10.59	10.60	1.00
	2	44.41	55.02	10.68	10.65	1.00
	3	22.13	41.19	10.72	10.55	1.02

Three load stages, respectively about 45, 70 and 90 percent of the ultimate capacity, were selected for analysis. After the forces were calculated, it was observed that the experimentally determined compressive and tensile forces were not equal. Generally the tensile force was greater. This difference increased with increasing load. Also, the differences were greatest for the instrumented section furthest from the bent. The differences are attributed to the effects of inclined cracking and a non-linear strain distribution[46]. The values of the compressive and tensile forces are listed in Table D-3, along with the experimentally determined lever arm between them.

In flanged sections such as the one tested, the length of the lever arm between tensile and compressive resultants should be well defined and insensitive to minor changes in reinforcement percentage and material properties. To investigate this possibility, an existing computer program was used to predict moment-curvature relationships, position of the neutral axis, length of lever arm, and other selected parameters. Using measured material properties, this computer program analyzes the section using suitably small elements of defined geometry and material. It has no provision for transverse variations in strain.

The lever arms predicted by the computer program agree within two percent with the experimentally determined lever arms listed in Table D-3. In view of this close correspondence, the experimentally determined lever arms were used in calculations to determine the value of the tensile and compressive resultants from the known bending moments.

Best results for the calculation of the resultant were found to be obtained by averaging the experimentally determined tensile and

compressive resultants. The average was then multiplied by the experimentally determined lever arm to obtain the experimental value of the bending moment. The moments determined in this manner for the three load stages are shown in Fig. D-21. Measured moments were always higher than applied moments. The values of $\frac{M\ test}{M\ appl}$ range from 1.04 to 1.13 with an average value of 1.09.

Since all three calculated moments were obtained for a region of nearly constant shear, the bending moment diagram between the sections should be linear. The best straight line between all three points was obtained using a least squares fit. The shear forces, as represented by the slope of the line, are listed in Table D-4.

Values for $\frac{V\ test}{V\ appl}$ are somewhat higher than might have been desired. This variation is due in part to the fact that errors in the moment values are magnified by the subtraction process needed to calculate the shears.

Findings. Tests of the girder element indicated that construction techniques were generally satisfactory. The only detail of concern was the effect that produced the horizontal shear distress in one web. This problem was partially attributed to difficulty in placing the concrete with the slightly oversized coarse aggregate. The larger aggregate tended to accumulate on the horizontal wires in the web and prevent uniform compaction directly beneath. A contributing factor may have been a tendency of the fresh concrete to settle out of the lower portion of web and into the lower flanges as that part of the web concrete was being placed. These possibilities suggested that extra

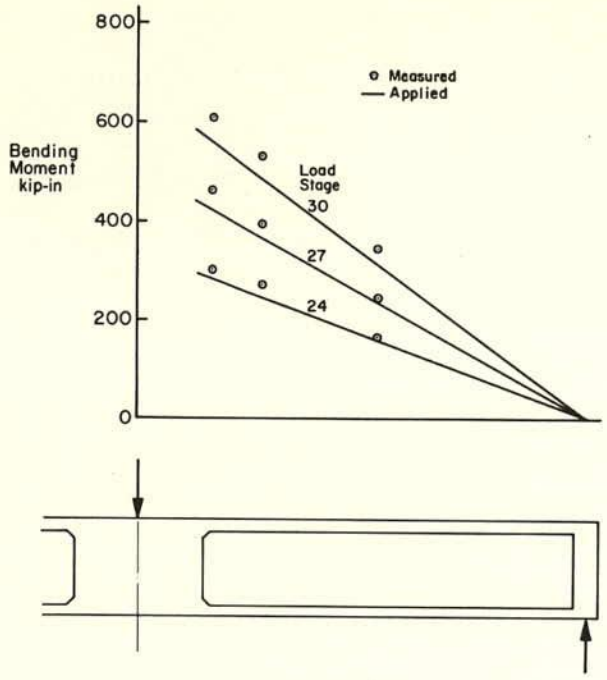

Fig. D-21 Relationship between Applied and Calculated Bending Moments for Girder Element

TABLE D-4 CALCULATED SHEAR FORCE FOR BEAM ELEMENT

Load Stage	Shear Force, V kips		V test / V appl.
	Applied	Test	
24	6.18	7.03	1.14
27	9.34	10.72	1.15
30	12.31	13.31	1.08

care in casting the model bridges was needed. However, no changes in technique appeared necessary unless further difficulties were encountered.

The instrumentation of the girder element provided the information needed. In addition, a workable method was developed for the determination of girder moments and shears from measured strains. Consequently, instrumentation and data analysis techniques used in the girder element test were also used for the model bridges.

Construction of Model Bridges

The construction sequence for both model bridges followed the order described in Appendix A. For the superstructure, these techniques were confirmed by construction and testing of the bridge girder element.

The column base and the column or columns for each model were precast in a suitable form at a location away from the main casting platform. They were then set in position under the platform. After reinforcement and formwork for the first casting were installed, the soffit and webs were cast in a single day. The top surface of the web concrete was purposely roughened to provide better bond with the next casting. After a curing period, the web forms were stripped, the deck forms installed, and the remainder of the reinforcement placed. Deck concrete was then cast in a single day.

Each model bridge was lifted from the casting platform using a strongback arrangement that enabled the elastic distribution of reactions between bent cap and abutment to be maintained. The double-column bridge during transport is shown in Fig. D-22. After the model was set in place in the testing area, temporary supports were provided.

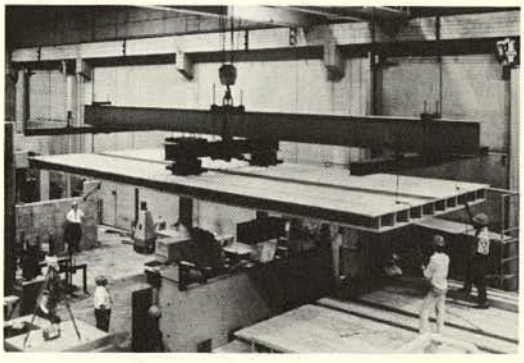

Fig. D-22 Transport of Double-Column Bridge Model Using Strongback Arrangement

End diaphragms were cast to close the boxes. Installation and final adjustment of the supports to reestablish the elastic distribution of reactions completed construction and positioning of the model.

After a portion of the load test had been completed, parapets were cast along each side of the deck. The parapets were cast in plywood forms that were clamped to the deck. Reinforcement protruding from the deck was provided to assure composite action between the parapet and deck. Open joints, about 0.5-in. wide were provided in the parapet at the quarter points of the spans and at the bent cap centerline. These joints were similar to those normally provided in bridges of this type.

Views of the single-column and double-column model bridges are shown in Figs. D-23 and D-24, respectively. In Fig. D-23, the reinforcement for the soffit, webs and part of the bent cap is in place. Formwork for the webs and for one side of the bent cap is also erected in the near half of the bridge.

Preparations for casting the deck of the double-column model bridge are shown in Fig. D-24. Deck and top bent cap reinforcement are in place for casting. The pieces of white cloth are attached as a safety measure to give visibility to the protruding handles of the jacks supporting the removable deck formwork.

Preparation for Test

Abutment Support. Abutment reactions were provided at points between each pair of webs, as shown in Fig. D-25. From the top, the support consisted of a roller with bearing plates, a load cell with 25 kip capacity, and a base plate with a means for precise height adjustment.

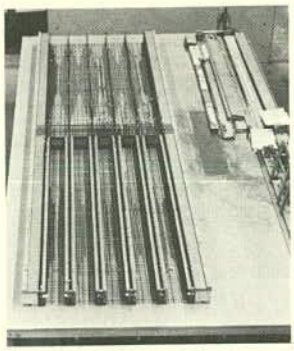

Fig. D-23 Construction of Single-Column Model Bridge

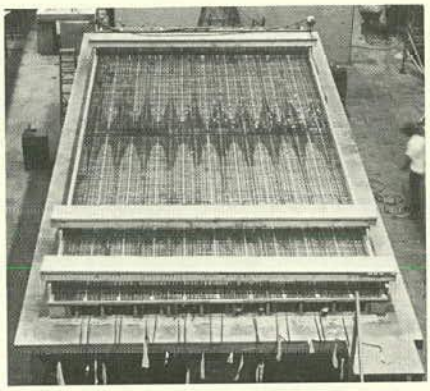

Fig. D-24 Construction of Double-Column Model Bridge

This height adjustment was needed to equalize reactions among the several supports at the start of testing. For the single-column bridge the height adjustment was accomplished by means of shims. A specially made differential screw, shown in Fig. D-25, was used for adjustment of the double-column bridge.

The diaphragms cast into the ends of the model bridges were uniformly prestressed over their depth to 500 psi. Prestress was applied through a 3/4-in. post-tensioning rod. To prevent horizontal movement of the ends of the bridge, the diaphragm prestressing rods were fastened to the stationary abutment support. This detail is shown in Fig. D-25.

Column Base. A view of the support at the base of a column is presented in Fig. D-26. To prevent cracking, the base block was eccentrically prestressed to a total force of 300 kips by means of five 1-in. diameter rods. The base blocks were supported at two points located 21-in. from the centerline of the bridge and on the centerline of the bent cap. Each support consisted of a spherical seat, a load cell of suitable capacity, and a 100 ton mechanical jack. This support equipment is visible in the foreground of Fig. D-26. By transferring the column reaction to a temporary support on the concrete block directly under the column, load cells of either 50 kip or 200 kip capacity could be inserted in the system. Consequently, the sensitivity could be increased or decreased as needed for a particular test.

The column base was restrained against horizontal movement longitudinally and transversely by a system of rods and struts.

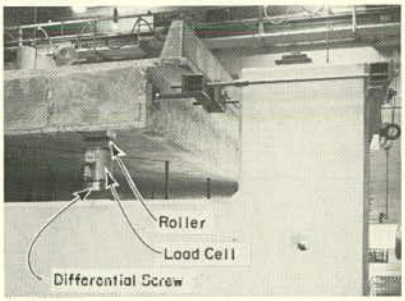

Fig. D-25 Abutment Support

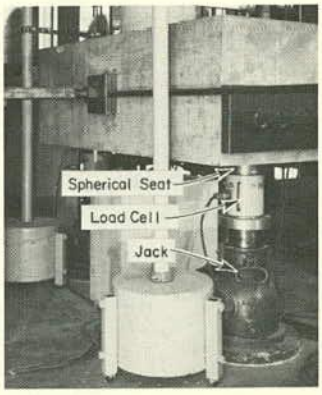

Fig. D-26 Column Support

Rotation about the longitudinal (spanwise) axis was controlled by the jacks and was measured by dial gages and level readings. Free rotation about the transverse axis was permitted.

Loading Apparatus. Three separate hydraulic systems were used to apply test loads to the models. The dead load system and the lane load portion of the live load system applied loads at the same points spaced at 3-ft. centers along the webs of the girders. A third system applied point loads to the bent cap. These concentrated loads included the point load portion of the AASHO live loads, as well as the dead load and uniform live load associated with the area tributary to the point of application.

As previously noted, the dead load system supplied the continuously applied dead load makeup, as well as required increments of dead load. Dead loads for all points were those calculated for an interior girder.

The lane load portion of the live load system applied forces through the same points as the dead load system. However, the actuating rods were centered on the particular lane, rather than being centered on the boxes. Thus, the resultants of the applied loads were in the correct lateral location. On the single-column model bridge, lane load could be applied to any one, to any two, or to all three lanes. For the double-column model, lanes 1 and 6, 2 and 5, and 3 and 4 were paired for live load. Load could be applied to any one, to any two, or to all three pairs.

The system applying points loads to the bent caps could apply load to either or both of lanes 1 and 3 of the single-column model.

For the double-column model, lanes 1, 3, 4, and 6 could be loaded in any combination. No provisions were made for bent cap point loads in lane 2 of the single-column model or for lanes 2 and 5 in the double-column model, since application at these locations over or in the vicinity of the column would not have affected the bent cap stresses.

The arrangement of loading apparatus for the application of dead load and distributed live load in the spans of the model bridges is shown for the single-column model in Fig. A-11. The arrangement for the double-column model was similar. The bent cap loading systems for the two model bridges are shown in Figs. D-27 and D-28. Details of the loading apparatus between the double-column model and the test floor are shown in Fig. D-29.

Instrumentation. The layout of strain gages for a representative instrumented girder is shown in Fig. D-18. The strain gage layout for the bent cap of the single-column model bridge is shown in Fig. D-30 and for the double-column model bridge in Fig. D-31.

Overall instrumentation patterns, including deflection measurement points, lines of Whittemore gage points, and load cell locations, are shown for the single-column model bridge in Fig. D-32 and for the double-column model bridge in Fig. D-33.

Test of Single-Column Model Bridge

General Planning of Test Program. As a first step in the test program, the dead load makeup was applied to bring the total load to 1.0D. Next, successively increasing loads were applied. At the service load intensity, response both to AASHO lane loads and to concentrated loads was measured.

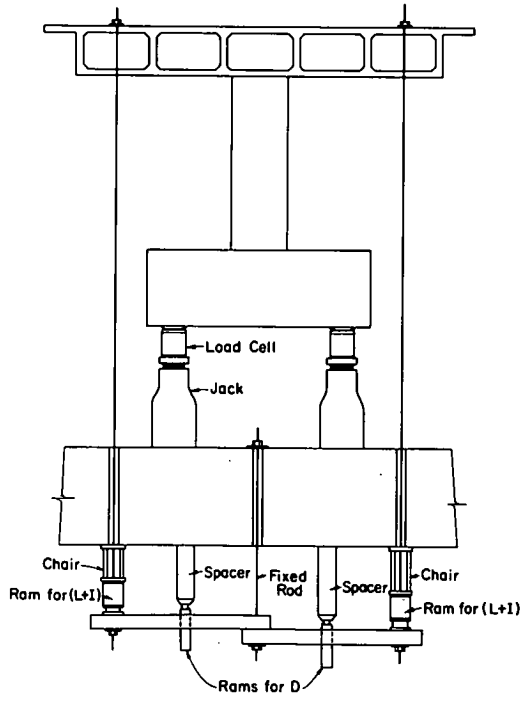

Fig. D-27 Loading System for Bent Cap of Single-Column Model Bridge

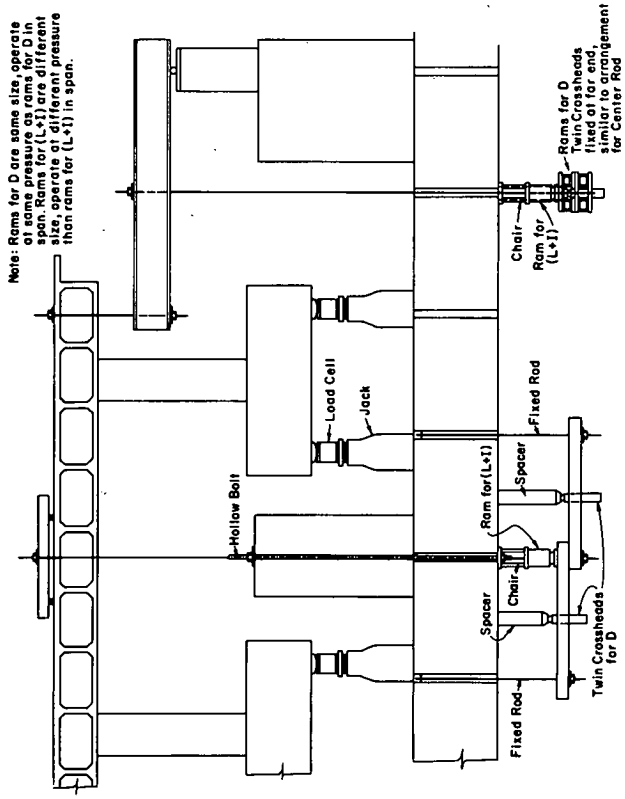

Fig. D-28 Loading System for Bent Cap of Double-Column Model Bridge

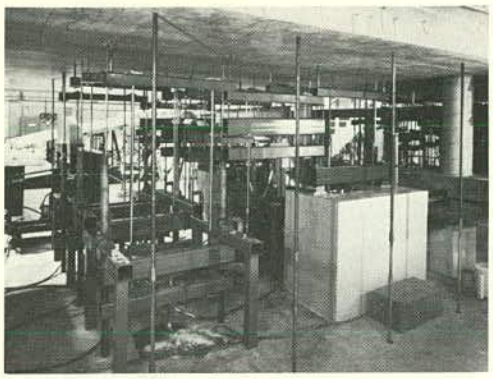

Fig. D-29 Double-Column Model Bridge Loading Apparatus

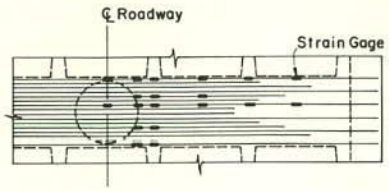

Fig. D-30 Strain Gages on Bent Cap Reinforcement for Single-Column Model Bridges

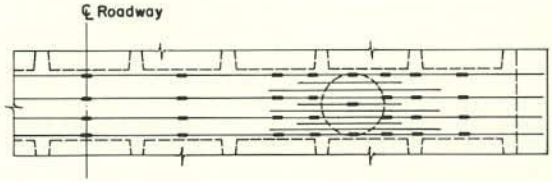

Fig. D-31 Strain Gages on Top Bent Cap Reinforcement for Double-Column Model Bridge

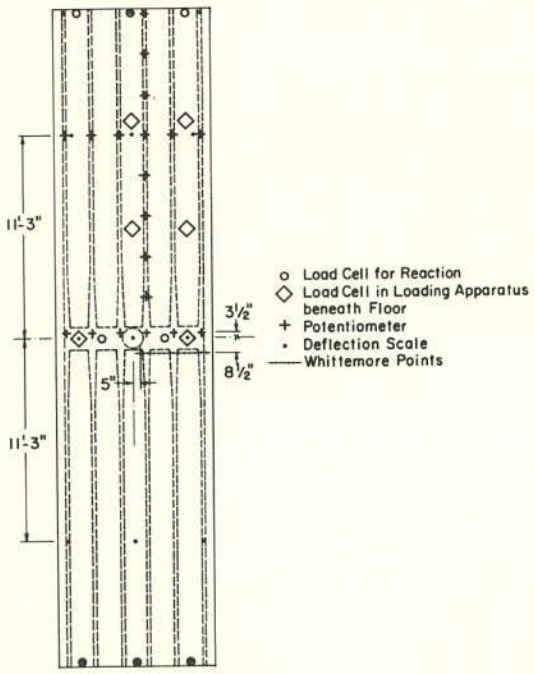

Fig. D-32 Instrumentation Layout for Single-Column Model Bridge

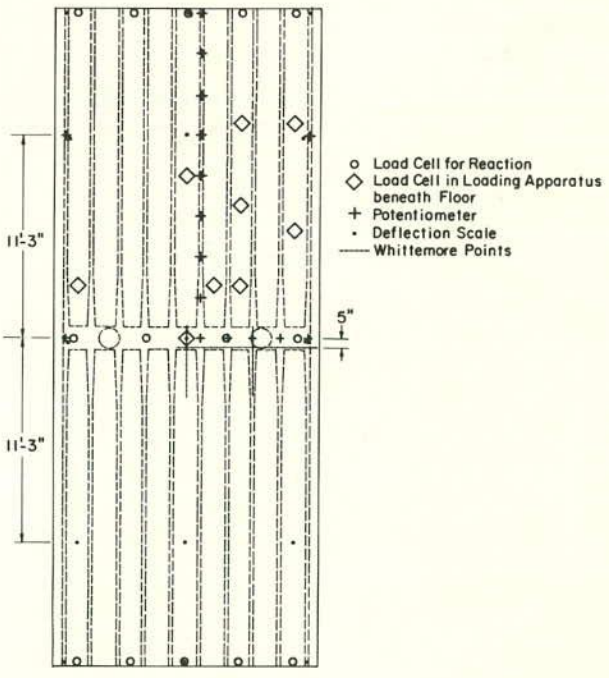

Fig. D-33 Instrumentation Layout for Double-Column Model Bridge

After application of the initial series of service load tests was completed, the parapet was added and the same tests were repeated. This was intended to show the effects of the parapet on behavior. Loadings of increasing intensity were then applied until capacity of the bridge was reached. After completion of the original program, additional tests were performed.

Materials. Material properties for the single-column model bridge are summarized in Tables D-5 and D-6.

Summary of Phases. Testing of the single-column model bridge was performed over a period of 70 days. For reference purposes, the main phases of the testing program are listed in Table D-7.

Loadings applied in Phase 1 were intended to provide a measure of the response of the model, without the participation of parapets, at loads in the service load range. Included were application of concentrated loads and equivalent AASHO service loadings. At the conclusion of these tests, only a few flexural cracks had developed in the positive moment regions and in the negative moment region over the column.

Following the casting of the parapets, the equivalent AASHO service loadings were again applied. This loading, designated Phase 2, provided a comparison of behavior under similar loadings with and without the parapet. In Phase 3, the bridge was intentionally subjected to a high overload. This overload produced substantial cracking in both negative and positive moment regions. A 4 kip concentrated load was applied at points on the roadway during Phase 4. This was intended to provide information on the response of the model after substantial cracking had occurred.

TABLE D-5 REINFORCEMENT PROPERTIES FOR SINGLE-COLUMN MODEL BRIDGE

Reinforcement	Yield Stress f_y, ksi	Tensile Strength f_{su}, ksi	Modulus of Elasticity E_s psi x 10^6
D1	70.7	71.1	26.6
D2	74.7	79.1	29.1
D5	75.5	83.8	29.3
No. 4	63.5	103.3	28.8

TABLE D-6 CONCRETE PROPERTIES FOR SINGLE-COLUMN MODEL BRIDGE

Concrete Location	Age at Start of Testing Days	Compressive Strength f'_c psi	Splitting Tensile Strength f_{sp} psi	Modulus of Elasticity E_c psi x 10^6
Bottom Slab, Webs, and Bent Cap	70	4030	500	3.8
Deck Slab	50	5330	600	4.3

TABLE D-7 TEST PROGRAM ON SINGLE-COLUMN BRIDGE

Phase	Description	Number of days from start of testing
1	Application of equivalent dead load, a 2 kip concentrated load at 3 ft. intervals along each web, and equivalent AASHO service loadings 1.0 [D + (L + I)]	1 to 11
-	Delay while parapets were cast and allowed to cure	12 to 31
2	Application of equivalent AASHO service loadings 1.0 [D + (L + I)]	32 to 35
3	Application of overload 1.75 (D) + 2.0 (L + I)	36
4	Application of a 4 kip concentrated load at 3 ft. intervals along each web	38 to 40
5	Application of equivalent AASHO ultimate loadings 1.5 (D) + 2.5 (L + I)	45 & 46
6	Test to destruction	47 to 49
7	Test to destruction of repaired bridge	61
8	Test to destruction of bent cap region	70

In Phase 5, combinations representing AASHO design ultimate loading conditions were applied to the bridge. These loadings were intended to show which combination subjected the bent cap to the highest stresses. The critical loading occurred with the maximum total load on the bridge, i.e., with all three traffic lanes loaded to 100 percent of the lane load (L + I).

Finally, in Phase 6, the bridge was loaded to destruction by proportionally increasing the most critical loading found in Phase 5. Distress occurred in the positive moment region of the box girders, at a section near the abutment. In this region there was a combination of bar cut-offs and splices in the main reinforcement.

Since the bent cap and adjacent superstructure were undamaged at the end of Phase 6, the region in which distress occurred was repaired by filling the ends of the cells with concrete. To maintain symmetry, the opposite end of the bridge was strengthened in a similar manner.

In Phase 7, the repaired bridge was tested to destruction. Under the loading, distress occurred again in the positive moment region. However, it was at a section approximately one-quarter of the span length from the bent cap where there was again a combination of bar cut-offs and splices.

In Phase 8, the bent cap region and adjacent superstructure, to one-quarter of the span length each side of the pier, were separated from the bridge and loaded to destruction. Distress occurred in the bent cap, due to a combination of flexure and shear. The ultimate load was close to that producing the calculated flexural capacity of the bent cap.

In the following sections, additional data concerning the testing and the behavior of the single-column bridge is presented.

Preparation. A thorough visual examination of the bridge was made prior to the removal of temporary shoring in the positive moment regions. No cracking was observed.

After the shoring was removed, the elevations of the reactions were adjusted until the reactions approximated those predicted by an elastic analysis. Some difficulty was experienced in making the individual reactions at each abutment equal. Individual reactions varying from 0.9 to 1.4 kips were accepted within the sum of 3.5 kips.

After adjustment of the reactions, it was observed that there was an upward curl of the superstructure. Deflection measurements indicated that the roadway surface at the ends of the bridge was 0.6 in. higher than at the bent cap. This curl was attributed primarily to the effect of differential shrinkage between the roadway slab and the lower part of the superstructure.

After the abutment reactions had been adjusted, the dead load makeup was applied to produce stress conditions equivalent to those caused by the dead load of the prototype. This 1.0D condition was maintained, as a minimum, during most of the period that the first six phases of the test program were conducted. The load was removed for two brief periods at the start of Phases 2 and 6 to obtain zero readings on instrumentation.

Dead load strains measured by both the electrical and mechanical gages located in the bent cap are compared in Fig. D-34. Agreement is satisfactory. It is important to note that the equivalent dead load

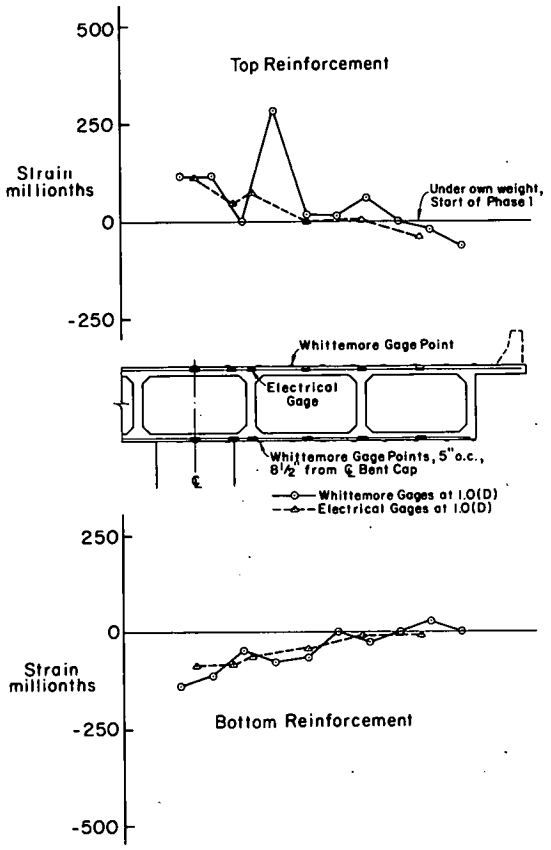

Fig. D-34 Measured Strains from Application of Equivalent Dead Load on Single-Column Model Bridge

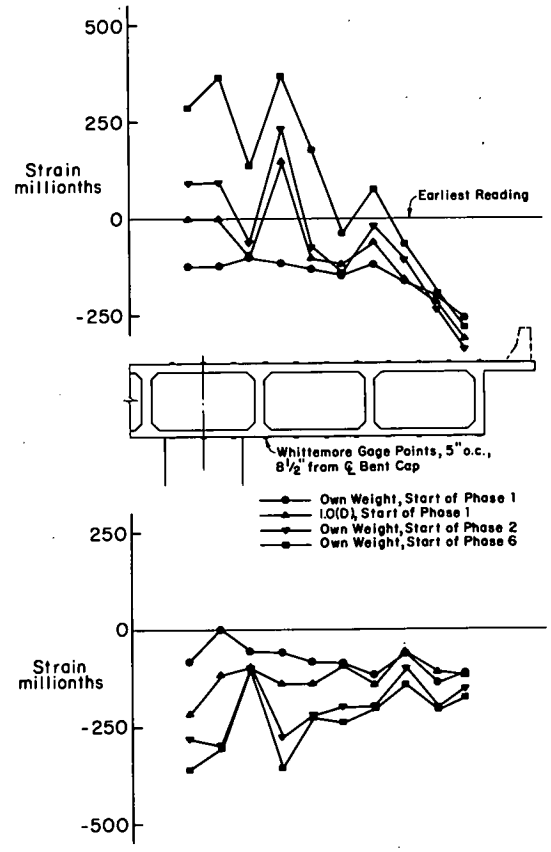

Fig. D-35 Mechanical Strain Gage Measurements on Bent Cap of Single-Column Model Bridge

condition, 1.0 (D) at the start of Phase 1, is the zero base for most of the data presented in the following sections. Fig. D-34 indicates that the strains under application of 1.0 (D) were so small that they could be considered negligible (less than 100 millionths). Also, there appeared to be no cracking of the bent cap except possibly at the location of the fourth Whittemore gage from the bridge centerline.

Time-Dependent Behavior. Lines of Whittemore gage points were placed on the bent cap and an interior box girder to provide long-term control during the three month period of the test program. Initial measurements were taken on the roadway slab before the model was removed from its form. Readings on the bottom slab were taken after the model had been moved from the form, placed in the testing area and shored to an equivalent no load condition. Strains measured with the model in identical unloaded conditions, at the start of Phases 1, 2, and 6, are shown in Figs. D-35 and D-36.

The strain data presented in Figs. D-35 and D-36 indicate that, at early ages, the model was subjected to compressive strains at both top and bottom. These strains are attributed to shrinkage. Later, residual strains of the same sign as those caused by loading are superimposed on the earlier shrinkage strains.

The observation that the compressive strains did not change significantly between Phases 2 and 6 indicates that the principal effects of shrinkage occurred at an early age. The measurements also indicate that there was a residual tensile strain of roughly 350 millionths, the equivalent of about 10 ksi, in the main bent cap and box girder reinforcement in the vicinity of the column at the start of

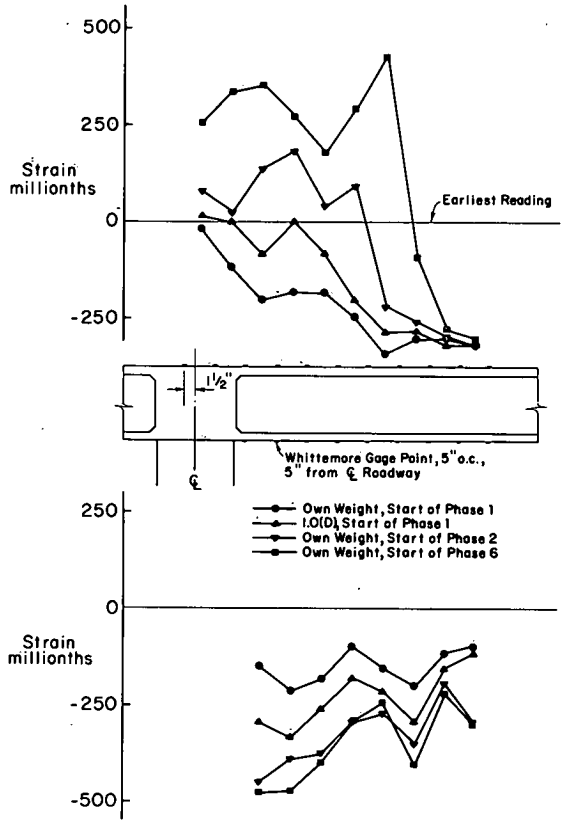

Fig. D-36 Mechanical Strain Gage Measurements on Girder of Single-Column Model Bridge

lane loading, equivalent to 640 pounds per linear ft., plus impact on the prototype, and two concentrated loads, equivalent to 18 kips plus impact. The concentrated loads were located 7.5 ft. either side of the centerline of the model bent cap, in each of the three traffic lanes shown in Fig. D-1. The load in the middle traffic lane was centered within the lane.

The first flexural cracking in the roadway, in the vicinity of the column, was observed under this loading. A deflection at the end of the bent cap of 0.06 in. was measured. The maximum deflection of the exterior web measured at the section of maximum positive moment was 0.22 in. Noting that the corresponding deflection under the equivalent dead load was 0.075 in., the corresponding maximum deflection of the prototype would be 1.19 in., or 1/900th of the span.

Next, the equivalent of the live loading shown in lanes 1 and 2 in Fig. D-1 was applied to the model. This loading, the critical AASHO design combination for the bent cap, produced a deflection at the end of the model bent cap of 0.014 in.

After application of loads in lanes 1 and 2, the equivalent of the live loading shown on all 3 lanes in Fig. D-1 was applied to the model at full 100 percent intensity. Under this loading, the deflection at the end of the bent cap was 0.007 in. These two loadings produced minor additional cracking in the roadway. Most of the cracking was in the direction of the centerline of the bent cap. The maximum measured width of any crack was 0.002 in.

The average reading of the first, second and third Whittemore gages from the bridge centerline along the top of the bent cap indicated

Phase 6, the test to destruction. Contributing to this residual strain is a compressive shrinkage strain ranging from 100 to 200 millionths before the start of Phase 1.

Phase 1. At the start of Phase 1, a 4 kip concentrated load was positioned at 3-ft. intervals along the two interior webs adjacent to the column. However, computations indicated that the 4 kip load, the equivalent of a 100 kip concentrated load on the prototype, would produce a reinforcement stress of 31 ksi when it was positioned to produce maximum positive moment on an exterior web. Since the 31 ksi stress was greater than the 24 ksi service load design stress, it was decided to apply only a 2 kip concentrated load. This load was subsequently positioned at 3-ft. intervals along each girder web.

Application of these concentrated loads to the bridge produced only minor cracking transverse to the girders in positive moment regions. Most of the cracks occurred between the exterior and first interior webs. Measurements of the total abutment reaction and column reaction were in reasonable agreement with values predicted by an elastic analysis for a 2 kip load located at different positions on a 2-span continuous beam. Strain response of the bent cap to the 2 kip load was so small that it could not be separated from residual and time-dependent effects. Values of measured deflection of the ends of the bent cap under the 2 kip load averaged 0.009 in., the equivalent of 0.045 in. in the prototype.

In the next part of Phase 1, several equivalent AASHO live loadings were applied. First, load was applied to produce maximum negative moment in the box girders. This consisted of a distributed

that the absolute stress in the main bent cap reinforcement due to the above three loading conditions was 2.5, 2.6, and 3.0 ksi tension, respectively. However, the measured response due to the application of any of these loads was about 0.5 ksi. This observation indicates that even at these low stresses the development of cracking in the roadway produced residual stresses in the reinforcement. These are attributed to the causes already discussed in Appendix A.

Following the application of the equivalent AASHO loadings, the 2 kip concentrated load was again positioned at 3-ft. intervals along each girder web. The behavior was similar to that observed previously. In this case, values of measured deflection of the ends of the bent cap under the 2 kip load varied, averaging 0.009 in. Stress in the bent cap reinforcement indicated by the electrical gages was in good agreement with that indicated by the mechanical Whittemore gages. However, the response indicated by application of specific loads was not consistent.

An overall indication of the deflections measured during Phase 1 is presented in Fig. D-37. These data indicate that from a percentage standpoint, there was substantial residual deflection in the model at the conclusion of these tests.

Phase 2. Following the 20-day period required to cast the parapets, the three AASHO loading conditions previously applied in Phase 1 were again applied. As described before, the first loading condition produced maximum negative moment in the girders. The second and third loading conditions were with lanes 1 and 2, and lanes 1, 2, and 3 loaded, respectively, as shown in Fig. D-1.

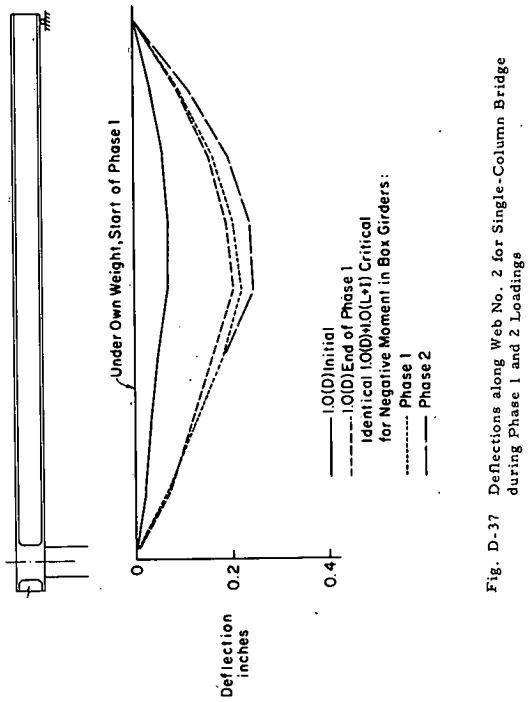

Fig. D-37 Deflections along Web No. 2 for Single-Column Bridge during Phase 1 and 2 Loadings

The deflection measured at the intersection of Web No. 1 and the bent cap for these three loading conditions was 0.005, 0.014, and 0.006 in., respectively. This can be compared with the deflections of 0.006, 0.014, and 0.007 in., respectively, measured for these loading conditions in Phase 1. It appears that the addition of the parapets increased the stiffness of the superstructure slightly. However, the stress in the bent cap reinforcement under Phase 2 loading was about 10 percent higher than that measured in Phase 1.

A comparison of the deflection of the model under the loading condition critical for negative moment in the box girders is shown in Fig. D-37. This comparison shows that the maximum deflections increased in Phase 2. However, it should be noted that the deflection response under the application of the equivalent dead load plus the live load was considerably less in Phase 2, indicating the effect of prior loading.

Phase 3. Before proceeding with further testing with a concentrated load in Phase 4, the model bridge was intentionally subjected to an overload of 0.75 times the dead load plus two times the equivalent of the live load conditions shown in Fig. D-1. This gave a total load of 1.75 D + 2.0 (L + I). All lanes were loaded with live load, with the loading in the middle lane off center.

The measured strain in the bent cap reinforcement before, at, and after this loading was applied is shown in Fig. D-38. Strains measured by the mechanical Whittemore gage were somewhat higher than the average strain determined from the electrical gages.

As seen in Fig. D-34, the strain in the main bent cap reinforcing bars under 1.0 (D) was insignificant. In Fig. D-38, the electrical

gages indicate that the maximum strain in the bent cap reinforcement under 1.75 D + 2.0 (L + I) was about 600 millionths, which is equivalent to a stress of 17 ksi.

The deflections in the model bridge under the 1.75 (D) + 2.0 (L + I) loading are indicated in Fig. D-39. The application of 1.75 (D) + 2.0 (L + I) produced an increase in residual deflection.

Phase 4. Application of a nominal 4 kip concentrated load at 3-ft. intervals along each box girder web provided confirmation of the elastic behavior of the structure and the distribution of reactions. The actual weight of the concentrated load was 4.23 kips. Measured reactions at the abutments and below the column were in excellent agreement with values predicted by analysis assuming that the structure as a whole acted like an elastic continuous beam.

Influence lines for bent cap deflection responses at the bent cap centerline with the load moving along the exterior and first interior girders are shown in Fig. D-40. Both model and prototype deflection scales are shown. The deflection at the end of the bent cap in a prototype structure, due to a 25 x 4.23 = 106 kip load at that point, would be expected to be about 5 x 0.018 = 0.09 in.

Influence lines for girder deflection responses at the point of maximum positive moment in each of the three girders, for the load moving along the girder, are shown in Fig. D-41.

Influence lines for girder deflection at the point of maximum positive moment in each of the three girders, for the load moving transversely across the section, are shown in Fig. D-42. The maximum deflection occurs at the exterior girder with the load at that point. This deflection would be about 0.22 in. in the prototype.

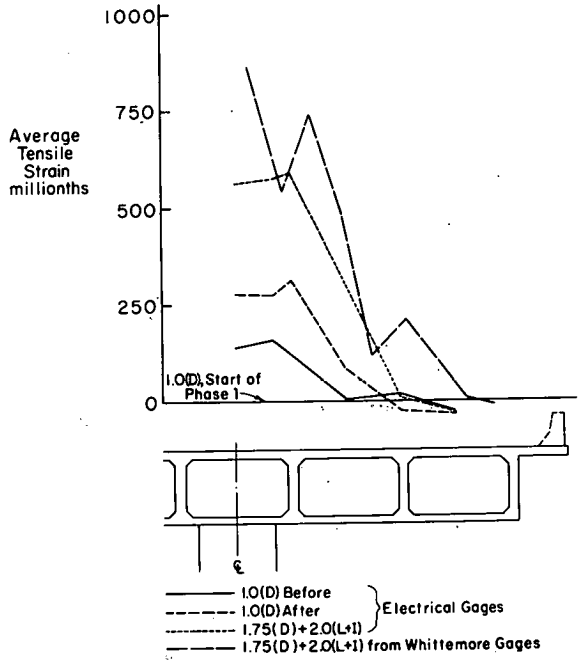

Fig. D-38 Strain in Bent Cap Reinforcement for Phase 3 Loading

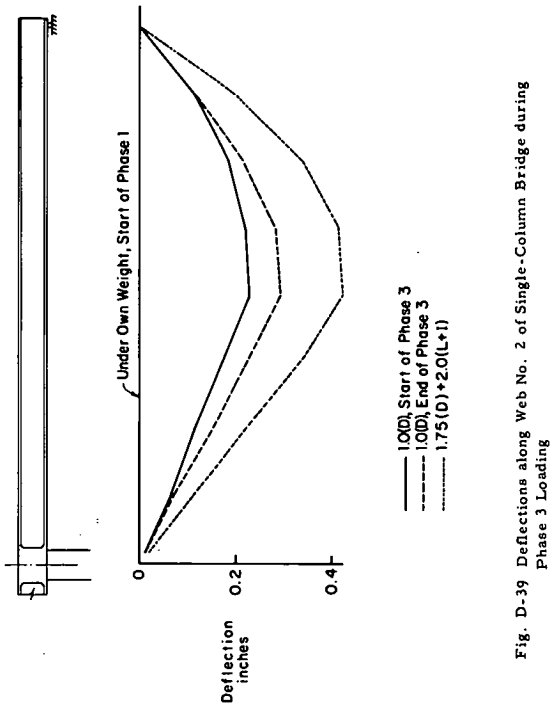

Fig. D-39 Deflections along Web No. 2 of Single-Column Bridge during Phase 3 Loading

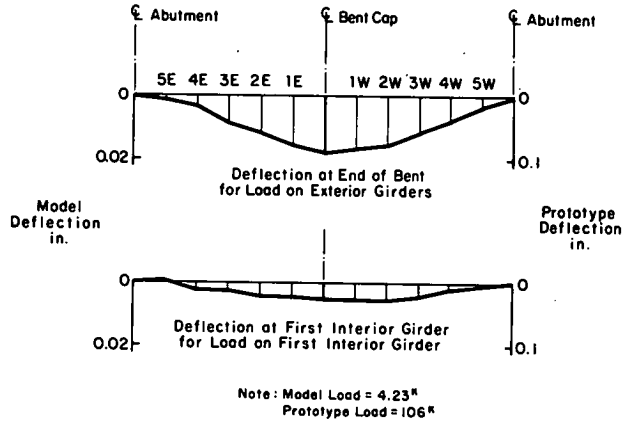

Fig. D-40 Influence Lines for Bent Cap Deflections

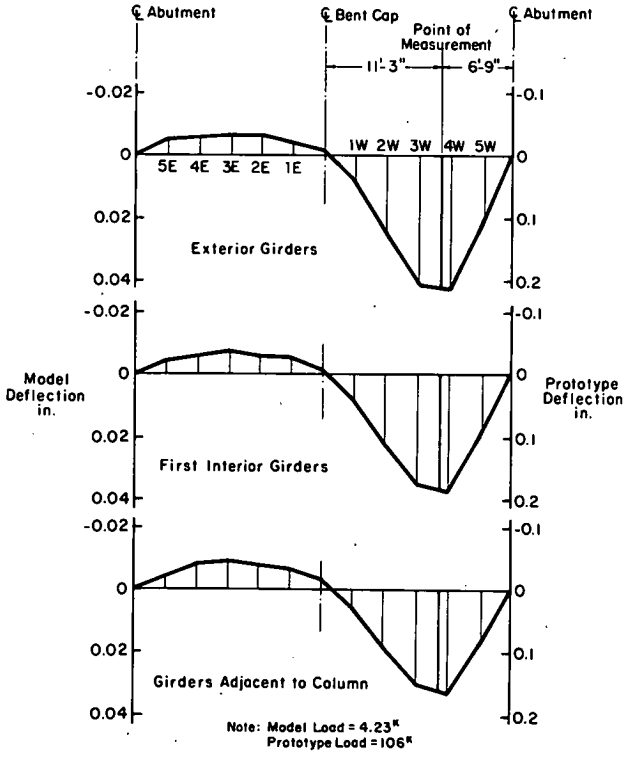

Fig. D-41 Influence Lines for Girder Deflections

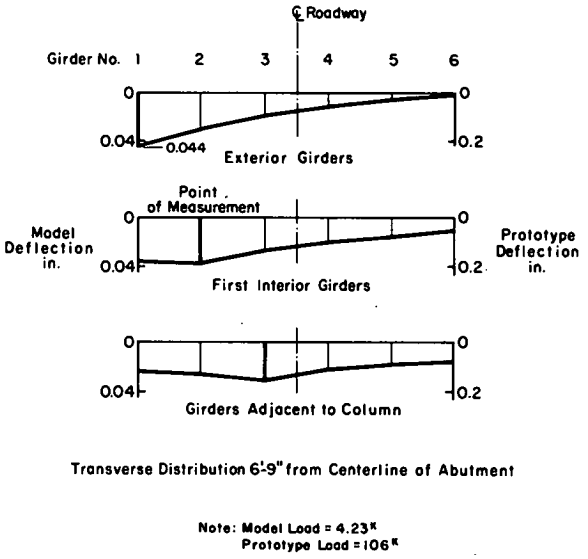

Fig. D-42 Influence Lines for Girder Deflections

Phase 5. In Phase 5, it was intended that loads representing various distributions of 1.5D + 2.5 (L + I) would be applied to the model. This planned value was obtained by dividing the design load factor, $1.35\ [D + \frac{5}{3}(L + I)]$ by $\phi = 0.9$, on the expectation that flexure would govern the behavior and that in the laboratory, $\phi = 1.0$. Due to errors in calculating the hydraulic pressures, however, the actual applied dead load was the equivalent of 1.37D.

First, the dead load was incremented to 1.37D. Next, 2.5 (L + I) was applied in lane 1. The load was then reduced to 1.37D. Next, 2.5 (L + I) was applied in lanes 1 and 2. The load was again reduced to 1.37D. Finally, 2.5 (L + I) was applied in all three lanes.

Fig. D-43 provides a comparison of the stress in the bent cap reinforcement under the first three Phase 5 loadings. This comparison is made at three sections through the bent cap. These are the centerline, the face of the column, and 3 in. in front of the face of the column. The data indicate that the highest stresses and the maximum stress response occur with all three lanes loaded. If the stress with all three lanes loaded is multiplied by the 0.9 factor for multiple lane loading[1], the response is still larger than for the other two cases. Consequently, it is concluded that the critical case is with all three lanes loaded. The data also indicate that the stresses at the face of the column and at a section one-quarter of the depth of the superstructure in front of the face of the column are approximately equal.

After the application of the first three loadings in Phase 5, the loadings for lane 1 and for lanes 1 and 2 were repeated with the dead load at the planned nominal 1.5D level. The responses to the

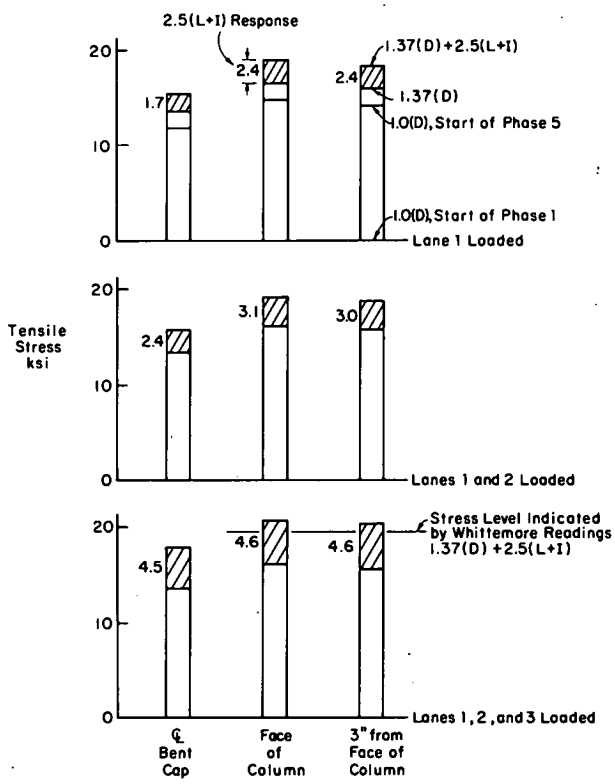

Fig. D-43 Stress in Bent Cap Reinforcement during Design Ultimate Test of Single-Column Model Bridge

2.5(L+I) loadings were the same as those shown in D-43. This indicated that the reduced dead load of the earlier series had little or no effect on the live load responses.

It should be noted that, due to the prior application of the 1.75D + 2.0 (L+I) load, none of these loadings is a new maximum. For this reason, the absolute values of the stresses should not be compared with those resulting from new maximum loadings. However, the responses can be compared with each other to determine critical load patterns.

Comparison of the stresses calculated from the Whittemore readings with those from the electrical gages again shows comparable results, as can be seen in Fig. D-43. The slightly lower stresses indicated by the Whittemore readings are attributed to the location of the gages being 1/2 in. outside of the edge of the bent cap.

Deflection response to Phase 5 loadings measured at the intersection of Web No. 1 and the bent cap, were 0.062, 0.066, and 0.040 in. under the application of 0.37(D) + 2.5 (L+I) load on lane 1, lanes 1 and 2 and lanes 1, 2, and 3 respectively. Measured crack widths in the roadway, in the vicinity of the column, were 0.008 in. or less.

Phase 6. In the test to destruction on the model bridge, load was applied in increments of a ratio, R, defined as the total applied load divided by the nominal design ultimate load. The nominal design ultimate load, R = 1.0, is 1.5 times the equivalent dead load of the prototype bridge plus 2.5 times the equivalent of the live loading shown in Fig. D-1. At the service load 1.0 [D + (L + I)], R is approximately equal to 0.6.

At the start of Phase 6, the equivalent dead load on the model was removed. In this condition, the model was resisting its own weight plus the weight of the loading apparatus, a total corresponding approximately to R = 0.1. Strains in the bent cap and adjacent box girder superstructure in this condition were previously shown in Figs. D-35 and D-36.

The measured deflection of exterior Web No. 1 during the test to destruction is shown in Fig. D-44. These plots show the deflection at the centerline of the bent cap and at the section of theoretical maximum positive moment, 6 ft. 9 in. from the abutment, assuming the superstructure acts as an elastic continuous beam. At R equal to about 1.8, the model was unloaded, as indicated by the dashed line, for an overnight rest period. It may be observed that the deflection at the section of maximum positive moment is about four times the deflection at the end of the bent cap. At the design service load of R = 0.6, the maximum deflection of 0.38 in. during the initial loading cycle corresponds to 1.90 in. in the prototype. This is about 1/570th of the span length.

Deflections of the bridge superstructure along transverse lines at the bent cap and at the section of maximum positive moment are shown in Fig. D-45. Deflections of the bent cap were measured at points located at the intersection of each web with a line 3.5 in from the centerline of the bent cap. Deflections of the superstructure along Web No. 3 are shown in Fig. D-46.

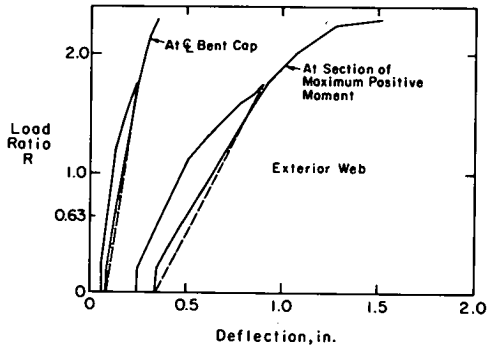

Fig. D-44 Deflection of Single-Column Model Bridge during Test to Destruction

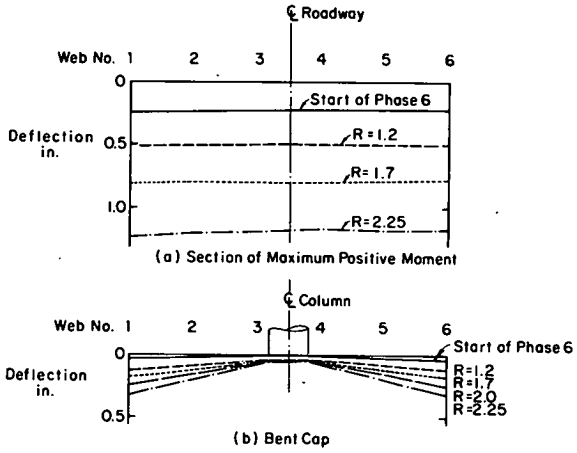

Fig. D-45 Transverse Distribution of Deflections for Single-Column Model Bridge during Test to Destruction

D-75

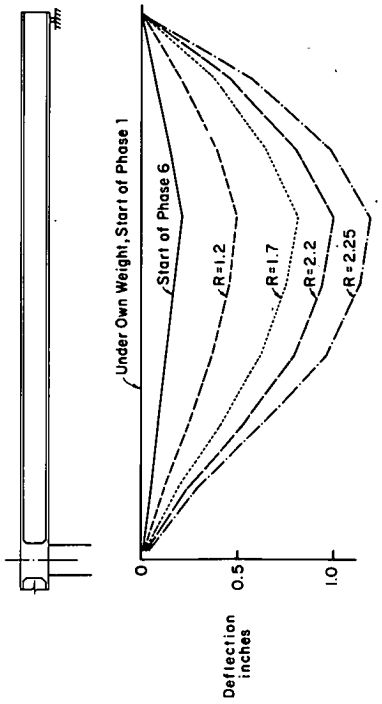

Fig. D-46 Deflections along Web No. 3 During Test to Destruction of Single-Column Model Bridge

D-77

D-78

The test was concluded when slip of lapped splices in the main box girder positive moment reinforcement occurred in a region where other bars were cut off. When this occurred, the load had just been raised to the level of R = 2.3. In Fig. D-47, a side view upward toward the superstructure shows the separation that occurred in the bottom slab at a section approximately 3 ft. from an abutment. A close view of the bottom slab below Web No. 2 is shown in Fig. D-48. Inspection disclosed that only one of the main D-5 reinforcing bars across the full width of the bottom slab was fractured. However, all of the auxiliary D-2 bars crossing the section were fractured.

In Fig. D-49, average measured strain in the bent cap reinforcement is plotted for several values of the load ratio, R. From this plot, it is evident that the maximum strain occurred at the edge of the column. The maximum measured strain was 1950 millionths which corresponds to a stress of 56 ksi.

Experimentally determined stresses in the bent cap flexural reinforcement are compared in Fig. D-50 with values of the stresses predicted by the Working Stress method. The experimental stress is calculated from the average strains at the face of the column, the location of maximum strain as shown in Fig. D-49.

The predicted stresses were calculated by assuming that the stress was 24 ksi for service load (taken to be R = 0.6) at the design section one-sixth the column diameter from the column centerline. The stress, assumed to be linearly related to moment, was then adjusted from the design section to the gaged section using the service load moments of Chapter 2.

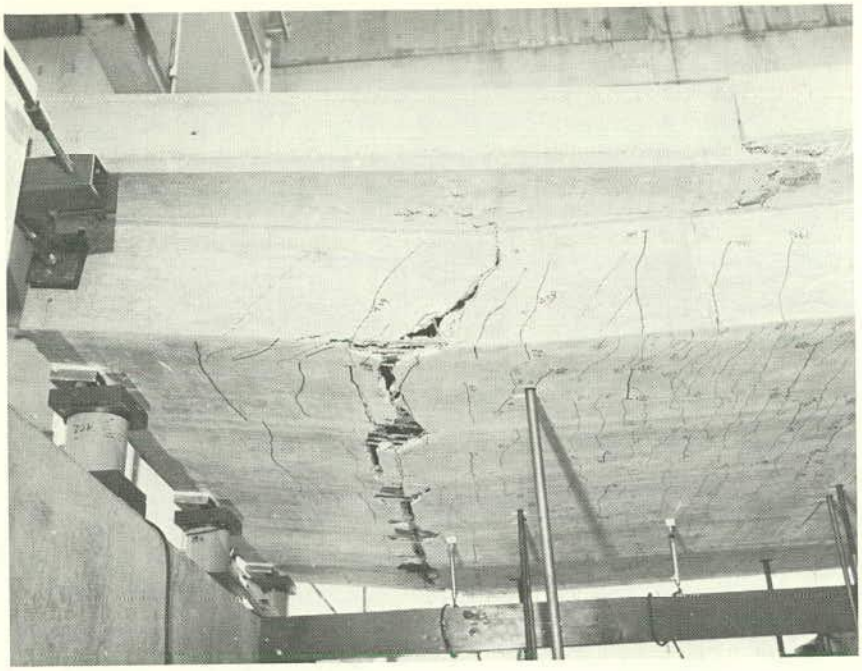

Fig. D-47 View of Region of Distress after Phase 6 Loading for Single-Column Model Bridge

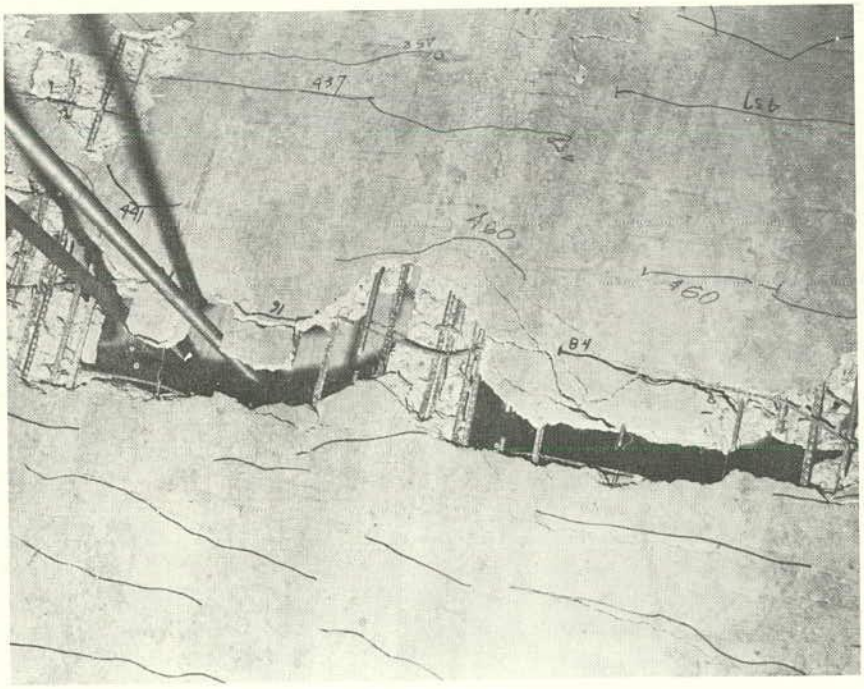

Fig. D-48 Bottom Slab Directly below Web No. 2 in Single-Column Model Bridge

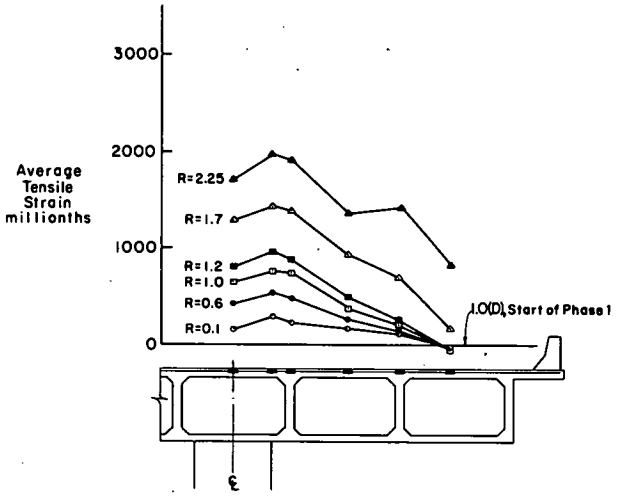

Fig. D-49 Strains in Bent Cap Reinforcement of Single-Column Model Bridge

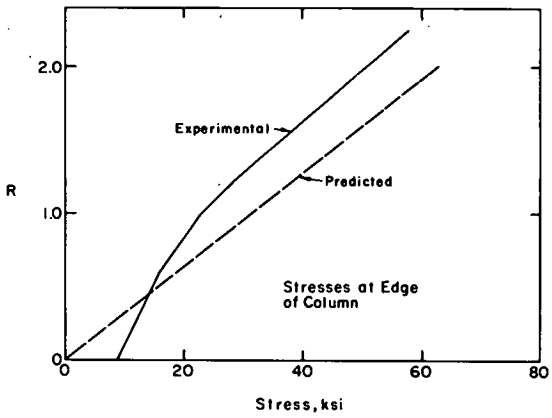

Fig. D-50 Predicted and Measured Stress in Bent Cap Reinforcement of Single-Column Model Bridge

This calculation did not take into account several factors that tend to reduce the measured stress as compared to the predicted. These factors include participation of surrounding superstructure in carrying the load, area of reinforcement greater than that required by the design, liberal assumptions of dead load in the original design, and the conservative nature of the Working Stress method.

The agreement between measured and predicted stresses seems to be satisfactory, considering the approximations involved.

Measured strains in the bent cap stirrups are shown in Fig. D-51. Maximum stirrup strains occurred midway between Web Nos. 2 and 3. Strains in the bent cap stirrups directly over the column were quite low.

Crack width measurements were taken at selected locations on the roadway surface in the vicinity of the column. These data, plotted in Fig. D-52, indicate substantial variation in crack widths depending on the location and orientation of the cracks. A photograph of the crack patterns taken after the end of the test is presented in Fig. D-53. As shown by the dashed lines in Fig. D-52, the width of cracks transverse to the box girders are considerably greater between the webs than directly over them. These wider cracks were located beyond the ends of the shorter flexural reinforcement in the girders. In this region, only a small amount of reinforcement crossed the crack. Cracks across the bent cap near the column were somewhat narrower than those in the box girders. However, widths of cracks that formed at higher loads near bar cut offs in the bent cap were substantial when first observed. Widths of these cracks increased rapidly with load.

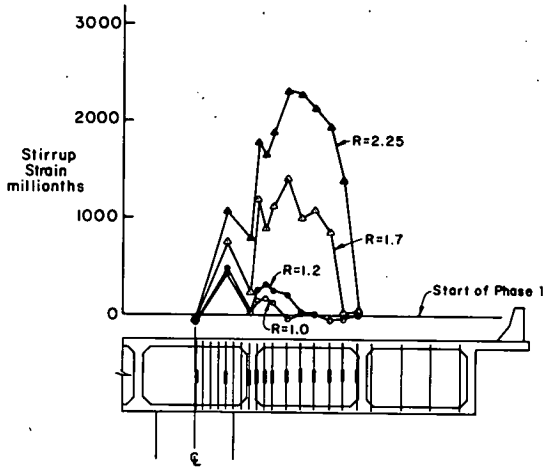

Fig. D-51 Strains in Bent Cap Stirrups of Single-Column Model Bridge

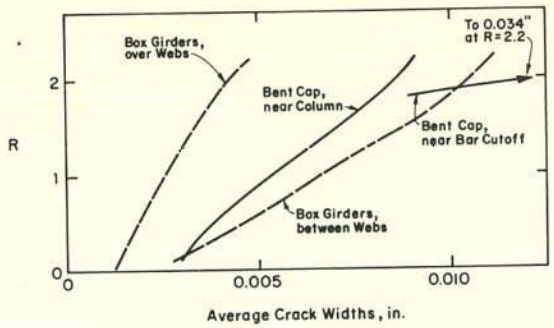

Fig. D-52 Measured Crack Widths in Roadway of Single-Column Model Bridge

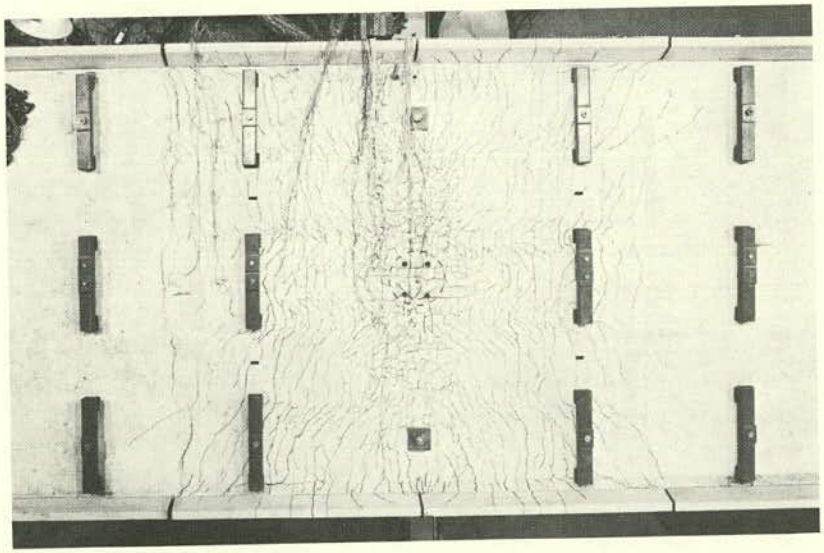

Fig. D-53 View of Crack Pattern in Roadway Slab Directly over the Column of Single-Column Model Bridge

Phase 7. Testing was resumed after repairs had been made on the end of the bridge where the distress had occurred. In this process, the bridge was restored to its proper alignment. Next, a length of 6 ft. of each box girder cell was filled with concrete and was reinforced vertically.

A similar arrangement was used to strengthen the opposite end of the bridge, since it appeared that a tension failure was imminent in this region as well. In addition, external stirrups were placed on all the webs in the span that failed. These stirrups were located in the vicinity of the point of inflection, approximately 4-1/2 ft. from the centerline of the bent cap. This region had been damaged as the initial failure occurred.

It was estimated that about 4 kips of weight was added at each end of the bridge in repairing the box girders. For analysis, it was assumed that 85 percent of this weight was distributed to the abutment and 15 percent to the column.

The critical bent cap loading condition, with all three lanes loaded, was incremented to destruction. Failure again occurred at R equal to 2.3. Collapse occurred in the same span as before, but in the region located at the interior end of the positive moment steel cut-offs. It again appeared to be caused by loss of anchorage at splices of the main bars.

Phase 8. Since the bent cap of the bridge was still undamaged, the ends of the model were severed at sections located approximately one-quarter of the span on either side of the centerline of the bent cap. The remaining portion, shown in Fig. D-54, was subjected to a loading consisting of concentrated forces, P/2, applied near the severed

end of each box girder web, 3 ft. from the centerline of the bent cap. Additional concentrated forces equal to P were also applied at the intersection of the centerline of the bent cap and the center of the exterior boxes, 3 ft. from the centerline of the column. This loading approximated the loading on the bent cap in the preceding tests.

As indicated by Fig. D-55, the measured strength of the bent cap was approximately 40 percent greater than the capacity expected assuming a critical section at the face of the column. This suggests that the reinforcement in adjacent parts of the deck was also effective in resisting the external movement on transverse sections through the bent cap.

The side view of the damaged region, shown in Fig. D-56, shows substantial shear distress in the bent cap. Close inspection showed that several stirrups were fractured. However, the main shear crack appears to have started as a flexural crack in the region where several main bent cap bars were terminated. At the last load stage before the test was terminated, a strain of 2,200 millionths was measured on a bar at this location. This indicated that yielding was imminent. At this load stage, strains near and slightly above the yield strain were also measured at sections at the face of the column and 3 in. from the face of the column. The failure was therefore considered to be due to flexure, but the shear reinforcement in the vicinity of the bar cut-offs was apparently insufficient to allow substantial yielding.

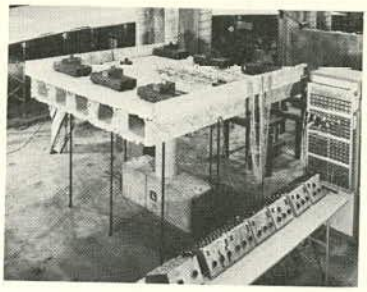

Fig. D-54 View of Test of Bent Cap Portion of Single-Column Model Bridge

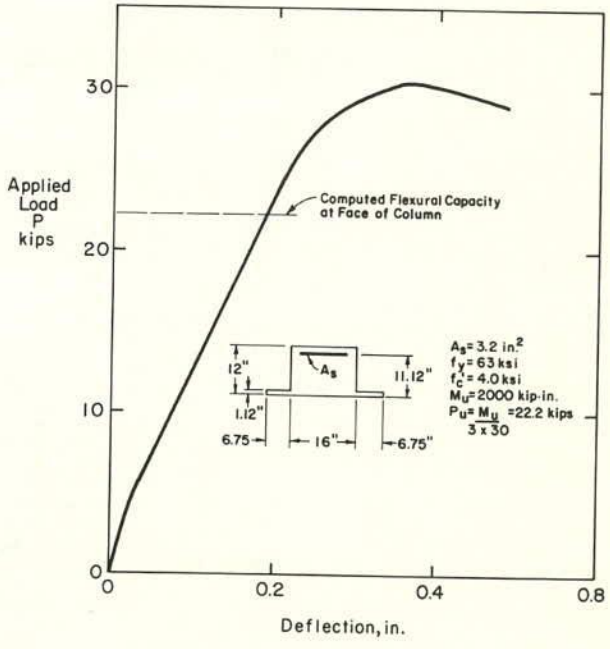

Fig. D-55 Deflection at End of Bent Cap for Test of Bent Cap Portion of Single-Column Model Bridge

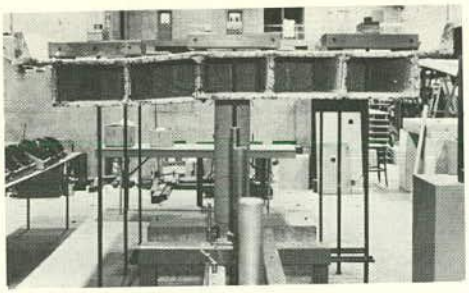

Fig. D-56 Side View Showing Distress of Bent Cap Portion of Single-Column Model Bridge

Test of Double-Column Model Bridge

General Planning of Test Program. As was the case for the single-column model bridge, the test program included the application of the dead load makeup followed by measurement of the response to a series of loads of successively increasing magnitude. However, some of the lower intensity loads applied to the single-column model were not applied to the double-column model bridge, since it had been found in the test of the single-column model that the effects of the low intensity loads were difficult to interpret due to the small quantities involved.

Materials. Material properties for the double-column model bridge are summarized in Tables D-8 and D-9.

Summary of Phases. Testing of the double-column model bridge was performed over a period of 25 days. For reference, the phases of the testing program are listed and briefly described in Table D-10.

Outline of Program. The test program for Phases 1 and 2 in the double-column model bridge paralleled that for the same phases in the single-column model. The response to various equivalent AASHO service loadings before (Phase 1) and after (Phase 2) the addition of parapets was measured. No concentrated loads were applied to the double-column model in these phases.

In Phase 3, the equivalent AASHO loadings 1.5 D + 2.5 (L + I) in distributions most highly stressing the various locations in the model were applied. The results provided information on the critical loading for the bent cap. This series of loadings was equivalent to the loadings applied in Phase 5 of the tests on the single-column model bridge. No preceding overload had been applied, however.

TABLE D-8 REINFORCEMENT PROPERTIES FOR DOUBLE-COLUMN MODEL BRIDGE

Reinforcement	Yield Stress f_y, ksi	Tensile Strength f_{su}, ksi	Modulus of Elasticity E_s psi x 10^6
D1	70.7	71.1	26.6
D2	57.9	67.6	29.0
D5	74.4	82.3	30.1
No. 4	63.1	104.8	27.4

TABLE D-9 CONCRETE PROPERTIES FOR DOUBLE-COLUMN MODEL BRIDGE

Concrete Location	Age at Start of Testing Days	Compressive Strength f'_c psi	Splitting Tensile Strength f_{sp} psi	Modulus of Elasticity E_c psi x 10^6
Bottom Slab, Webs, and Bent Cap	107	3450	410	3.1
Deck Slab	76	4610	540	3.9

TABLE D-10 TEST PROGRAM OF DOUBLE-COLUMN BRIDGE

Phase	Description	Number of days from start of testing
1	Application of equivalent dead load and various equivalent AASHO service loadings 1.0 [D + (L + I)]	1 to 4
-	Delay while parapets were cast and allowed to cure	5 to 19
2	Application of equivalent AASHO service loadings 1.0 [D + (L + I)]	20
3	Application of equivalent AASHO ultimate loadings 1.5 D + 2.5 (L + I)	21 to 22
4	Special tests, including application of concentrated loads, and settlement and rotation of columns	22 to 24
5	Test to destruction	25

In Phase 4, a series of special tests was conducted. These included application of a 4 kip concentrated load successively at points spaced at 3 ft. intervals along each web, and the introduction of known rotations and displacements at the base of the columns.

Finally, in Phase 5, the bridge was loaded to destruction by incrementally applying multiples of an equivalent loading of 1.5 (D) + 2.5 (L + I) on all six lanes. Collapse occurred due to a combination of the effects of flexure and shear in the box girders adjacent to the bent cap at a load 2.2 [1.5 (D) + 2.5 (L + I)].

Preparation. The bridge was carefully examined for cracking prior to the start of testing. One 4-ft. long crack was found in the bottom slab, almost exactly on the centerline of the roadway. This crack started at the side of the bent cap. Several other short cracks, also parallel to the centerline of the roadway, were found extending from loading rod holes, near the bent cap. A few similar cracks were found extending from loading rod holes in the roadway slab. All of these cracks were indicative of differential shrinkage between the bent cap and adjacent superstructure.

Following the removal of shoring, the elevations of the supports were adjusted until the reactions approximated those predicted by an elastic analysis. The total weight of the model bridge and the loading equipment suspended from it was 41.2 kips. Reactions at the column bases were 14.0 and 14.3 kips. The five reactions at each abutment varied from 1.2 to 1.4 kips. As for the single-column model bridge, an upward curl of the roadway surface, measured to be 0.5 in., was observed at this stage.

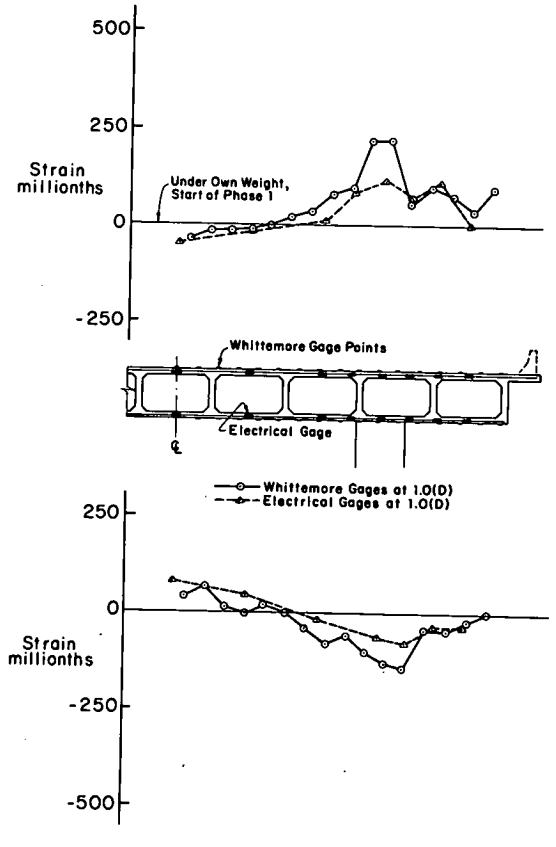

Fig. D-57 Measured Strains from Application of Equivalent Dead Load to Double-Column Model Bridge

After the reactions were set, the dead load makeup was applied to produce conditions equivalent to the dead load of the prototype. As in the case of the single-column bridge, this loading was maintained, as a minimum, during the testing period, except for brief periods when the model was unloaded to obtain zero readings on instrumentation. These unloading periods occurred at the start of Phases 2, 3, and 5. A comparison of the strains measured by electrical and Whittemore gages in the bent cap when the loading was 1.0 (D) is shown in Fig. D-57. The strains measured were similar to those found for similar loading on the single-column model bridge.

Time-Dependent Behavior. The double-column bridge was somewhat older than the single-column bridge at the start of testing. However, the period of testing was less than half as long, as seen by comparing Tables D-7 and D-10.

As in the case of the single-column model bridge, strains throughout the term of the test were monitored by means of the Whittemore mechanical strain gage. Initial measurements were taken with the model bridge in the form, or shortly after its removal. Subsequent measurements were taken at selected times.

Data presented in Fig D-58 and D-59 show the deformation which had taken place at the start of testing and also at the start of Phase 5, the test to destruction. For these sets of measurements, the model bridge was supporting its own weight, plus the weight of loading equipment. In addition, Figs. D-58 and D-59 include strain data with the double-column bridge under equivalent dead load at the start of Phase 1. A pattern similar to that observed in the single-column model bridge was obtained.

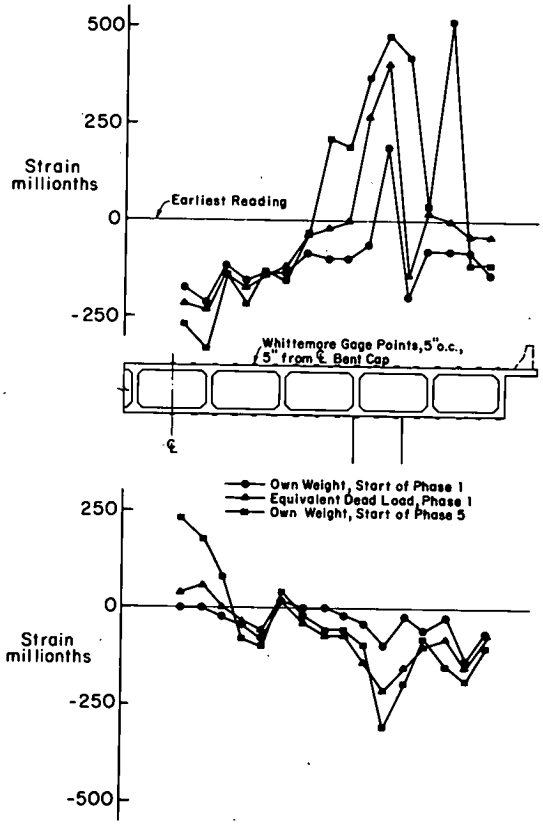

Fig. D-58 Mechanical Strain Gage Measurements on Bent Cap of Double-column Model Bridge

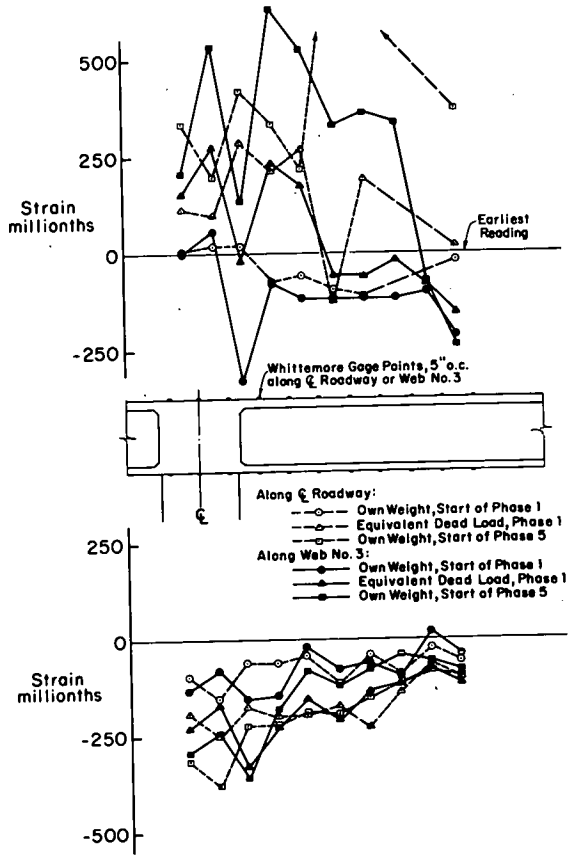

Fig. D-59 Mechanical Strain Gage Measurements on Girders of Double-Column Model Bridge

D-98

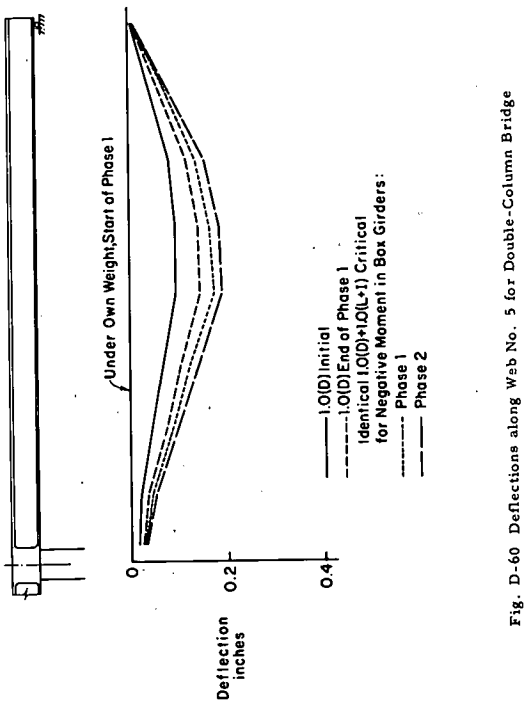

Fig. D-60 Deflections along Web No. 5 for Double-Column Bridge

D-100

Phase 1. The first live loading applied to the bridge consisted of a distributed lane load, equivalent to 640 pounds per linear ft. plus impact, and two concentrated loads each equivalent to 18 kips plus impact, located 37.5 ft. (7.5 ft. in the model) either side of the centerline of the bent cap in each of the six traffic lanes. With the dead load, this loading was equivalent to a 1.0 (D) + 1.0 (L + I) loading on all six lanes of the prototype producing maximum negative moment in the box girders. No reduction was made in live load intensity for the multiple lane loading.

The deflection of Web No. 5, adjacent to the centerline of the roadway, under Phase 1 loading, is shown in Fig. D-60. The maximum deflection of Web No. 5 was 0.19 in. Deflection of the bent cap at its intersection with this web was 0.03 in. Noting that the maximum deflection of Web No. 5 under the equivalent dead load was 0.10 in., the corresponding maximum deflection of the prototype under 1.0 (D) + 1.0 (L + I) would be 1.08 in. or 1/1000th of the span. The corresponding maximum deflection determined from measurements on an exterior web of the single-column model bridge was 1.19 in. The double-column bridge deflection was less even though on the average each box girder in it carried 20 percent more live load than did the single-column bridge girder.

Subsequently, individual lane loads and concentrated loads were applied to further condition the superstructure. These loadings demonstrated that, as for the single-column bridge, the overall behavior was essentially linear although the measured strain response at specific locations was quite erratic.

D-99

Next, loading equivalent to that shown in Fig. D-2 was applied. Besides the loading equivalent to 640 lbs. per linear ft. plus impact on each lane, concentrated loads equivalent to 26 kips plus impact were applied on the bent cap in lanes 1, 3, 4, and 6. The application of this live loading produced a deflection of the bent cap at its cantilevered end and at its intersection with the centerline of the roadway of 0.003 in. and 0.005 in. respectively.

Phase 2. The parapets cast on the double-column model bridge were similar to those on the single-column bridge. Again, open joints were provided at the centerline of the bent cap and at the quarter points of the span. During the 15-day period in which the parapets were cast and allowed to cure, the model was maintained under an equivalent dead load condition. Subsequently, several of the AASHO loading conditions previously applied in Phase 1 were reapplied.

A comparison of the deflection of the model under the loading condition critical for negative moment in the box girders is given in Fig. D-60. This comparison shows that the maximum deflections increased by about 10 percent. However, it should be noted that the deflection response under the application of the equivalent dead load plus the live load was considerably less in Phase 2, indicating the effect of prior loading.

Phase 3. In Phase 3, the equivalent AASHO ultimate loads were applied to obtain information on the critical loading for the bent cap. Values of stress, computed from the average measured strain of four gages at each of three locations on the bent cap reinforcement, are plotted as bar graphs in Fig. D-61.

D-101

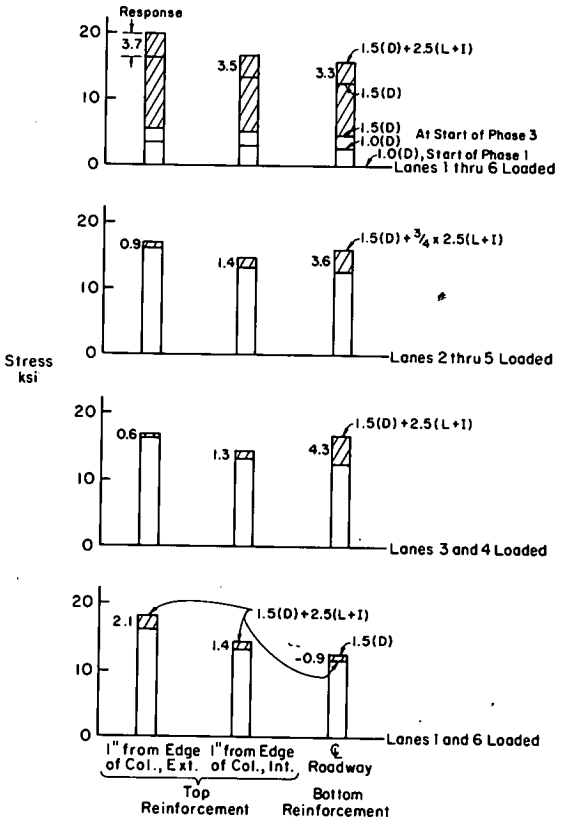

Fig. D-61 Stress in Bent Cap Reinforcement of Double-Column Model Bridge

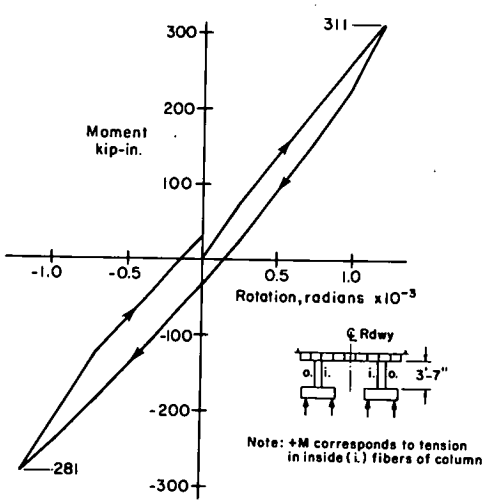

Fig. D-62 Moment Required to Rotate Column Bases of Double-Column Model Bridge

As indicated in the upper graph in Fig. D-61, the stresses in the bent cap reinforcement at all three locations had increased by about 3 ksi under the equivalent 1.0 (D) loading between the start of Phase 1 and the start of Phase 3. First, the dead load was increased to 1.5 (D), resulting in the increase in stress shown in Fig. D-61. Next, live load equivalent to 2.5 times the loading shown in Fig. D-2 was applied on all six lanes. This loading produced the maximum stresses shown by the bars in the upper graph. The response is shown as the crosshatched portion of the bar. When this equivalent live load was removed, the stresses shown as the line across the crosshatched portion of the bar remained. These stresses were substantially greater than those measured previously under the application of 1.5 (D). This resulted because the applied load was a new maximum.

Subsequently, distributed lane loads equivalent to 2.5 (L + I) were applied successively to lanes 2 through 5, 3 and 4, and 1 and 6. The maximum stresses measured under these loadings are also plotted in Fig. D-61. Between each of the loadings, the stresses under the 1.5 (D) load condition were the same as those measured after the initial application of load on all six lanes. Loading on lanes 2 through 5 was applied at 75 percent intensity to comply with AASHO specifications for multiple lane loadings.

Examination of the dead and live load stresses shown in Fig. D-61 indicates that they are about one-half of the corresponding design stresses for the prototype given in Table D-1. It is also evident that the critical live loading for the top bent cap reinforcement over the column is with load on all six lanes. Even if the stress responses of 3.7 and 3.5 ksi based on the 1.5 D condition after loading near the exterior and interior

edges of the column are multiplied by 0.75, to account for the AASHO specification for loading on multiple lanes, they would be greater than for any of the other loading conditions. The maximum measured stress in the bottom reinforcement occurred with the live load on lanes 3 and 4 in accord with the design of the prototype.

Phase 4. Several special tests were conducted on the model in Phase 4. First, because it had been difficult to distinguish between a pinned or fixed condition at the base of the columns in any of the prior loading conditions, vertical displacements and rotations were applied to the bases. It was found, however, that small vertical displacements could not be reliably correlated with a change in the column reaction.

For example, when a vertical settlement of 0.1 in. was introduced at both columns, while the model was being maintained under its equivalent dead load condition, the measured change in the sum of both reactions was 6.8 kips. Using a modulus of elasticity of 3.5×10^6 psi the average of measured values for the concrete in the superstructure, and using the gross section properties of the superstructure, the predicted settlement for this change in the reactions was 0.21 in. This large inconsistency between the measured change in reactions and predicted settlement was attributed to friction and other restraints in the loading system. This was verified by the observation that only a small part of the decrease of 6.8 kips at the bases of the columns was found as an increase in the abutment reactions.

The moment required to produce rotation at the base of the columns was determined for different conditions. One of these is plotted in Fig. D-62. For this condition, both column bases were rotated

simultaneously in opposite directions, first to produce tension on the "inside" fibers, nearest the centerline of the roadway, and subsequently to produce compression on the "outside" fibers. The rotations were applied by means of the two mechanical jacks at the support points beneath each column. The elevation of the base was held constant.

Based on the average of the values of maximum moment producing a rotation of 0.0012 radians, equal to 296 kip-in. or 24.7 kip-ft., the corresponding relation between moment and rotation in the prototype would be (24.7 x 125)/1.2 = 2570 kip-ft. per 0.001 radian.

When the base of only one column was rotated, a moment of 270 kip-in. was required to produce a rotation of 0.0012 radians. When both columns were rotated simultaneously in the same direction, moments of 235 kip-in. were required to produce the same rotation.

Prior to application of the 4-kip concentrated load at 3-ft. intervals along the webs of the bridge, concentrated loads of 1, 2 and 4 kips were applied successively at the intersections of the centerline of the bent cap and Web No. 1, centerline of the roadway, and Web No. 10. Loads of 1, 2 and 4 kips on the model are equivalent to 25, 50, and 100 kips respectively, on the prototype.

The stress response in the top and bottom reinforcement of the bent cap, shown in Fig. D-63, was small under application of the concentrated loads. However, the response is linear with load, and consistent with location.

Influence lines for stress in the bent cap reinforcement at three locations are shown in Fig. D-64. These influence lines show the effect of a 4 kip concentrated load applied within one third of the span

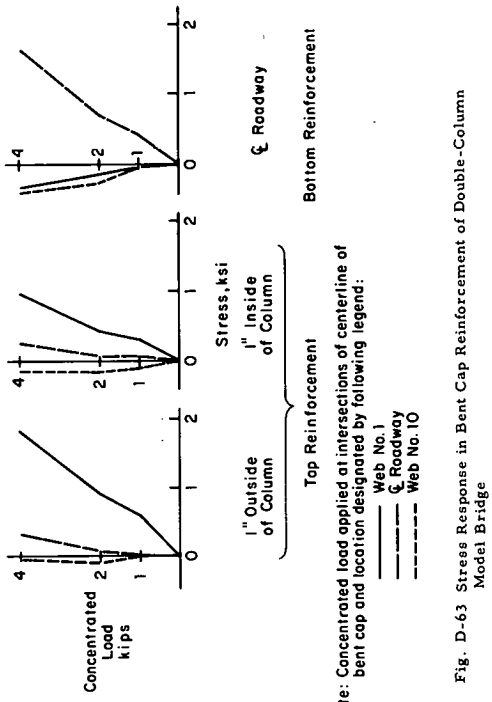

Fig. D-63 Stress Response in Bent Cap Reinforcement of Double-Column Model Bridge

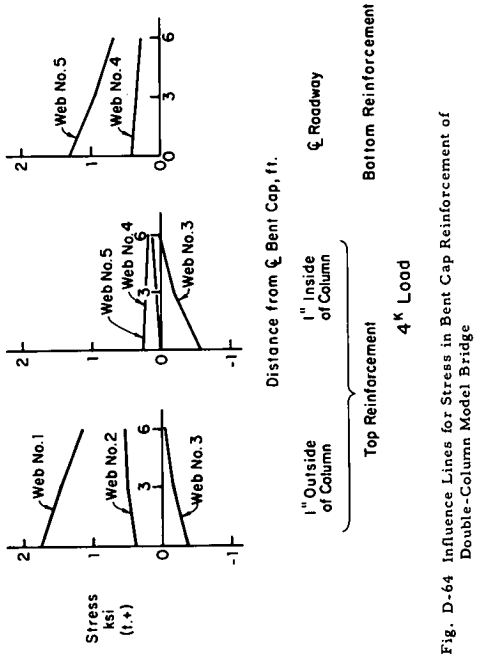

Fig. D-64 Influence Lines for Stress in Bent Cap Reinforcement of Double-Column Model Bridge

from the centerline of the bent cap. Stress response of the top reinforcement on the inside of the column is small when concentrated loads are applied between the columns.

Phase 5. The test to destruction was carried out following procedures similar to those used for the single-column model bridge. Again, load was applied in increments of a ratio, R, defined as the total applied load divided by the nominal design ultimate load. The nominal design ultimate load, R = 1.0, is 1.5 times the equivalent dead load of the prototype bridge plus 2.5 times the live load shown in Fig. D-2.

Measured deflections of Web No. 5, nearest to the centerline of the roadway, and of Web No. 1, the exterior web, during the test to destruction are shown in Fig. D-65. By comparison with deflections measured in the test on the single-column bridge, shown in Fig. D-44, it may be noted that the maximum deflections of the bent cap and the superstructure of both bridges were approximately equal.

Transverse deflections at the bent cap and at the section of theoretical maximum positive moment are shown in Fig. D-66. Longitudinal deflections along Web No. 5 are shown in Fig. D-67. In Fig. D-66 it may be noted that the bent cap deflections, at R = 2.2, are nearly equal at the end and at the centerline of the roadway. In Fig. D-67 it may be seen that the maximum longitudinal deflection occurred at midspan rather than the theoretical section of maximum positive moment. As in the case of the single-column bridge, it appears that a concentration of rotation exists at the intersection of the bent cap and the superstructure, leading to behavior between that of a simple and continuous span.

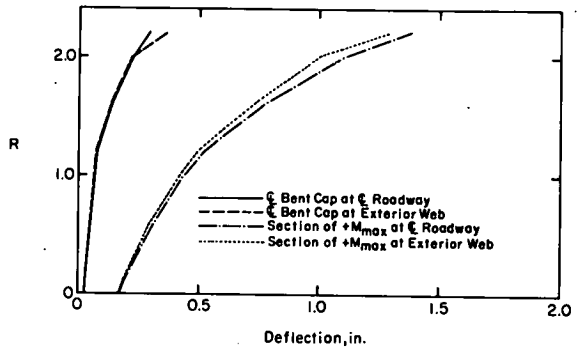

Fig. D-65 Deflections of Double-Column Model Bridge during Test to Destruction

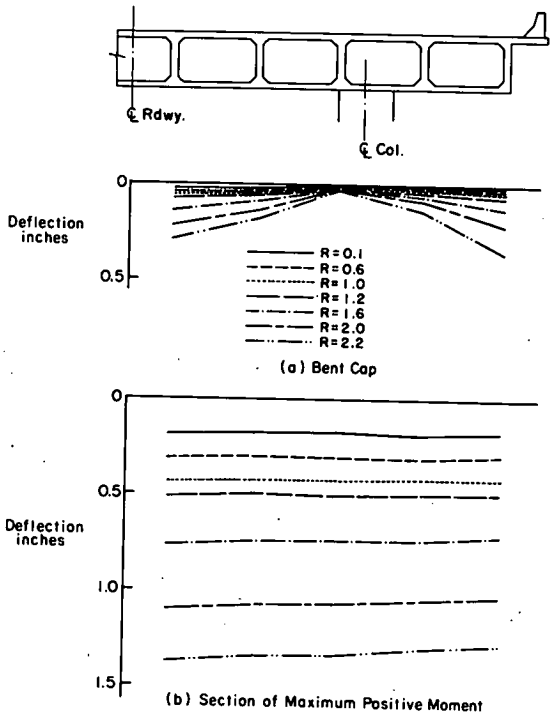

Fig. D-66 Transverse Distribution of Deflections for Double-Column Model Bridge during Test to Destruction

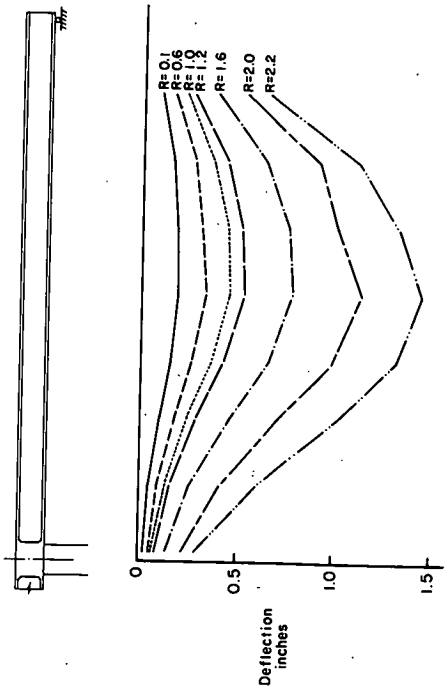

Fig. D-67 Deflections along Web No. 5 during Test to Destruction of Double-Column Model Bridge

Collapse of the model occurred after the application of the load equivalent to 2.2 [1.5 D + 2.5 (L + I)]. The collapse was apparently caused by the combination of the effects of flexure and shear in the box girders adjacent to the bent cap. The first indication of distress was a line of spalling of the girder lower flanges along the face of the bent cap near a column. Within a period of about one minute, the spalling progressed approximately 2 ft. along this line toward the center of the bridge. At this time sounds of several fractures of reinforcement were heard; it was later determined that the fractures occurred in box girder stirrups. After this event, the line of spalling increased rapidly in length, extending both toward and beyond the center of the bridge and toward the exterior web. Finally, sudden and complete destruction of the compression zone of the girders occurred along the line of spalling, resulting in the collapse of the bridge.

A view of the exterior of Web No. 1 after the test was completed is shown in Fig. D-68. The distress appeared to initiate at the intersection of Web No. 3 and the bent cap, where spalling of the bottom slab was observed. A view of this region, after the test was complete, is shown in Fig. D-69. This photo was taken, with respect to Fig. D-68, from behind the column. The potentiometer in the foreground of Fig. D-69 is located at the intersection of Web No. 4 and a line parallel to, and 1 in. to the near side of, the centerline of the bent cap. The line of Whittemore points furthest in the background is located along Web No. 3. The separation in the slab, at Web No. 3, extends upward from the bottom surface at a flat angle to the intersection of the junction of the web, bottom slab, and face of the bent cap. It then extends along

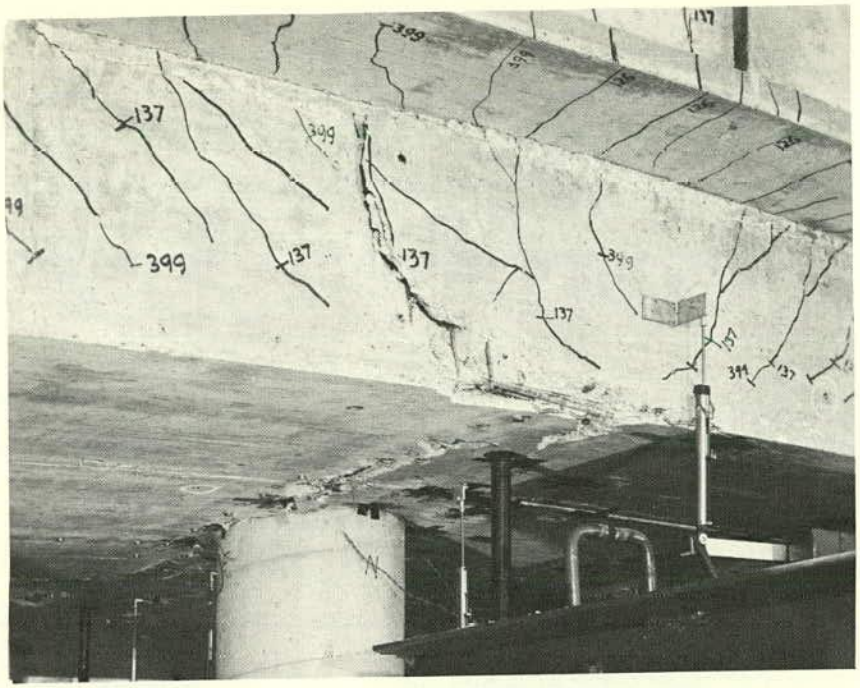

Fig. D-68 Web No. 1 after Test to Destruction of Double-Column Model Bridge

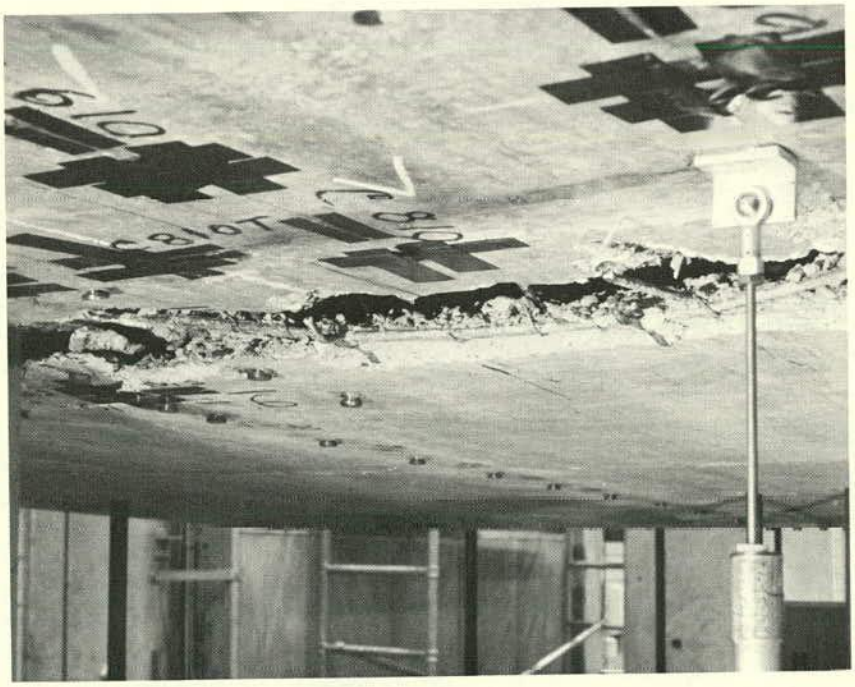

Fig. D-69 Region of Initial Spalling after Test to Destruction of Double-Column Model Bridge

this junction for approximately 4 in. Finally, it extends upward through the web at an angle of about 45 degrees. Cracking in Web No. 4 was quite similar. Several stirrups were fractured in both these webs. Cracking in Web Nos. 2 and 5 was more like that shown in Fig. D-68 for Web No. 1. There were no fractured stirrups in these webs.

Strains measured in the top and bottom bent cap reinforcement of the double-column model bridge are shown in Fig. D-70. As can be seen, the location of maximum strain for the top reinforcement is not within the column. Rather it is at a section located outside of the column. In this case, the maximum strain was measured at a location beyond a point where some of the reinforcement in the negative moment region was cut off.

Fig. D-70 shows that the location of zero stress in the bottom bent cap reinforcement was near Web No. 4 at low load, but moved toward the column at higher load.

Experimentally determined stresses in the bent cap flexural reinforcement are compared with approximate values of the stresses predicted by the Working Stress method in Fig. D-71. The experimental stress for negative moment is taken at the section 1 in. outside the exterior face of the column. The stress for positive moment is taken at the bridge centerline.

The predicted values were determined by assuming that the stress was 24 ksi at the relevant critical design section at service load (taken to be R = 0.6) for the critical load distribution. Adjustment was then made to account for applied loading conditions and location of measurement.

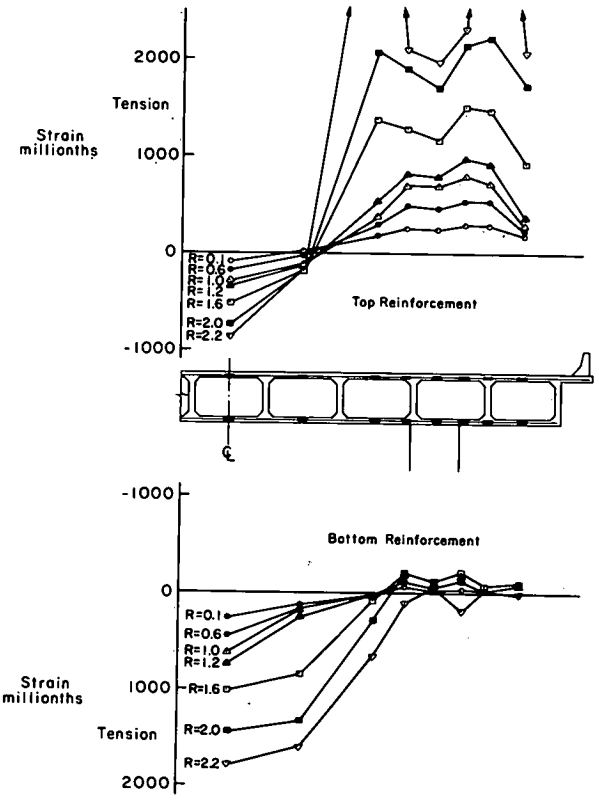

Fig. D-70 Strains in Bent Cap Reinforcement of Double-Column Model Bridge

For the negative moment case, the applied load was the same (6 lanes loaded) as assumed in the design, but the critical design section was taken 1/6 column diameter inside the column centerline. The predicted stress for Fig. D-71 was obtained at R = 0.6 by multiplying the 24 ksi design stress by the ratio of the indicated moment at the gaged section to that at the design section. To do this, service load moments of Chapter 2 were used.

The positive moment stress was measured at the point assumed critical in the design. However, the design load distribution was lanes 3 and 4 loaded, rather than all lanes loaded. The predicted stresses were adjusted according to the difference in moments as calculated by the design method.

The approximate calculations do not take into account such factors as stress reduction due to participation of surrounding superstructure, round off to a higher value of the design area of reinforcement, liberal assumptions of dead load in the original design, and the conservative nature of the working stress method. On the other hand, two factors tending to increase the measured stresses were not taken into account. These include the stress concentration due to bar cutoffs and the reduced effectiveness of the ungaged short bars.

The agreement between measured and predicted stresses in the negative moment region is reasonable, considering the approximations involved. The correspondence in the positive moment region was not as good and may have been influenced by the tendency for the interior span of the bent cap to behave as a built-in beam, with clear-span moments substantially less than the centerline-dimension moments assumed in the design.

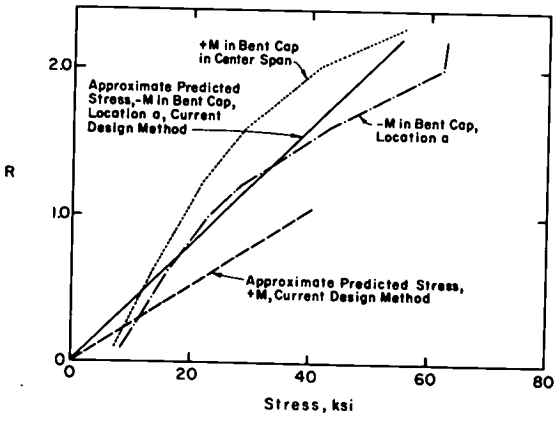

Fig. D-71 Predicted and Measured Stresses in Bent Cap Reinforcement of Double-Column Model Bridge

Measured strains in stirrup reinforcement in the bent cap are shown in Fig. D-72. High stirrup strains were measured in regions both inside and outside the columns. The data indicate that the design of the bent cap in shear was adequate, since stirrup strains approached yield as the flexural reinforcement yielded.

Data obtained from a limited number of crack width measurements on the roadway surface are summarized in Fig. D-73. The solid line is the average of measurements on cracks normal to the beat cap reinforcement located about 3 in. outside either edge of the column. The dotted lines are the average of measurements on a generally continuous crack normal to the box girder reinforcement and located approximately 22 in. from the centerline of the bent cap. Consequently, the dotted line for the box girder crack widths between webs is in a region beyond where the main box girder reinforcement was cut off. By comparison with data presented in Fig. D-52, it is evident the crack widths observed on the double-column model were comparable to those of the single-column model bridge.

A photograph of the crack patterns in the roadway is shown in Fig. D-74. It is evident that the crack pattern in the vicinity of both columns is like that shown for the single-column model in Fig. D-53. The patterns, in the vicinity of the columns, are similar to those commonly observed around slab-column junctions.

Analysis of Data-Model Bridge Tests

General Approach. Moments and shears for the instrumented girders of the single-column and double-column model bridges were determined from the experimental data using slightly modified versions

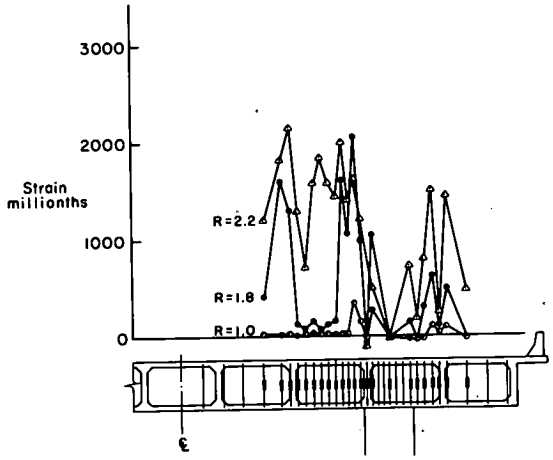

Fig. D-72 Strains in Bent Cap Stirrups of Double-Column Model Bridge

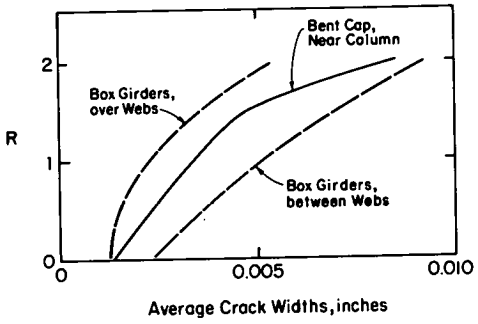

Fig. D-73 Measured Crack Widths in Roadway of Double-Column Model Bridge

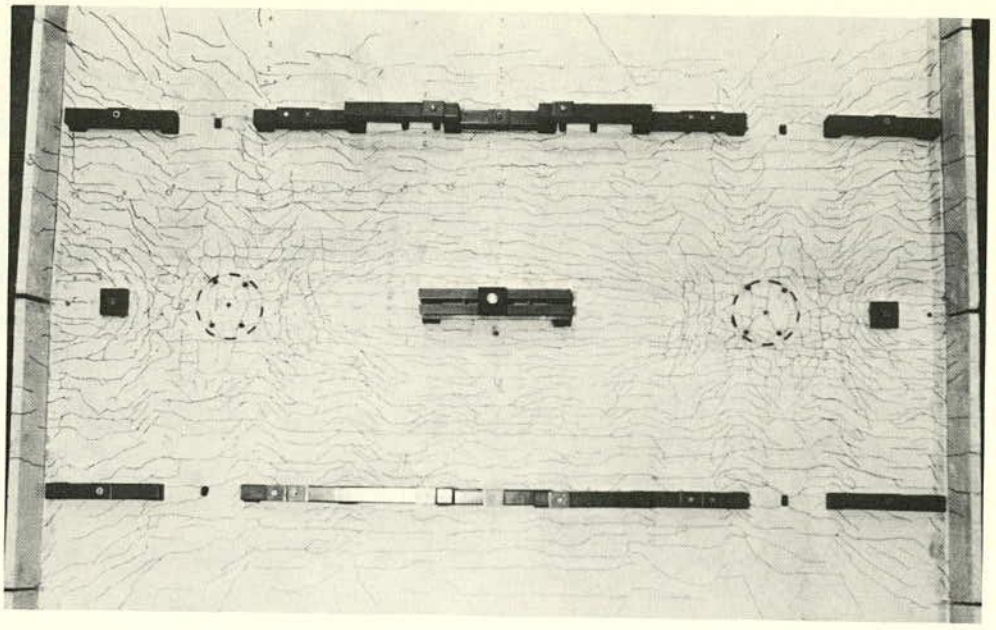

Fig. D-74 View of Cracking in Roadway Slab of Double-Column Model Bridge

of the procedure developed for the bridge element. Slight differences in the layout of strain gages and reinforcement, plus the differences in bent cap width, necessitated modifications in the analysis of the interior girder data. For the exterior girders, the lack of a portion of the compression flange also required modification of the analysis.

Final values for moment and shear in each girder were determined by adjusting the experimentally determined value of each in the same proportion so that the sum of the shears and moments for all the girders equalled the sum for the particular cross section calculated using the measured loads and reactions.

Three load stages were selected for analysis from each of the model bridges. Selection was based on the following criteria:

1. The strains at each location should be a new maximum for that location.
2. The strains at all locations should be large enough so that response to the loading predominated over random effects.

The first criterion was selected following the reasoning developed in Appendix A that the only unique value for a strain at a given point was that obtained when loading caused that strain to be a new maximum. According to this, loadings to strains that were not new maximums might well produce linear, repeatable responses, but the response rate would never be the same as the original. Furthermore, the rate would not be easily predictable.

The second criterion was a recognition of the fact that the strain data would always contain a random element. The smaller the strain, presumably the larger the influence of the random element. Application of this criterion sharply restricted the choice of loadings, since the strains at the section most remote from the bent cap were quite small throughout the tests.

Determination of Absolute Value of Strains. The analysis was performed using absolute strains. These were obtained by summing the response to load and the residual in the unloaded condition before the start of the phase containing the load. The residual was determined from the Whittemore gages as the difference between the strains in the model bridges under their own weight and the strains under the same conditions at the start of the phase containing the load. The difference was reduced by a small calculated amount to allow for creep and shrinkage between the two phases. Consequently, the residual was that caused entirely by loading. In some cases, particularly for the section most remote from the bent cap, the residual strains were a large proportion of the absolute values.

Calculation of Moments and Shears. The calculation of moments and shears from strains was performed in the same manner as for the bridge element. Measured stress-strain relationships were used in each case. For every girder at every cross-section, the calculated lever arm was compared with the theoretical value. In the case of the third section most remote from the bent cap, it was necessary to make an assumption about the effectiveness of the bars cut off just beyond the section. Analysis of the measured strains in the bridge element

showed that up to a strain of 1100 millionths, the cut-off bars were fully effective. Thereafter, the increase in strain was only at one quarter the rate of that in adjacent continuous bars. This criterion was used in the analysis.

Moments and Shears in the Single-Column Model Bridge. Application of the criteria of selection of loads for analysis limited the study to loads in Phase 6, the test to destruction. Loads at R = 1.2, 1.7 and 2.25 were selected. These loads are respectively 52, 70, and 98 percent of the measured ultimate capacity of R = 2.3. Thus they fall approximately in the range between service load (R = 0.6 referred to design ultimate for these bridges) and ultimate capacity.

Moments and shears were determined for the three instrumented girders. The length of lever arms calculated from the strains agreed with the theoretical values. This indicated that the analysis was not being affected by possible axial forces. At the instrumented sections closest to the bent cap, experimentally determined tensile and compressive resultants were approximately equal for the first two loads. For all other cases, the tensile force was considerably greater than the compressive force.

Total moments across the three sections were on the average 6 percent greater than the moment calculated by statics. Total shear force for the three load levels were respectively 36, 22, and 7 percent greater than the statical values.

Values of the experimentally determined shear force in each girder are given in Fig. D-75 as a percentage of the total of the three.

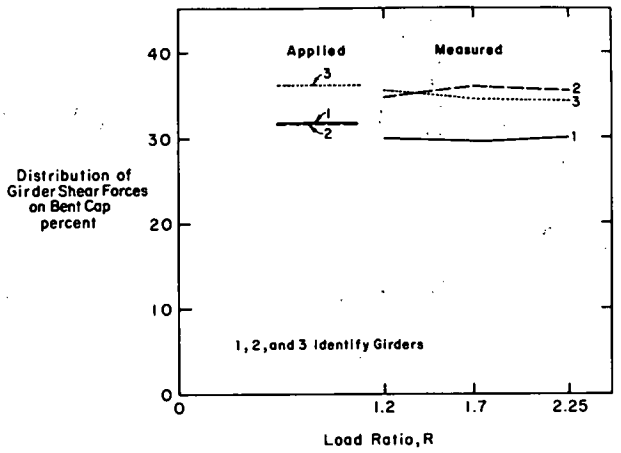

Fig. D-75 Girder Shear Force Distribution at Bent Cap for Single-Column Model Bridge

The measured distributions do not vary significantly with increase in load. The small decrease in the percentage of load carried by girder No. 3 at higher loads may have been caused by flexural yielding in the negative moment reinforcement occurring first in this girder.

The applied distribution of shears is also shown in Fig. D-75. Girders Nos. 1 and 2 have the same shear because the same dead load was assigned to each, and the live load lane is centered on them. It appears that girder No. 2 was carrying some of the load originally applied to the other girders.

Moments and Shears in the Double-Column Model Bridge. As for the single-column bridge, the loads selected for analysis were all selected from in the test to destruction, in this case, Phase 5. Loads of R = 1.2, 1.6 and 2.0 were selected. These loads are respectively 55, 73, and 91 percent of the measured ultimate capacity of R = 2.2. The loads fall into the same range utilized in the analysis of the single-column bridge. At the highest load selected, the strains at certain locations in the cross-sections most remote from the bent cap reached maximum values. Decreasing strains at higher loads were probably due to internal redistribution of forces.

Calculated tensile resultants were always greater than the compressive resultants. The experimental lever arms agreed with the theoretical values. Very good agreement between the total experimentally determined moment and the statical moment based on external forces was obtained for all three sections. The calculated shear forces agreed within 1, 6, and 8 percent for the three loads considered.

Values of the distribution of the experimentally determined shears for one-half of the bridge are shown in Fig. D-76. Generally the measured values are constant for increasing load. Distribution of the shears between the various girders is complicated by the unequal loads applied to them. However, it appears that the girders spanning into the cantilever portion of the bent cap carried more load than was applied to them.

Conclusions. The obtained distributions do not show sufficient evidence to warrant any change in the assumption that loads applied to the individual girders travel straight along the girders to the bent cap. Furthermore, the analysis provided evidence to justify the application of equal loads to the webs of the bent cap specimens.

Load Distribution Characteristics of the Bridges. To assess the experimentally determined load distribution characteristics of the model bridges, the ratio of the load in a girder (girder shear) to the load applied on the girder was determined. This experimental ratio of output girder shear to input girder load is compared in Chapter 2 with the distribution characteristics assumed in the design and predicted by the analysis.

The load distribution characteristics were calculated for each girder, considered as part of the group of instrumented girders in a bridge. The input per girder was taken to be that portion of the total load on the group that was applied to the girder. The output per girder was taken to be the portion carried by the girder of the total calculated shear for the group. Thus, the ratio of output to input indicated what part of its applied load a particular girder delivered to the bent cap.

Input and output percentages are shown in Fig. D-75 for the single-column model bridge and in Fig. D-76 for the double-column

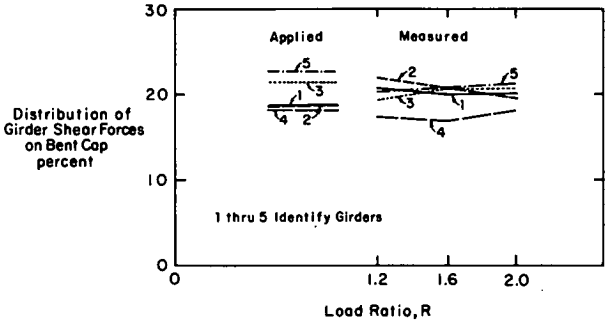

Fig. D-76 Girder Shear Force Distribution at Bent Cap for Double-Column Model Bridge

TABLE D-11 PERCENT DISTRIBUTION OF SHEARS

Model Bridges		Girder 1	2	3	4	5
Single-Column	Input	32	32	36	-	-
	Output	30	35	35	-	-
Double-Column	Input	19	19	21	18	23
	Output	20	20	21	18	21

model bridge. For the purposes of Chapter 2, average values of distribution were used, rounded off to the nearest whole percent. This approximation was felt to be consistent with the accuracy of the data. The results are shown in Table D-11.

Input for any girder was taken to be the hydraulically applied load on the girder web. It should be noted that this loading assigned the same dead load to the exterior girders as to the interior girders, whereas in actuality the cross sectional area for the exterior girders was only 82 percent of that for the interior girders. Thus, somewhat greater relative dead load was applied to the exterior girders than to the interior girders than might have been assigned on the basis of girder cross sections. However, it was felt that this small departure from the calculated distribution of dead load would not affect the load distribution characteristics of the bridges as defined by the girder output to input ratios.

Loadings on the Bent Cap. Bent cap loadings, including the effects of girder shears at the bent cap, are compared in Chapter 2. The "Experimental Distributions" were calculated using the measured distributions of shear shown in Figs. D-75 and D-76, and summarized in Table D-11.

For the discussion in Chapter 2 the girder shears for the single-column bent cap were determined using a hybrid procedure. Total shear for the three girders considered was computed as the center reaction for an elastic continuous prismatic beam of two equal spans, pin supported, and loaded with the applied live loads and assumed dead load associated with service conditions. This total shear was then distributed to each girder according to the measured output shears shown in Table D-11.

For the double-column bent cap, total shear for five girders considered was calculated on the assumption of continuous beam action. This total shear was then distributed to each girder according to the measured output shears shown in Table D-11.

Continuous Beam Action. To determine whether or not the model bridges acted like two-span continuous beams in the spanwise direction, the measured ratios of abutment reaction to total reaction were computed and compared in Table D-12 with those calculated. The measured ratios represent the effects of all hydraulically applied loads at the particular load stage. The calculated loads were obtained by applying the nominal values of the same hydraulically applied loads to a two-span continuous elastic prismatic beam. The correspondence between measured and predicted loads is well within the limits of experimental error. Consequently, it is concluded that, for purposes of predicting reactions, the models acted like continuous beams.

TABLE D-12 CONTINUOUS BEAM ACTION

Model Bridge	Load	Ratio - Abutment Reaction / Total Reaction	
		Measured	Calculated
Single-Column	R = 1.2	.149	.151
	R = 1.7	.151	.151
	R = 2.25	.149	.151
Double-Column	R = 1.2	.146	.149
	R = 1.6	.147	.149
	R = 2.0	.149	.149

APPENDIX E

MODEL BENT TESTS

Introduction

Behavior of the bent cap portion of the concrete box girder bridges when subjected to known loads was determined by tests on five model bent caps. Four of these represented single-column bridges and one represented a double-column bridge. The loading, selected on the basis of the results from tests on two model bridges, was the same for all webs in a model.

The bent cap models were utilized to investigate the following items from the list of specific objectives in Chapter 1:

Effective width of the bent cap in tension and compression.

Location of the critical cross-sections for design of the bent cap.

Effect of flaring the column.

Effect of spreading the bent cap reinforcement.

The model bents were intended to represent a transverse strip of bridge superstructure. The strip modeled is parallel to and includes the bent cap and the column of the prototype bridges shown in Figs. 3, 4, and 5 of Chapter 1. The width of each specimen was equal to the full width of the bridge. Analytical studies reported in Appendix B indicated that the transverse inflection position in the box girders is a slightly curved line approximately one-fourth of the span length from the centerline of the bent cap. The observation during testing

that the model bridges behaved as continuous beams having inflection points at one-fourth the span from the center support tended to confirm this finding. Accordingly, it was decided that the model bent caps should extend to one-fourth of the span length either side of the centerline of the bent cap.

Variables adopted for the test program are summarized in Table E-1. The first single-column bent cap model had a cylindrical column, and was geometrically quite similar to the bent cap portion of the single-column model bridge. The next two bent cap specimens had different amounts of flare in the column. The fourth model had the main bent cap flexural reinforcement spread out into the adjacent portion of the deck that had been thickened for the purpose. Dimensions of the models are shown in Figs. 11 through 14.

The double-column bent cap model was geometrically quite similar to the bent cap portion of the double column model bridge. This bent cap model served to show the effect of a change in the moment-to-shear ratio in the negative moment region of the bent cap. In addition, behavior of the positive moment region could also be investigated. Dimensions are shown in Figs. 16 and 17.

Design Procedure. Isometric views showing total superimposed loads applied to the single-and double-column model bents are shown in Figs. E-1 and E-2, respectively. Self weight of the models is not included. The loading, A, at the ends of the girders, represents the shear from dead load, live load and impact transmitted from the missing portion of the structure. The loads, B, along the girders, represent

TABLE E-1 MODEL BENT CAP TEST SPECIMENS

Specimen Mark	Single Column Two-Fifths Scale	Double Column One-Fifth Scale	Column Flare			Deck Slab	
			None	Two Times Col. Dia.	Three Times Col. Dia.	Uniform	Thickened Near Bent
SC-3	X		X			X	
SF-4	X			X		X	
SF-5	X				X	X	
ST-6	X		X				X
DC-9		X	X			X	

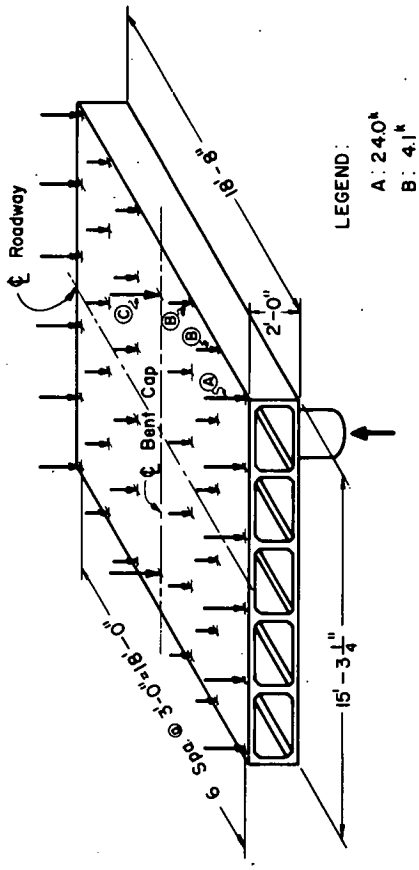

Fig. E-1 Design Ultimate Superimposed Load on Single-Column Bent Cap Specimen

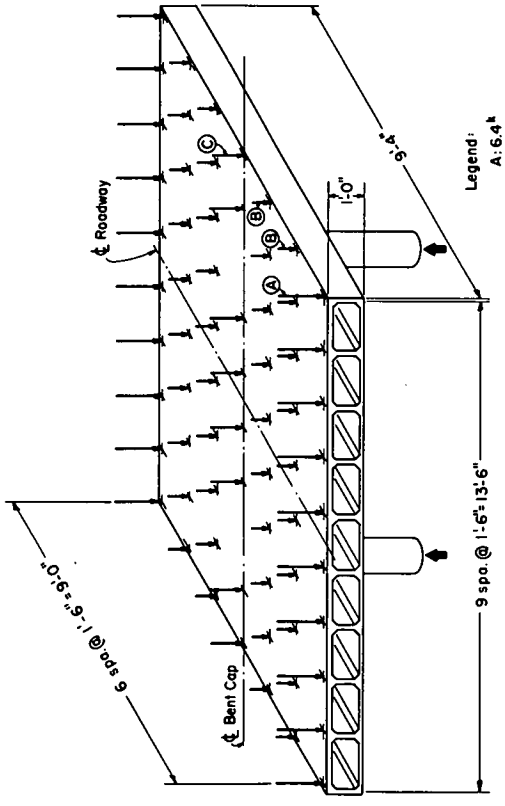

Fig. E-2 Design Ultimate Superimposed Load on Double-Column Bent Cap Specimen

the distributed dead loads and lane live loads. The loads, C, applied to the bent cap represent dead load, lane live loads, and concentrated live loads. The numerical values shown are for the design ultimate load condition.

The column bases were grouted to steel plates seated in a mortar bed on the laboratory test floor. Symmetrical loading of the single-column models produced no overturning moment, and the small moment introduced into the column base of the double-column model was insufficient to cause any tension. Consequently, the base acted as if fully restrained.

With the overall geometry and loading of the single and double-column specimens defined, the following design procedure was used:

1. The test specimens were proportioned to satisfy strength criteria[19].
2. A load factor for the design of the bent cap was selected to make its strength comparable to that of the supporting column. The basic load factor[19] was U = 1.35 (D + 1.67 L)*. Dividing by the strength modification factor, ϕ, of 0.75 for a spiral column, the design ultimate loading on the bent cap was taken as U = 1.8 D + 3.0 L.
3. Since the single-column prototype carries three traffic lanes, each of the six girders was assumed to carry one-half traffic lane. Likewise, since the double-column prototype carries six traffic lanes, each of the ten girders was considered to carry six-tenths traffic lane.

*This load factor has since been superseded by the value U = 1.30 (D + 1.67 L) in the AASHO Specifications[24].

4. Loads were assumed to be carried longitudinally to the bent cap along each girder web and then transversely to the column.
5. The critical bent cap design section was assumed to be located one-quarter of the depth of the superstructure outside the extreme edge of the round or flared columns. This assumption was based on preliminary analysis of data obtained from the tests of the model bridges. For the double-column specimen, the critical section for positive moment was taken at the center of the bent. Moment calculations were based on centerline dimensions.
6. The effective compressive flange width for the bent cap was taken to satisfy the AASHO Specifications[1] for box girders.
7. Flexural reinforcement in the bent cap was proportioned to carry the design ultimate loads.
8. To facilitate strain measurements along the length of the bent cap reinforcement, all bent cap reinforcement in the single-column specimens was run full length. Similarly, for the double-column specimen, all negative moment bent cap reinforcement extended the full length of the cantilever. All positive moment bent cap reinforcement was carried beyond the point of inflection toward the column. In spite of the seemingly arbitrary choice of bar lengths, the resulting reinforcement was essentially the same as if the bar cut-offs had been precisely calculated to be the minimum required to meet the design requirements.

9. When the reinforcement was spread near the bent cap, a greater number of smaller size bars uniformly distributed over the entire width of the bent cap and the thickened portion of the deck slab was used. The total area of reinforcement was kept the same as in the similar specimen without spread reinforcement.
10. Flexural and shear reinforcement in the box girders and shear reinforcement in the bent cap was proportioned to carry ten percent more shear and moment than required to develop the flexural capacity of the bent cap. The purpose of this was to bias the design in an attempt to have first distress occur in the bent cap.
11. The following material properties were used in design: Compressive strength of concrete at 28 days, f'_c = 3500 psi Yield stress of reinforcement, f_y = 60,000 psi.
12. Clearances and other dimensions were scaled as appropriate from the single- and double-column bridges described in Appendix D.
13. Wherever possible, hot-rolled deformed reinforcing bar sizes that modeled prototype reinforcement were used.

In following this design procedure, it was found that the shears were low enough to permit the use of non-flared box girder webs and a bent cap width equivalent to the one used in the double-column bridge. The deck and soffit slab reinforcement was scaled from the prototype bridge design.

The prototype column was designed by the strength method. A 5-ft. diameter column containing approximately 1.1 percent reinforcement was found to be adequate for both the single- and the double-column bridges. The dimensions and reinforcement were scaled down for the model bent cap specimens.

In the flared columns, the circular column reinforcement, including the ties was continued through the flared portion of the columns. Supplementary reinforcement was placed around the flare periphery. This reinforcement amounted to at least 0.5 percent of the net unreinforced area at the top of the flare. Ties for the flared reinforcement were placed at the same spacing as those for the circular column.

Details of Model Bents

Details of the single- and double-column bent cap specimens are shown in Figs. E-3 through E-30.

Physical properties of the concrete and steel used in the specimens are listed in Tables E-2 and E-3. Representative stress-strain curves for the model concrete and reinforcement are given in Appendix A (Figs. A-8 and A-9). Appendix A also contains a general discussion of the materials selected for the specimens.

Construction of Model Bents

The single- and double-column specimens were constructed in three stages. First the column was cast. Next, the soffit and webs of the box girders and the bent cap were cast. Finally, roadway deck slab concrete was placed.

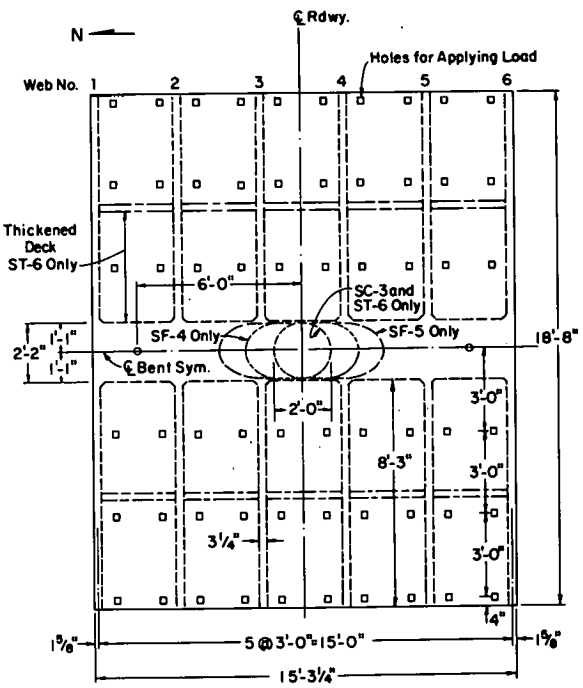

Fig. E-3 Plan of Single-Column Bent Cap Specimens

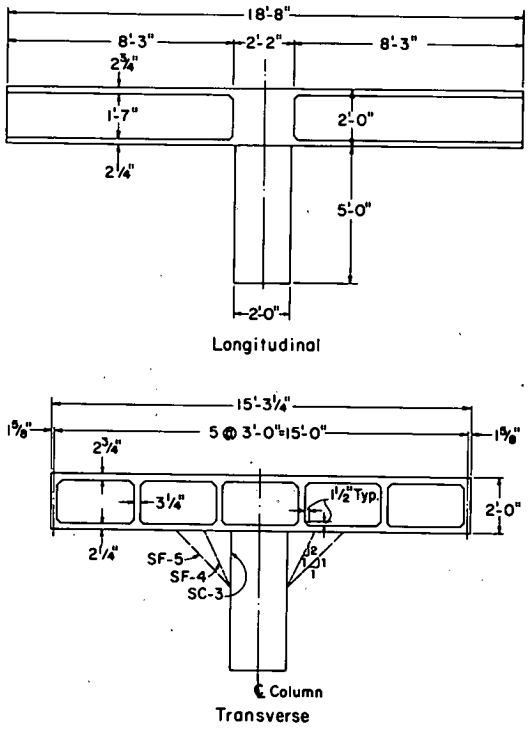

Fig. E-4 Section Details for Specimens SC-3, SF-4, and SF-5

E-11

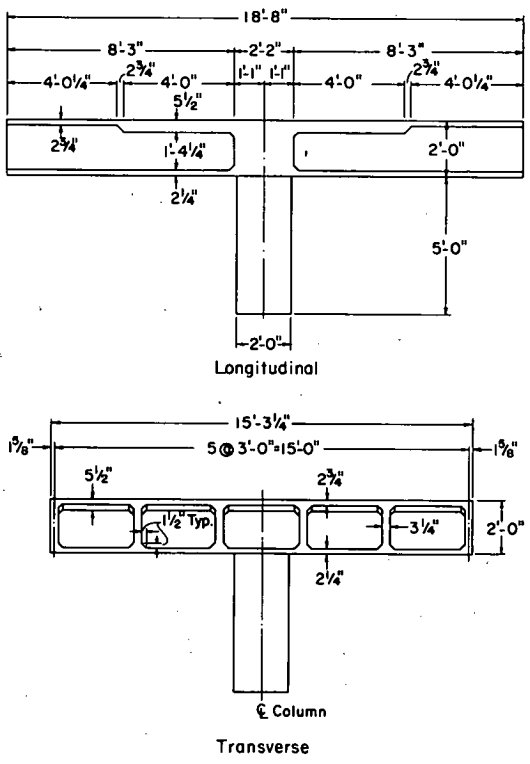

Fig E-5 Section Details for Specimen ST-6

E-12

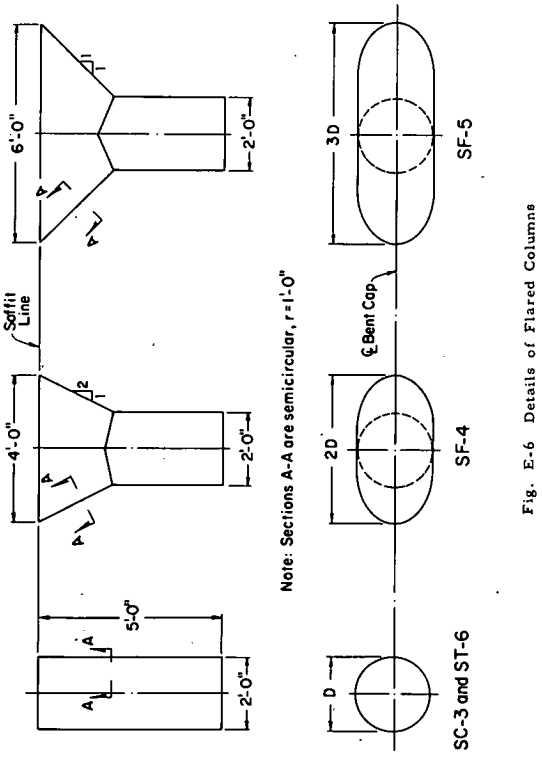

Fig. E-6 Details of Flared Columns

E-13

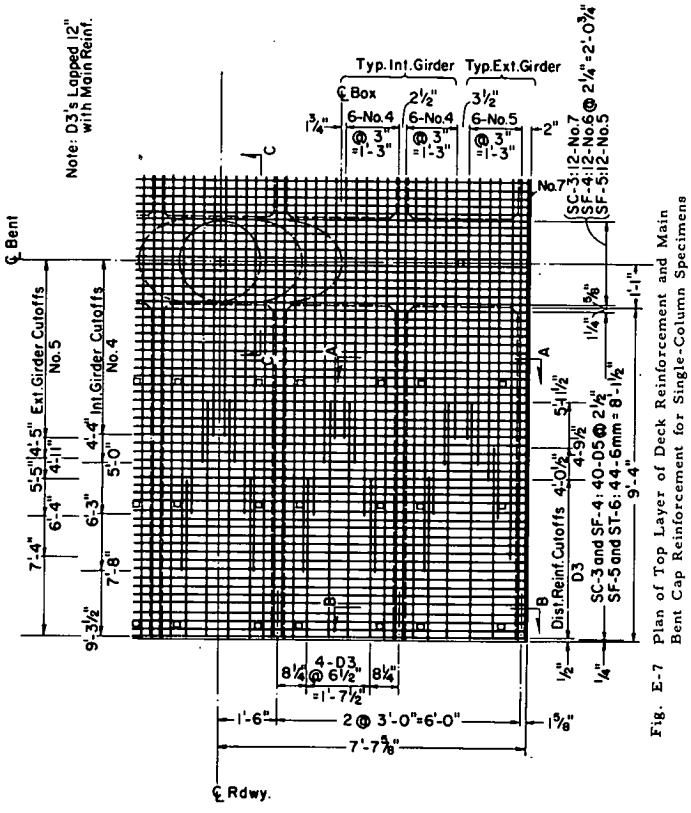

Fig. E-7 Plan of Top Layer of Deck Reinforcement and Main Bent Cap Reinforcement for Single-Column Specimens

E-14

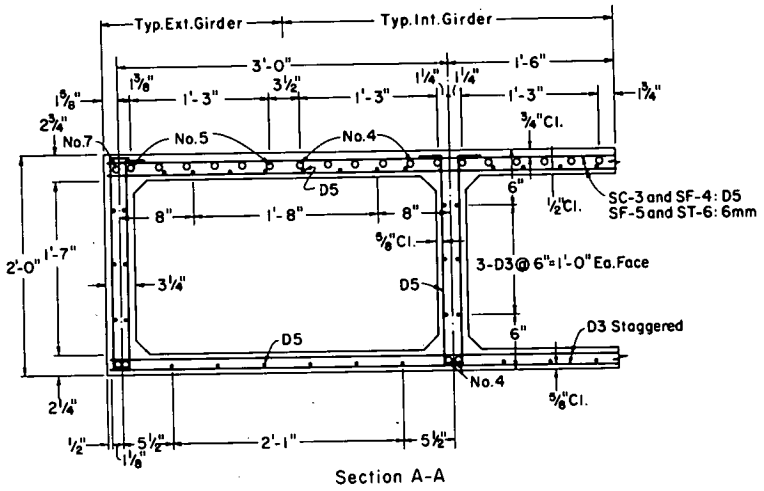

Fig. E-10 Section of Girders Near Bent Cap of Single-Column Specimens

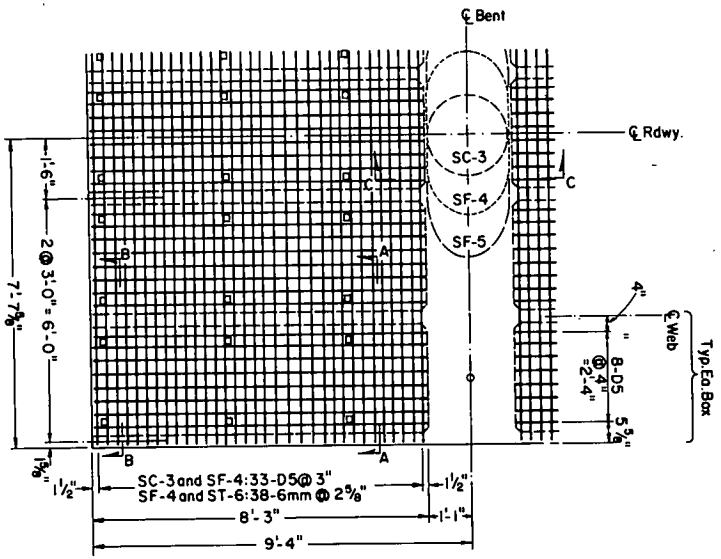

Fig. E-8 Plan of Bottom Layer of Deck Reinforcement for Single-Column Specimens

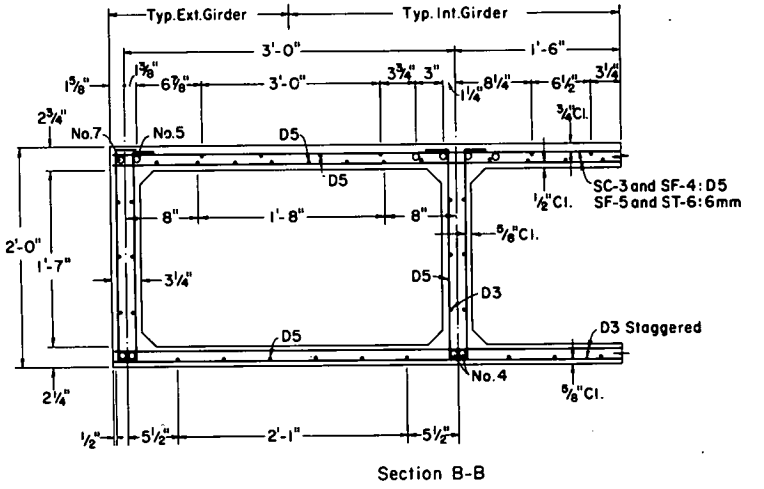

Fig. E-11 Section of Girders Near End of Single-Column Specimens

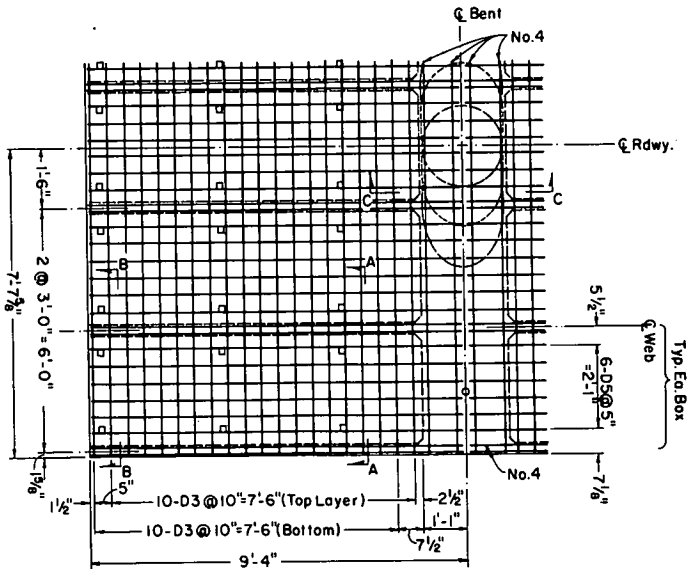

Fig. E-9 Plan of Bottom Slab Reinforcement and Bottom Bent Cap Reinforcement for Single-Column Specimens

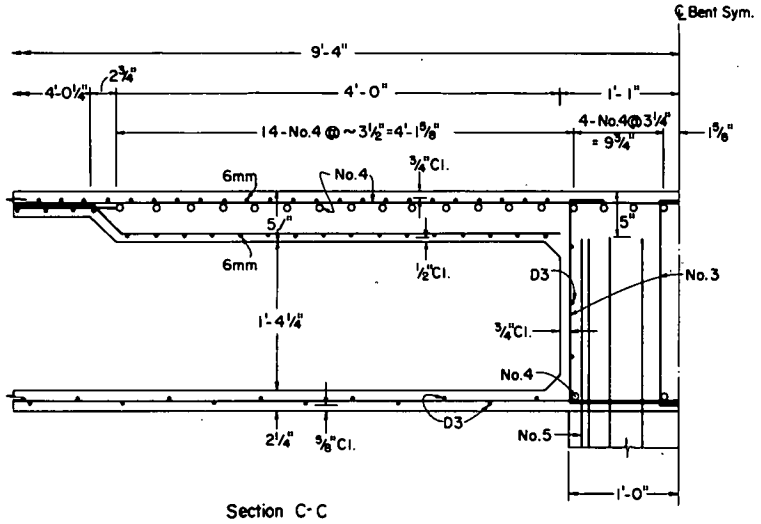

Fig. E-14 Details of Specimen ST-6

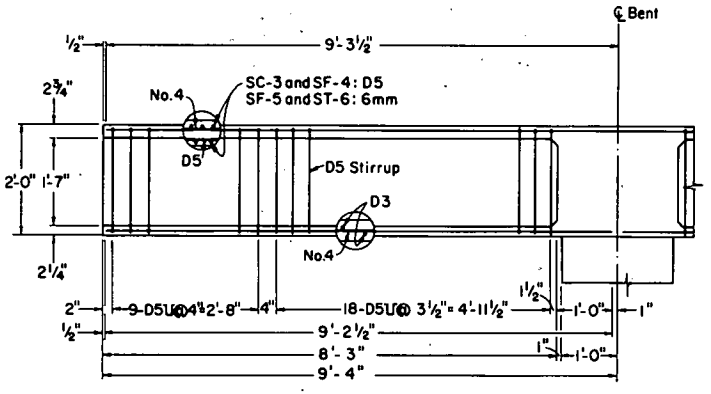

Fig E-12 Elevation of Girder for Single-Column Specimens

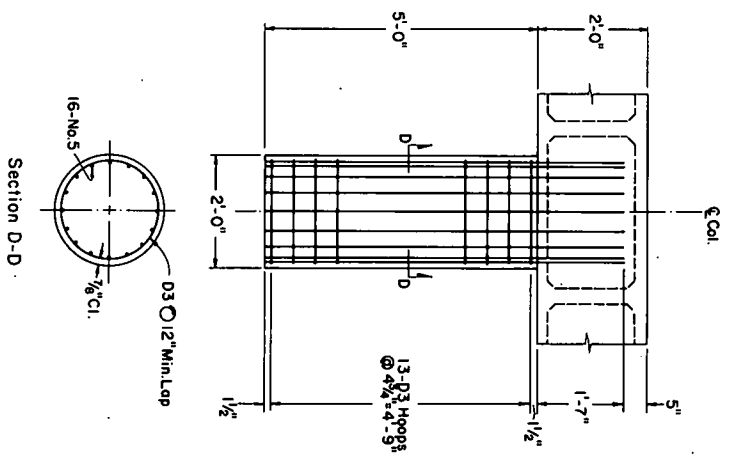

Fig. E-15 Column Reinforcement for Specimens SC-3 and ST-6

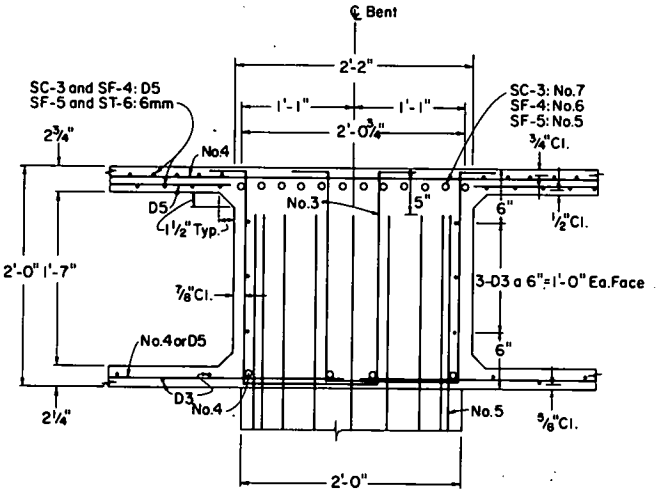

Fig. E-13 Section of Bent Cap of Specimens SC-3, SF-4, and SF-5

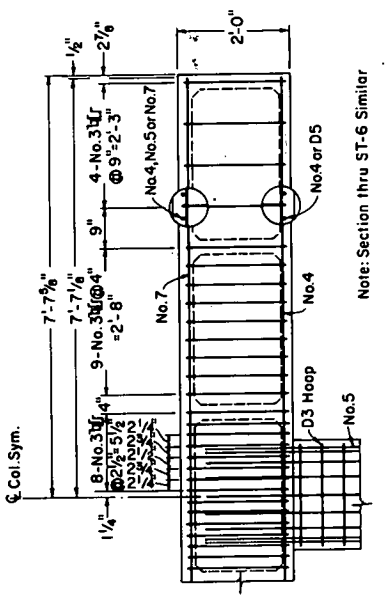

Fig. E-16 Bent Cap Reinforcement for Specimens SC-3 and ST-6

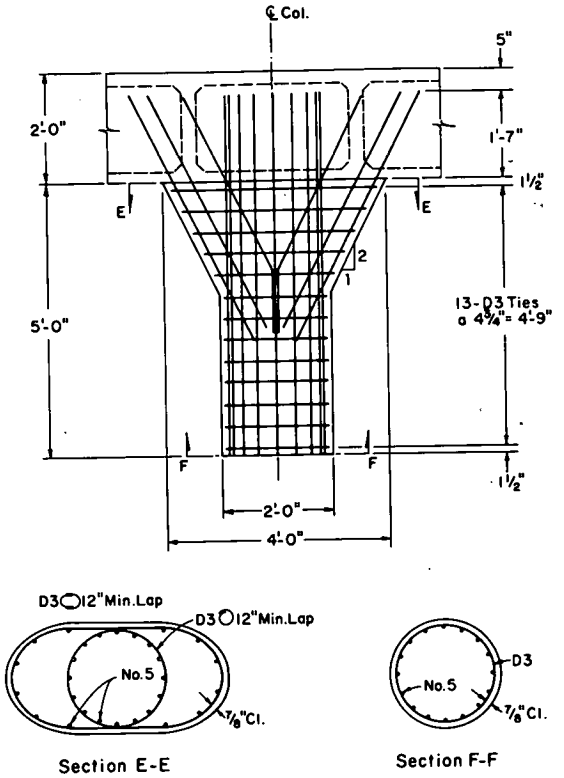

Fig. E-17 Column Reinforcement for Specimen SF-4

E-23

E-24

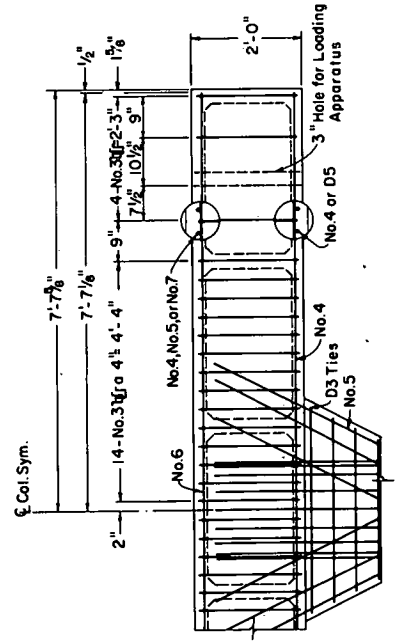

Fig. E-18 Bent Cap Reinforcement for Specimen SF-4

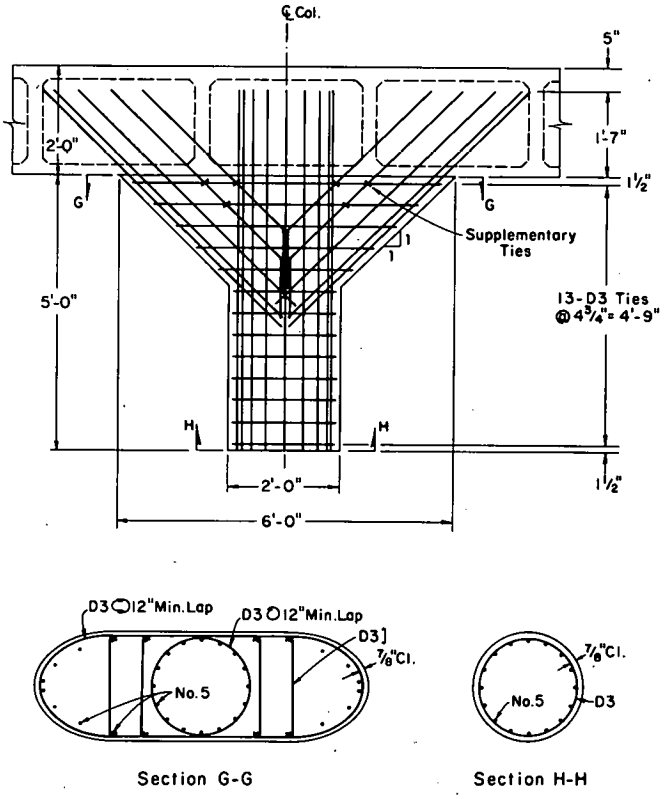

Fig. E-19 Column Reinforcement for Specimen SF-5

E-25

E-26

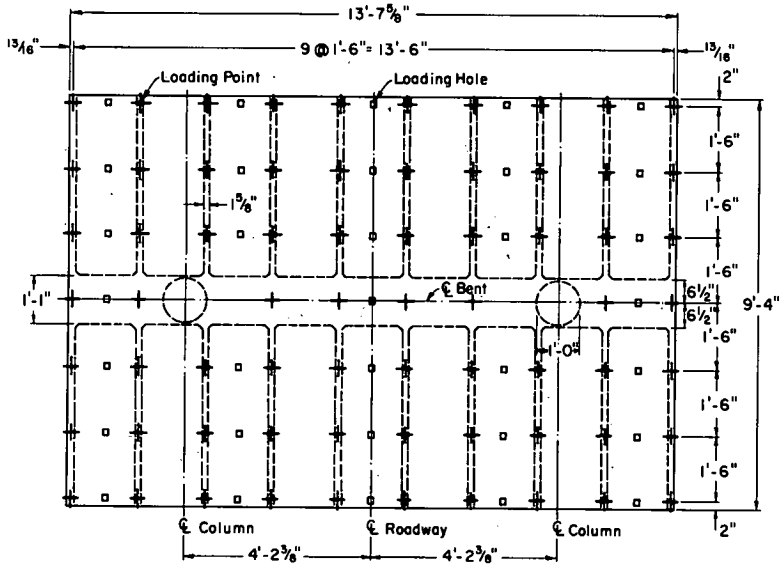

Fig. E-22 Plan of Double-Column Bent Cap Specimen DC-9

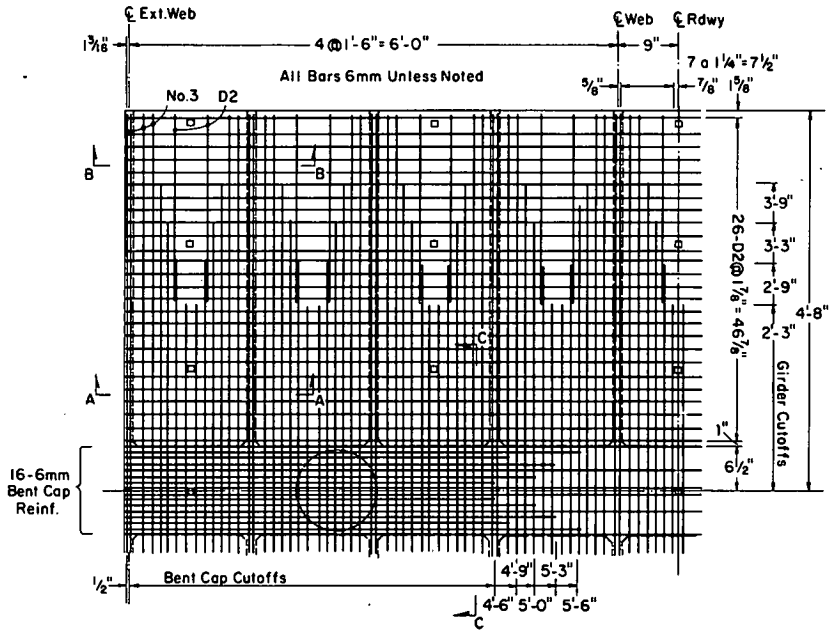

Fig. E-23 Plan of Top Layer of Deck Reinforcement and Main Bent Cap Reinforcement for DC-9

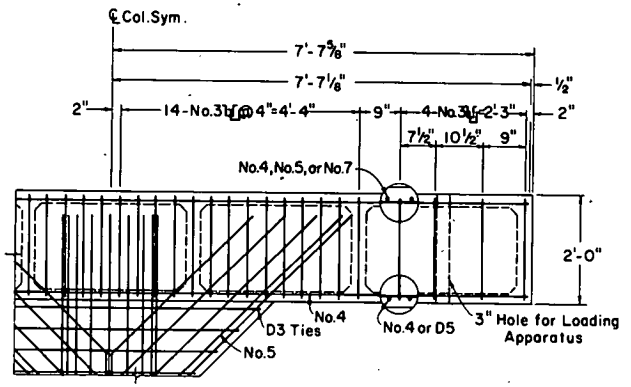

Fig. E-20 Bent Cap Reinforcement for Specimen SF-5

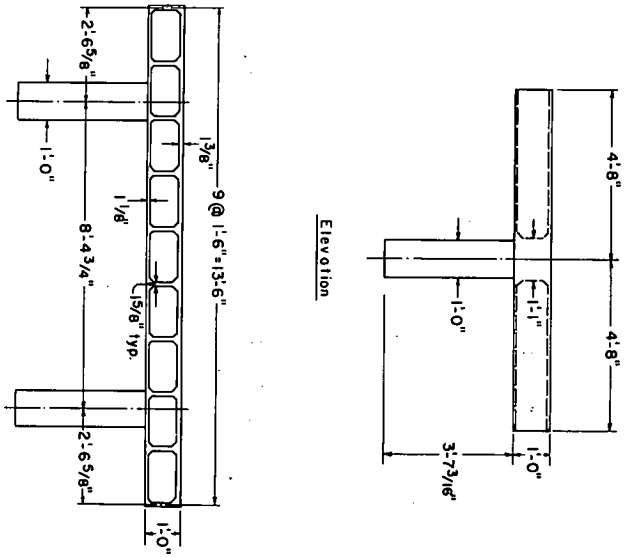

Fig. E-21 Elevation and Section of Double-Column Bent Cap Specimen DC-9

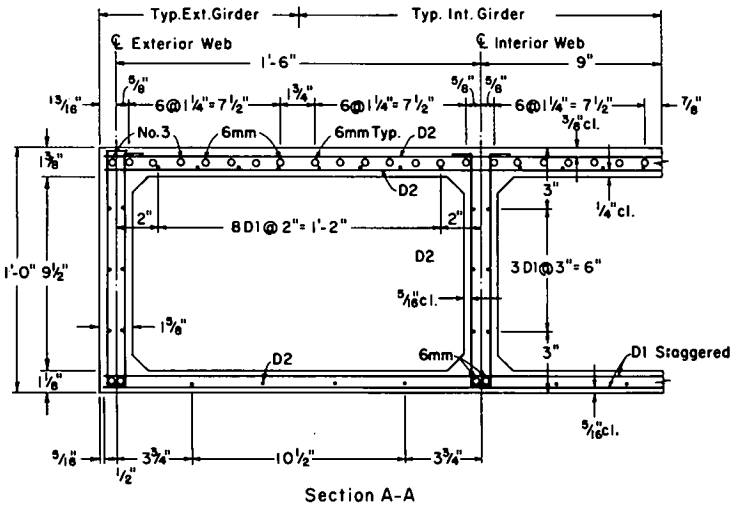

Fig. E-26 Section of Girders Near Bent Cap of Specimen DC-9

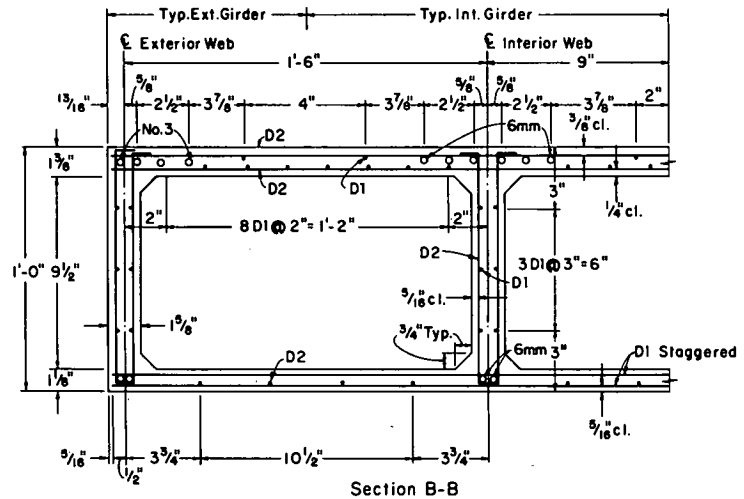

Fig. E-27 Section of Girders Near End of Specimen DC-9

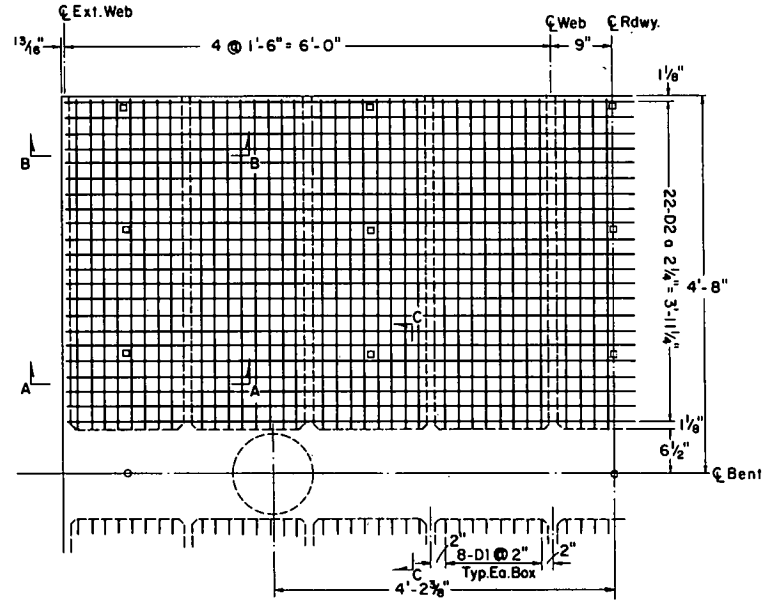

Fig. E-24 Plan of Bottom Layer of Deck Reinforcement for DC-9

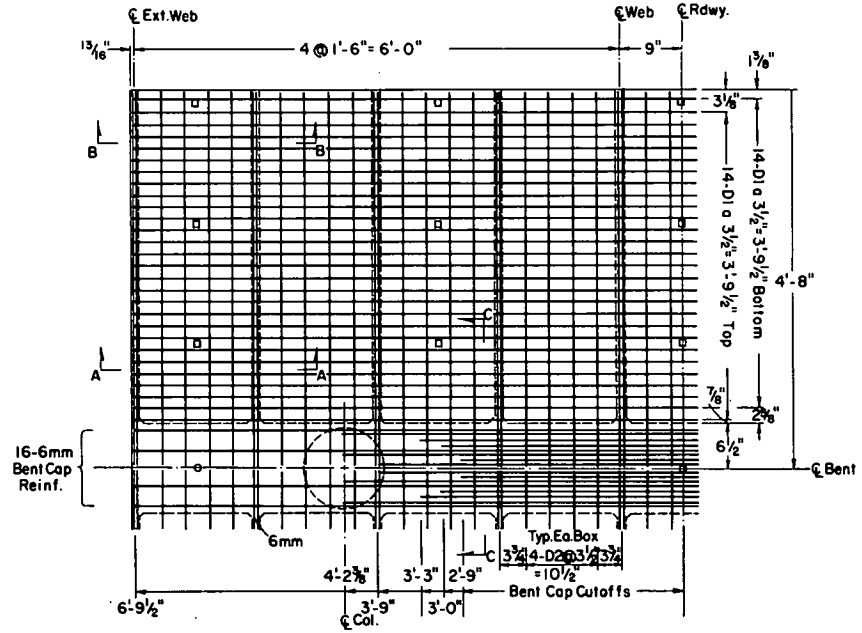

Fig. E-25 Plan of Bottom Slab Reinforcement and Bottom Bent Cap Reinforcement for DC-9

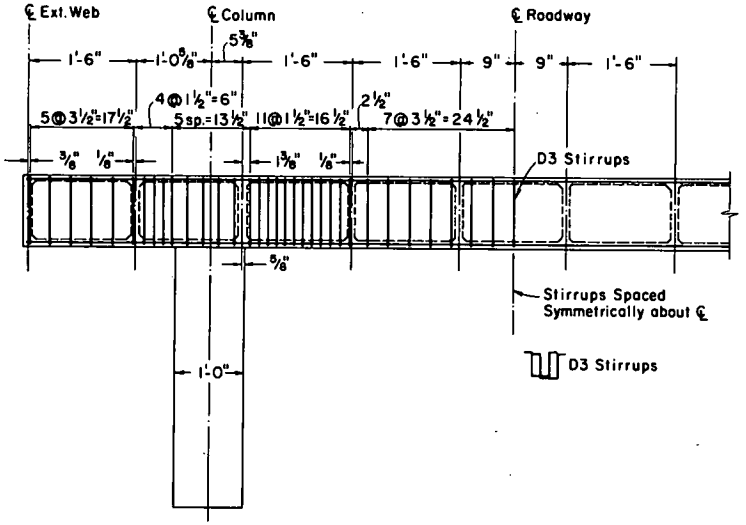

Fig. E-30 Bent Cap Reinforcement for Specimen DC-9

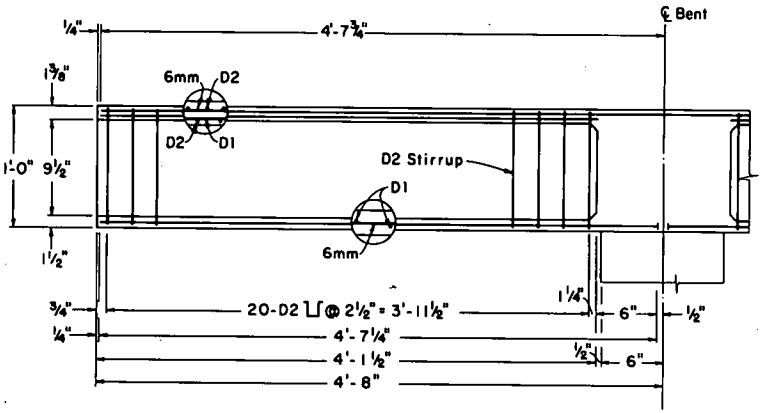

Fig. E-28 Elevation of Girder for Specimen DC-9

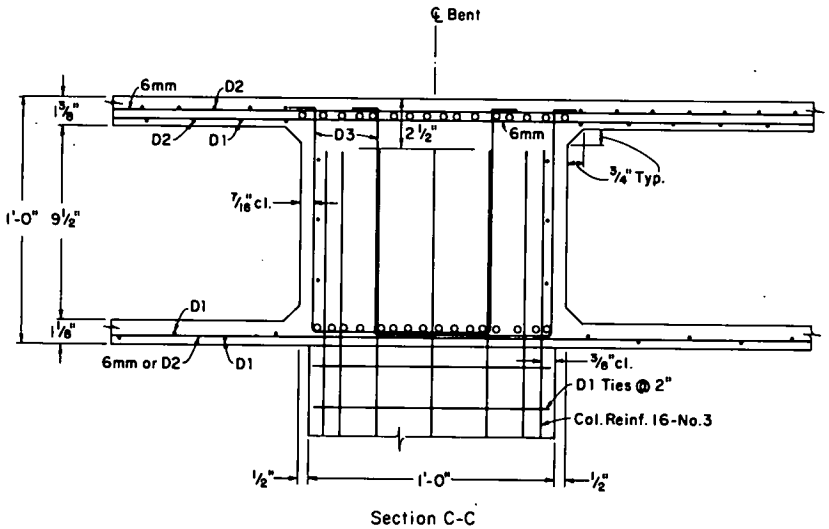

Fig. E-29 Section of Bent Cap of Specimen DC-9

TABLE E-2 PROPERTIES OF MODEL CONCRETE AT TEST

Specimen	Location *	f'_c psi	f_{sp} psi	E_c psi x 10^6
SC-3	1	3520	-	3.23
	2	3210	450	2.92
	3	3390	420	2.85
SF-4	1	3600	-	3.33
	2	4330	500	3.36
	3	3860	480	2.99
SF-5	1	3910	-	3.25
	2	3700	470	3.02
	3	3810	470	3.09
SF-6	1	3900	-	-
	2	4670	530	3.75
	3	3720	480	3.16
DC-9	1	4000	-	3.70
	2	3840	440	3.20
	3	4420	505	3.65

*1 - column
2 - bottom slab, girder webs, bent cap
3 - deck slab

TABLE E-3 PROPERTIES OF REINFORCEMENT

Specimen	Bar or Wire	D1	D2	D3	D5	6mm	No. 3	No. 4	No. 5	No. 6	No. 7
SC-3	f_y, ksi	-	-	69.3	69.9	-	81.5	62.6	69.6	-	64.8
	f_{su}, ksi	-	-	76.6	79.0	-	126.4	98.4	116.8	-	112.3
	E_s, psi x 10^6	-	-	28.7	28.1	-	29.0	26.1	28.4	-	27.5
SF-4	f_y, ksi	-	-	71.5	66.5	-	77.0	62.1	69.7	64.6	-
	f_{su}, ksi	-	-	77.5	76.7	-	118.7	98.5	117.6	109.3	-
	E_s, psi x 10^6	-	-	28.0	29.1	-	27.1	27.2	29.3	28.0	
SF-5	f_y, ksi	-	-	69.6	83.5	71.2	77.1	62.1	70.0	-	-
	f_{su}, ksi	-	-	76.2	95.0	97.1	118.6	97.8	117.6	-	-
	E_s, psi x 10^6	-	-	29.8	29.1	32.0	26.8	26.8	27.6	-	-
SF-6	f_y, ksi	-	-	67.3	83.4	72.0	77.2	63.1	69.8	-	69.8
	f_{su}, ksi	-	-	73.9	95.9	98.8	119.8	98.5	112.8	-	111.5
	E_s, psi x 10^6	-	-	26.6	30.3	28.8	28.3	26.7	28.1	-	27.2
DC-9	f_y, ksi	70.7	65.5	71.5	-	70.5	75.5	-	-	-	-
	f_{su}, ksi	70.3	69.6	77.5	-	96.0	118.3	-	-	-	-
	E_s, psi x 10^6	27.8	26.3	29.0	-	30.2	26.6	-	-	-	-

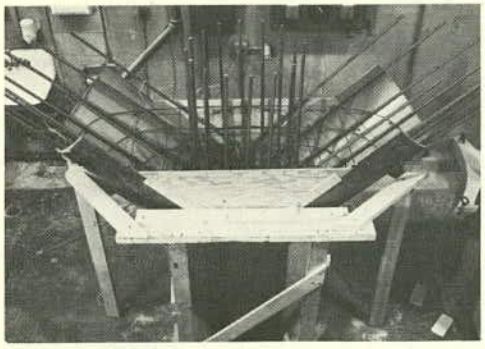

Fig. E-31 Column Formwork for Specimen SF-5

Columns. After fabrication, each column reinforcing cage was positioned in a heavy cardboard form as shown in Fig. E-31. The column concrete was then placed and was consolidated with internal vibrators. The completed column was stripped and positioned under the same elevated platform previously used for construction of the model bridges. The superstructure was cast on this platform.

Soffit Slab, Webs, and Bent Cap. After the column was in position, construction of the soffit slab of the box girders, the girder webs, and the bent cap was begun. Each box girder web cage, consisting of the longitudinal girder compressive reinforcement, the girder stirrups, and the longitudinal temperature reinforcement, was prefabricated. These cages were positioned on the casting platform along with the longitudinal and transverse reinforcement for the soffit slab. Forms for the girder webs were then attached as shown in Fig. E-32.

Next, a pre-assembled bent cap reinforcement cage was lowered over the column reinforcement and tied to the box girder compressive reinforcement that extended into the bent cap. This cage included the bent cap compressive reinforcement, the bent cap stirrups, the bent cap temperature reinforcement, and the cage stiffening bars at the top corners of the stirrups. One of the bent cap reinforcing cages is shown in Fig. E-33.

The procedure for casting was intended to eliminate voids in the girder webs caused by concrete flowing out into the soffit slab after the web had been filled. First, the bottom portions of adjacent webs were filled to the level of the lowest longitudinal web bar, and the concrete in the soffit slab between those webs was placed. At this

Fig. E-32 Girder Reinforcement and Formwork for Specimen SC-3

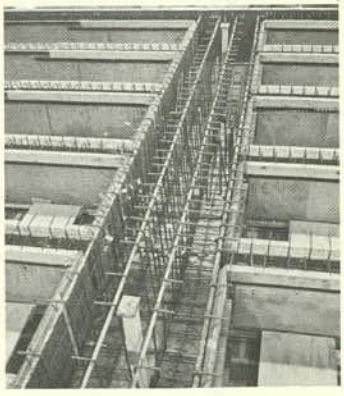

Fig. E-33 Bent Cap Reinforcement and Formwork for Specimen SF-5

time, the casting operation was interrupted until the concrete had taken its initial set. Following this holding period, the remainder of the webs and the bent cap were filled to the top of the web forms. The partially hardened concrete first cast prevented settlement of the additional concrete as it was placed in the webs. This procedure was used in all of the specimens except SC-3, where the girder webs were cast to their full height in one operation.

Deck Slab. The third stage of construction started with assembly of the deck forms and placing of the deck reinforcement. The bottom mat of deck reinforcement and the main longitudinal reinforcement in the top of the bent cap were placed first. Next, the box girder negative moment reinforcement was placed on top of the bent cap reinforcement as shown in Fig. E-34. A final layer of transverse reinforcement in the deck slab was then tied to the box girder negative moment bars.

After the deck concrete was cast and cured, the specimen was lifted from the form with lifting chains attached to anchors cast into the top of the column. The test specimen was then positioned for testing and loading apparatus and instrumentation were installed.

Loading Apparatus and Instrumentation

Loading Apparatus. A hydraulic system was used to apply the loads shown in Figs. E-1 and E-2 for the single- and the double-column specimens. Since the tests were of short duration, it was not necessary to apply the dead load deficiency of the model separately, as had been done in the model bridge tests.

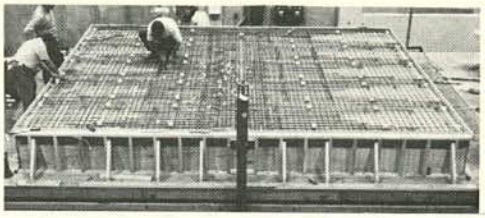

Fig. E-34 Placement of Reinforcement in Roadway Deck Slab for Specimen SC-3

For the double-column bent cap, a lever system was used to adapt the pattern of applied loads to the hole spacing of the test floor.

Photographs of the test setups for the single- and double-column specimens are shown in Figs. 15 and 18, respectively.

Instrumentation. The bent cap models were instrumented to measure loads, deflections, concrete strains, and steel strains. Instrumentation was concentrated in one quadrant of each specimen.

Applied loads were determined from measured hydraulic pressures. As a check on the hydraulic system, load cells were also used to monitor forces at selected locations.

Vertical deflections were measured at the four corners and along the box girder webs in one quadrant of each specimen. Linear potentiometers having a 4-in. total travel were fixed between the specimen and the test floor to measure deflections. In addition, level readings were taken at selected locations to verify potentiometer readings.

Strain gages were located at the following five levels over the superstructure depth:

1. On concrete at the bottom surface of the soffit slab.
2. On the bottom layer of soffit slab reinforcement, and the bottom longitudinal reinforcement in the bent cap.
3. On concrete at the top surface of the soffit slab.
4. On the bottom layer of deck slab reinforcement.
5. On the top layer of deck slab reinforcement, and the top longitudinal reinforcement in the bent cap.

Layouts for the strain gages in the single- and double-column models are shown in Figs. E-35 and E-36. The location of the gages, as shown in the figures, was similar at each of the five levels, but not all of the gages shown were included at each level.

Strains were also measured on the bent cap and box girder web stirrups, the column and column flare reinforcement and surface concrete, and the bent cap temperature reinforcement.

A Whittemore mechanical strain gage with a 5-in. gage length was used to measure strains along the top and bottom surface of the bent cap in the single-column specimens. These measurements were taken to determine the changes in the bent cap strains as the specimen was removed from the formwork and prepared for testing. Readings of these gages were also made during testing.

Crack patterns were marked with a felt tipped pen on the deck slab during testing. At selected locations, crack widths were measured using a hand microscope containing a scale having 0.001-in. divisions.

Tests of Single-Column Bents

Loading Sequence. The initial zero condition for tests of each single-column bent was taken after removal of shoring. At this time, the specimen was supporting its own weight plus that of the loading apparatus. The specimens were inspected for initial cracks before and after removal of the shoring.

A service load test and a test to destruction were carried out on each specimen. For the service load test, the dead and live loads were each applied in four increments to 1.0 D + 1.0 (L + I). After reaching the service load, the specimen was unloaded. For the test to

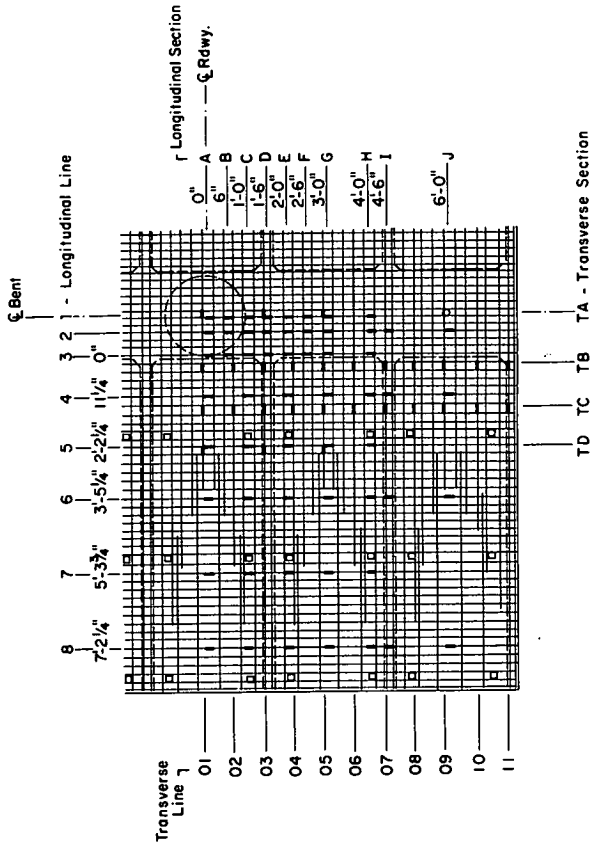

Fig. E-35 Strain Gage Layout for Single-Column Model Bents

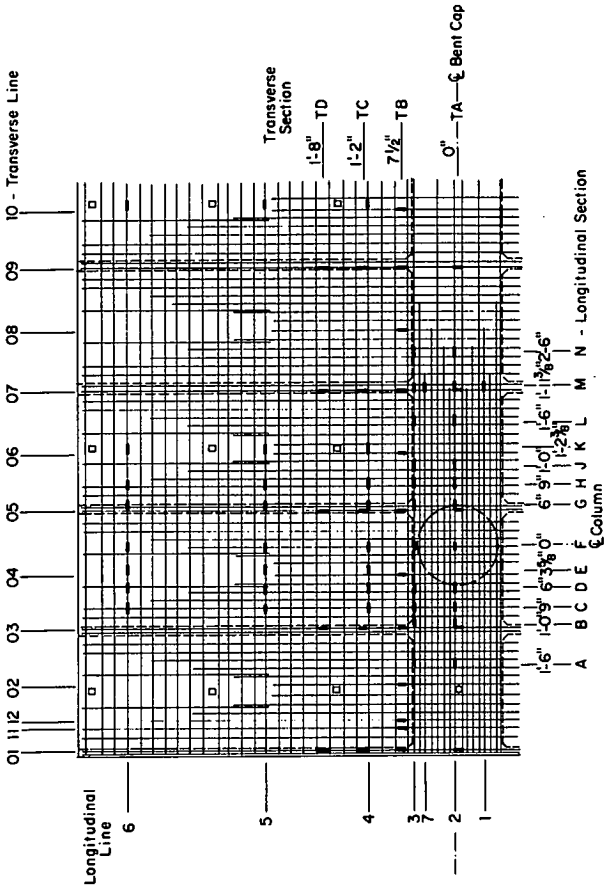

Fig. E-36 Strain Gage Layout for Double-Column Model Bent

destruction, usually carried out on the day following the service load test, the loads were applied in increments of 0.05 of the design ultimate load [1.8 D + 3.0 (L + I)] until collapse occurred.

Test of Specimen SC-3. Specimen SC-3 had deck and soffit slabs of uniform thickness, and a straight circular column.

Load versus deflection curves for SC-3 are shown in Fig. E-37. The load is given as the ratio, K, of the total applied load to the design ultimate load. Thus, K = 1.0 represents the load corresponding to 1.8 D + 3.0 (L + I). The deflections plotted are those at the end of the bent cap and the end of the exterior girder. The initial loops in the curves represent the service load test.

The difference in deflections for the two curves is the net deflection of the exterior girder. Potentiometer readings not shown here indicated that the net deflections of each of the three girders measured was nearly equal.

Major events of the test are indicated on the load-deflection plots. Flexural cracking was first observed in both the box girders and the bent cap while the structure was carrying 0.5 D. The maximum crack width measured at the service load level was 0.007 in., over a girder web. The maximum crack width measured in the bent cap was 0.006 in.

In Fig. E-37, points indicating yielding represent first yielding of a reinforcing bar, not general yielding. First yielding of the box girder tensile reinforcement was observed at K = 0.95. First yielding of the bent cap tensile reinforcement was observed at K = 1.1.

At the design ultimate load, K = 1.0, there was no visual evidence of structural distress. It was not until a load of K = 1.15

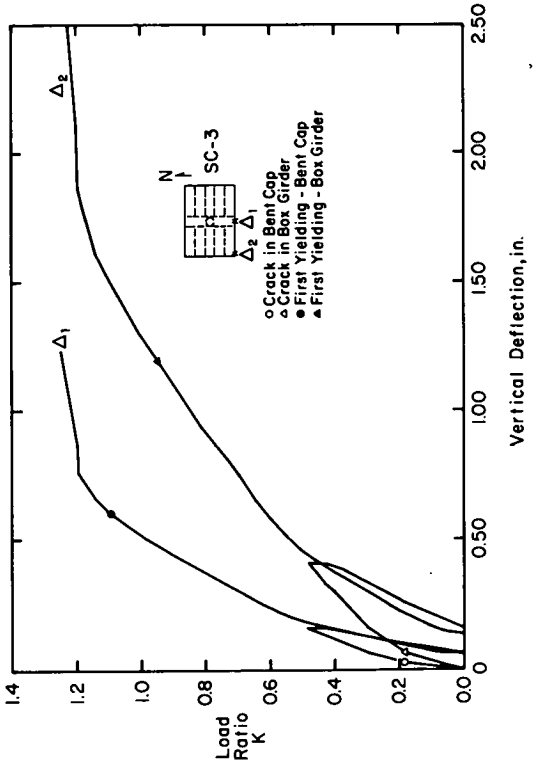

Fig E-37 Load-Deflection Curves for Specimen SC-3

that spalling of concrete on the bottom of the soffit slab was observed. This spalling was seen at the intersection of the centerline of the bent cap with the north exterior girder web.

At a load K = 1.20, horizontal cracks developed in several of the box girder webs on both sides of the bent cap. These cracks formed, in all cases, at the level of the longitudinal temperature reinforcement located in the box girder webs. A possible explanation for this cracking is that horizontal planes of weakness developed in the webs because of settling of the concrete below the longitudinal bars after casting.

In addition to the horizontal cracks, spalling of concrete on the bottom of the soffit slab at the intersection of the bent cap with the south exterior girder web was also observed at K = 1.20.

The test terminated after the load had been increased to K = 1.25. At this load, horizontal shear distress developed in an interior box girder web west of the bent cap. The failure plane, shown in Fig. E-39, propagated nearly the entire length of the girder. A photograph of the top of SC-3 after the test was terminated is shown in Fig. E-38. A felt-tipped pen was used to accent the cracks so they would show clearly in the photo.

Average longitudinal bent cap strains measured in Specimen SC-3 are plotted in Fig. E-40. These plots were prepared from measurements of tensile strains in the No. 7 reinforcing bars and compressive strains in the concrete along the bottom face of the bent cap.

Although the peak tensile strains are located at the face of the column, the strains 6 in. to either side of this point do not differ greatly from the maximum. At a load of K = 1.0, the reinforcement nearly reached the design yield strain.

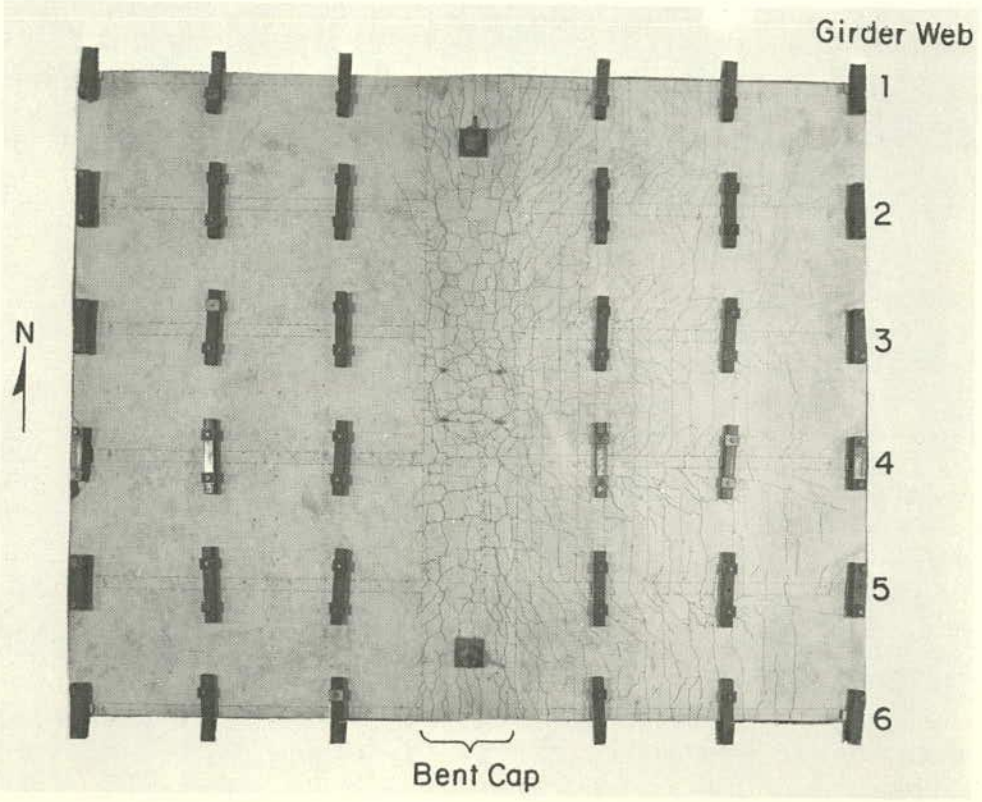

Fig. E-38 Deck Cracking of Specimen SC-3 at End of Test

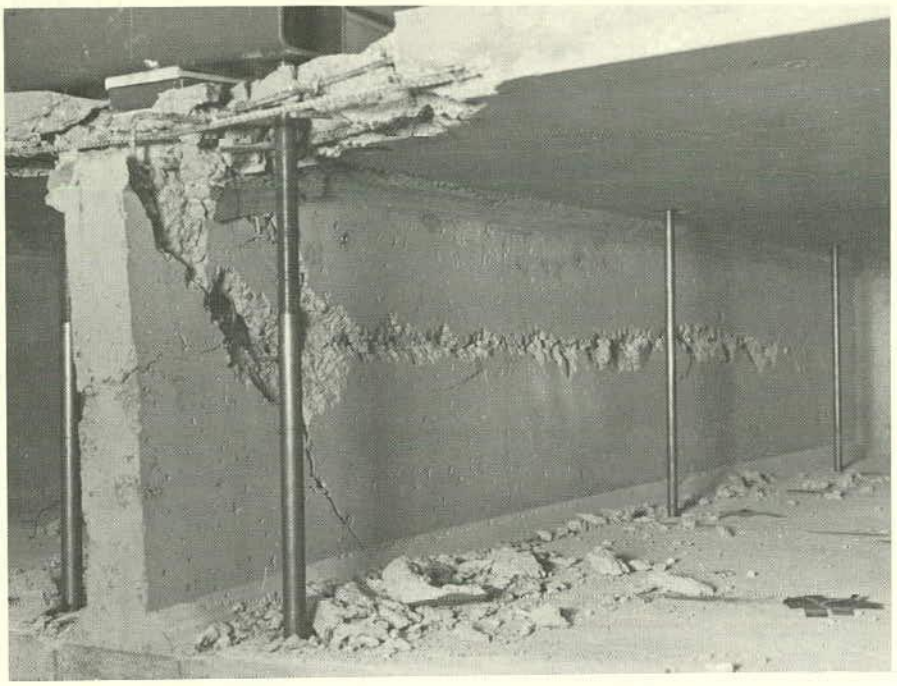

Fig. E-39 Detail of Horizontal Shear Distress of Girder Web No. 4 Specimen SC-3

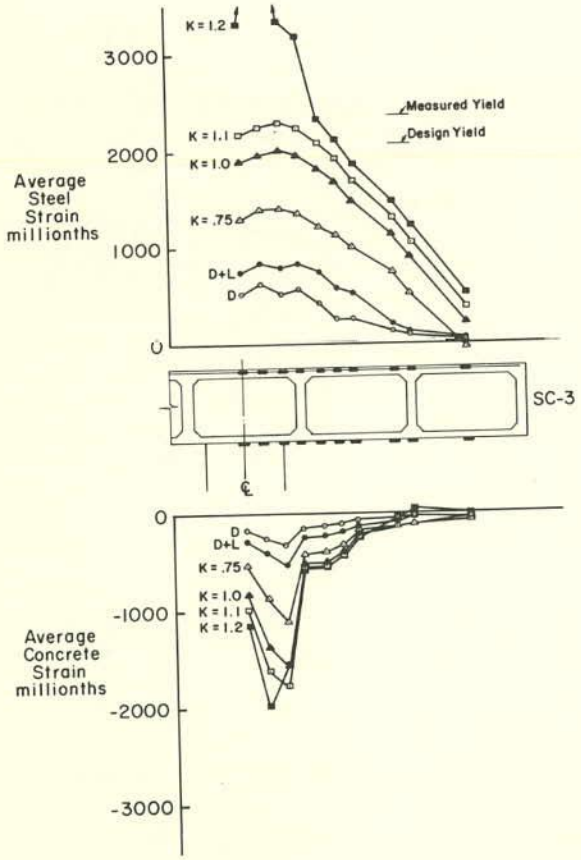

Fig. E-40 Longitudinal Strains in Bent Cap of Specimen SC-3

Compressive strains along the bottom of the bent cap were generally small. In the vicinity of the column, however, higher strains were observed as expected.

Strains in the bent cap stirrups are shown in Fig. E-41. Only small strains were observed at service load conditions. While strains in stirrups over the column were negligible at all loads, outside of the column flexural and inclined cracking in the bent cap at higher loads resulted in significant increases in stirrup strains. In most of the stirrups, strains did not reach the design yield value.

Longitudinal strains measured in the box girders along the face of the bent cap are shown in Fig. E-42. The observed higher tensile strains over the girder webs compared to the values between the webs are indicative of shear lag. At K = 1.0, the peak strains were greater than those corresponding to the design yield stress.

Longitudinal compressive strains along the bottom of the soffit slab were nearly uniform at service conditions. As the load was increased, the concrete in the exterior girder became more highly strained than in the interior girders.

Test of Specimen SF-4. Specimen SF-4 represents a single-column prototype with deck and soffit slabs of uniform thickness and a variable column cross section. The column cross section of the model was circular to 2 ft. below the soffit and then was flared at a two-to-one slope until it intersected the bent cap. At the top of the column, the flare span was two times the circular column diameter as shown in Fig. E-6.

Load versus deflection curves are shown for SF-4 in Fig. E-43. As before, the deflections are at the end of the bent cap and the end

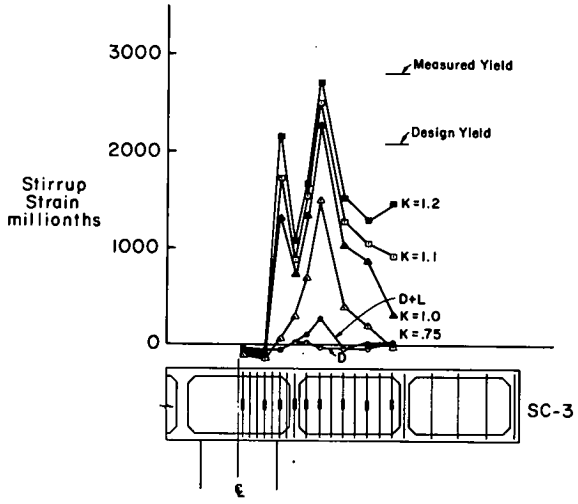

Fig. E-41 Strains in Bent Cap Stirrups of Specimen SC-3

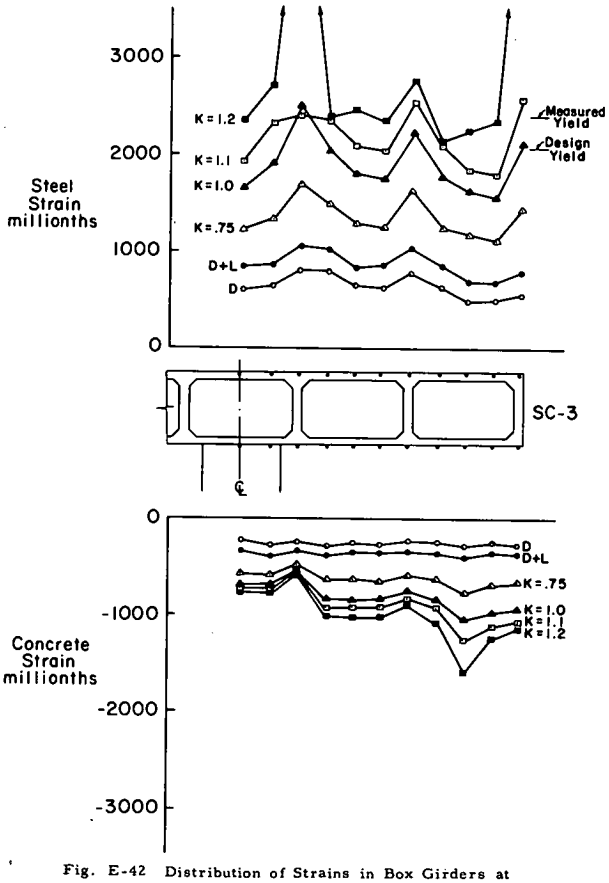

Fig. E-42 Distribution of Strains in Box Girders at Face of Bent Cap of Specimen SC-3

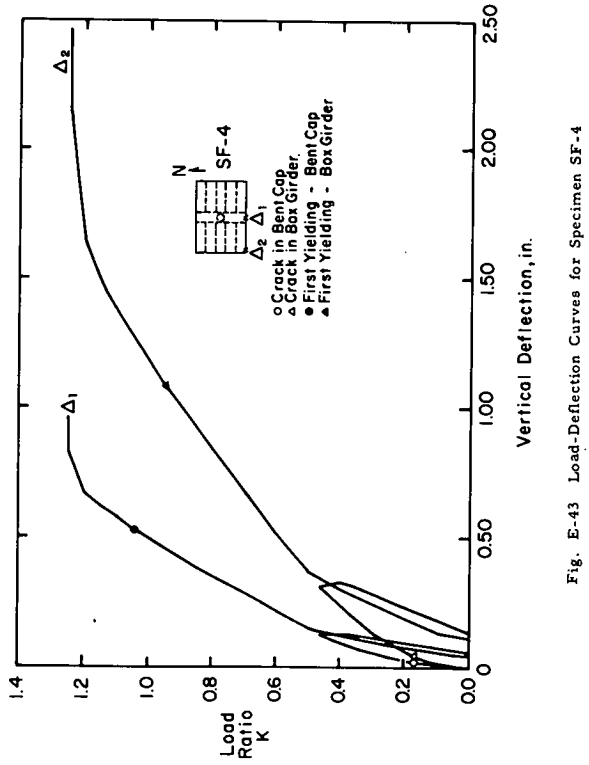

Fig. E-43 Load-Deflection Curves for Specimen SF-4

of an exterior girder. Flexural cracking of the deck slab in the bent cap and the box girders was first observed while the specimen was maintaining 0.5 D. At service load, inclined cracks were present in the box girder webs. Inclined cracks in the bent cap were found at K = 0.70. The maximum crack width measured at service load was 0.0065 in. at a flexural crack in the bent cap.

The longitudinal box girder reinforcement started to yield at K = 0.95. Longitudinal bent cap reinforcement did not begin to yield until the load K = 1.05 was reached.

With the design ultimate load K = 1.0 applied to the specimen, no visible signs of structural distress were evident. Cracks along the deck slab-girder web and soffit slab-girder web joints did, however, indicate distortion of the box sections.

Spalling of the concrete in an exterior girder at the centerline of the bent cap was observed at K = 1.2. Additional spalling along the periphery of the column was observed at K = 1.25.

The end of the test came while the load was being increased to K = 1.30. Concrete in the exterior girder soffit crushed at the bent cap, and the soffit slab in that quadrant was torn away along the bent cap toward the column. The region of distress is shown in Fig. E-44; the view is looking toward the column from the end of the bent. The crack pattern of the deck slab after failure is shown in Fig. E-45.

Average strains in the bent cap main reinforcing bars and in the concrete along the bottom face of the bent cap are plotted in Fig. E-46. The tensile steel strains are fairly uniform within 6-in. either side of the face of support, and tend to decrease toward the column centerline.

Fig. E-44 Crushed Concrete of Specimen SF-4

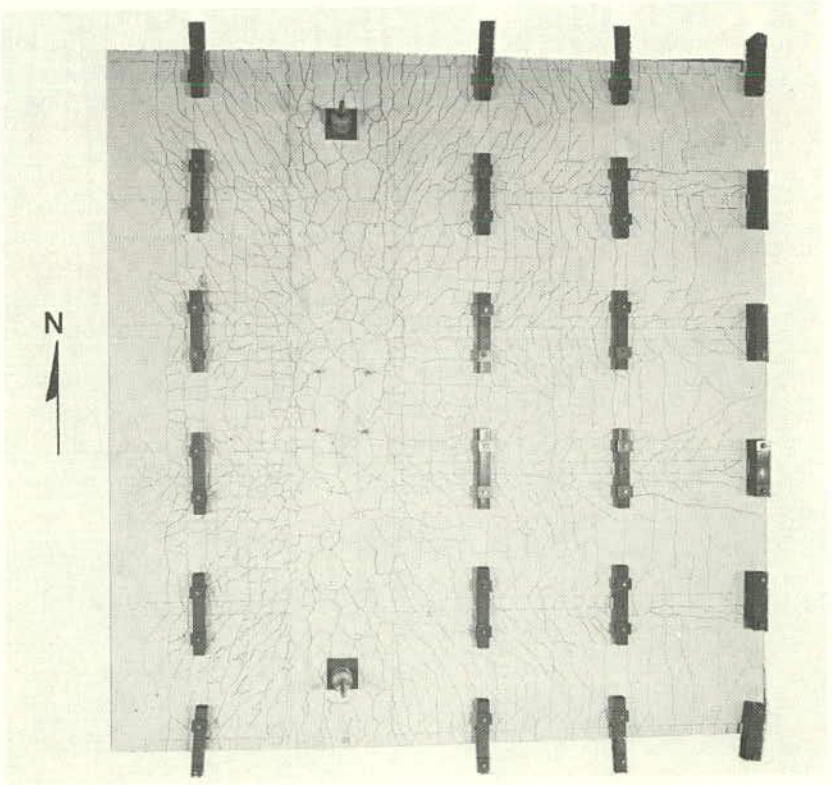

Fig. E-45 Deck Cracking of Specimen SF-4 at End of Test

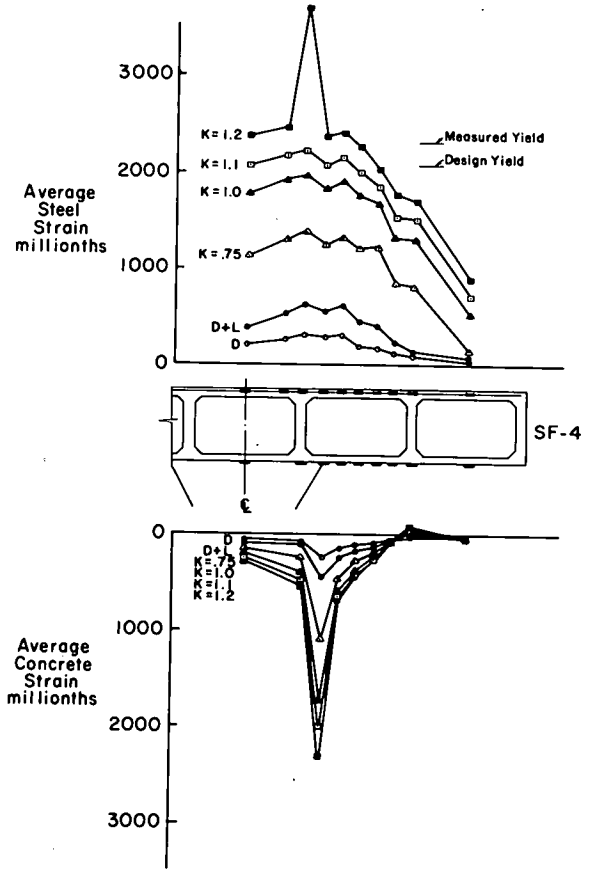

Fig. E-46 Longitudinal Strains in Bent Cap of Specimen SF-4

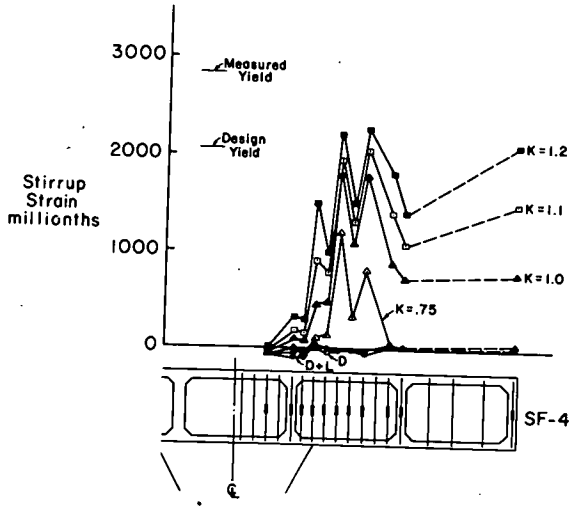

Fig. E-47 Strains in Bent Cap Stirrups of Specimen SF-4

At the design ultimate load, the average steel strains approach the design yield value.

Compressive strains in the concrete at the bottom of the bent cap were small, except at the face of the support. At this location, concentrations of stress were caused by the change in section and the curve in the face of the support.

Measured strains in the bent cap stirrups are shown in Fig. E-47. The strains were negligible at the service load level. Several stirrups had just reached their design yield at the design ultimate load. Only small strains were recorded on those stirrups located over the column.

Longitudinal strains in the box girders of SF-4 are shown in Fig. E-48. The strains plotted are those at the face of the bent cap. Shear lag is evident from the tensile strains that peak over the girder webs and diminish at the box centerline. At design ultimate load, K = 1.0, the longitudinal reinforcement near the webs had yielded, while the bars near the center of the boxes had not. Compressive strains in the concrete were essentially uniform under service load conditions.

Test of Specimen SF-5. Specimen SF-5 represents a single-column prototype with deck and soffit slabs of uniform thickness, and a variable column cross section. The column cross section was circular to a distance 2 ft. below the soffit and then was flared at a one-to-one slope until it intersection the bent cap. At the top of the column, the flare span was three times the circular column diameter as shown in Fig. E-6.

Load-deflection curves for Specimen SF-5 are given in Fig. E-49. Deflections plotted are those at the south end of the bent cap and at the end of the south exterior girder. Flexural cracking of the box girders was

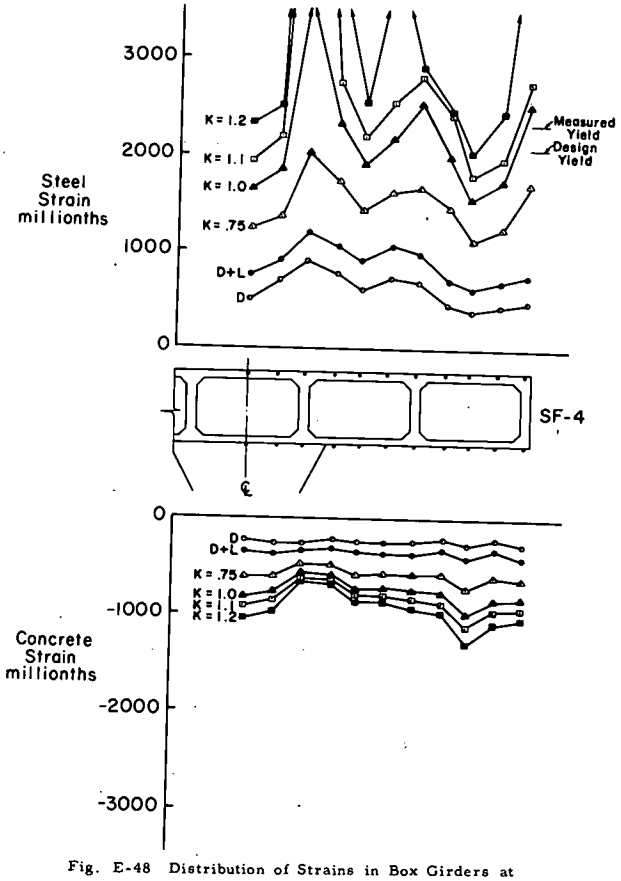

Fig. E-48 Distribution of Strains in Box Girders at Face of Bent Cap of Specimen SF-4

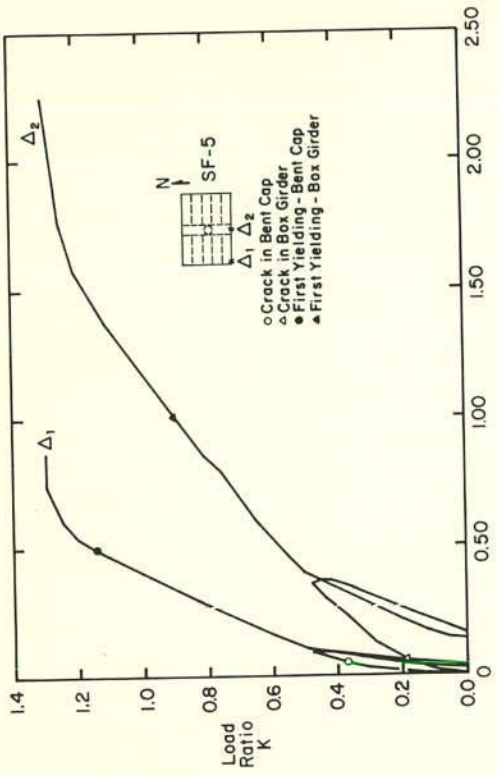

Fig. E-49 Load-Deflection Curves for Specimen SF-5

first observed in the deck at 0.5 D. This was followed by cracking in the bent cap when the entire dead load was applied. At the service load [1.0 D + 1.0 (L + I)], the maximum measured crack width was 0.007 in. Diagonal cracks were observed in the box girder webs at service load. However, none were seen in the bent cap. Distortion of the box girder cells was indicated at service load by the pattern of longitudinal cracks observed along the girders adjacent to the deck and soffit slabs.

Initial yielding of the box girder longitudinal reinforcement was noted at K = 0.90. Yielding of the bent cap reinforcement followed at K = 1.15.

The end of the test for Specimen SF-5 was similar to that of SF-4. While no evidence of structural distress was found at the design ultimate load, spalling of concrete in an exterior girder at its intersection with the centerline of the bent cap was observed at K = 1.20. With the application of load K = 1.25, spalling of concrete in both exterior girders and in the soffit slab at the face of the column was observed.

After load K = 1.30 had been applied, incipient failure was indicated by further spalling of the concrete at the face of the column and along the longitudinal centerline of the bent cap. This spalling was seen to start at the column and propagate toward the exterior girder. While maintaining the load K = 1.30, collapse occurred with crushing of the concrete in the soffit slab along the face of the bent cap. A photograph of the region of distress is shown in Fig. E-50. The view is of the bottom of the bent cap looking toward the column. The crack pattern marked on top of the deck slab is shown in Fig. E-51.

Fig. E-50 Crushed Concrete of Specimen SF-5

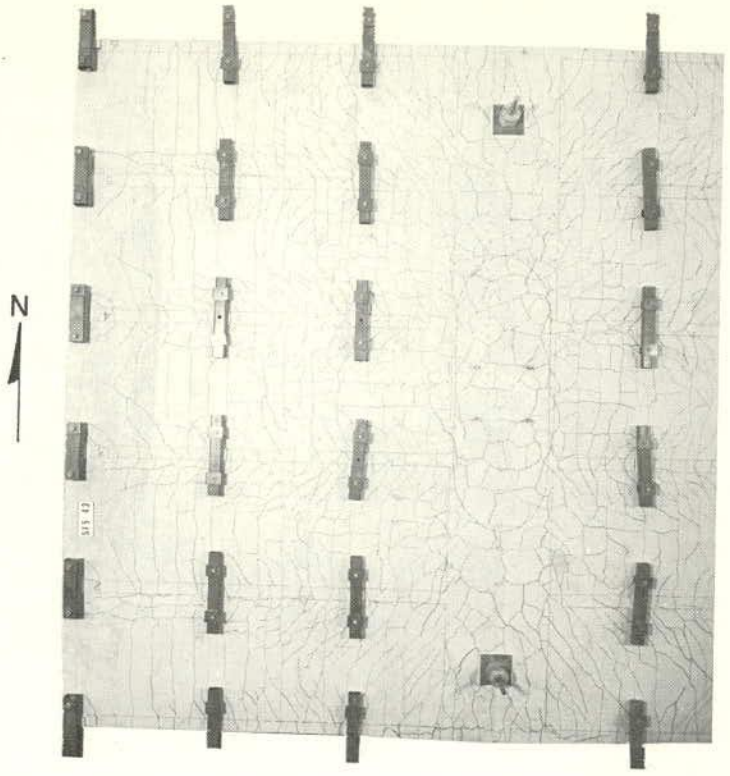

Fig. E-51 Deck Cracking of Specimen SF-5 at End of Test

Distribution of longitudinal strains measured in the bent cap has been plotted in Fig. E-52. At K = 1.0, average tensile strains had not reached the design yield value. Concrete strains, uniformly low under service conditions, were higher near the face of the support at higher loads.

Strains measured on the bent cap stirrups for Specimen SF-5 are shown in Fig. E-53. Strains in stirrups located above the column were small. As seen in Fig. E-53, only one of the instrumented stirrups yielded. The stress in this stirrup, located at the intersection of the exterior girder with the bent cap, was affected by the flexure and shear cracking of the exterior girder.

Fig. E-54 is a cutaway view showing the crack pattern in the bent cap. Similar patterns were observed in Specimens SC-3 and SF-4.

Longitudinal strains measured at the face of the bent cap in the box girders are plotted in Fig. E-55. As in previous models of the series, the effects of shear lag are evident. The measured tensile strains in the girder webs are significantly larger than those at the center of the box cells. At K = 1.0, strains in the girder webs exceeded design yield, whereas the strains at the center of the box cells did not. Concrete strains were slightly larger than those observed in Specimens SC-3 and SF-4.

Test of Specimen ST-6. Specimen ST-6 represents a prototype with a single column of constant circular cross section and with bent cap flexural reinforcement spread into the deck. To accommodate the spread reinforcement, the deck slab was thickened to twice its original thickness for a distance of 48 in. on either side of the bent cap as shown in Fig. E-5. The total area of flexural reinforcement was the same as in Specimen SC-3.

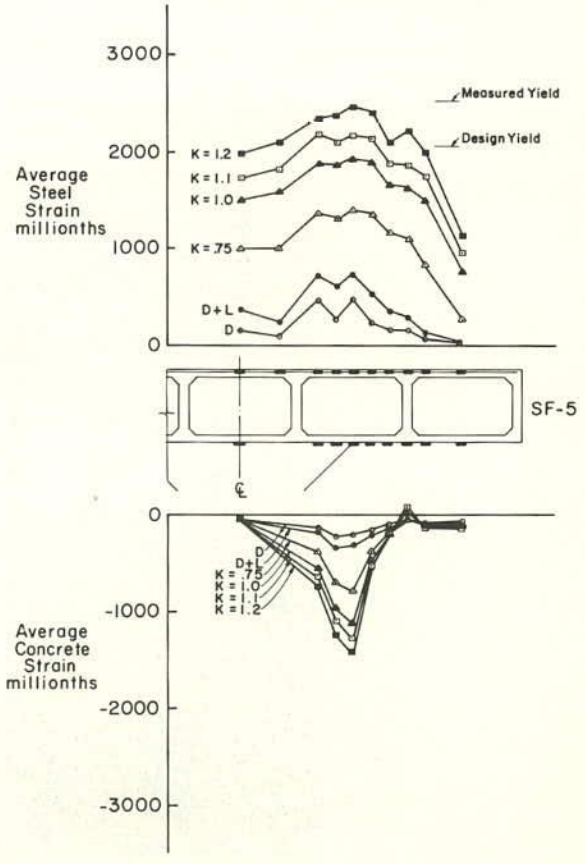

Fig. E-52 Longitudinal Strains in Bent Cap of Specimen SF-5

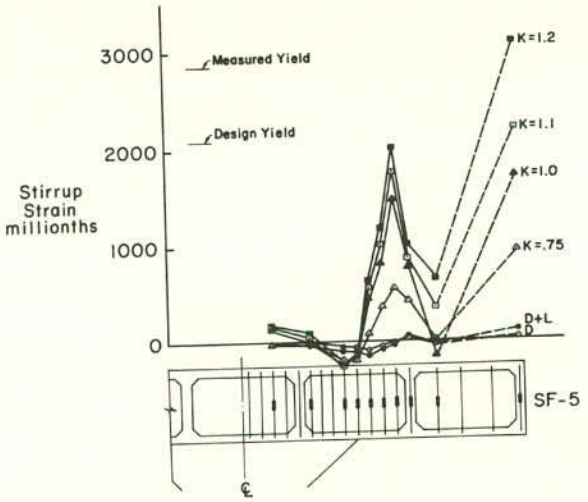

Fig. E-53 Strains in Bent Cap Stirrups of Specimen SF-5

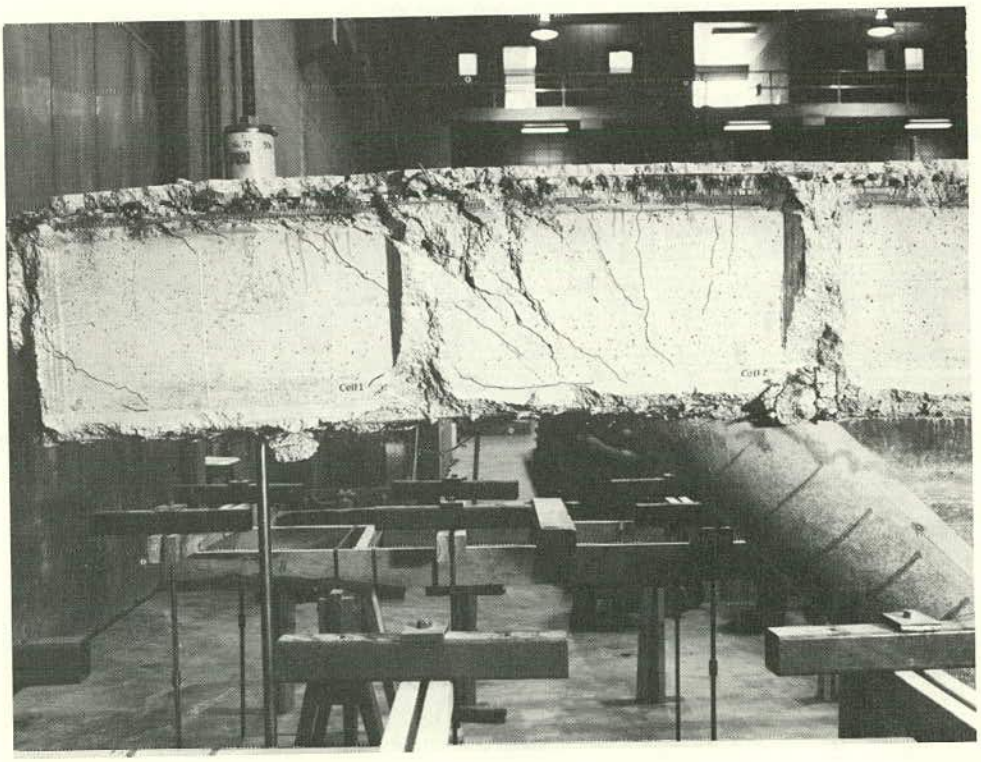

Fig. E-54 Cutaway View of Bent Cap

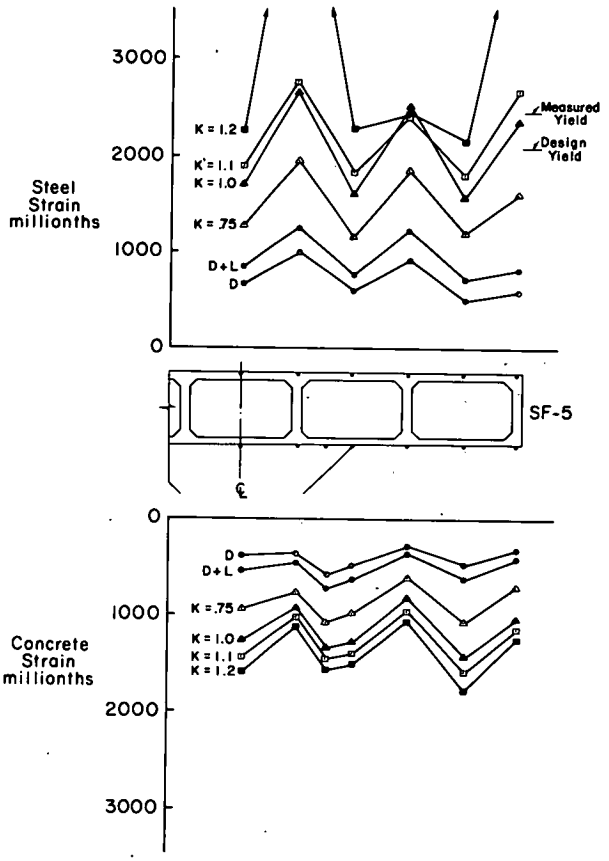

Fig. E-55 Distribution of Strains in Box Girders at Face of Bent Cap of Specimen SF-5

Load-deflection curves for ST-6 are shown in Fig. E-56. Deflections at the end of the bent cap and the end of the south exterior girder are plotted. Cracking in the bent cap and the box girders was observed before the full dead load was applied. The maximum measured crack width at service load was 0.010 in.

At the service load level, shear distortion of the box girder cells was apparent from the pattern of longitudinal cracks that developed along the web-to-flange joints of the box sections.

At K = 1.0, the design ultimate load, spalling of the concrete around the periphery of the column was observed. After the load was increased to K = 1.15, particles of concrete were seen flaking off around the column. However, no other visual signs of distress were evident.

The test ended at a load of K = 1.20. As the load was applied, a large increase in deflection was noted and spalling of the concrete at the intersection of the centerline of the bent cap with the exterior girder was observed. Collapse was gradual as the concrete around the column and along the bent cap began crushing. Fig. E-57 shows the zone of crushed concrete at the end of the test. The crack pattern marked on the deck slab after collapse of the specimen is shown in Fig. E-58.

In contrast to the previous three specimens, initial yielding of the bent cap reinforcement in ST-6 was observed at a lower load level than was initial yielding of the box girder flexural reinforcement. Yielding of the reinforcement within the bent cap occurred at K = 0.65, well below the design ultimate load. Tensile strains in the bent cap reinforcement dropped off significantly for bars located outside the bent cap web. This observation indicated that the effectiveness of a reinforcing bar in resisting the applied moment decreased as the distance

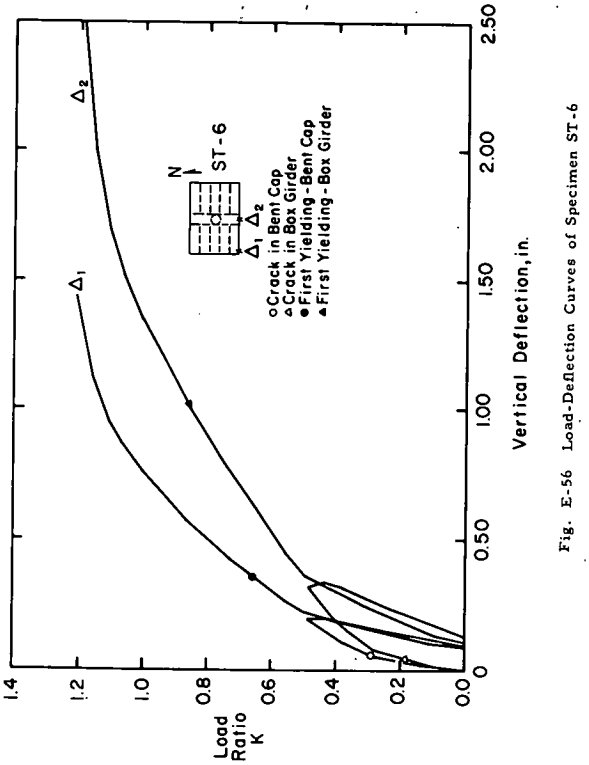

Fig. E-56 Load-Deflection Curves of Specimen ST-6

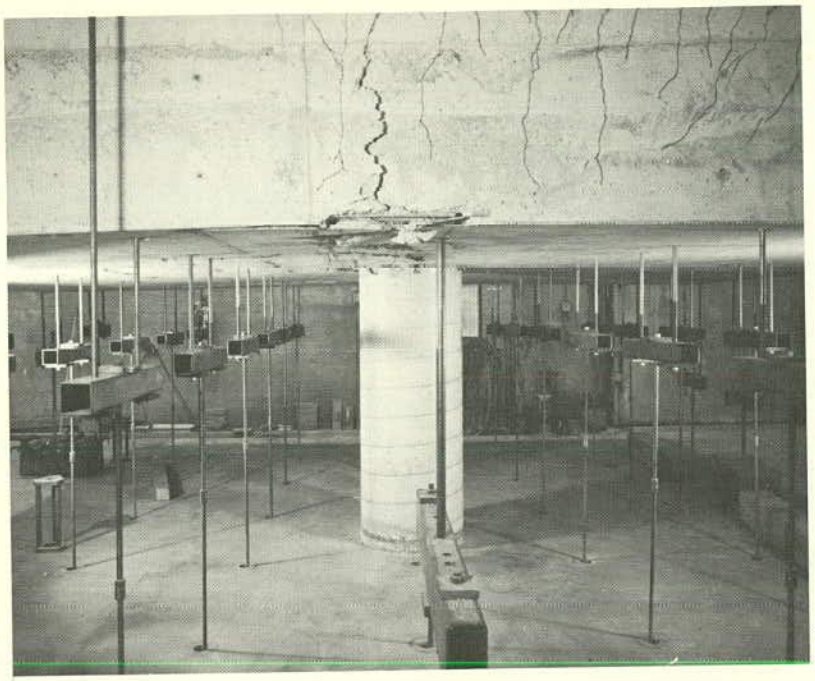

Fig. E-57 Crushed Concrete of Specimen ST-6

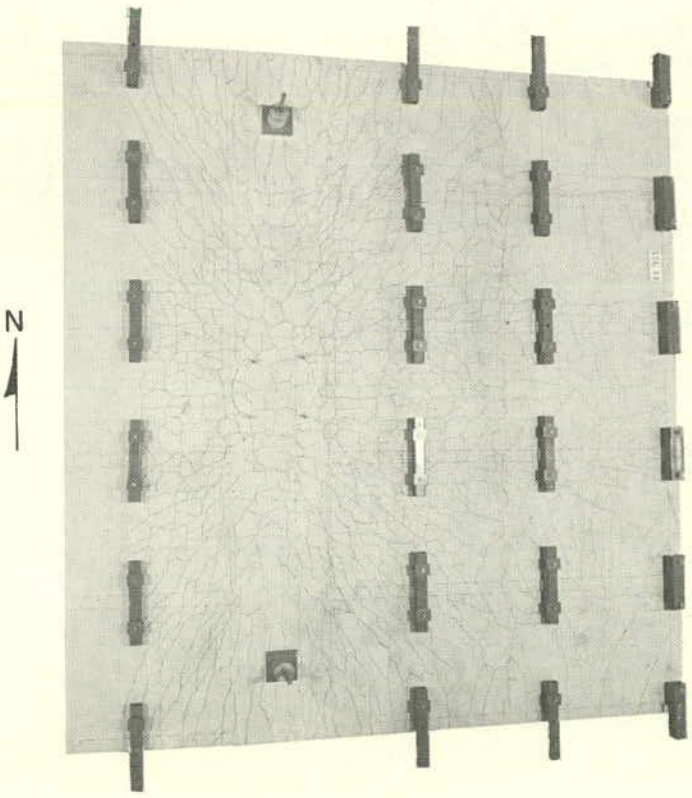

Fig. E-58 Deck Cracking of Specimen ST-6 at End of Test

between the bar and the bent cap web increased. The inefficiency of the bars located outside the bent cap web resulted in the relatively early yielding of the bars within the bent cap web. This also resulted in ST-6 having a more flexible bent cap than SC-3.

Figure E-59 shows strains measured in the bent cap stirrups for Specimen ST-6. As was the case for the other single-column specimens, stirrup strains were small at service load. At subsequent higher loadings, measured strains indicated the stirrups over the column were not stressed significantly. However, a number of stirrups outside the column reached their design yield strain.

The distribution of the measured longitudinal strains in the box girders at the face of the bent cap is shown in Fig. E-60. At K = 1.0, the strains indicate that the box girder tensile reinforcement had essentially reached its design yield. Peaking of the tensile strains over the girder webs was not as distinct in this specimen as it was in the previous specimens which did not have thickened decks. The compressive strains show a definite peak at the exterior girder.

Test of Double-Column Bent

Loading Sequence. The planned loading sequence for the double-column bent, Specimen DC-9, was the same as for the single-column bents. A service load test of 1.0D + 1.0 (L + I), was applied. This was followed by removal of superimposed load and then by the test to destruction. Again, load increments for the service load test were 0.25 D and 0.25 (L + I). For the test to destruction, increments were 0.05 K, where K = 1.0 is that load corresponding to 1.8 D + 3.0 (L + I).

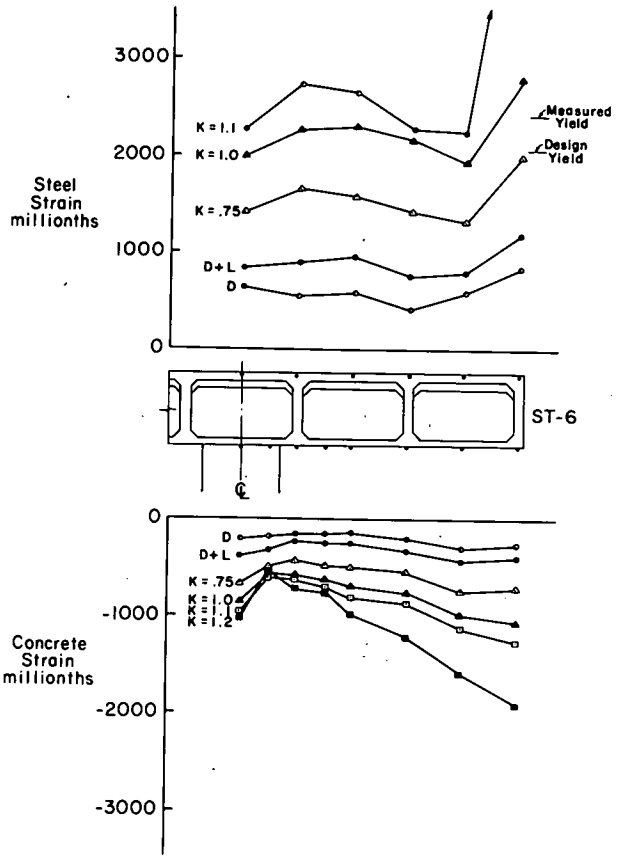

Fig. E-60 Distribution of Strains in Box Girders at Face of Bent Cap of Specimen ST-6

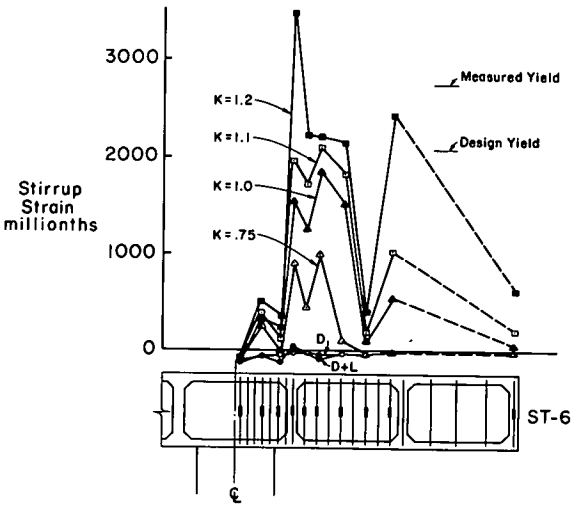

Fig. E-59 Strains in Bent Cap Stirrups of Specimen ST-6

The test to destruction ended with local distress at a load of K = 1.15. To gain more information on general structural behavior, the loading apparatus was rearranged to bypass the damaged area, and the test was continued, with load increments of K = 0.05 as before. Details are described below.

Test. Load-deflection curves for the bent cap at the end and at the centerline of roadway, for the corner of the specimen, and for the centerline of roadway at the end of the specimen are shown in Fig. E-61. As for the single-column bents, the service load tests have been converted to fractions of K load ratios giving equal column reactions.

Various events of the test are shown on the plots. First flexural cracking occurred in the girders at the face of the bent cap at 1.0 D. First cracking in the bent cap (circumferential cracking above the columns) was observed at 1.0 D + 0.75 (L + I). Minor web cracking in the exterior girder webs also was noted at this load. No other cracking was visible at the end of the service load test.

In the test to destruction, the first clearly defined negative moment flexural cracking in the bent cap was visible just outside the column at a load of K = 0.6. At the load K = 0.7, these flexural cracks were visible extending down into the bent cap.

The first clearly developed diagonal tension web crack, as opposed to the minor cracking observed earlier, occurred in the exterior girder web at a load of K = 0.85.

At K = 0.9, a loading rod fractured and the applied load was reduced to zero. After the loading apparatus was repaired and strengthened, testing resumed. These events appear as a break in the load deflection curve.

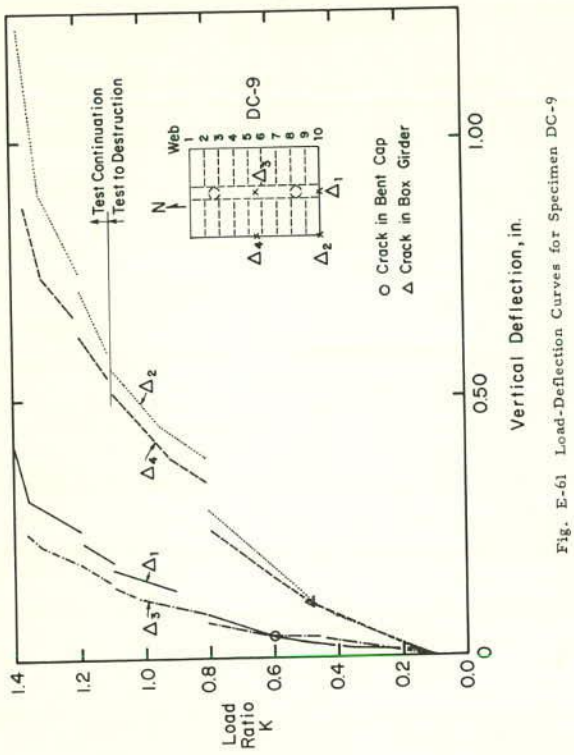

Fig. E-61 Load-Deflection Curves for Specimen DC-9

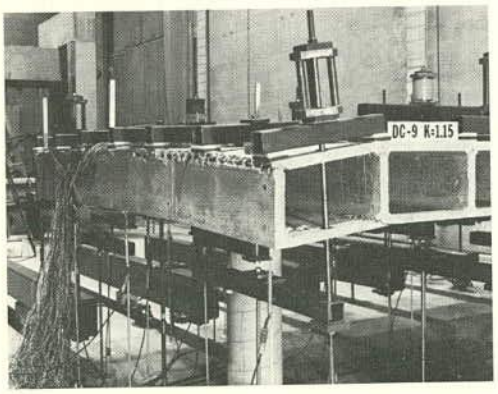

Fig. E-62 Initial Area of Distress During Test to Destruction on Double-Column Bent DC-9

As load was increased, no marked changes in behavior were noted through K = 1.10. Just as the load reached K = 1.15, the east portion of exterior girder 10 (south side of specimen) developed horizontal shear distress in the construction joint between web and deck. This was apparently due to incomplete compaction of the concrete. Since no data were obtained at the load K = 1.15, K = 1.10 represents the highest load for which a complete set of data exists.

Fig. E-62 shows the area of distress. As can be seen, damage was limited to the exterior girder and the adjacent deck and soffit.

Due to the local nature of the distress that terminated the test to destruction, it was decided to continue the testing on the relatively undamaged portions of the structure. To continue the test while maintaining, for stability, symmetry of loading, it was necessary to deactivate all the girder loading apparatus on Webs 9 and 10 and replace it with the statically equivalent equal force at the centroid of the deactivated loads. This force was applied at the location of the existing south load point on the bent cap centerline.

Since the west ends of Webs 9 and 10 in the deactivated area, as well as the south load point on the bent cap centerline, were in the instrumented southwest quadrant of the specimen, the change in load pattern meant that readings from the instrumentation, though available, were no longer a valid indication of the original load carrying mechanism of the structure.

New optical level targets were installed in the essentially unaffected north portion of the structure so that deflections could be monitored during the test continuation. The test continuation portion of Fig. E-61 was plotted from these data.

The break in the load-deflection curve for the test continuation at a load of K = 1.20 resulted from an unloading to correct difficulties in the loading system. Load was increased in the usual increments to K = 1.40, with no significant changes in behavior. Impending distress in the compression flange of the exterior girder, similar to that observed in the single-column bent specimens, was observed at higher loads.

Just as the load reached K = 1.40, crushing in the compression flanges of the box girder began in the north end of the bent cap and, combined with shearing distortion, spread along the east junction of bent cap and girder soffit through the first three boxes. The distress then continued outward as a hinging of the deck and soffit along the north side of the fourth web. The load was reduced to zero and the testing terminated. This mode of collapse is similar to that observed in several of the single-column bent cap specimens. A photograph of the specimen after test is shown in Fig. E-63.

Average strains in the main bent cap reinforcement are shown in Fig. E-64. For the top reinforcement in the negative moment region, it can be seen that the location of the maximum average strain moved from the column center at low loads to a point 6 in. beyond the exterior column face at high loads. Yield strain was not reached at any of the loads shown.

Strains on the interior side of the column were lower than those on the exterior side. The point of zero strain showed some shift at higher loads but not as much as was found in the double-column bridge. Compressive strains in the positive moment region were relatively small.

Fig. E-63 Crushed Concrete of Double-Column Bent DC-9

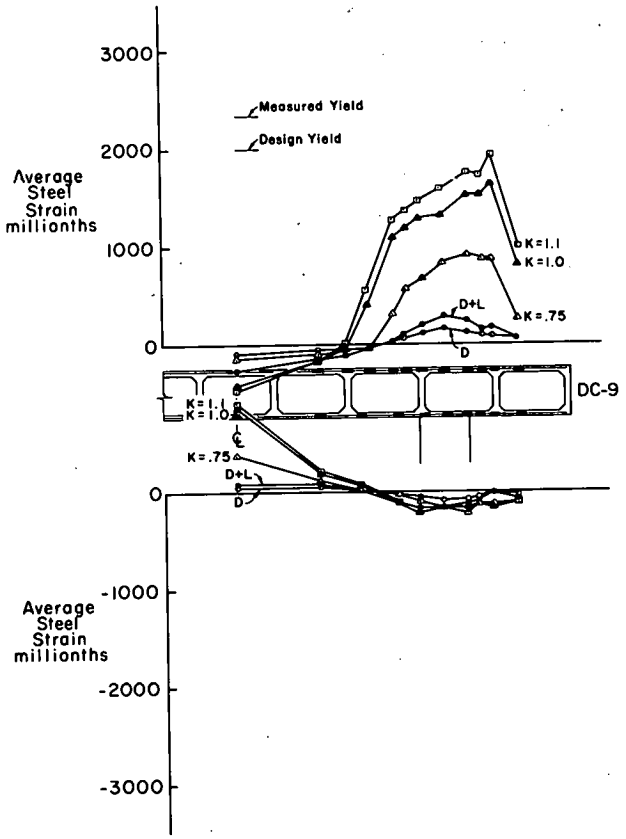

Fig. E-64 Longitudinal Strains in Bent Cap of Specimen DC-9

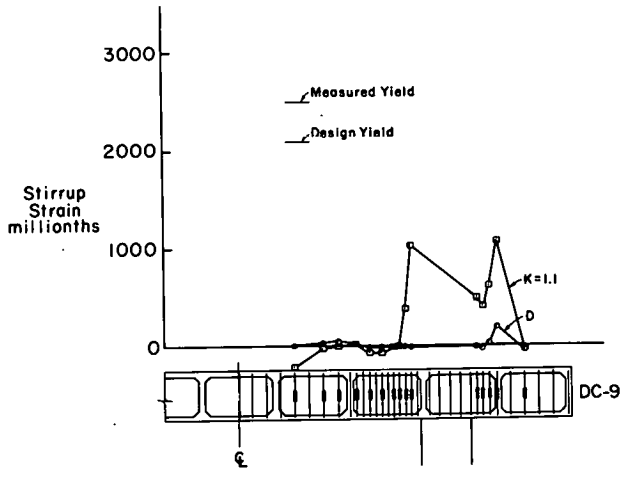

Fig. E-65 Strains in Bent Cap Stirrups of Specimen DC-9

Considering the bottom reinforcement in the positive moment region, it can be seen that the maximum tensile strain at K = 1.0 was about 900 millionths, less than half the yield strain predicted by design. This implies that bending moments in the region were substantially less than those calculated in design.

Measurements indicated that the point of zero strain in the bottom reinforcement migrated very little with increasing load. Also, compressive strains in the negative moment region were small.

Strains in the bent cap stirrups are shown in Fig. E-65. Strains were negligible at all locations except in the immediate vicinity of the column. Even there maximum strains were only about half the yield strain.

Longitudinal strains in the girders along the face of the bent cap are shown in Fig. E-66. The upper portion of the figure shows the variation of strains in the main girder reinforcement. The lower portion of the figure shows the measured strains in the extreme lower fiber of the concrete.

The strains in the concrete were uniformly distributed (the exception for one location at high loads does not appear to be significant) and of quite small magnitude. However, the reinforcement strains showed the same variations between locations on web centerlines and box centerlines already noted in previous tests of the bars above the webs. The bars nearest the column were the more highly strained, and at K = 1.1, the strains at one location were at yield. This was the highest strain measured anywhere in the structure at this load. However,

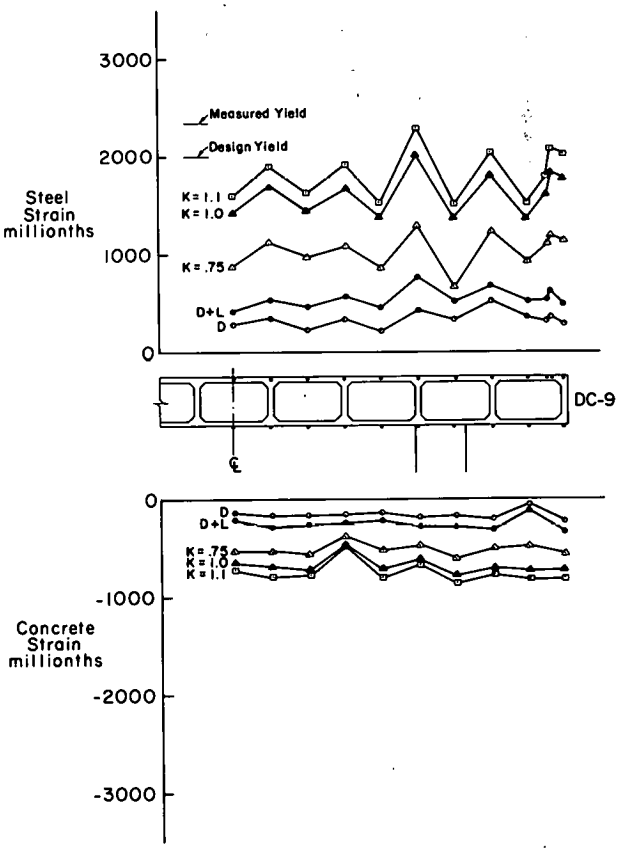

Fig. E-66 Distribution of Strains in Box Girders at Face of Bent Cap Specimen DC-9

the average strain for the girder reinforcement was well below yield. Consequently, the moment capacity of the girders was not developed.

Bent Data Analysis

Analysis of the tests of the four single-column and the double-column bent cap specimens was carried out in the following sequence:

1. Effect of column flare
2. Effective slab width for bent cap design
3. Effect of spreading bent cap tensile reinforcement
4. Location of critical section for bent cap design

The analysis was based primarily on the measured strains in the concrete and reinforcement.

The object of the analysis was to evaluate the observed response of the bent cap specimens so that design recommendations based on this response could be developed.

Determination of Absolute Strains. As discussed in Appendix A, one of the problems encountered in the interpretation of the experimental results was the determination of the absolute value of strain for any particular load. This problem was less acute in the model bent tests than in the model bridge tests because fewer cycles of loading were applied and a shorter time elapsed between each cycle in the bent tests.

In interpreting the data for the bent cap specimens, the original zero, point A in Fig. A-14, was used as the datum for strains measured during both the service and ultimate load tests. Most of the analysis was performed on the data from two loads, service load and design ultimate load, K = 1.0. These data were selected because they represented respectively, a load of an intermediate level and one of a high level. The high level

load, however, was not so high that local distress had begun to cause internal redistribution of forces.

Effect of Column Flare. Model bents with the column flared in the plane of the bent were studied to determine if the flared column would act as effectively as a cylindrical column having the same cross section as that at the top of the flare. Stresses in the concrete of the flare were also investigated.

Specimens SF-4 and SF-5, shown in Fig. E-6, had single columns with two-to-one and one-to-one flares, respectively. The tests of these two specimens, along with SC-3 which had a circular cylindrical column, provided the data for the analysis. Except for the flare detail, all three specimens had the same nominal dimensions. As a result of the design assumptions already listed, the main flexural reinforcement consisted of 12-No. 7 bars for SC-3, 12-No. 6 bars for SF-4 and 12-No. 5 bars for SF-5, as shown in Fig. E-13.

The effect of column flare on bent cap deflections at service load and at K = 1.0 is shown in Fig. E-67. At both loads, the smallest deflection is produced with the largest flare. Deflections for ST-6, also shown, exceed those of the other specimens.

The distributions of longitudinal strains in the main flexural reinforcement and in the concrete at the bottom of the bent cap for SC-3, SF-4, and SF-5 are shown in Fig. E-68. The strains plotted are those measured at K = 1.0. For ease in making comparisons, the distance between the face of the support and the center of the exterior web has been drawn as though it was constant for the three specimens. The face of the support was defined as the most extreme point, in the longitudinal direction of the bent cap, of the column or flare.

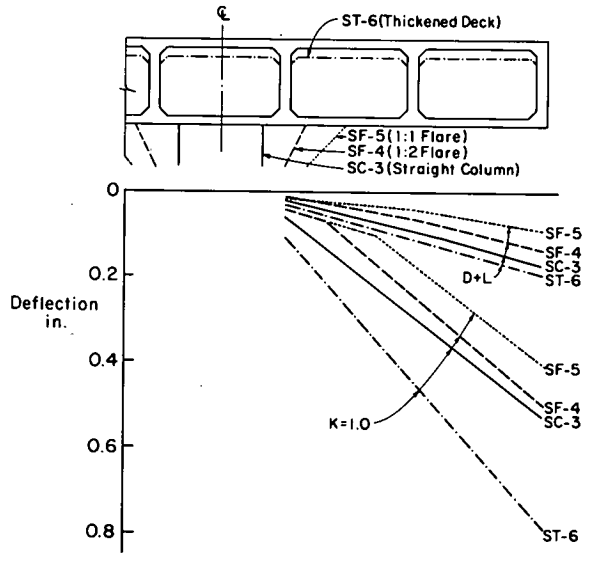

Fig. E-67 Effect of Column Flare and Spread Reinforcement on Bent Cap Deflections

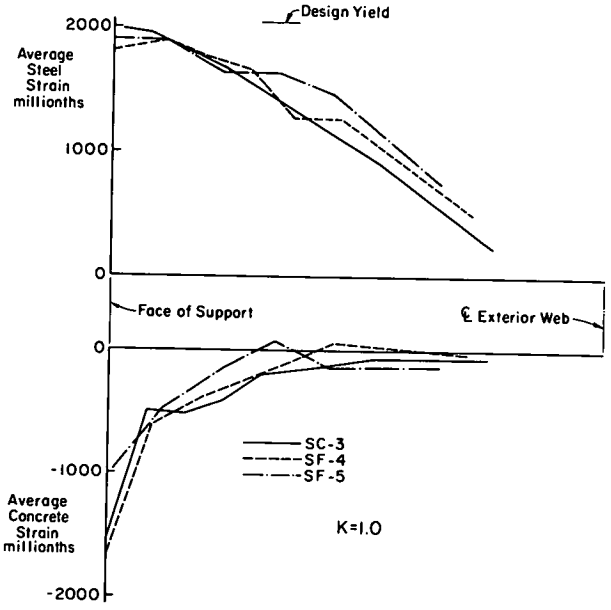

Fig. E-68 Distribution of Average Strains in Bent Cap Between Face of Support and End of Bent Cap

Figure E-68 shows that the distributions of reinforcement strains along the bent cap closely coincided for the three specimens. The shapes of the curves in the vicinity of the face of support are similar. The compressive strains measured on the bottom face of the bent cap also match for the straight and flared column models. Based on the bent cap strains, it can be concluded that the flared columns were as effective as an equivalent cylindrical column.

To determine if the concrete in the most highly stressed region of the flare showed any signs of distress, strains measured on the face of the flared column 3 in. below the bottom of the bent cap for SF-4 and SF-5 were plotted against load in Fig. E-69. The concrete strain in SF-5, containing the widest flare, was slightly greater than the corresponding strain in SF-4. In neither specimen, however, does the strain at the design ultimate load indicate that the concrete in the flare was overstressed, since maximum strains are well below the usually accepted limit of 3000 millionths.

Effective Slab Width. An analysis was made to determine the extent of participation of the soffit and deck slabs in resisting the bending moment applied to the bent cap. The situation is analagous to that in T-beams where the flanges effectively participate in resisting the moment applied to the section. While studies of T-beams have been primarily directed toward determining the effectiveness of the flanges in compression[7, 18] the present study was intended to investigate the effectiveness of the tension flanges as well as the compression flanges.

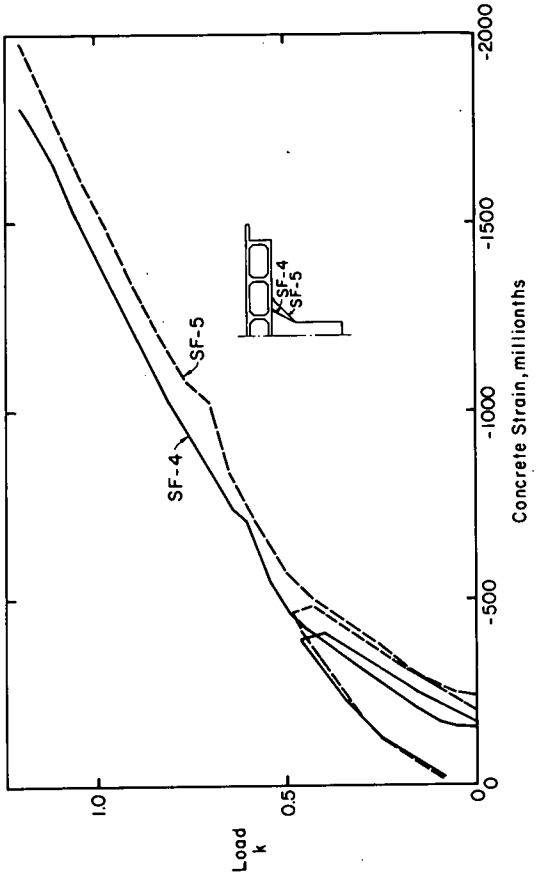

Fig. E-69 Load vs. Concrete Strains Measured on Flared Columns of SF-4 and SF-5

In single-column bents, and in the negative moment regions of double-column bents, the deck and the soffit slabs serve as the tension and the compression flanges, respectively. In the positive moment region of double-column bents, the roles of the deck and soffit slabs are reversed.

To obtain a measure of the participation of the deck and soffit slabs, the transverse distributions of strains parallel to the longitudinal centerline of the bent cap were analyzed. These distributions, for strains measured at the face of the support, are plotted in Fig. E-70 for K = 1.0. The reinforcement strains are those in the main tensile reinforcement for the bent cap and the top reinforcement in the deck slab. Concrete strains are those on the bottom surface of the soffit slab.

As can be seen in Fig. E-70, strains decrease with increasing distance from the bent cap. This is indicative of shear lag in the slabs, and results in a reduced effectiveness of the slab portions farther away from the bent cap. The transverse strain distributions for SC-3, SF-4, and SF-5 are discussed in more detail below. Discussion of Specimen ST-6, which had spread reinforcement, is reserved for a later section.

Considering first the negative moment tensile strains, Fig. E-70 indicates that out to about 36 in. from the bent cap centerline, the decrease of strain for SC-3, SF-4, and SF-5 is similar. Beyond this point, however, the deck strains in SC-3 and SF-4 are much higher than those in SF-5. This difference can be attributed to shearing distortion of the box girders shown in Fig. E-71. The shearing distortion results in a secondary strain gradient in the deck and soffit slabs. These strains

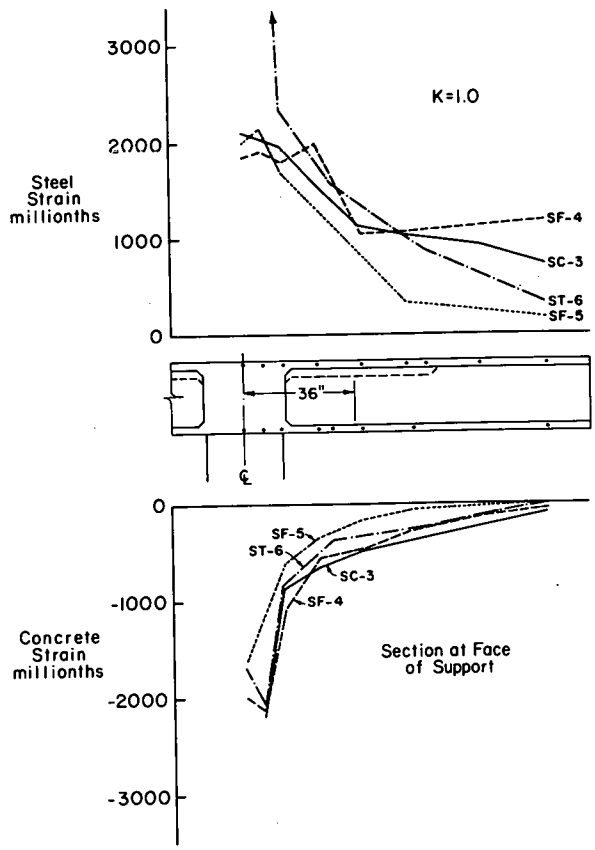

Fig. E-70 Transverse Distribution of Strains at Face of Support in Single-Column Bents

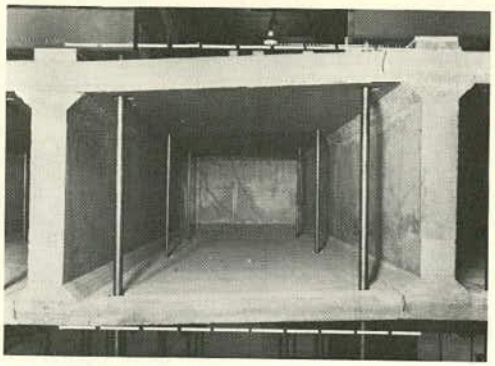

Fig. E-71 Shearing Distortion of Box Girder for Specimen SF-5

are greatest near the webs of the box section. For Specimens SC-3 and SF-4, the sections along which the strains in Fig. E-70 were measured are located such that the secondary strain gradient would result in an increase in the strains in the top steel of the deck slab. For Specimen SF-5, on the other hand, the section at the face of the flared column is located at the centerline of a box section. Here, the influence of the secondary strain gradient is not significant. Consequently, the steel strain distribution plotted for SF-5 in Fig. E-70 is considered to be the one most indicative of the participation of the deck slab in resisting the moment applied to the bent cap.

Since strain gages were not placed on the bottom layer of deck slab reinforcement at every longitudinal section, the influence of the secondary effects described above could not be quantified. However, for those sections where strains were measured, the expected pattern of strains due to shearing distortion of the boxes was confirmed.

To summarize, the results in Fig. E-70 indicate that the deck slab reinforcement in SC-3, SF-4, and SF-5 did contribute to the moment resistance of the bent cap. The effectiveness of this reinforcement, however, decreased rapidly as its distance from the bent cap increased.

In addition to the negative moment tensile strains, negative moment compressive strains are also shown in Fig. E-70. Because of high strain concentrations at the intersection of the bent cap with the support, the decrease in the concrete compressive strains is accentuated at the section along the support face. Therefore, Fig. E-72 showing the strain distributions for each specimen along a section 6 in. outside the face of the support is included.

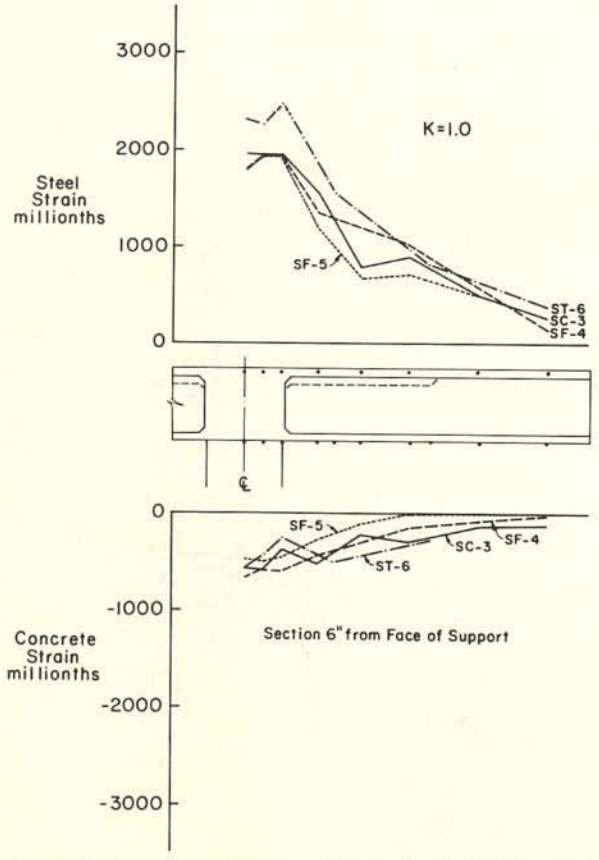

Fig. E-72 Transverse Distribution of Strains in Single-Column Bents

E-97

The transverse distributions of compressive strains shown in Fig. E-72 are similar for SC-3, SF-4, and SF-5. This indicates that the soffit slab acted as a compressive flange in resisting the applied bent cap moment. The effectiveness of the soffit slabs decreased in portions of the slab farther from the bent cap in a manner similar to that observed in T-beam flanges. It should be noted that the comments given above regarding secondary effects also apply to the concrete strains measured on the bottom of the soffit slab.

Results similar to those shown in Figs. E-70 and E-72 were obtained in the negative moment regions of the double-column bent cap model, DC-9. Transverse strain distributions for DC-9 are given in Fig. E-73. The steel strains plotted are those along a section at the exterior face of a column and at a section 3 in. outside the column. This section, at one-fifth scale, is equivalent to the section shown in Fig. E-72 for the two-fifth-scale single-column bent specimens. Similarity to strain distributions of the single-column bents indicates that the strain decreased with increasing distance from the bent cap was similar in the negative moment region of the double column bent.

The transverse strain distributions at the section of maximum positive moment in DC-9 are shown in Fig. E-74. The strains plotted are those measured on the top layer of deck reinforcement and the bottom layer of soffit reinforcement. Strain distributions are given both for K = 0.75 and K = 1.0 to show the changes that occurred between these two load stages.

At K = 0.75, the strain distribution patterns are similar to those obtained in the negative moment regions. In this case, strains

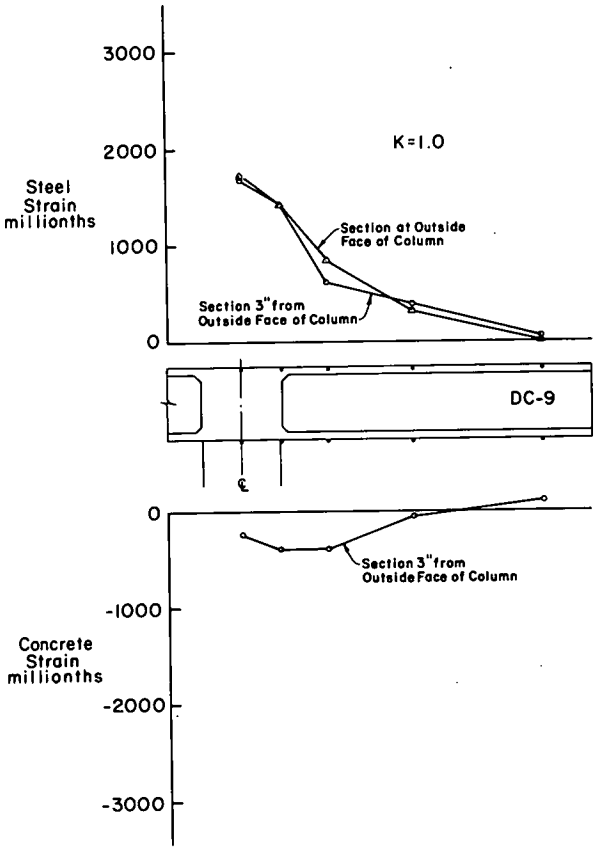

Fig. E-73 Transverse Distribution of Strains in Negative Moment Sections of Double-Column Bent

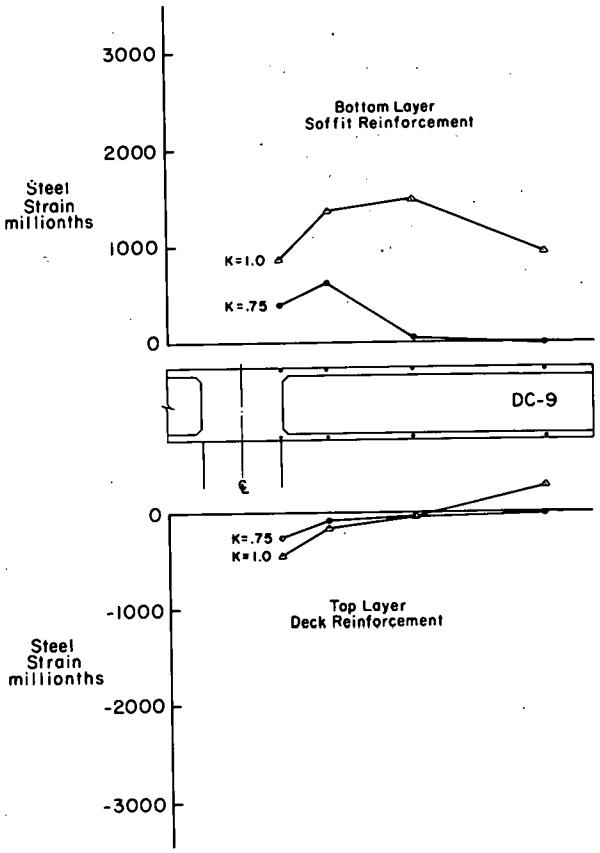

Fig. E-74 Transverse Distribution of Strains in Positive Moment Section of Double-Column Bent

decreased as the distance from the bent cap increased. As expected, the soffit slab is in tension and the deck slab is in compression. After the load was increased to K = 1.0, the measured strains indicate that both slabs were in tension over approximately one-half the length of the box girders. The existence of the tensile strains indicated by the strain gages was confirmed by tensile cracking of the deck slab. The source of the redistribution of internal forces that caused the cracking was not determined.

Effect of Spreading Bent Cap Tensile Reinforcement. As previously described, specimen ST-6 had a thickened deck to accommodate a portion of the bent cap reinforcement as shown in Fig. E-14. Spread bent cap reinforcement is used when the width of the bent cap web is not great enough to accommodate all the flexural reinforcement. In such cases the reinforcement would be expected to be rather heavy. However, for ease in comparison of results, the total amount of reinforcement in ST-6 was made the same as in SC-3.

Figure E-75 is a plot of the transverse distribution of strains parallel to the longitudinal centerline of the bent cap for Specimen ST-6. The strains, measured at the face of the column, are plotted at several levels of load. Within the width of the thickened deck, the strains are those on the main tensile reinforcement. Beyond the thickened deck, the strains are those on the top layer of deck slab reinforcement. The concrete strains were measured on the bottom surface of the soffit slab.

It is evident from the figure that reinforcement at the extremities of the thickened deck was much less effective than that located closer to the bent cap. At a load of K = 0.75, for example, the reinforcement

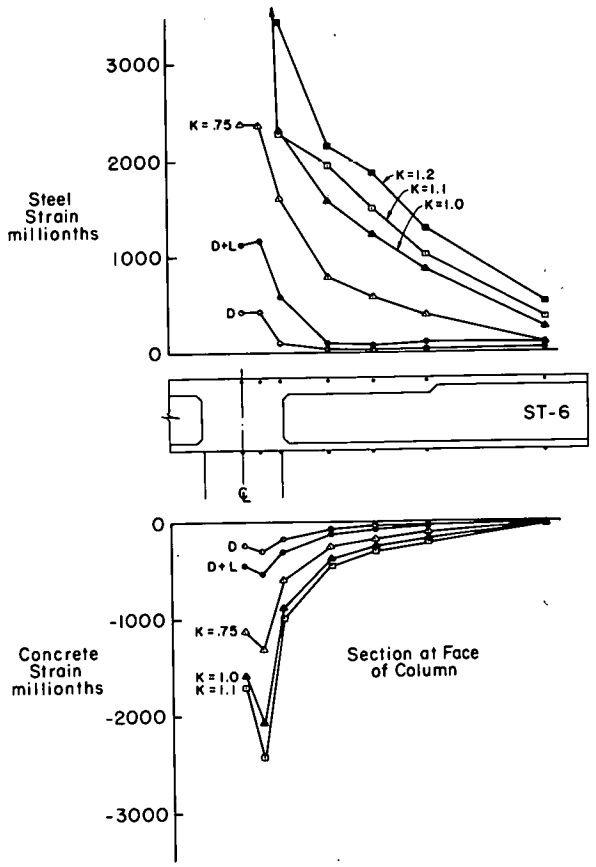

Fig. E-75 Transverse Distribution of Strains Parallel to Longitudinal Centerline of Bent Cap Specimen ST-6

strain measured at the end of the thickened deck was less than 20 percent of the maximum strain at the center of the bent cap.

As can be seen by comparison with Figs. E-70 and E-72, the rate of strain decrease for bars more remote from the bent cap in ST-6 is similar to that found in the other single-column bent caps. However, due to the fact that much of the main reinforcement is only partially effective in ST-6, the strain in the more highly stressed reinforcement is increased above that in the other specimens.

The higher stresses in the reinforcement over the bent cap web are also reflected in larged deflections for ST-6 compared to the otherwise similar SC-3. These deflections are shown in Fig. E-67.

Location of Critical Section for Bent Cap Design. The most significant requirement for a critical design section is that it be located where the maximum stresses occur. This is essential for design of both the negative and positive moment reinforcement.

Variations of the average longitudinal tensile and compressive strains in the single-column bent caps are presented in Fig. E-76. These curves show that reinforcement strains are at a maximum at or near the face of support, but that strain gradients in either direction are small in the immediate vicinity. Reinforcement strains at the center of the support tend to be smaller than at the face of support, presumably because the support serves to increase the effective depth of the bent cap.

It is evident from the results shown in Fig. E-76 that design of the bent cap for negative moment based on a critical section at the centerline of the column would be unrealistic, since this is not the location of maximum stress. The data support the selection of the critical section at or near the face of the column.

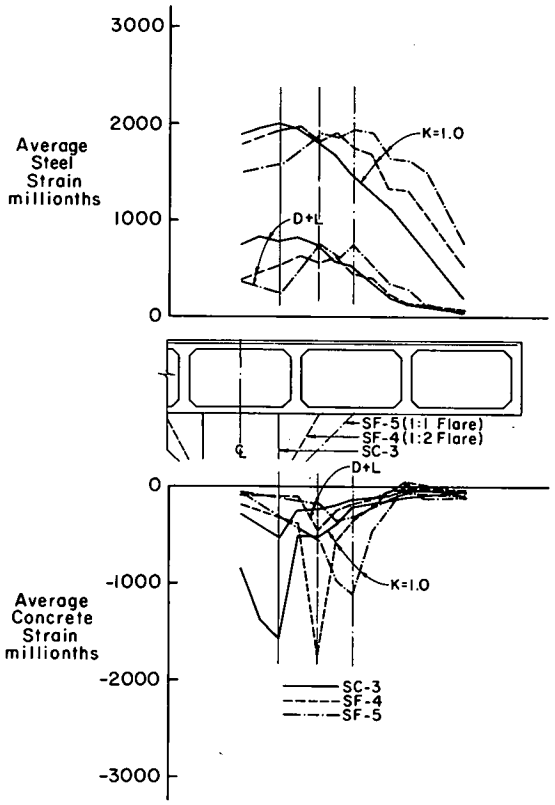

Fig. E-76 Distribution of Average Strains in Bent Cap of Specimens SC-3, SF-4 and SF-5

Figure E-64 shows the variations in the average longitudinal tensile and compressive strains in the double-column bent cap. These results show that the maximum negative moment tensile strains occur in the vicinity of the face of the support, as was the case for the single-column specimens. The maximum positive moment tensile strains occur at midspan of the bent cap as expected.

Published reports of the

NATIONAL COOPERATIVE HIGHWAY RESEARCH PROGRAM

are available from:

Transportation Research Board
National Academy of Sciences
2101 Constitution Avenue
Washington, D.C. 20418

Rep. No.	Title
—*	A Critical Review of Literature Treating Methods of Identifying Aggregates Subject to Destructive Volume Change When Frozen in Concrete and a Proposed Program of Research—Intermediate Report (Proj. 4-3(2)), 81 p., $1.80
1	Evaluation of Methods of Replacement of Deteriorated Concrete in Structures (Proj. 6-8), 56 p., $2.80
2	An Introduction to Guidelines for Satellite Studies of Pavement Performance (Proj. 1-1), 19 p., $1.80
2A	Guidelines for Satellite Studies of Pavement Performance, 85 p.+9 figs., 26 tables, 4 app., $3.00
3	Improved Criteria for Traffic Signals at Individual Intersections—Interim Report (Proj. 3-5), 36 p., $1.60
4	Non-Chemical Methods of Snow and Ice Control on Highway Structures (Proj. 6-2), 74 p., $3.20
5	Effects of Different Methods of Stockpiling Aggregates—Interim Report (Proj. 10-3), 48 p., $2.00
6	Means of Locating and Communicating with Disabled Vehicles—Interim Report (Proj. 3-4), 56 p. $3.20
7	Comparison of Different Methods of Measuring Pavement Condition—Interim Report (Proj. 1-2), 29 p., $1.80
8	Synthetic Aggregates for Highway Construction (Proj. 4-4), 13 p., $1.00
9	Traffic Surveillance and Means of Communicating with Drivers—Interim Report (Proj. 3-2), 28 p., $1.60
10	Theoretical Analysis of Structural Behavior of Road Test Flexible Pavements (Proj. 1-4), 31 p., $2.80
11	Effect of Control Devices on Traffic Operations—Interim Report (Proj. 3-6), 107 p., $5.80
12	Identification of Aggregates Causing Poor Concrete Performance When Frozen—Interim Report (Proj. 4-3(1)), 47 p., $3.00
13	Running Cost of Motor Vehicles as Affected by Highway Design—Interim Report (Proj. 2-5), 43 p., $2.80
14	Density and Moisture Content Measurements by Nuclear Methods—Interim Report (Proj. 10-5), 32 p., $3.00
15	Identification of Concrete Aggregates Exhibiting Frost Susceptibility—Interim Report (Proj. 4-3(2)), 66 p., $4.00
16	Protective Coatings to Prevent Deterioration of Concrete by Deicing Chemicals (Proj. 6-3), 21 p., $1.60
17	Development of Guidelines for Practical and Realistic Construction Specifications (Proj. 10-1), 109 p., $6.00
18	Community Consequences of Highway Improvement (Proj. 2-2), 37 p., $2.80
19	Economical and Effective Deicing Agents for Use on Highway Structures (Proj. 6-1), 19 p., $1.20
20	Economic Study of Roadway Lighting (Proj. 5-4), 77 p., $3.20
21	Detecting Variations in Load-Carrying Capacity of Flexible Pavements (Proj. 1-5), 30 p., $1.40
22	Factors Influencing Flexible Pavement Performance (Proj. 1-3(2)), 69 p., $2.60
23	Methods for Reducing Corrosion of Reinforcing Steel (Proj. 6-4), 22 p., $1.40
24	Urban Travel Patterns for Airports, Shopping Centers, and Industrial Plants (Proj. 7-1), 116 p., $5.20
25	Potential Uses of Sonic and Ultrasonic Devices in Highway Construction (Proj. 10-7), 48 p., $2.00
26	Development of Uniform Procedures for Establishing Construction Equipment Rental Rates (Proj. 13-1), 33 p., $1.60
27	Physical Factors Influencing Resistance of Concrete to Deicing Agents (Proj. 6-5), 41 p., $2.00
28	Surveillance Methods and Ways and Means of Communicating with Drivers (Proj. 3-2), 66 p., $2.60
29	Digital-Computer-Controlled Traffic Signal System for a Small City (Proj. 3-2), 82 p., $4.00
30	Extension of AASHO Road Test Performance Concepts (Proj. 1-4(2)), 33 p., $1.60
31	A Review of Transportation Aspects of Land-Use Control (Proj. 8-5), 41 p., $2.00
32	Improved Criteria for Traffic Signals at Individual Intersections (Proj. 3-5), 134 p., $5.00
33	Values of Time Savings of Commercial Vehicles (Proj. 2-4), 74 p., $3.60
34	Evaluation of Construction Control Procedures—Interim Report (Proj. 10-2), 117 p., $5.00
35	Prediction of Flexible Pavement Deflections from Laboratory Repeated-Load Tests (Proj. 1-3(3)), 117 p., $5.00
36	Highway Guardrails—A Review of Current Practice (Proj. 15-1), 33 p., $1.60
37	Tentative Skid-Resistance Requirements for Main Rural Highways (Proj. 1-7), 80 p., $3.60
38	Evaluation of Pavement Joint and Crack Sealing Materials and Practices (Proj. 9-3), 40 p., $2.00
39	Factors Involved in the Design of Asphaltic Pavement Surfaces (Proj. 1-8), 112 p., $5.00
40	Means of Locating Disabled or Stopped Vehicles (Proj. 3-4(1)), 40 p., $2.00
41	Effect of Control Devices on Traffic Operations (Proj. 3-6), 83 p., $3.60
42	Interstate Highway Maintenance Requirements and Unit Maintenance Expenditure Index (Proj. 14-1), 144 p., $5.60
43	Density and Moisture Content Measurements by Nuclear Methods (Proj. 10-5), 38 p., $2.00
44	Traffic Attraction of Rural Outdoor Recreational Areas (Proj. 7-2), 28 p., $1.40
45	Development of Improved Pavement Marking Materials—Laboratory Phase (Proj. 5-5), 24 p., $1.40
46	Effects of Different Methods of Stockpiling and Handling Aggregates (Proj. 10-3), 102 p., $4.60
47	Accident Rates as Related to Design Elements of Rural Highways (Proj. 2-3), 173 p., $6.40
48	Factors and Trends in Trip Lengths (Proj. 7-4), 70 p., $3.20
49	National Survey of Transportation Attitudes and Behavior—Phase I Summary Report (Proj. 20-4), 71 p., $3.20

* Highway Research Board Special Report 80.

Rep. No. Title

50 Factors Influencing Safety at Highway-Rail Grade Crossings (Proj. 3-8), 113 p., $5.20
51 Sensing and Communication Between Vehicles (Proj. 3-3), 105 p., $5.00
52 Measurement of Pavement Thickness by Rapid and Nondestructive Methods (Proj. 10-6), 82 p., $3.80
53 Multiple Use of Lands Within Highway Rights-of-Way (Proj. 7-6), 68 p., $3.20
54 Location, Selection, and Maintenance of Highway Guardrails and Median Barriers (Proj. 15-1(2)), 63 p., $2.60
55 Research Needs in Highway Transportation (Proj. 20-2), 66 p., $2.80
56 Scenic Easements—Legal, Administrative, and Valuation Problems and Procedures (Proj. 11-3), 174 p., $6.40
57 Factors Influencing Modal Trip Assignment (Proj. 8-2), 78 p., $3.20
58 Comparative Analysis of Traffic Assignment Techniques with Actual Highway Use (Proj. 7-5), 85 p., $3.60
59 Standard Measurements for Satellite Road Test Program (Proj. 1-6), 78 p., $3.20
60 Effects of Illumination on Operating Characteristics of Freeways (Proj. 5-2) 148 p., $6.00
61 Evaluation of Studded Tires—Performance Data and Pavement Wear Measurement (Proj. 1-9), 66 p., $3.00
62 Urban Travel Patterns for Hospitals, Universities, Office Buildings, and Capitols (Proj. 7-1), 144 p., $5.60
63 Economics of Design Standards for Low-Volume Rural Roads (Proj. 2-6), 93 p., $4.00
64 Motorists' Needs and Services on Interstate Highways (Proj. 7-7), 88 p., $3.60
65 One-Cycle Slow-Freeze Test for Evaluating Aggregate Performance in Frozen Concrete (Proj. 4-3(1)), 21 p., $1.40
66 Identification of Frost-Susceptible Particles in Concrete Aggregates (Proj. 4-3(2)), 62 p., $2.80
67 Relation of Asphalt Rheological Properties to Pavement Durability (Proj. 9-1), 45 p., $2.20
68 Application of Vehicle Operating Characteristics to Geometric Design and Traffic Operations (Proj. 3-10), 38 p., $2.00
69 Evaluation of Construction Control Procedures—Aggregate Gradation Variations and Effects (Proj. 10-2A), 58 p., $2.80
70 Social and Economic Factors Affecting Intercity Travel (Proj. 8-1), 68 p., $3.00
71 Analytical Study of Weighing Methods for Highway Vehicles in Motion (Proj. 7-3), 63 p., $2.80
72 Theory and Practice in Inverse Condemnation for Five Representative States (Proj. 11-2), 44 p., $2.20
73 Improved Criteria for Traffic Signal Systems on Urban Arterials (Proj. 3-5/1), 55 p., $2.80
74 Protective Coatings for Highway Structural Steel (Proj. 4-6), 64 p., $2.80
74A Protective Coatings for Highway Structural Steel—Literature Survey (Proj. 4-6), 275 p., $8.00
74B Protective Coatings for Highway Structural Steel—Current Highway Practices (Proj. 4-6), 102 p., $4.00
75 Effect of Highway Landscape Development on Nearby Property (Proj. 2-9), 82 p., $3.60

Rep. No. Title

76 Detecting Seasonal Changes in Load-Carrying Capabilities of Flexible Pavements (Proj. 1-5(2)), 37 p., $2.00
77 Development of Design Criteria for Safer Luminaire Supports (Proj. 15-6), 82 p., $3.80
78 Highway Noise—Measurement, Simulation, and Mixed Reactions (Proj. 3-7), 78 p., $3.20
79 Development of Improved Methods for Reduction of Traffic Accidents (Proj. 17-1), 163 p., $6.40
80 Oversize-Overweight Permit Operation on State Highways (Proj. 2-10), 120 p., $5.20
81 Moving Behavior and Residential Choice—A National Survey (Proj. 8-6), 129 p., $5.60
82 National Survey of Transportation Attitudes and Behavior—Phase II Analysis Report (Proj. 20-4), 89 p., $4.00
83 Distribution of Wheel Loads on Highway Bridges (Proj. 12-2), 56 p., $2.80
84 Analysis and Projection of Research on Traffic Surveillance, Communication, and Control (Proj. 3-9), 48 p., $2.40
85 Development of Formed-in-Place Wet Reflective Markers (Proj. 5-5), 28 p., $1.80
86 Tentative Service Requirements for Bridge Rail Systems (Proj. 12-8), 62 p., $3.20
87 Rules of Discovery and Disclosure in Highway Condemnation Proceedings (Proj. 11-1(5)), 28 p., $2.00
88 Recognition of Benefits to Remainder Property in Highway Valuation Cases (Proj. 11-1(2)), 24 p., $2.00
89 Factors, Trends, and Guidelines Related to Trip Length (Proj. 7-4), 59 p., $3.20
90 Protection of Steel in Prestressed Concrete Bridges (Proj. 12-5), 86 p., $4.00
91 Effects of Deicing Salts on Water Quality and Biota—Literature Review and Recommended Research (Proj. 16-1), 70 p., $3.20
92 Valuation and Condemnation of Special Purpose Properties (Proj. 11-1(6)), 47 p., $2.60
93 Guidelines for Medial and Marginal Access Control on Major Roadways (Proj. 3-13), 147 p., $6.20
94 Valuation and Condemnation Problems Involving Trade Fixtures (Proj. 11-1(9)), 22 p., $1.80
95 Highway Fog (Proj. 5-6), 48 p., $2.40
96 Strategies for the Evaluation of Alternative Transportation Plans (Proj. 8-4), 111 p., $5.40
97 Analysis of Structural Behavior of AASHO Road Test Rigid Pavements (Proj. 1-4(1)A), 35 p., $2.60
98 Tests for Evaluating Degradation of Base Course Aggregates (Proj. 4-2), 98 p. $5.00
99 Visual Requirements in Night Driving (Proj. 5-3), 38 p., $2.60
100 Research Needs Relating to Performance of Aggregates in Highway Construction (Proj. 4-8), 68 p., $3.40
101 Effect of Stress on Freeze-Thaw Durability of Concrete Bridge Decks (Proj. 6-9), 70 p., $3.60
102 Effect of Weldments on the Fatigue Strength of Steel Beams (Proj. 12-7), 114 p., $5.40
103 Rapid Test Methods for Field Control of Highway Construction (Proj. 10-4), 89 p., $5.00
104 Rules of Compensability and Valuation Evidence for Highway Land Acquisition (Proj. 11-1), 77 p., $4.40

Rep. No. *Title*

105 Dynamic Pavement Loads of Heavy Highway Vehicles (Proj. 15-5), 94 p., $5.00
106 Revibration of Retarded Concrete for Continuous Bridge Decks (Proj. 18-1), 67 p., $3.40
107 New Approaches to Compensation for Residential Takings (Proj. 11-1(10)), 27 p., $2.40
108 Tentative Design Procedure for Riprap-Lined Channels (Proj. 15-2), 75 p., $4.00
109 Elastomeric Bearing Research (Proj. 12-9), 53 p., $3.00
110 Optimizing Street Operations Through Traffic Regulations and Control (Proj. 3-11), 100 p., $4.40
111 Running Costs of Motor Vehicles as Affected by Road Design and Traffic (Proj. 2-5A and 2-7), 97 p., $5.20
112 Junkyard Valuation—Salvage Industry Appraisal Principles Applicable to Highway Beautification (Proj. 11-3(2)), 41 p., $2.60
113 Optimizing Flow on Existing Street Networks (Proj. 3-14), 414 p., $15.60
114 Effects of Proposed Highway Improvements on Property Values (Proj. 11-1(1)), 42 p., $2.60
115 Guardrail Performance and Design (Proj. 15-1(2)), 70 p., $3.60
116 Structural Analysis and Design of Pipe Culverts (Proj. 15-3), 155 p., $6.40
117 Highway Noise—A Design Guide for Highway Engineers (Proj. 3-7), 79 p., $4.60
118 Location, Selection, and Maintenance of Highway Traffic Barriers (Proj. 15-1(2)), 96 p., $5.20
119 Control of Highway Advertising Signs—Some Legal Problems (Proj. 11-3(1)), 72 p., $3.60
120 Data Requirements for Metropolitan Transportation Planning (Proj. 8-7), 90 p., $4.80
121 Protection of Highway Utility (Proj. 8-5), 115 p., $5.60
122 Summary and Evaluation of Economic Consequences of Highway Improvements (Proj. 2-11), 324 p., $13.60
123 Development of Information Requirements and Transmission Techniques for Highway Users (Proj. 3-12), 239 p., $9.60
124 Improved Criteria for Traffic Signal Systems in Urban Networks (Proj. 3-5), 86 p., $4.80
125 Optimization of Density and Moisture Content Measurements by Nuclear Methods (Proj. 10-5A), 86 p., $4.40
126 Divergencies in Right-of-Way Valuation (Proj. 11-4), 57 p., $3.00
127 Snow Removal and Ice Control Techniques at Interchanges (Proj. 6-10), 90 p., $5.20
128 Evaluation of AASHO Interim Guides for Design of Pavement Structures (Proj. 1-11), 111 p., $5.60
129 Guardrail Crash Test Evaluation—New Concepts and End Designs (Proj. 15-1(2)), 89 p., $4.80
130 Roadway Delineation Systems (Proj. 5-7), 349 p., $14.00
131 Performance Budgeting System for Highway Maintenance Management (Proj. 19-2(4)), 213 p., $8.40
132 Relationships Between Physiographic Units and Highway Design Factors (Proj. 1-3(1)), 161 p., $7.20

Rep. No. *Title*

133 Procedures for Estimating Highway User Costs, Air Pollution, and Noise Effects (Proj. 7-8), 127 p., $5.60
134 Damages Due to Drainage, Runoff, Blasting, and Slides (Proj. 11-1(8)), 23 p., $2.80
135 Promising Replacements for Conventional Aggregates for Highway Use (Proj. 4-10), 53 p., $3.60
136 Estimating Peak Runoff Rates from Ungaged Small Rural Watersheds (Proj. 15-4), 85 p., $4.60
137 Roadside Development—Evaluation of Research (Proj. 16-2), 78 p., $4.20
138 Instrumentation for Measurement of Moisture—Literature Review and Recommended Research (Proj. 21-1), 60 p., $4.00
139 Flexible Pavement Design and Management—Systems Formulation (Proj. 1-10), 64 p., $4.40
140 Flexible Pavement Design and Management—Materials Characterization (Proj. 1-10), 118 p., $5.60
141 Changes in Legal Vehicle Weights and Dimensions—Some Economic Effects on Highways (Proj. 19-3), 184 p., $8.40
142 Valuation of Air Space (Proj. 11-5), 48 p., $4.00
143 Bus Use of Highways—State of the Art (Proj. 8-10), 406 p., $16.00
144 Highway Noise—A Field Evaluation of Traffic Noise Reduction Measures (Proj. 3-7), 80 p., $4.40
145 Improving Traffic Operations and Safety at Exit Gore Areas (Proj. 3-17) 120 p., $6.00
146 Alternative Multimodal Passenger Transportation Systems—Comparative Economic Analysis (Proj. 8-9), 68 p., $4.00
147 Fatigue Strength of Steel Beams with Welded Stiffeners and Attachments (Proj. 12-7), 85 p., $4.80
148 Roadside Safety Improvement Programs on Freeways—A Cost-Effectiveness Priority Approach (Proj. 20-7), 64 p., $4.00
149 Bridge Rail Design—Factors, Trends, and Guidelines (Proj. 12-8), 49 p., $4.00
150 Effect of Curb Geometry and Location on Vehicle Behavior (Proj. 20-7), 88 p., $4.80
151 Locked-Wheel Pavement Skid Tester Correlation and Calibration Techniques (Proj. 1-12(2)), 100 p., $6.00
152 Warrants for Highway Lighting (Proj. 5-8), 117 p., $6.40
153 Recommended Procedures for Vehicle Crash Testing of Highway Appurtenances (Proj. 22-2), 19 p., $3.20
154 Determining Pavement Skid-Resistance Requirements at Intersections and Braking Sites (Proj. 1-12), 64 p., $4.40
155 Bus Use of Highways—Planning and Design Guidelines (Proj. 8-10), 161 p., $7.60
156 Transportation Decision-Making—A Guide to Social and Environmental Considerations (Proj. 8-8(3)), 135 p., $7.20
157 Crash Cushions of Waste Materials (Proj. 20-7), 73 p., $4.80
158 Selection of Safe Roadside Cross Sections (Proj. 20–7), 57 p., $4.40
159 Weaving Areas—Design and Analysis (Proj. 3-15), 119 p., $6.40

Rep. No. *Title*

160 Flexible Pavement Design and Management—Systems Approach Implementation (Proj. 1-10A), 54 p., $4.00

161 Techniques for Reducing Roadway Occupancy During Routine Maintenance Activities (Proj. 14-2), 55 p., $4.40

162 Methods for Evaluating Highway Safety Improvements (Proj. 17-2A), 150 p., $7.40

163 Design of Bent Caps for Concrete Box-Girder Bridges (Proj. 12-10), 124 p., $6.80

Synthesis of Highway Practice

No. *Title*

1 Traffic Control for Freeway Maintenance (Proj. 20-5, Topic 1), 47 p., $2.20

2 Bridge Approach Design and Construction Practices (Proj. 20-5, Topic 2), 30 p., $2.00

3 Traffic-Safe and Hydraulically Efficient Drainage Practice (Proj. 20-5, Topic 4), 38 p., $2.20

4 Concrete Bridge Deck Durability (Proj. 20-5, Topic 3), 28 p., $2.20

5 Scour at Bridge Waterways (Proj. 20-5, Topic 5), 37 p., $2.40

6 Principles of Project Scheduling and Monitoring (Proj. 20-5, Topic 6), 43 p., $2.40

7 Motorist Aid Systems (Proj. 20-5, Topic 3-01), 28 p., $2.40

8 Construction of Embankments (Proj. 20-5, Topic 9), 38 p., $2.40

No. *Title*

9 Pavement Rehabilitation—Materials and Techniques (Proj. 20-5, Topic 8), 41 p., $2.80

10 Recruiting, Training, and Retaining Maintenance and Equipment Personnel (Proj. 20-5, Topic 10), 35 p., $2.80

11 Development of Management Capability (Proj. 20-5, Topic 12), 50 p., $3.20

12 Telecommunications Systems for Highway Administration and Operations (Proj. 20-5, Topic 3-03), 29 p., $2.80

13 Radio Spectrum Frequency Management (Proj. 20-5, Topic 3-03), 32 p., $2.80

14 Skid Resistance (Proj. 20-5, Topic 7), 66 p., $4.00

15 Statewide Transportation Planning—Needs and Requirements (Proj. 20-5, Topic 3-02), 41 p., $3.60

16 Continuously Reinforced Concrete Pavement (Proj. 20-5, Topic 3-08), 23 p., $2.80

17 Pavement Traffic Marking—Materials and Application Affecting Serviceability (Proj. 20-5, Topic 3-05), 44 p., $3.60

18 Erosion Control on Highway Construction (Proj. 20-5, Topic 4-01), 52 p., $4.00

19 Design, Construction, and Maintenance of PCC Pavement Joints (Proj. 20-5, Topic 3-04), 40 p., $3.60

20 Rest Areas (Proj. 20-5, Topic 4-04), 38 p., $3.60

21 Highway Location Reference Methods (Proj. 20-5, Topic 4-06), 30 p., $3.20

22 Maintenance Management of Traffic Signal Equipment and Systems (Proj. 20-5, Topic 4-03) 41 p., $4.00

23 Getting Research Findings into Practice (Proj. 20-5, Topic 11) 24 p., $3.20

24 Minimizing Deicing Chemical Use (Proj. 20-5, Topic 4-02), 58 p., $4.00

25 Reconditioning High-Volume Freeways in Urban Areas (Proj. 20-5, Topic 5-01), 56 p., $4.00

26 Roadway Design in Seasonal Frost Areas (Proj. 20-5, Topic 3-07), 104 p., $6.00

27 PCC Pavements for Low-Volume Roads and City Streets (Proj. 20-5, Topic 5-06), 31 p., $3.60

28 Partial-Lane Pavement Widening (Proj. 20-5, Topic 5-05), 30 p., $3.20

29 Treatment of Soft Foundations for Highway Embankments (Proj. 20-5, Topic 4-09), 25 p., $3.20

30 Bituminous Emulsions for Highway Pavements (Proj. 20-5, Topic 6-10), 76 p., $4.80

31 Highway Tunnel Operations (Proj. 20-5, Topic 5-08), 29 p., $3.20

32 Effects of Studded Tires. (Proj. 20-5, Topic 5-13), 46 p., $4.00

33 Acquisition and Use of Geotechnical Information (Proj. 20-5, Topic 5-03), 40 p., $4.00

THE TRANSPORTATION RESEARCH BOARD is an agency of the National Research Council, which serves the National Academy of Sciences and the National Academy of Engineering. The Board's purpose is to stimulate research concerning the nature and performance of transportation systems, to disseminate information that the research produces, and to encourage the application of appropriate research findings. The Board's program is carried out by more than 150 committees and task forces composed of more than 1,800 administrators, engineers, social scientists, and educators who serve without compensation. The program is supported by state transportation and highway departments, the U.S. Department of Transportation, and other organizations interested in the development of transportation.

The Transportation Research Board operates within the Commission on Sociotechnical Systems of the National Research Council. The Council was organized in 1916 at the request of President Woodrow Wilson as an agency of the National Academy of Sciences to enable the broad community of scientists and engineers to associate their efforts with those of the Academy membership. Members of the Council are appointed by the president of the Academy and are drawn from academic, industrial, and governmental organizations throughout the United States.

The National Academy of Sciences was established by a congressional act of incorporation signed by President Abraham Lincoln on March 3, 1863, to further science and its use for the general welfare by bringing together the most qualified individuals to deal with scientific and technological problems of broad significance. It is a private, honorary organization of more than 1,000 scientists elected on the basis of outstanding contributions to knowledge and is supported by private and public funds. Under the terms of its congressional charter, the Academy is called upon to act as an official—yet independent—advisor to the federal government in any matter of science and technology, although it is not a government agency and its activities are not limited to those on behalf of the government.

To share in the tasks of furthering science and engineering and of advising the federal government, the National Academy of Engineering was established on December 5, 1964, under the authority of the act of incorporation of the National Academy of Sciences. Its advisory activities are closely coordinated with those of the National Academy of Sciences, but it is independent and autonomous in its organization and election of members.

TRANSPORTATION RESEARCH BOARD
National Research Council
2101 Constitution Avenue, N.W.
Washington, D.C. 20418

ADDRESS CORRECTION REQUESTED

NON-PROFIT ORG.
U.S. POSTAGE
PAID
WASHINGTON, D.C.
PERMIT NO. 42970

0000019X003
GLENN ANSCHUTZ

ST HWY COMM KANSAS
STATE OFFICE BLDG
TOPEKA KS 66612